Summary of the Bulletin of the International Seismological Centre

2012

July – December

Volume 49 Issue 7-12

www.isc.ac.uk

isc-mirror.iris.washington.edu

ISSN 2309-236X

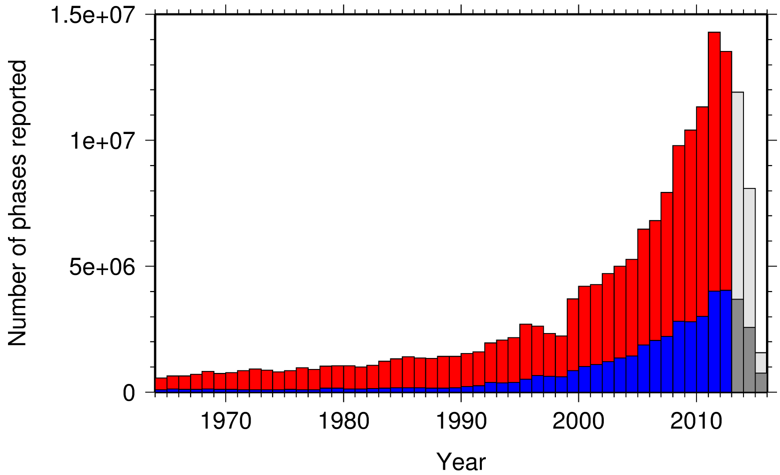

The number of phases (red) and number of amplitudes (blue) collected by the ISC for events each year since 1964. The data in grey covers the current period where data are still being collected before the ISC review takes place and are accurate at the time of publication. See Section 7.3.

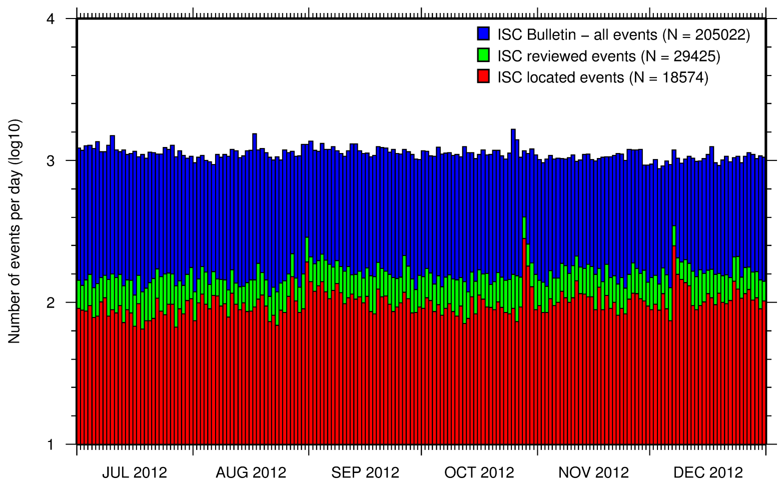

The number of events within the Bulletin for the current summary period. The vertical scale is logarithmic. See Section 8.1.

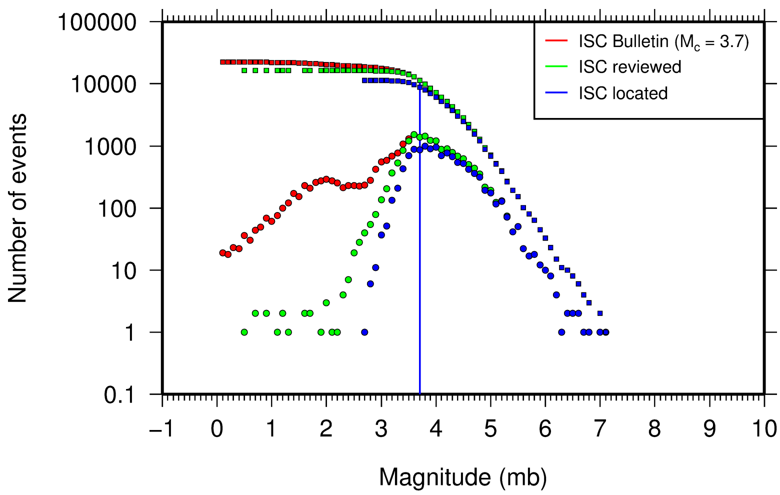

Frequency and cumulative frequency magnitude distribution for all events in the ISC Bulletin, ISC reviewed events and events located by the ISC. The magnitude of completeness (M_C) is shown for the ISC Bulletin. Note: only events with values of m_b are represented in the figure. See Section 8.4.

Contents

1 Preface **1**

2 The International Seismological Centre **2**

2.1 The ISC Mandate . . . 2

2.2 Brief History of the ISC . . . 3

2.3 Former Directors of the ISC and its U.K. Predecessors . . . 4

2.4 Member Institutions of the ISC . . . 5

2.5 Sponsoring Organisations . . . 11

2.6 Data Contributing Agencies . . . 12

2.7 ISC Staff . . . 22

3 Availability of the ISC Bulletin **26**

4 Citing the International Seismological Centre **27**

5 Summary of Seismicity, July - December 2012 **29**

6 Notable Events **33**

6.1 The 30th August 2012, M_W 6.7 Jan Mayen Earthquake . . . 33

6.1.1 Introduction . . . 33

6.1.2 The 30th August 2012 Earthquake . . . 34

6.1.3 Fore- and Aftershock Activity in Connection with the 30th August 2012 Event . . . 35

6.1.4 Summary . . . 39

6.1.5 Acknowledgements . . . 39

6.1.6 References . . . 39

6.2 The October 2012 magnitude (M_W) 7.8 earthquake offshore Haida Gwaii, Canada . . . 41

6.2.1 Introduction . . . 41

6.2.2 Historical Seismicity and Tectonics . . . 42

6.2.3 Mainshock of the October 2012 Earthquake Sequence . . . 45

6.2.4 Physical Impacts . . . 47

6.2.5 Community Decimal Intensities . . . 51

6.2.6 Source Characteristics . . . 53

6.2.7 Coulomb Stress Studies and Overall Rupture Characteristics . . . 53

6.2.8 GPS Observed Crustal Displacements . . . 59

6.2.9 Tsunami . . . 61

6.2.10 Conclusions . . . 67
6.2.11 Acknowledgements . . . 67
6.2.12 References . . . 67

7 Statistics of Collected Data **73**
7.1 Introduction . . . 73
7.2 Summary of Agency Reports to the ISC . . . 73
7.3 Arrival Observations . . . 78
7.4 Hypocentres Collected . . . 85
7.5 Collection of Network Magnitude Data . . . 87
7.6 Moment Tensor Solutions . . . 92
7.7 Timing of Data Collection . . . 95

8 Overview of the ISC Bulletin **97**
8.1 Events . . . 97
8.2 Seismic Phases and Travel-Time Residuals . . . 106
8.3 Seismic Wave Amplitudes and Periods . . . 112
8.4 Completeness of the ISC Bulletin . . . 115
8.5 Magnitude Comparisons . . . 116

9 The Leading Data Contributors **121**
9.1 The Largest Data Contributors . . . 121
9.2 Contributors Reporting the Most Valuable Parameters . . . 124
9.3 The Most Consistent and Punctual Contributors . . . 130

10 Appendix **132**

11 Glossary of ISC Terminology **149**

12 Acknowledgements **153**

References **154**

1

Preface

Dear Colleague,

This is the second and concluding 2012 issue of the Summary of the ISC Bulletin that remains the most fundamental reason for continued operations at the ISC. This issue covers seismic events that occurred during the period from July to December.

This publication presents a description of the ISC data available on the attached DVD-ROM and from the ISC website. It contains information on the ISC, its Members, Sponsors and Data Providers. It offers analysis of the data contributed to the ISC by many seismological agencies worldwide as well as analysis of the data in the ISC Bulletin itself. This somewhat smaller issue misses some of the standard information on routine procedures usually published in the first issue of each year.

We continue publishing invited articles describing notable seismic events in this period – the M_W 6.7 Jan Mayen earthquake in August and the M_W 7.8 Haida Gwaii earthquake in October.

We hope that you find this relatively new publication useful in your work. If your home-institution or company is unable, for one reason or another, to support the long-term international operations of the ISC in full by becoming a Member, then, please, consider subscribing to this publication by contacting us at admin@isc.ac.uk.

With kind regards to our Data Contributors, Members, Sponsors and users,

Dr Dmitry A. Storchak
Director
International Seismological Centre (ISC)

2

The International Seismological Centre

2.1 The ISC Mandate

The International Seismological Centre (ISC) was set up in 1964 with the assistance of UNESCO as a successor to the International Seismological Summary (ISS) to carry forward the pioneering work of Prof. John Milne, Sir Harold Jeffreys and other British scientists in collecting, archiving and processing seismic station and network bulletins and preparing and distributing the definitive summary of world seismicity.

Under the umbrella of the International Association of Seismology and Physics of the Earth Interior (IASPEI/IUGG), the ISC has played an important role in setting international standards such as the International Seismic Bulletin Format (ISF), the IASPEI Standard Seismic Phase List (SSPL) and both the old and New IASPEI Manual of the Seismological Observatory Practice (NMSOP-2) (www.iaspei.org/projects/NMSOP.html).

The ISC has contributed to scientific research and prominent scientists such as John Hodgson, Eugine Herrin, Hal Thirlaway, Jack Oliver, Anton Hales, Ola Dahlman, Shigeji Suehiro, Nadia Kondorskaya, Vit Karnik, Stephan Müller, David Denham, Bob Engdahl, Adam Dziewonski, John Woodhouse and Guy Masters all considered it an important duty to serve on the ISC Executive Committee and the Governing Council.

The current mission of the ISC is to maintain:

- the ISC **Bulletin** – the longest continuous definitive summary of World seismicity (collaborating with ∼130 seismic networks and data centres around the world). (www.isc.ac.uk/iscbulletin/)
- the **International** Seismographic Station Registry (**IR**, jointly with the World Data Center for Seismology, Denver). (www.isc.ac.uk/registries/)
- the IASPEI Reference Event List (Ground Truth, **GT**, jointly with IASPEI). (www.isc.ac.uk/gtevents/)

These are fundamentally important tasks. Bulletin data produced, archived and distributed by the ISC for almost 50 years are the definitive source of such information and are used by thousands of seismologists worldwide for seismic hazard estimation, for tectonic studies and for regional and global imaging of the Earth's structure. Key information in global tomographic imaging is derived from the analysis of ISC data. The ISC Bulletin served as a major source of data for such well known products as the ak135 global 1-D velocity model and the EHB (*Engdahl et al.*, 1998) and Centennial (*Engdahl and Villaseñor*, 2002) catalogues. It presents an important quality-control benchmark for the Comprehensive Nuclear-Test-Ban Treaty Organization (CTBTO). Hypocentre parameters from the ISC Bulletin are used by the Data Management Center of the Incorporated Research Institutions for Seismology (IRIS DMC) to serve event-oriented user-requests for waveform data. The ISC-GEM Bulletin is a cornerstone of the ISC-GEM Global Instrumental Reference Earthquake Catalogue for Global Earthquake risk Model (GEM).

The ISC relational database currently holds approximately 90 Gb of unique data. The ISC Bulletin contains over 5 million seismic events: earthquakes, chemical and nuclear explosions, mine blasts and mining induced events. At least 1.5 million of them are regional and teleseismically recorded events that have been reviewed by the ISC analysts. The ISC Bulletin contains approximately 150 million individual seismic station readings of arrival times, amplitudes, periods, SNR, slowness and azimuth, reported by approximately 17,000 seismic stations currently registered in the IR. Over 6,000 stations have contributed to the ISC Bulletin in recent years. This number includes the numerous sites of the USArray. The IASPEI GT List currently contains 7802 events for which latitude, longitude and depth of origin are known with high confidence (to 5 km or better) and seismic signals were recorded at regional and/or teleseismic distances.

2.2 Brief History of the ISC

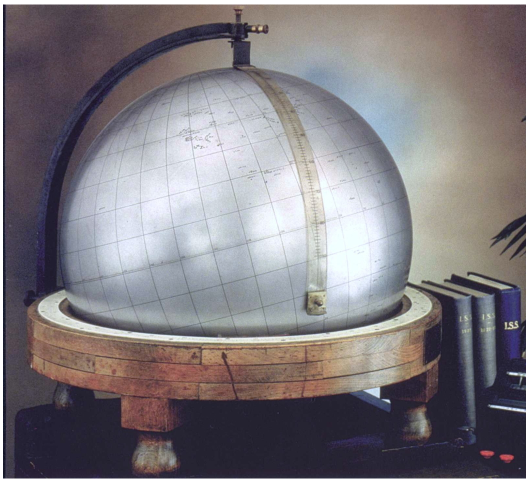

Figure 2.1: *The steel globe bearing positions of early seismic stations was used for locating positions of earthquakes for the International Seismological Summaries.*

Earthquake effects have been noted and documented from the earliest times, but it is only since the development of earthquake recording instruments in the latter half of the 19th century that a proper study of their occurrence has been possible. After the first teleseismic observation of an earthquake in 1889, the need for international exchange of readings was recognised in 1895 by Prof. John Milne and by Ernst von Rebeur Paschwitz together with Georg Gerland, resulting in the publication of the first international seismic bulletins. Milne's "Shide Circulars" were issued under the auspices of the Seismological Committee of the British Association for the Advancement of Science (BAAS), while co-workers of Gerland at the Central Bureau of the International Association of Seismology worked independently in Strasbourg (BCIS).

Following Milne's death in 1913, Seismological Bulletins of the BAAS were continued under Prof. H.H. Turner, later based at Oxford University. Upon formal post-war dissolution of the International Association of Seismology in 1922 the newly founded Seismological Section of the International Union of Geodesy and Geophysics (IUGG) set up the International Seismological Summary (ISS) to continue at Oxford under Turner, to produce the definitive global catalogues from the 1918 data-year onwards, under the auspices of IUGG and with the support of the BAAS.

ISS production, led by several professors at Oxford University, and Sir Harold Jeffreys at Cambridge University, continued until it was superseded by the ISC Bulletin, after the ISC was formed in Edinburgh in 1964 with Dr P.L. Willmore as its first director.

During the period 1964 to 1970, with the help of UNESCO and other international scientific bodies, the ISC was reconstituted as an international non-governmental body, funded by interested institutions from various countries. Initially there were supporting members from seven countries, now there are almost 60, and member institutions include national academies, research foundations, government departments and research institutes, national observatories and universities. Each member, contributing a minimum unit of subscription or more, appoints a representative to the ISC's Governing Council, which meets every two years to decide the ISC's policy and operational programme. Representatives from the International Association of Seismology and Physics of the Earth's Interior also attend these meetings. The Governing Council appoints the Director and a small Executive Committee to oversee the ISC's operations.

Figure 2.2: *ISC building in Thatcham, Berkshire, UK.*

In 1975, the ISC moved to Newbury in southern England to make use of better computing facilities there. The ISC subsequently acquired its own computer and in 1986 moved to its own building at Pipers Lane, Thatcham, near Newbury. The internal layout of the new premises was designed for the ISC and includes not only office space but provision for the storage of extensive stocks of ISS and ISC publications and a library of seismological observatory bulletins, journals and books collected over many tens of years.

In 1997 the first set of the ISC Bulletin CD-ROMs was produced (not counting an earlier effort at USGS). The first ISC website appeared in 1998 and the first ISC database was put in day-to-day operations from 2001.

Throughout 2009-2011 a major internal reconstruction of the ISC building was undertaken to allow for more members of staff working in mainstream ISC operations as well as major development projects such as the CTBTO Link, ISC-GEM Catalogue and the ISC Bulletin Rebuild.

2.3 Former Directors of the ISC and its U.K. Predecessors

John Milne
Publisher of the Shide Cicular Reports on Earthquakes
1899-1913

Herbert Hall Turner

Seismological Bulletins of the BAAS

1913-1922
Director of the ISS
1922-1930

Harry Hemley Plaskett
Director of the ISS
1931-1946

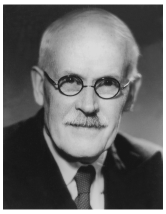

Harold Jeffreys
Director of the ISS
1946-1957

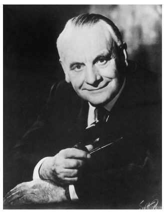

Robert Stoneley
Director of the ISS
1957-1963

P.L. (Pat) Willmore
Director of the ISS
1963-1970
Director of the ISC
1964-1970

Edouard P. Arnold
Director of the ISC
1970-1977

Anthony A. Hughes
Director of the ISC
1977-1997

Raymond J. Willemann
Director of the ISC
1998-2003

Avi Shapira
Director of the ISC
2004-2007

2.4 Member Institutions of the ISC

Article IV(a-b) of the ISC Working Statutes stipulates that any national academy, agency, scientific institution or other non-profit organisation may become a Member of the ISC on payment to the ISC of a sum equal to at least one unit of subscription and the nomination of a voting representative to serve on the ISC's governing body. Membership shall be effective for one year from the date of receipt at the ISC of the annual contribution of the Member and is thereafter renewable for periods of one year.

The ISC is currently supported with funding from its 62 Member Institutions and a four-year Grant Award EAR-1417970 from the US National Science Foundation.

Figures 2.3 and 2.4 show major sectors to which the ISC Member Institutions belong and proportional financial contributions that each of these sectors make towards the ISC's annual budget.

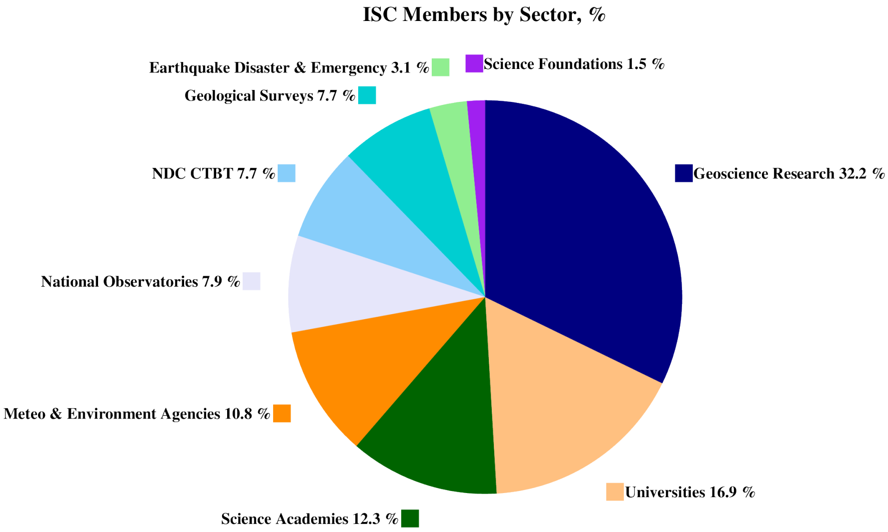

Figure 2.3: Distribution of the ISC Member Institutions by sector in year 2013 as a percentage of total number of Members.

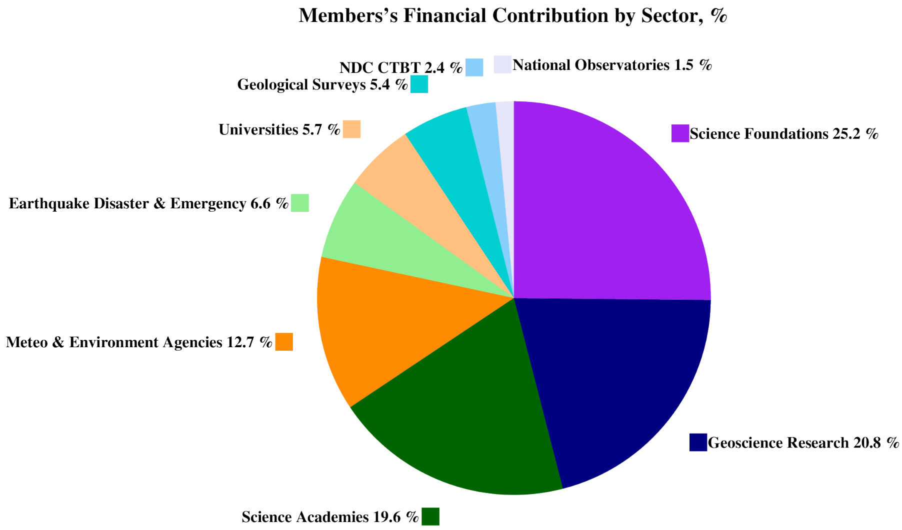

Figure 2.4: Distribution of Member's financial contributions to the ISC by sector in year 2013 as a percentage of total annual Member contributions.

There follows a list of all current Member Institutions with a category (1 through 9) assigned according to the ISC Working Statutes. Each category relates to the number of membership units contributed.

Centre de Recherche en Astronomie, Astrophysique et Géophysique (CRAAG)
Algeria
www.craag.dz
Category: 1

Instituto Nacional de Prevención Sísmica (INPRES)
Argentina
www.inpres.gov.ar
Category: 1

Geoscience Australia
Australia
www.ga.gov.au
Category: 3

The University of Melbourne
Australia
www.unimelb.edu.au
Category: 1

Seismology Research Centre
Australia
www.seis.com.au
Category: 1

Bundesministerium für Wissenschaft und Forschung
Austria
www.bmbwk.gv.at
Category: 2

Centre of Geophysical Monitoring (CGM) of the National Academy of Sciences of Belarus
Belarus
www.cgm.org.by
Category: 1

Observatoire Royal de Belgique
Belgium
www.astro.oma.be
Category: 1

Universidade de São Paulo, Centro de Sismologia
Brazil
www.sismo.iag.usp.br
Category: 1

The Geological Survey of Canada
Canada
gsc.nrcan.gc.ca
Category: 4

Department of Geophysics, University of Chile
Chile
ingenieria.uchile.cl
Category: 1

China Earthquake Administration
China
www.gov.cn
Category: 5

Institute of Earth Sciences, Academia Sinica
Chinese Taipei
www.earth.sinica.edu.tw
Category: 1

Geological Survey Department
Cyprus
www.moa.gov.cy
Category: 1

Academy of Sciences of the Czech Republic
Czech Republic
www.cas.cz
Category: 2

Geological Survey of Denmark and Greenland - GEUS
Denmark
www.geus.dk
Category: 2

National Research Institute for Astronomy and Geophysics (NRIAG), Cairo
Egypt
www.nriag.sci.eg
Category: 1

The University of Helsinki
Finland
www.helsinki.fi
Category: 2

Institute National des Sciences de l'Univers
France
www.insu.cnrs.fr
Category: 4

Laboratoire de Détection et de Géophysique/CEA
France
www-dase.cea.fr
Category: 2

Bundesanstalt für Geowissenschaften und Rohstoffe
Germany
www.bgr.bund.de
Category: 4

GeoForschungsZentrum Potsdam
Germany
www.gfz-potsdam.de
Category: 2

The Seismological Institute, National Observatory of Athens
Greece
www.noa.gr
Category: 1

The Hungarian Academy of Sciences
Hungary
www.mta.hu
Category: 1

The Icelandic Meteorological Office
Iceland
www.vedur.is
Category: 1

India Meteorological Department
India
www.imd.ernet.in
Category: 4

Iraqi Seismic Network
Iraq
www.imos-tm.com
Category: 1

Dublin Institute for Advanced Studies
Ireland
www.dias.ie
Category: 1

The Geophysical Institute of Israel
Israel
www.gii.co.il
Category: 1

Soreq Nuclear Research Centre (SNRC)
Israel
www.soreq.gov.il
Category: 1

Istituto Nazionale di Oceanografia e di Geofisica Sperimentale
Italy
www.ogs.trieste.it
Category: 1

Istituto Nazionale di Geofisica e Vulcanologia
Italy
www.ingv.it
Category: 3

University of the West Indies
Jamaica
www.mona.uwi.edu
Category: 1

Japan Agency for Marine-Earth Science and Technology (JAMSTEC)
Japan
www.jamstec.go.jp
Category: 3

The Japan Meteorological Agency (JMA)
Japan
www.jma.go.jp
Category: 5

Earthquake Research Institute, University of Tokyo
Japan
www.eri.u-tokyo.ac.jp
Category: 3

National Institute of Polar Research (NIPR)
Japan
www.nipr.ac.jp
Category: 1

Natural Resources Authority, Amman
Jordan
www.nra.gov.jo
Category: 1

Institute of Geophysics, National University of Mexico
Mexico
www.igeofcu.unam.mx
Category: 1

The Royal Netherlands Meteorological Institute
Netherlands
www.knmi.nl
Category: 2

Institute of Geological and Nuclear Sciences
New Zealand
www.gns.cri.nz
Category: 3

The University of Bergen
Norway
www.uib.no
Category: 2

Stiftelsen NORSAR
Norway
www.norsar.no
Category: 2

Institute of Geophysics, Polish Academy of Sciences
Poland
www.igf.edu.pl
Category: 1

Instituto Português do Mar e da Atmosfera
Portugal
www.ipma.pt
Category: 2

Red Sísmica de Puerto Rico
Puerto Rico
redsismica.uprm.edu
Category: 1

Korean Meterological Administration
Republic of Korea
www.kma.go.kr
Category: 1

National Institute for Earth Physics
Romania
www.infp.ro
Category: 1

Russian Academy of Sciences
Russia
www.ras.ru
Category: 5

Environmental Agency of Slovenia
Slovenia
www.arso.gov.si
Category: 1

Council for Geoscience
South Africa
www.geoscience.org.za
Category: 1

Institut Cartogràfic i Geològic de Catalunya (ICGC)
Spain
www.igc.cat
Category: 1

Uppsala Universitet
Sweden
www.uu.se
Category: 2

National Defence Research Establishment
Sweden
www.foi.se
Category: 1

The Swiss Academy of Sciences
Switzerland
www.scnat.ch
Category: 2

University of the West Indies
Trinidad and Tobago
sta.uwi.edu
Category: 1

Disaster and Emergency Management Presidency
Turkey
www.deprem.gov.tr
Category: 2

Kandilli Observatory and Earthquake Research Institute
Turkey
www.koeri.boun.edu.tr
Category: 1

The Royal Society of London
United Kingdom
www.royalsociety.org
Category: 6

AWE Blacknest
United Kingdom
www.blacknest.gov.uk
Category: 1

British Geological Survey
United Kingdom
www.bgs.ac.uk
Category: 2

University of Texas at Austin
U.S.A.
www.utexas.edu
Category: 1

Incorporated Research Institutions for Seismology
U.S.A.
www.iris.edu
Category: 1

The National Science Foundation of the United States. (Grant No. EAR-1417970)
U.S.A.
www.nsf.gov
Category: 9

National Earthquake Information Center, U.S. Geological Survey
U.S.A.
www.neic.usgs.gov
Category: 2

In addition the ISC is currently in receipt of grants from the International Data Centre (IDC) of the Preparatory Commission of the Comprehensive Nuclear-Test-Ban Treaty Organization (CTBTO), the Global Earthquake risk Model Foundation (GEM), FM Global, Lighthill risk Network, OYO and USGS (Award G14AC00149).

2.5 Sponsoring Organisations

Article IV(c) of the ISC Working Statutes stipulates any commercial organisation with an interest in the objectives and/or output of the ISC may become an Associate Member of the ISC on payment of an Associate membership fee, but without entitlement to representation with a vote on the ISC's governing body.

www.reftek.com

REF TEK designs and manufactures application specific, high-performance, battery-operated, field-portable geophysical data acquisition devices for the global market. With over 35 years of experience, REF TEK provides customers with complete turnkey solutions that include high resolution recorders, broadband sensors, state-of-the-art communications (V-SAT, GPRS, etc), installation, training, and continued customer support. Over 7,000 REF TEK instruments are currently being used globally for multiple applications. From portable earthquake monitoring to telemetry earthquake monitoring, earthquake aftershock recording to structural monitoring and more, REF TEK equipment is suitable for a wide variety of application needs.

GeoSIG swiss made to measure http://www.geosig.com/

GeoSIG provides earthquake, seismic, structural, dynamic and static monitoring and measuring solutions As an ISO Certified company, GeoSIG is a world leader in design and manufacture of a diverse range of high quality, precision instruments for vibration and earthquake monitoring. GeoSIG instruments are at work today in more than 100 countries around the world with well-known projects such as the NetQuakes installation with USGS and Oresund Bridge in Denmark. GeoSIG offers off-the-shelf solutions as well as highly customised solutions to fulfil the challenging requirements in many vertical markets including the following:

- Earthquake Early Warning and Rapid Response (EEWRR)
- Seismic and Earthquake Monitoring and Measuring
- Industrial Facility Seismic Monitoring and Shutdown
- Structural Analysis and Ambient Vibration Testing
- Induced Vibration Monitoring
- Research and Scientific Applications

2.6 Data Contributing Agencies

In addition to its Members and Sponsors, the ISC owes its existence and successful long-term operations to its 142 seismic bulletin data contributors. These include government agencies responsible for national seismic networks, geoscience research institutions, geological surveys, meteorological agencies, universities, national data centres for monitoring the CTBT and individual observatories. There would be no ISC Bulletin available without the regular stream of data that are unselfishly and generously contributed to the ISC on a free basis.

The Institute of Seismology, Academy of Sciences of Albania
Albania
TIR

Centre de Recherche en Astronomie, Astrophysique et Géophysique
Algeria
CRAAG

Instituto Nacional de Prevención Sísmica
Argentina
SJA

Universidad Nacional de La Plata
Argentina
LPA

National Survey of Seismic Protection
Armenia
NSSP

Geoscience Australia
Australia
AUST

Österreichischer Geophysikalischer Dienst
Austria
VIE

International Data Centre, CTBTO
Austria
IDC

Republic Center of Seismic Survey
Azerbaijan
AZER

Centre of Geophysical Monitoring
Belarus
BELR

Royal Observatory of Belgium
Belgium
UCC

Observatorio San Calixto
Bolivia
SCB

Sarajevo Seismological Station
Bosnia and Herzegovina
SAR

Instituto Astronomico e Geofísico
Brazil
VAO

Geophysical Institute, Bulgarian Academy of Sciences
Bulgaria
SOF

Canadian Hazards Information Service, Natural Resources Canada
Canada
OTT

Departamento de Geofísica, Universidad de Chile
Chile
GUC

China Earthquake Networks Center
China
BJI

Institute of Earth Sciences, Academia Sinica
Chinese Taipei
ASIES

Red Sismológica Nacional de Colombia
Colombia
RSNC

Sección de Sismología, Vulcanología y Exploración Geofísica
Costa Rica
UCR

Seismological Survey of the Republic of Croatia
Croatia
ZAG

Cyprus Geological Survey Department
Cyprus
NIC

Geophysical Institute, Academy of Sciences of the Czech Republic
Czech Republic
PRU

West Bohemia Seismic Network
Czech Republic
WBNET

The Institute of Physics of the Earth (IPEC)
Czech Republic
IPEC

Geological Survey of Denmark and Greenland
Denmark
DNK

Observatoire Géophysique d'Arta
Djibouti
ARO

Servicio Nacional de Sismología y Vulcanología
Ecuador
IGQ

National Research Institute of Astronomy and Geophysics
Egypt
HLW

University of Addis Ababa
Ethiopia
AAE

Institute of Seismology, University of Helsinki
Finland
HEL

Institut de Physique du Globe
France
STR

Laboratoire de Détection et de Géophysique/CEA
France
LDG

Centre Sismologique Euro-Méditerranéen (CSEM/EMSC)
France
CSEM

Laboratoire de Géophysique/CEA
French Polynesia
PPT

Seismological Observatory Skopje
FYR Macedonia
SKO

Seismic Monitoring Centre of Georgia
Georgia
TIF

Alfred Wegener Institute for Polar and Marine Research
Germany
AWI

Seismological Observatory Berggießhübel, TU Bergakademie Freiberg
Germany
BRG

Bundesanstalt für Geowissenschaften und Rohstoffe
Germany
BGR

Geophysikalisches Observatorium Collm
Germany
CLL

National Observatory of Athens
Greece
ATH

Department of Geophysics, Aristotle University of Thessaloniki
Greece
THE

Hong Kong Observatory
Hong Kong
HKC

Geodetic and Geophysical Research Institute
Hungary
BUD

Icelandic Meteorological Office
Iceland
REY

India Meteorological Department
India
NDI

National Geophysical Research Institute
India
HYB

Badan Meteorologi, Klimatologi dan Geofisika
Indonesia
DJA

Tehran University
Iran
TEH

International Institute of Earthquake Engineering and Seismology (IIEES)
Iran
THR

Iraqi Meteorological and Seismology Organisation
Iraq
ISN

Dublin Institute for Advanced Studies
Ireland
DIAS

The Geophysical Institute of Israel
Israel
GII

Dipartimento per lo Studio del Territorio e delle sue Risorse (RSNI)
Italy
GEN

Istituto Nazionale di Geofisica e Vulcanologia
Italy
ROM

Istituto Nazionale di Oceanografia e di Geofisica Sperimentale (OGS)
Italy
TRI

MedNet Regional Centroid - Moment Tensors
Italy
MED_RCMT

Osservatorio Sismologico Universita di Bari
Italy
OSUB

Station Géophysique de Lamto
Ivory Coast
LIC

Jamaica Seismic Network
Jamaica
JSN

National Research Institute for Earth Science and Disaster Prevention
Japan
NIED

National Institute of Polar Research
Japan
SYO

Japan Meteorological Agency
Japan
JMA

The Matsushiro Seismological Observatory
Japan
MAT

Jordan Seismological Observatory
Jordan
JSO

National Nuclear Center
Kazakhstan
NNC

Seismological Experimental Methodological Expedition
Kazakhstan
SOME

Institute of Seismology, Academy of Sciences of Kyrgyz Republic
Kyrgyzstan
KRNET

Kyrgyz Seismic Network
Kyrgyzstan
KNET

Latvian Seismic Network
Latvia
LVSN

National Council for Scientific Research
Lebanon
GRAL

Geological Survey of Lithuania
Lithuania
LIT

Macao Meteorological and Geophysical Bureau
Macao, China
MCO

Geological Survey Department Malawi
Malawi
GSDM

Malaysian Meteorological Service
Malaysia
KLM

Red Sismica del Noroeste de Mexico (RESOM)
Mexico
ECX

Instituto de Geofísica de la UNAM
Mexico
MEX

Institute of Geophysics and Geology
Moldova
MOLD

Seismological Institute of Montenegro
Montenegro
PDG

Centre National de Recherche
Morocco
CNRM

Department of Mines and Geology, Ministry of Industry of Nepal
Nepal
DMN

Koninklijk Nederlands Meteorologisch Instituut
Netherlands
DBN

Institute of Geological and Nuclear Sciences
New Zealand
WEL

Stiftelsen NORSAR
Norway
NAO

University of Bergen
Norway
BER

Sultan Qaboos University
Oman
OMAN

Micro Seismic Studies Programme, PINSTECH
Pakistan
MSSP

Manila Observatory
Philippines
QCP

Philippine Institute of Volcanology and Seismology
Philippines
MAN

Institute of Geophysics, Polish Academy of Sciences
Poland
WAR

Instituto Geofisico do Infante Dom Luiz
Portugal
IGIL

Sistema de Vigilância Sismológica dos Açores
Portugal
SVSA

Instituto Português do Mar e da Atmosfera, I.P.
Portugal
INMG

Korea Meteorological Administration
Republic of Korea
KMA

National Institute for Earth Physics
Romania
BUC

Yakutiya Regional Seismological Center, GS SB RAS
Russia
YARS

Baykal Regional Seismological Centre, GS SB RAS
Russia
BYKL

Geophysical Survey of Russian Academy of Sciences
Russia
MOS

Institute of Environmental Problems of the North, Russian Academy of Sciences
Russia
IEPN

Sakhalin Experimental and Methodological Seismological Expedition, GS RAS
Russia
SKHL

Mining Institute of the Ural Branch of the Russian Academy of Sciences
Russia
MIRAS

North Eastern Regional Seismological Centre, GS RAS
Russia
NERS

Altai-Sayan Seismological Centre, GS SB RAS
Russia
ASRS

Kola Regional Seismic Centre, GS RAS
Russia
KOLA

Kamchatkan Experimental and Methodical Seismological Department, GS RAS
Russia
KRSC

Saudi Geological Survey
Saudi Arabia
SGS

Seismological Survey of Serbia
Serbia
BEO

Geophysical Institute, Slovak Academy of Sciences
Slovakia
BRA

Environmental Agency of the Republic of Slovenia
Slovenia
LJU

Ministry of Mines, Energy and Rural Electrification
Solomon Islands
HNR

Council for Geoscience
South Africa
PRE

Real Instituto y Observatorio de la Armada
Spain
SFS

Institut Cartogràfic de Catalunya
Spain
MRB

Instituto Geográfico Nacional
Spain
MDD

University of Uppsala
Sweden
UPP

Swiss Seismological Sevice (SED)
Switzerland
ZUR

National Syrian Seismological Center
Syria
NSSC

Thai Meteorological Department
Thailand
BKK

University of the West Indies
Trinidad and Tobago
TRN

Institut National de la Météorologie
Tunisia
TUN

The Earthquake Research Center
Ataturk University
Turkey
ATA

Kandilli Observatory and Research Institute
Turkey
ISK

Disaster and Emergency Management Presidency
Turkey
DDA

Subbotin Institute of Geophysics, National Academy of Sciences
Ukraine
SIGU

Dubai Seismic Network
United Arab Emirates
DSN

British Geological Survey
United Kingdom
BGS

IASPEI Working Group on Reference Events
U.S.A.
IASPEI

United States Geological Survey
U.S.A.
USGS

National Earthquake Information Center
U.S.A.
NEIC

IRIS Data Management Center
U.S.A.
IRIS

The Global CMT Project
U.S.A.
GCMT

Red Sísmica de Puerto Rico
U.S.A.
RSPR

Pacific Northwest Seismic Network
U.S.A.
PNSN

National Center for Scientific Research
Vietnam
PLV

Yemen National Seismological Center
Yemen
DHMR

Geological Survey Department of Zambia
Zambia
LSZ

Goetz Observatory
Zimbabwe
BUL

Seismic Institute of Kosovo

SIK

CWB
Chinese Taipei
TAP

East African Network

EAF

2.7 ISC Staff

Listed below are the staff (and their country of origin) who were employed at the ISC at the time of this ISC Bulletin Summary.

- Dmitry Storchak
- Director
- Russia/United Kingdom

- Maureen Aspinwall
- Administration Officer
- United Kingdom

- James Harris
- System and Database Administrator
- United Kingdom

- John Eve
- Data Collection Officer
- United Kingdom

- Emily Delahaye
- Seismologist/Lead Analyst
- Canada

- Blessing Shumba
- Seismologist/Analyst
- Zimbabwe

- Rosemary Wylie
- Analyst
- United Kingdom

- Rebecca Verney
- Analyst
- United Kingdom

- Wayne Richardson
- Senior Seismologist
- New Zealand

- Domenico Di Giacomo
- Seismologist
- Italy

- Konstantinos Lentas
- Seismologist/Developer
- Greece

- Przemek Ozgo
- Junior System Administrator
- Poland

- Natalia Safronova
- Historical Data Entry Officer
- Russia

- Elizabeth Ball
- Historical Data Entry Officer
- United Kingdom

- Daniela Catanescu
- Historical Data Entry Officer
- Romania

3

Availability of the ISC Bulletin

The ISC Bulletin is available from the following sources:

- Web searches
  The entire ISC Bulletin is available directly from the ISC website via tailored searches.
  (www.isc.ac.uk/iscbulletin/search)
  (isc-mirror.iris.washington.edu/iscbulletin/search)

  - Bulletin search - provides the most verbose output of the ISC Bulletin in ISF or QuakeML.
  - Event catalogue - only outputs the prime hypocentre for each event, producing a simple list of events, locations and magnitudes.
  - Arrivals - search for arrivals in the ISC Bulletin. Users can search for specific phases for selected stations and events.

- CD-ROMs/DVD-ROMs

  CDs/DVDs can be ordered from the ISC for any published volume (one per year), or for all back issues of the Bulletin (not including the latest volume). The data discs contain the Bulletin as a PDF, in IASPEI Seismic Format (ISF), and in Fixed Format Bulletin (FFB) format. An event catalogue is also included, together with the International Registry of seismic station codes.

- FTP site

  The ISC Bulletin is also available to download from the ISC ftp site, which contains the Bulletin in PDF, ISF and FFB formats. (ftp://www.isc.ac.uk)
  (ftp://isc-mirror.iris.washington.edu)

Mirror service

A mirror of the ISC database, website and ftp site is available at IRIS DMC (isc-mirror.iris.washington.edu), which benefits from their high-speed internet connection, providing an alternative method of accessing the ISC Bulletin.

4

Citing the International Seismological Centre

Data from the ISC should always be cited. This includes use by academic or commercial organisations, as well as individuals. A citation should show how the data were retrieved and may be in one of these suggested forms:

Data retrieved from the ISC web site:

- International Seismological Centre, On-line Bulletin, http://www.isc.ac.uk, Internatl. Seis. Cent., Thatcham, United Kingdom, 2015.

Data transcribed from the IASPEI reference event bulletin:

- International Seismological Centre, Reference Event Bulletin, http://www.isc.ac.uk, Internatl. Seis. Cent., Thatcham, United Kingdom, 2015.

Data transcribed from the EHB bulletin:

- International Seismological Centre, EHB Bulletin, http://www.isc.ac.uk, Internatl. Seis. Cent., Thatcham, United Kingdom, 2015.

Data copied from ISC CD-ROMs/DVD-ROMs:

- International Seismological Centre, Bulletin Disks 1-2012 [CD-ROM], Internatl. Seis. Cent., Thatcham, United Kingdom, 2015.

Data transcribed from the printed Bulletin:

- International Seismological Centre, Bull. Internatl. Seis. Cent., 2015(1), Thatcham, United Kingdom, 2015.

The ISC is named as a valid data centre for citations within American Geophysical Union (AGU) publications. As such, please follow the AGU guidelines when referencing ISC data in one of their journals. The ISC may be cited as both the institutional author of the Bulletin and the source from which the data were retrieved.

BibTex entry example:

```
@manual{ISCcitation2015,
author = "International Seismological Centre",
title = "On-line Bulletin",
organization = "Int. Seis. Cent.",
note = "http://www.isc.ac.uk",
address = "Thatcham, United Kingdom",
year = "2015"
}
```

5

Summary of Seismicity, July - December 2012

During the last six months of 2012, the largest earthquake, M_W 7.8 on October 28 centred in the Haida Gwaii archipelago (Queen Charlotte Islands region), generated a generally small but nearly Pacific-wide tsunami but there were no reported deaths. The other shallow earthquakes of M_W 7 or more during this interval also had small tsunami recorded.

There were at least 48 deaths reported for the M_W 7.4 earthquake on November 7 off the coast of Guatemala, and many buildings were damaged. There were at least two deaths reported for the M_W 7.6 earthquake in Costa Rica in September and one death reported for the M_W 7.6 earthquake in the Philippines Islands region in August.

The M_W 6.5 earthquake on August 11 in the Iran-Armenia-Azerbaijan border region was the most lethal earthquake in this summary period, with at least 306 deaths reported, and there was much damage and infrastructure disruption in the epicentral region.

For other earthquakes less than M_W 7, there were at least 81 deaths and much damage reported for the M_W 5.6 earthquake on September 7 in Yunnan, China, which was followed by an M_W 5.3 earthquake within an hour. Elsewhere, there were at least 26 deaths reported for the M_W 6.8 earthquake on November 11 in Myanmar, at least 6 deaths reported for the M_W 6.3 earthquake in August in Sulawesi, at least 1 death reported for the M_W 5.0 earthquake in July in southeastern China and at least 1 death reported for the M_W 5.3 earthquake in October in southern Italy.

The number of events in this Bulletin Summary categorised by type are given in Table 5.1.

Table 5.1: *Summary of events by type between July and December 2012.*

damaging earthquake	15
felt earthquake	1709
felt mine explosion	1
known earthquake	178028
known chemical explosion	5218
known induced event	2459
known mine explosion	1665
known rockburst	36
known experimental explosion	88
suspected earthquake	10765
suspected chemical explosion	273
suspected induced event	8
suspected mine explosion	4828
suspected rockburst	433
unknown	851
total	206377

Table 5.2: *Summary of the earthquakes of magnitude Mw ≥ 7 between July and December 2012.*

Date	lat	lon	depth	Mw	Flinn-Engdahl Region
2012-10-28 03:04:07	52.68	-132.17	7	7.8	Queen Charlotte Islands region
2012-08-14 02:59:38	49.75	145.31	590	7.7	Sea of Okhotsk
2012-09-05 14:42:07	10.02	-85.39	20	7.6	Costa Rica
2012-08-31 12:47:35	10.81	126.83	44	7.6	Philippine Islands region
2012-11-07 16:35:49	14.03	-92.07	38	7.4	Near coast of Chiapas
2012-08-27 04:37:19	12.13	-88.66	15	7.4	Off coast of central America
2012-09-30 16:31:34	1.91	-76.37	155	7.3	Colombia
2012-12-07 08:18:23	37.82	144.16	35	7.3	Off east coast of Honshu
2012-12-10 16:53:09	-6.50	129.87	161	7.1	Banda Sea

The period between July and December 2012 produced 9 earthquakes with $M_W \geq 7$; these are listed in Table 5.2.

Figure 5.1 shows the number of moderate and large earthquakes in the second half of 2012. The distribution of the number of earthquakes should follow the Gutenberg-Richter law.

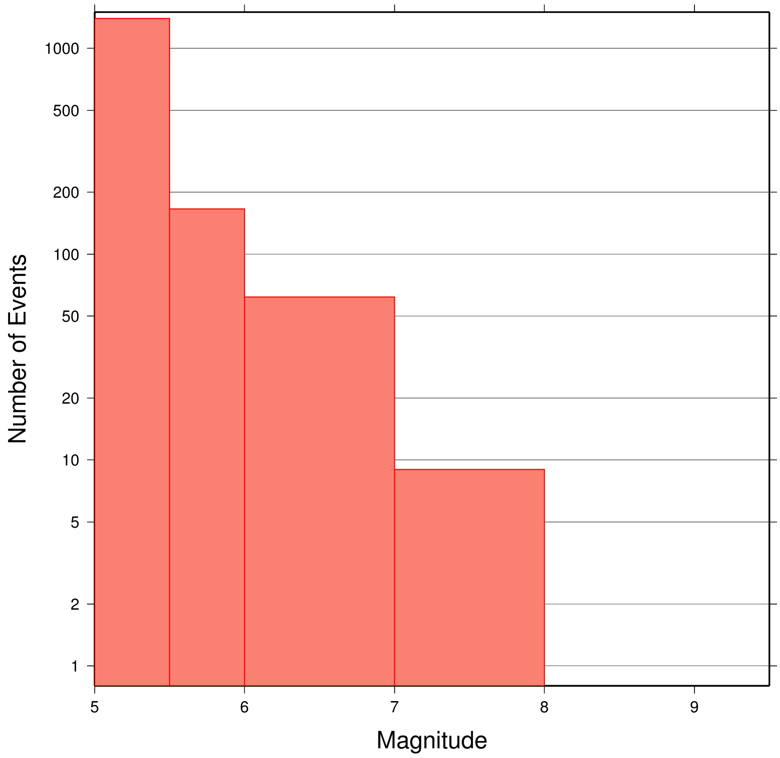

Figure 5.1: *Number of moderate and large earthquakes between July and December 2012. The non-uniform magnitude bias here correspond with the magnitude intervals used in Figures 5.2 to 5.5.*

Figures 5.2 to 5.5 show the geographical distribution of moderate and large earthquakes in various magnitude ranges.

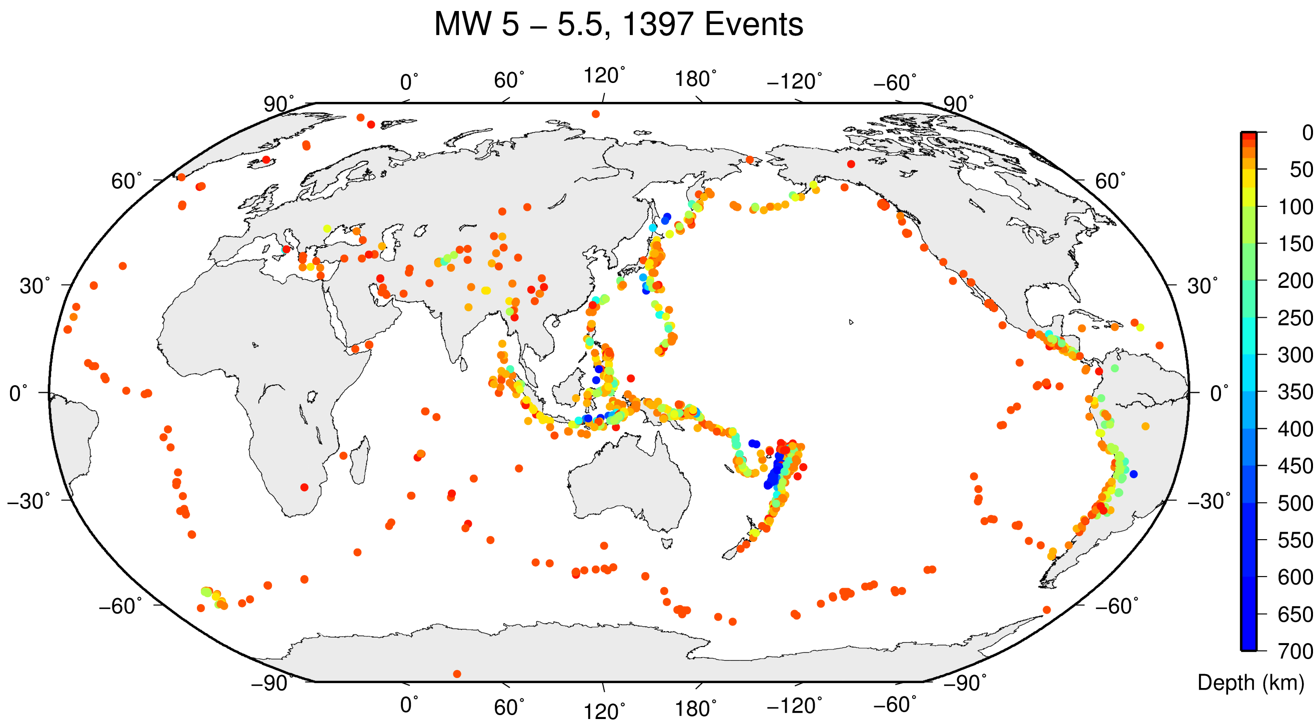

Figure 5.2: *Geographic distribution of magnitude 5-5.5 earthquakes between July and December 2012.*

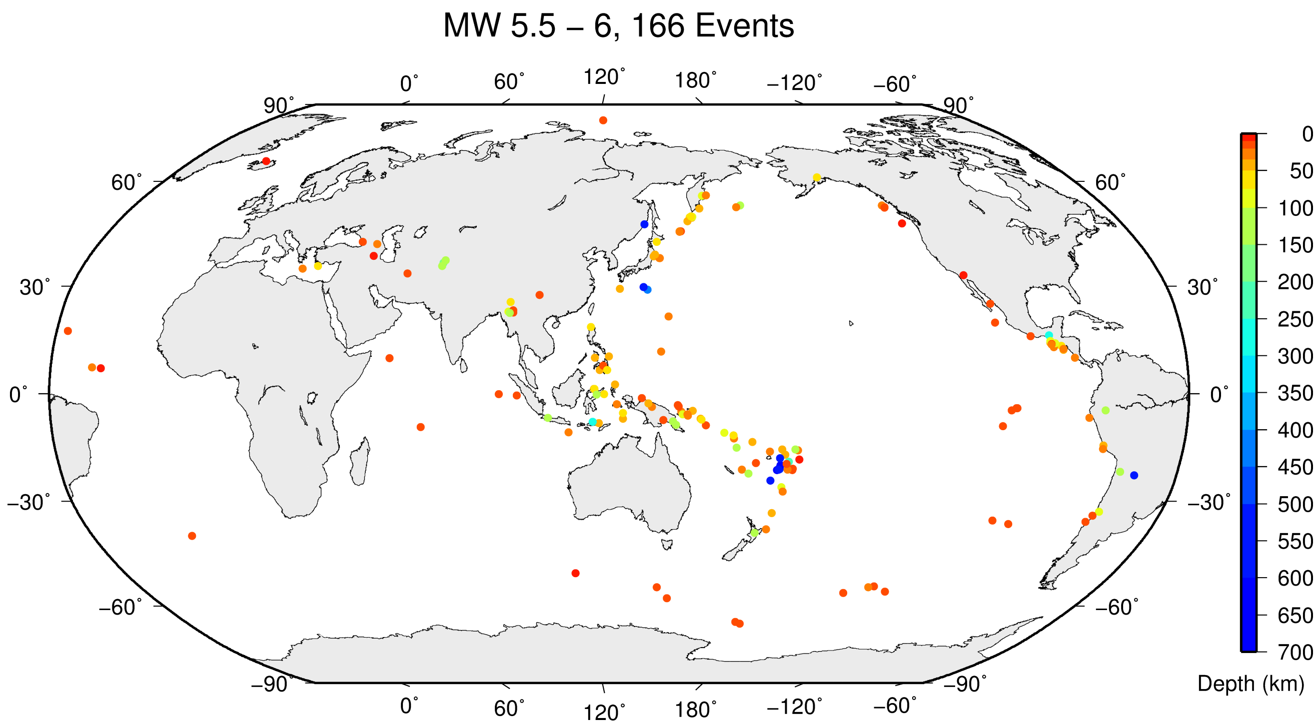

Figure 5.3: *Geographic distribution of magnitude 5.5-6 earthquakes between July and December 2012.*

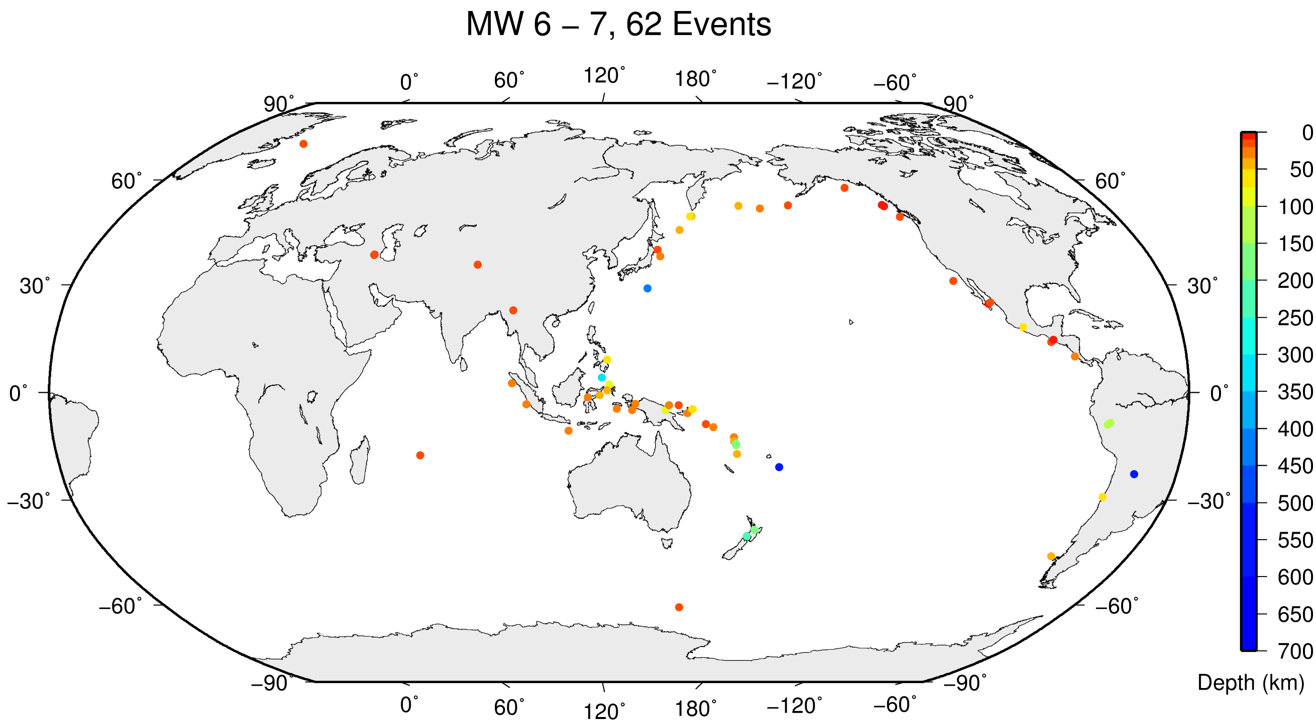

Figure 5.4: *Geographic distribution of magnitude 6-7 earthquakes between July and December 2012.*

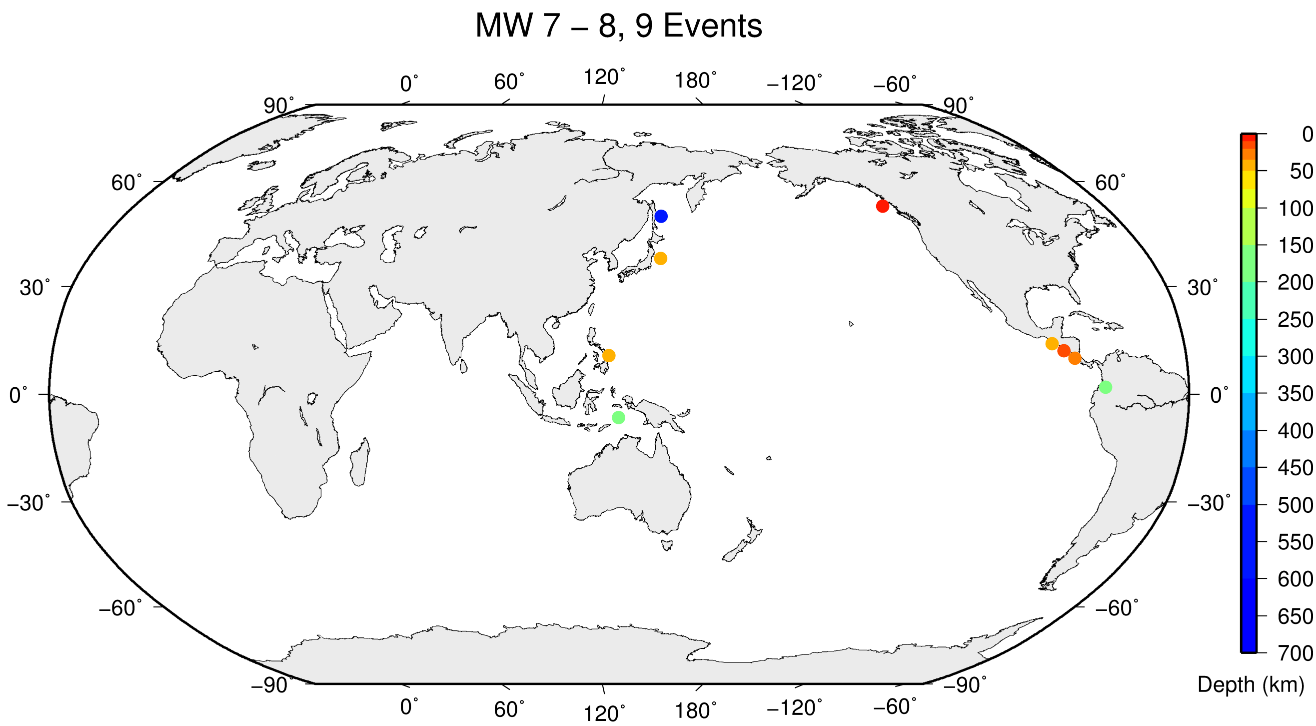

Figure 5.5: *Geographic distribution of magnitude 7-8 earthquakes between July and December 2012.*

6

Notable Events

6.1 The 30th August 2012, M_W 6.7 Jan Mayen Earthquake

Mathilde B. Sørensen
Dept. of Earth Science
University of Bergen
Norway

6.1.1 Introduction

On 30th August 2012, a magnitude (M_W) 6.7 earthquake occurred along the Jan Mayen Fracture Zone (JMFZ), a major transform structure off-setting the Kolbeinsey and Mohns ridges in the North Atlantic Ocean (see Figure 6.1 for the locations of all tectonic structures referred to herein). This was the third $M \geq 6.0$ event to occur along the JMFZ in the last decade and followed intense clusters of foreshock activity during the months prior to the event.

The Jan Mayen region is characterized by the geodynamic processes associated with the interaction between the JMFZ and the slowly spreading Kolbeinsey and Mohns ridges. South of the JMFZ, the Jan Mayen Island is a volcanic island located at the northern part of the Jan Mayen Ridge, a continental fragment torn off eastern Greenland as spreading shifted from the Aegir Ridge to the Kolbeinsey Ridge during the Oligocene (Talwani and Eldholm, 1977). The Island itself is much younger and of volcanic origin. Jan Mayen hosts an active volcano, the Beerenberg volcano, which last erupted in 1985. To the north of the Island is the Jan Mayen Platform, which is characterized by normal faults striking NE, parallel to the spreading axis of the Mohns Ridge.

The Jan Mayen region has a high level of seismicity, mainly associated with the JMFZ, but also with the spreading ridges. Rodriguez-Pérez and Ottemöller (2014) presented 13 events of tectonic origin that had occurred since 1951 within the magnitude range $5.8 \leq M \leq 7.0$. The authors illustrated that almost the entire JMFZ had ruptured at least once during this time period. Most recently, two $M \geq 6.0$ earthquakes occurred along the JMFZ in April 2004 ($M = 6.3$) and January 2011 ($M = 6.1$). The locations of these events are shown, alongside the 2012 event in Figure 6.1. Slip distributions for five $M_W \geq 5.8$ events in the JMFZ, including the three most recent events, are presented by Rodriguez-Pérez and Ottemöller (2014). They found that the events had relatively simple slip distributions with the exception of the 2012 event which had two main asperities and a more complex source time function.

Earthquakes in the Jan Mayen region are monitored by the Norwegian National Seismic Network (NNSN) which operates two stations with vertical short-period seismometers and one broadband station on the

Island. In addition, there is an IMS station that is operated by NORSAR. Data from the NNSN serve as the basis for the work presented herein.

This article presents an overview of the August 2012 event and its source characteristics, as derived by Rodriguez-Pérez and Ottemöller (2014). The fore- and aftershock activity which has been recorded in connection with the event is then presented and compared to recent event sequences recorded in connection with other large earthquakes in the Jan Mayen region.

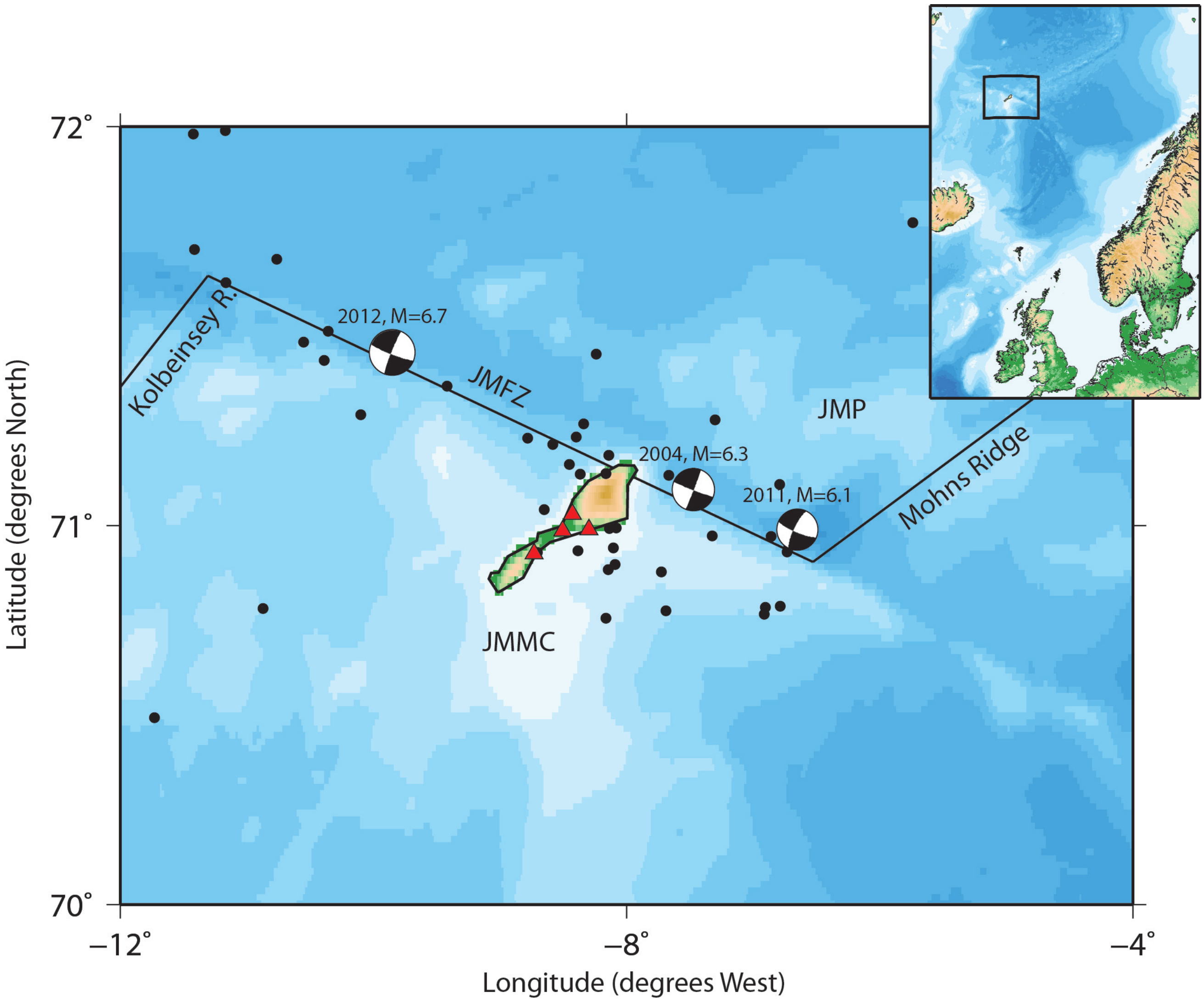

Figure 6.1: The Jan Mayen region in the North Atlantic Ocean. $M \geq 5.0$ earthquakes since 1900, as recorded by the NNSN, are marked as black dots. Focal mechanisms are shown for the three recent $M \geq 6.0$ earthquakes. The locations of seismic stations on Jan Mayen are marked as red triangles. The approximate location of the plate boundary is indicated by the black line. JMFZ: Jan Mayen Fracture Zone, JMMC: Jan Mayen Microcontinent, JMP: Jan Mayen Platform.

6.1.2 The 30th August 2012 Earthquake

The 30th August 2012 earthquake had a moment magnitude (M_W) of 6.7 and ruptured with an almost pure left-lateral strike-slip focal mechanism (Figure 6.1). The event is located in the northern part of the JMFZ, in an area devoid of any large earthquakes since the occurrence of a $M = 7.0$ event in 1951.

Rodriguez-Pérez and Ottemöller (2014) performed a slip inversion and studied the source parameters of this event. They found that the 2012 event ruptured a 42 x 20 km fault plane. The slip distribution was complex, exhibiting two main asperities with up to 1.6 m slip (Figure 6.2). The average static stress drop was determined to be 2.59 MPa with a static stress drop of 4.23 MPa on the asperities covering *ca.* 21% of the fault plane.

6.1.3 Fore- and Aftershock Activity in Connection with the 30th August 2012 Event

The 30th August 2012 earthquake was preceded by two clusters of strong foreshock activity. Figure 6.3 presents a histogram of the daily number of earthquakes in 2012 in the region covered by the map in Figure 6.1, based on data from the NNSN. On average, 2.5 earthquakes were recorded daily during this period. Three distinct clusters of increased activity are observed on 11th-13th June, 13th-16th July, and following the main shock on 30th August. If the three clusters of enhanced activity are excluded from the average calculation, the daily average drops to 1.4 events. During the June cluster, 44 earthquakes were recorded within a three day period. These events were in the magnitude range 1.5 $\leq M_L \leq$ 2.9 and could not be associated with any specific main shock. The July cluster consisted of 82 events that occurred within a four day period (44 events occurred on 14th July) in the magnitude range 1.1 $\leq M_L$ $\leq$ 3.9. There was no distinct main shock associated to this cluster. Following the second cluster, the seismicity level was slightly above average, but it dropped shortly before the occurrence of the main shock.

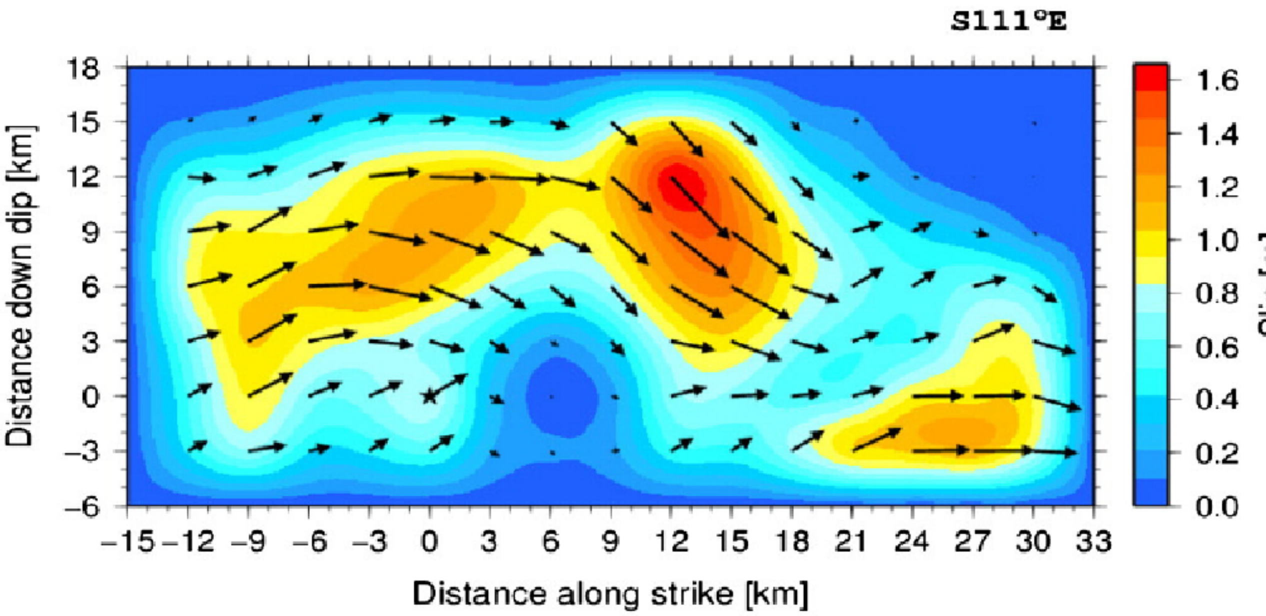

Figure 6.2: *Slip distribution for the 30th August 2012 earthquake inferred from teleseismic recordings. From Rodriguez-Pérez and Ottemöller (2014).*

To study the two clusters of events preceding the main shock in more detail, event locations are shown in Figures 6.4a and 6.4b for the months of June and July, respectively. Events occurring in the two clusters are marked as red. The vast majority of these cluster events are located in the epicentral area of the 30th August M_W = 6.7 earthquake and can thus be considered as foreshocks. Figure 6.4c shows the seismicity recorded during the first month after the 30th August event. There is strong aftershock

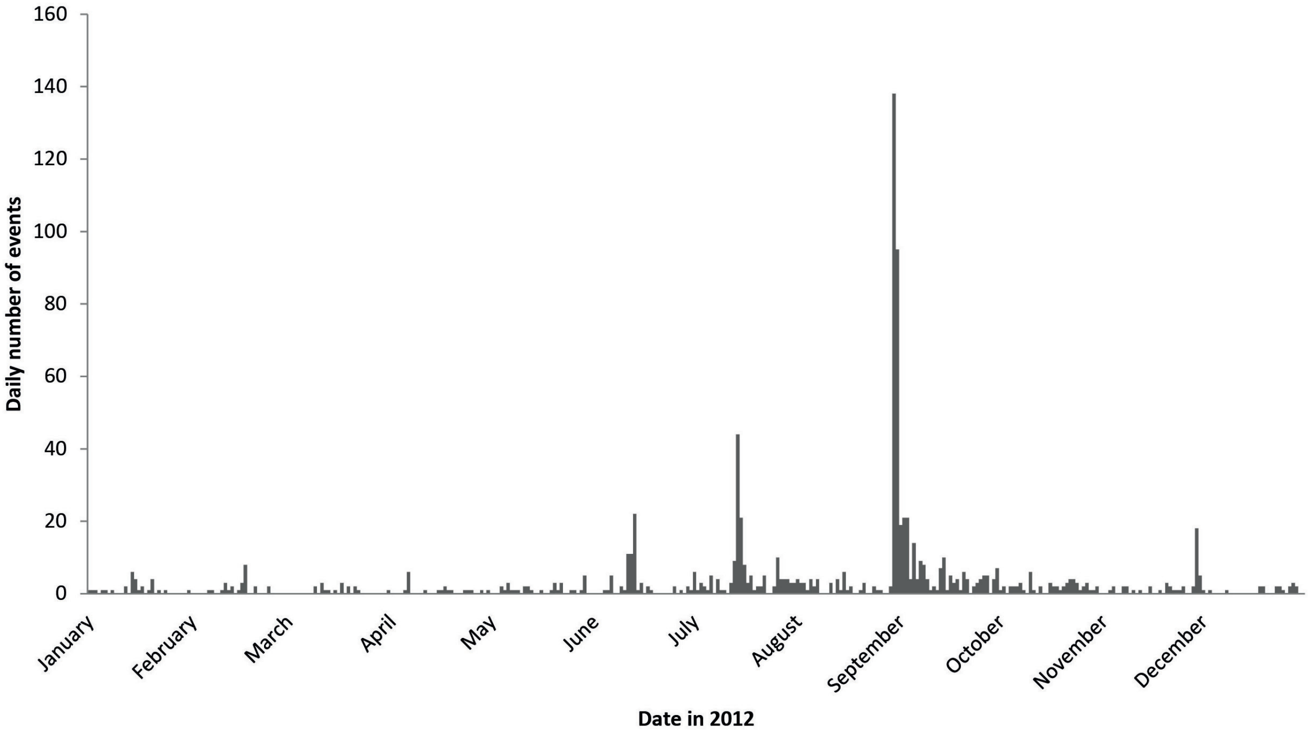

Figure 6.3: *Histogram showing the daily number of earthquakes in the Jan Mayen region, as recorded by the NNSN, in 2012.*

activity in the epicentral area, and the aftershock distribution indicates that the rupture propagated mainly from the epicenter, towards the SE. This is in agreement with the results of Rodriguez-Pérez and Ottemöller (2014). In addition to the aftershock activity near the rupturing fault plane, an increased level of seismicity is observed along the JMFZ and in the Jan Mayen Microcontinent .

Especially noteworthy are two clusters of events located NW and SE of the Jan Mayen Island, between -9 $^\circ$ and -8 $^\circ$ longitude, respectively (highlighted by the red squares in Figure 6.4c). Due to the station configuration on the Island however, these events are associated with relatively large location uncertainties. The event locations are highly sensitive to the S-arrival time and a slight change in the phase reading can lead to the event location jumping from one cluster to the other. It is thus not certain whether these events represent one or two clusters. There is, however, a strong indication that the events are not located in the JMFZ, but in the continental fragment.

It is not clear if and how these cluster events are linked to the 30$^{\text{th}}$ August earthquake, but some insight can be gained by studying the temporal evolution of seismicity in the region during the months June-September 2012. Figure 6.5 shows, in addition to the spatial seismicity distribution (top left), the temporal seismicity distribution as a function of both latitude (top right) and longitude (bottom left). The clusters of seismicity in June and July are clearly seen in these plots of temporal seismicity distribution. The aftershock activity following the 30$^{\text{th}}$ August event is also evident, and it is interesting to observe that the clusters of strong activity in the Jan Mayen Microcontinent are activated immediately after the occurrence of the main shock. This strongly supports a direct link between the main shock and these events, though we do not currently have a detailed explanation for their occurrence. Future Coulomb stress transfer modeling may give us further insight into this problem.

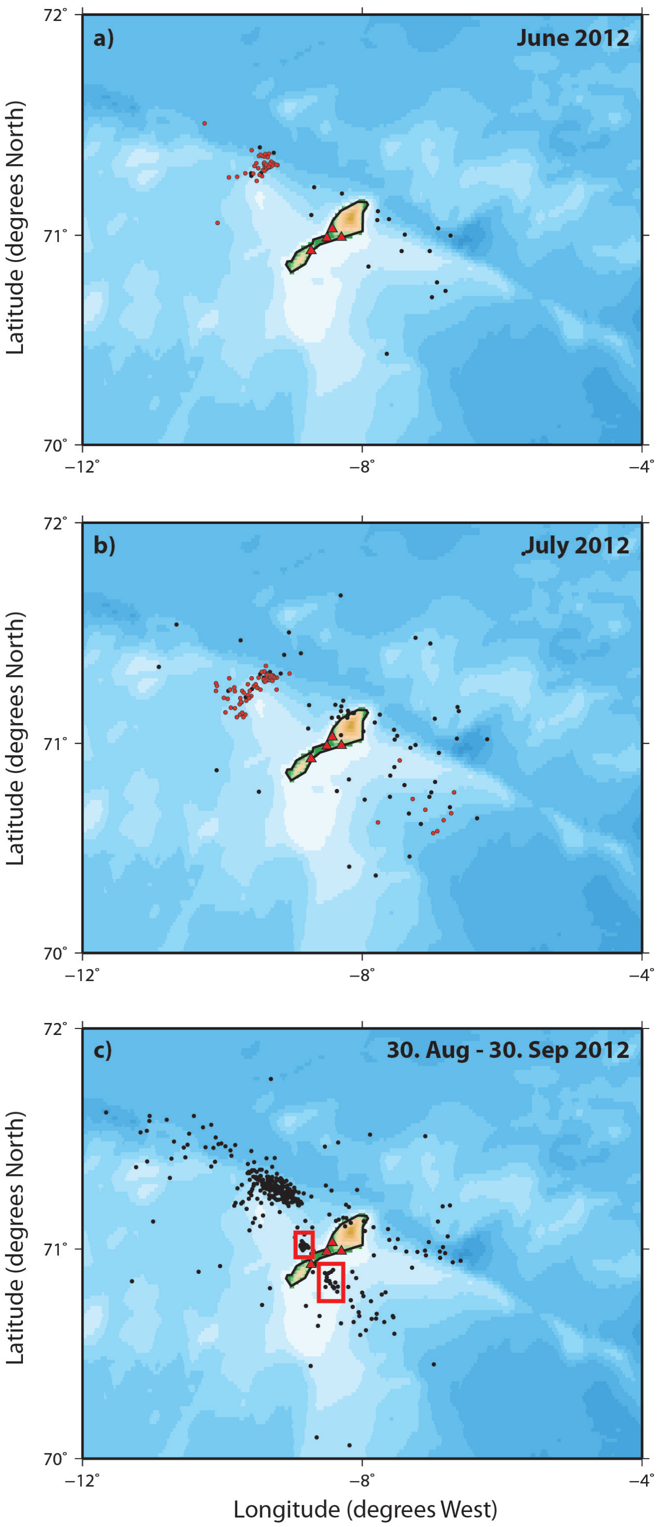

Figure 6.4: *Seismicity (dots) recorded by the NNSN during (a) June 2012, (b) July 2012, and (c) the period 30th August – 30th September 2012. (a,b) Cluster events in June and July are marked as red. (c) The aftershock clusters in the Jan Mayen Microcontinent are marked with red squares. The seismic stations on Jan Mayen are marked as red triangles.*

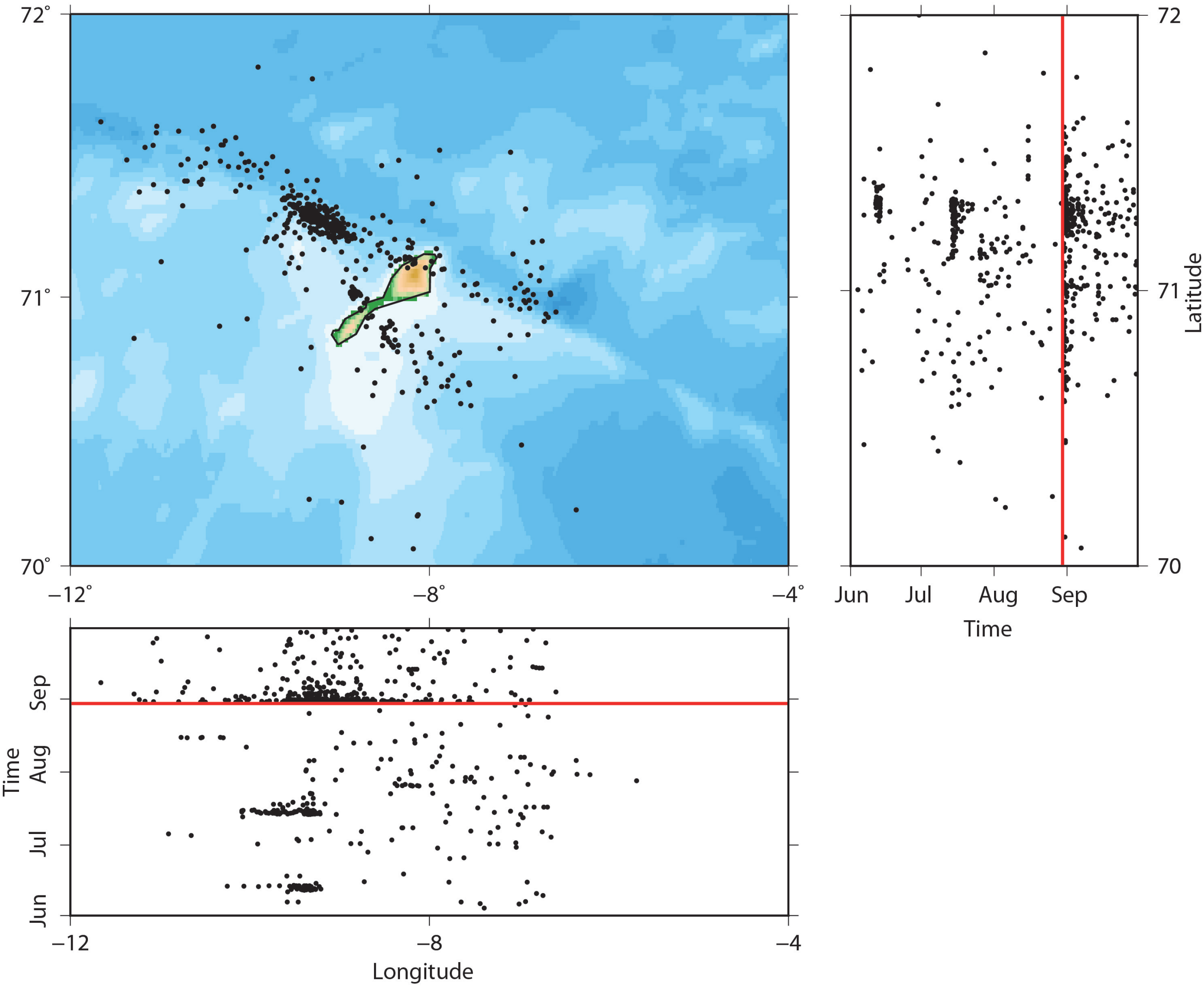

Figure 6.5: *Spatial (top left) and temporal (top right and bottom left) seismicity distributions in the Jan Mayen region during the months June-September 2012. The origin time of the 30th August event is indicated by the red lines in the temporal seismicity distribution plots.*

Similar plots to the one presented in Figure 6.5 have been prepared for the 2004 and 2011 $M \geq 6.0$ earthquakes to see if they were preceded by similar clusters of foreshock activity or if they triggered aftershocks in the Jan Mayen Microcontinent (Figure 6.6). Figure 6.6a shows a cluster of activity in June 2003 in the epicentral area of the 2004 earthquake. This sequence contained 60 events that occurred within a three day period, starting with a $M_W = 4.1$ event on 19$^{\text{th}}$ June. Figure 6.6b shows no clear foreshock clusters prior to the 2011 event, though increased seismicity levels were observed in a larger area containing the epicentral area in late February and early September 2010. Neither the 2004 event nor the 2011 event triggered noteworthy activity in the Jan Mayen Microcontinent. There was, however, significant activity in the Jan Mayen Platform, to the north of the JMFZ, in connection with both of these events.

In a study focused on the 2004 earthquake, Sørensen *et al.* (2007) showed that the event triggered distinct clusters of aftershocks in the Jan Mayen Platform. Coulomb stress modeling showed that these events occurred in a region of increased stress due to the 2004 event, thus supporting the hypothesis that stress triggering may play an important role in controlling the aftershock distribution of large strike-slip earthquakes in the JMFZ.

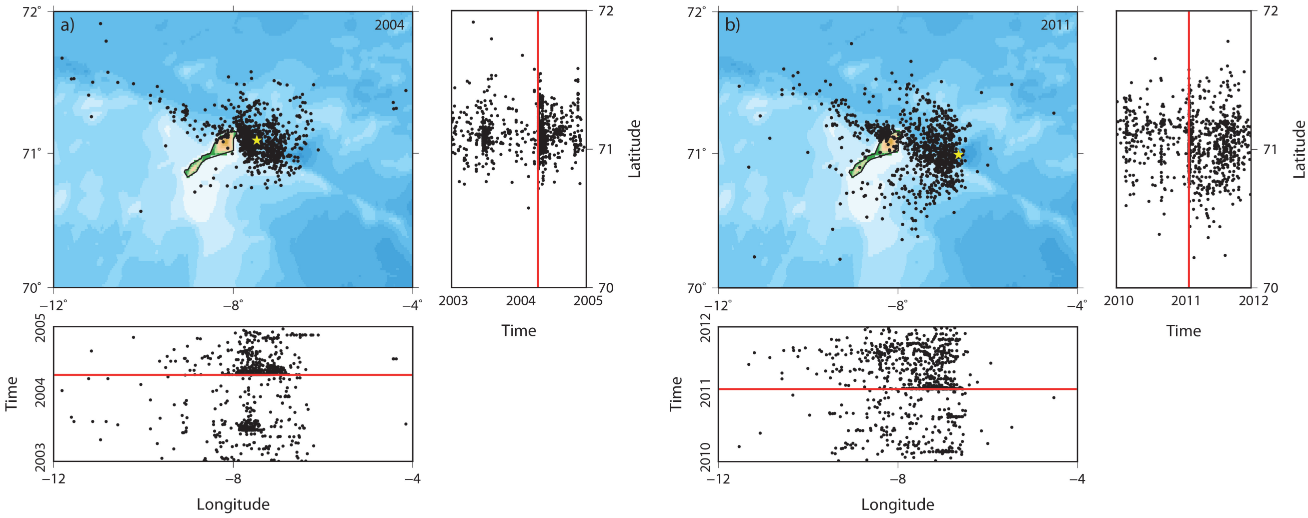

Figure 6.6: *As Figure 6.5 for earthquake sequences throughout (a) 2003-2004, and (b) 2010-2011. The epicentral locations of the 2004 and 2011 $M \geq 6.0$ earthquakes are shown as yellow stars in the spatial seismicity distribution plots.*

6.1.4 Summary

The 30[th] August 2012 Jan Mayen earthquake was the third $M \geq 6.0$ earthquake to occur along the JMFZ in the last decade. It ruptured a *ca.* 42 km-long segment of the northern part of the fracture zone that had not ruptured since 1951. The event was characterized by two intense clusters of foreshock activity in the epicentral region in June and July 2012. Following the event, aftershocks were observed mainly along the ruptured fault plane, but also along the entire fracture zone. Two clusters of aftershock activity in the Jan Mayen Microcontinent are also thought to be associated to this event. A comparison with two $M \geq 6.0$ events in 2004 and 2011 shows that the 2012 event is unique in terms of the clustered nature of both its foreshock activity and the aftershock activity in the Jan Mayen Microcontinent. A previous study of the 2004 $M \geq 6.0$ earthquake supports the hypothesis that these aftershocks are caused by Coulomb stress transfer in connection with the 30[th] August 2012 earthquake.

6.1.5 Acknowledgements

The data presented in this article was provided by the Norwegian National Seismic Network. Most of the data processing was done by Berit Marie Storheim. Many figures were plotted using the Generic Mapping Tools (Wessel *et al.*, 2013). I thank Lars Ottemöller for comments on the manuscript.

6.1.6 References

Rodriguez-Pérez, Q. and L. Ottemöller (2014). Source study of the Jan Mayen transform fault strike-slip earthquakes, *Tectonophysics*, 628, 71-84.

Sørensen, M.B., L. Ottemöller, J. Havskov, K. Atakan, B. Hellevang and R.B. Petersen (2007). Tectonic Processes in the Jan Mayen Fracture Zone based on Earthquake Occurrence and Bathymetry, *Bull. Seism. Soc. Am.*, 97(3), 772-779.

Talwani, M. and O. Eldholm (1977). Evolution of the Norwegian-Greenland Sea, *Bull. Geol. Soc. Am.*, 88, 969-999.

Wessel, P., W. H. F. Smith, R. Scharroo, J. F. Luis, and F. Wobbe (2013). Generic Mapping Tools: Improved version released, *EOS Trans. AGU*, 94, 409-410.

6.2 The October 2012 magnitude (M_W) 7.8 earthquake offshore Haida Gwaii, Canada

Alison L. Bird[1], John F. Cassidy[1&2], Honn Kao[1&2], Lucinda J. Leonard[1&2], Trevor I. Allen[1], Lisa Nykolaishen[1], Herb Dragert[1], Tiegan E. Hobbs[3], Amir M. Farahbod[4], Jan M. Bednarski[1], Thomas S. James[1], Maurice Lamontagne[5], Shao-Ju Shan[1], Roy D. Hyndman[1], Isaac V. Fine[6], Josef Y. Cherniawsky[6], Camille D. Brillon[1], Kelin Wang[1&2] and Garry C. Rogers[1&2]

Alison L. Bird
Geological Survey of Canada
Natural Resources Canada
Sidney, British Columbia
Canada

1. Geological Survey of Canada, Natural Resources Canada, Sidney, British Columbia, Canada.
2. School of Earth and Ocean Sciences, University of Victoria, Victoria, British Columbia, Canada.
3. School of Earth and Atmospheric Sciences, Georgia Institute of Technology, Atlanta, Georgia, Unites States of America.
4. Geological Survey of Canada, Natural Resources Canada, Vancouver, British Columbia, Canada.
5. Geological Survey of Canada, Natural Resources Canada, Ottawa, Ontario, Canada.
6. Canadian Hydrographic Service, Department of Fisheries and Oceans, Sidney, British Columbia, Canada.

6.2.1 Introduction

The Haida Gwaii archipelago (formerly known as the Queen Charlotte Islands) is located off the coast of central British Columbia (BC), Canada (Figure 6.7). While approximately 150 islands make up Haida Gwaii, there are two main islands: the northern Graham Island and southern Moresby Island; the two are separated by the narrow Skidegate Channel. Approximately 5,000 people live on Haida Gwaii, mostly in six small communities, five of them on Graham Island.

On the evening of 27th October 2012 (8:04pm local time), a magnitude (M_W) 7.8 earthquake occurred along a previously only hypothesised thrust fault off the west coast of Moresby Island. This was the second largest earthquake in Canada's written history. It was felt throughout much of British Columbia and as far away as the Yukon, Alberta and Montana, roughly 1600 km from the epicentre. In some locations (notably on Haida Gwaii) the perceivable shaking lasted 1.5 - 2 minutes, with very strong shaking for about 30 seconds. Strong ground motions recorded in the region reached a maximum horizontal acceleration of 0.2g. Fortunately, this earthquake resulted in very limited damage partly because of the relatively large distance (more than 60 km) between population centres and the fault rupture, and partly because of seismic resistance of the generally low, wood-frame construction found on the islands. We examine the earthquake rupture characteristics and crustal displacements, along with various physical effects from the shaking (including ground motions, tsunami, landslides, building damage and the loss of hot springs), catalogued by field crews and reported by the inhabitants of Haida

Gwaii and the surrounding regions. These will serve as a guide toward understanding the potential impact from future large earthquakes on the various Haida Gwaii communities.

6.2.2 Historical Seismicity and Tectonics

The Queen Charlotte Fault (QCF), a near-vertical fault running along the west coast of Haida Gwaii and north into south-eastern Alaska, is a transpressional boundary between the Pacific and North American Plates (Bird 1997, Bird *et al.*, 1997; Figure 6.8). Little was known in detail about the distribution of earthquakes in this region before the establishment of a local seismograph network between 1982 and 1987. Some sizeable earthquakes had been recorded by the regional seismic network in previous decades, however, including a magnitude (M_W) 7 in 1929 (Milne, 1956), an M_S 8.1 event off north-western Graham Island in 1949 (the largest instrumentally recorded earthquake in Canadian history; Bostwick, 1984) and an M_W 7.4 in 1970 (Lamontagne *et al.*, 2008). The rupture zones of these events, as defined by their aftershock distribution, suggested a seismic gap (Rogers, 1986) remained along the southernmost portion of the QCF.

The network installed in the 1980's revealed not only intense seismicity along the plate boundary region but also a more extensive pattern of activity than that associated simply with the QCF, with substantial activity shown to occur up to 150 km east of the fault, in particular under Graham Island and Hecate Strait (Bird 1997, Bird *et al.*, 1997; Ristau *et al.*, 2007).

Pacific - North America relative plate motion is roughly 50 mm/year (DeMets *et al.*, 1990 and 2010; Hyndman, 2015) with a discrepancy between plate motion and fault strike of 15° to 20° – varying along-fault and greatest along the southern section of the QCF. This leads to a small, but significant component of oblique convergence at approximately 15 mm/year that is believed to have initiated at ∼6 Ma, resulting in under-thrusting at the margin (Bird 1997, Bird *et al.*, 1997; Barrie *et al.*, 2013; Hyndman, 2015). The total under-thrusting has been too small to instigate Benioff-Wadati seismicity or arc volcanism but is indicated by: (1) a trench: the Queen Charlotte Trough, into which the converging oceanic plate bows downward, and an adjacent offshore flexural bulge, the Oshawa Rise; (2) the Queen Charlotte Terrace (QCT), interpreted to be an accretionary sedimentary prism; (3) seismic receiver function delineation of the under-thrusting Pacific Plate; (4) heat flow decreasing landward as predicted for under-thrusting; (5) low gravity offshore and high gravity onshore, consistent with subduction; and (6) late Tertiary uplift and erosion of the western coasts of the islands (Hyndman, 2015). Oblique convergence is partitioned into nearly margin-normal under-thrusting relative to the Terrace, which itself is moving along the margin, and margin-parallel transform motion on the Queen Charlotte Fault just off the coast, which produced the aforementioned M 8.1 earthquake in 1949.

Focal mechanisms for the region have been dominantly strike-slip, but with a considerable component of thrust, especially for earthquakes along the section of fault adjacent to Moresby Island in the south (Bird 1997, Bird *et al.*, 1997; Ristau *et al.*, 2007). This is consistent with the oblique convergence across the dominantly strike-slip QCF in the area where the fault changes strike into a somewhat more E-W orientation along this southern section of the QCF, giving the fault a dog-leg appearance.

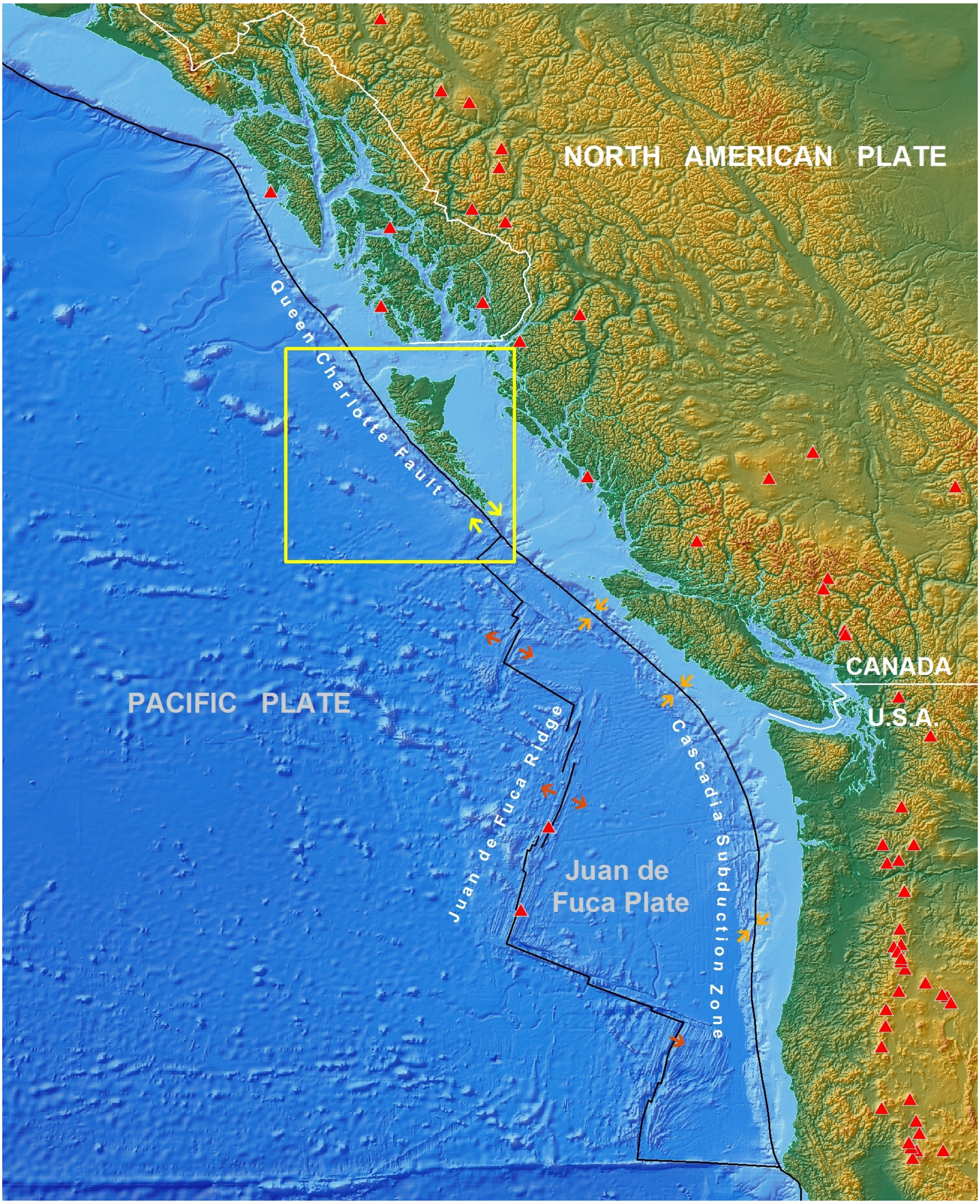

Figure 6.7: *Regional tectonic setting off the west coast of British Columbia in western Canada, with the area of study indicated by the yellow box. Arrows show relative plate motion across plate boundaries, and red triangles indicate volcanic features.*

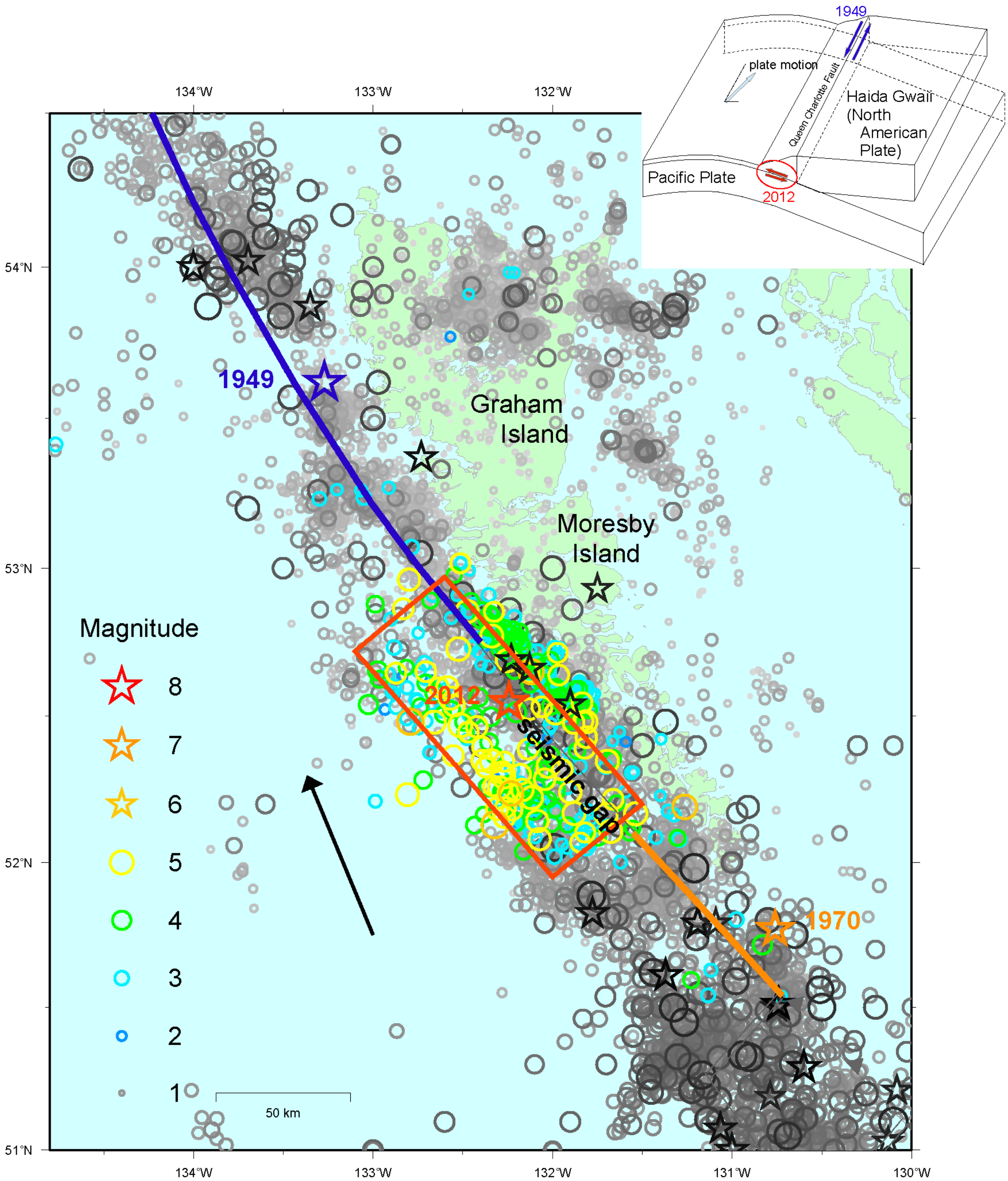

Figure 6.8: *Tectonic setting and historical seismicity (1898 through 2013) of Haida Gwaii, off the coast of British Columbia, with the Queen Charlotte Fault marking the transpressional boundary between the Pacific and North American Plates; the arrow indicates Pacific Plate motion, at roughly 50 mm/y, relative to the North American Plate (from Bird and Lamontagne, 2015a). The rupture length of the M_W 8.1 earthquake in 1949 is shown in blue and that of the M_W 7.4 event in 1970 in orange; the rupture zone of the 2012 event is boxed in red. With the exception of the 1949 and 1970 mainshocks, seismicity that occurred before the M7.8 in 2012 is indicated in a grey scale. The inset figure is of a simplified fault model (adapted from James et al., 2013) showing thrust faulting beneath the Queen Charlotte Fault, with the 2012 M_W 7.8 thrust event (shown in red) believed to have occurred between the Pacific Plate and the accretionary prism. The 1949 M_S 8.1 ruptured along the transform margin to the north.*

6.2.3 Mainshock of the October 2012 Earthquake Sequence

The magnitude 7.8 earthquake of 27th October 2012 (20:04 Pacific Standard Time) is the second largest instrumentally recorded in Canadian history. It was of a predominantly thrust movement (Kao *et al.*, 2015) on a north-eastward dipping fault, believed to lie directly beneath the QCF (Figure 6.8 inset, adapted from James *et al.*, 2013). While the event occurred in the vicinity of the aforementioned seismic gap, it did not occur on the QCF, and it therefore did not release stress as anticipated along that section of fault. That section of the QCF was instead subjected to increased stress as a result of the M_W 7.8 event (Hobbs *et al.*, 2015a).

The mainshock was felt throughout British Columbia and as far away as the Yukon, Alberta and Montana, roughly 1600 km from the epicentre. Nevertheless, this earthquake resulted in limited damage partly due to the population centres being located at least 80 km from the epicentre and 60 km from the fault rupture. Figure 6.9 shows: a) the shaking recorded at the village of Queen Charlotte, at an epicentral distance of roughly 80 km; and b) the attenuation as seen at three regional strong motion seismic stations. Although there was little visible impact and there were few, minor injuries from this earthquake, many people were significantly traumatised by the experience, and by the numerous aftershocks that were felt throughout the following weeks (Bird and Lamontagne, 2015a).

Ground motion

The weak-motion seismic stations operating on Haida Gwaii at the time of the earthquake were saturated by the shaking. Three strong-motion Internet Accelerographs (IAs) in the region did, however, register the event clearly, to a maximum recorded acceleration of $0.2g$ (20% of gravitational acceleration; Rosenberger *et al.*, 2013; Figure 6.9a) in the village of Queen Charlotte at an epicentral distance of 80 km. Most people on Haida Gwaii are familiar with small-to-moderate earthquakes, and following the October 2012 event described having felt considerable shaking for about half-a-minute, at which point they assumed the shaking would diminish, as it had for earthquakes in the past. The shaking instead became much stronger. The perceivable shaking lasted roughly 1.5 minutes, with very strong shaking for about 30 seconds.

Field surveys

In the weeks following the mainshock, Natural Resources Canada (NRCan) technical crews visited the islands and the offshore region to service the existing network of seismometers and to install seven additional seismometers, seven GPS receivers and fourteen ocean-bottom seismometers (James *et al.*, 2013). The latter deployment was complemented by an airgun seismic survey to examine the structure of the rupture region. The land-based fieldwork was supplemented by surveys to map landslides and by expeditions in search of evidence of tsunami run-up. This fieldwork provided data critical in many of the studies outlined below. The seismic and GPS data gathered in the months to follow would be used to accurately locate the tens of thousands of aftershocks and to measure the coseismic crustal deformation associated with this event and the post-seismic relaxation. At time of printing, only ∼2%

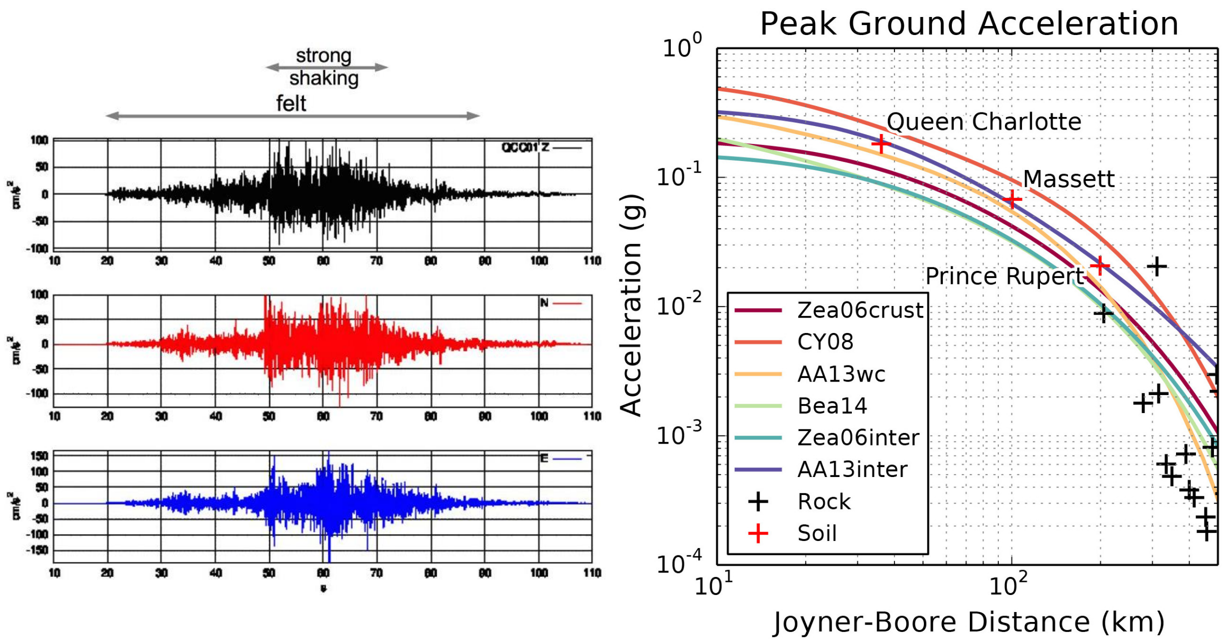

(a) (b)

Figure 6.9:
a) Shaking (acceleration) recorded by the three-component strong-motion Internet Accelerograph at the village of Queen Charlotte, with peak motion up to ~0.2g (~20% gravitational acceleration); this instrument is operated by the Ministry of Transportation and Infrastructure, BC (from Bird and Lamontagne, 2015a).

b) Peak ground acceleration (PGA) recorded at three strong-motion soil sites (red crosses) as well as weak-motion sites on rock (black crosses), shown against well-established ground-motion models for subduction interface environments for an M_W 7.8 earthquake. Ground-motion predictions assume a VS30 of 1,500 m/s appropriate for BC coastal rock sites (Atkinson, 2005). Ground-motion models are shown for subduction interface (Atkinson and Adams, 2013: "AA13inter"; Zhao et al., 2006: Zea06inter) and crustal (Atkinson and Adams, 2013: "AA13wc"; Akkar et al., 2014: "Aea14"; Zhao et al., 2006: Zea06crust) models (after Allen and Brillon, 2015).

of the approximately 100,000 recorded aftershocks have been located by analysts, although automated locations have been acquired for roughly 60%.

Spatiotemporal distribution of events during the first week of aftershocks

Farahbod and Kao (2015) systematically relocated 1229 aftershocks (M_L 1.4 – 5.8) that occurred during the first week of the 2012 Haida Gwaii aftershock sequence by re-examining continuous seismic waveforms of the Canadian National Seismograph Network (CNSN). These efforts primarily benefited from the data recorded at seven stations operated by the CNSN on Haida Gwaii. Whenever corresponding arrivals could be identified, waveforms from other nearby stations in the region were also included to maximise the data constraint. The key principle of the strategy to increase location accuracy is to extract as much information as possible from existing waveforms (Roberts *et al.*, 1989; Ottemöller *et al.*, 2012). In this regard, travel-time differences between P and S phases from at least the three closest stations were measured. Through this process, the presence of numerous micro-aftershocks were revealed in the recordings from the closest station (BNB; Figure 6.10); phases from these micro-events were often wrongly associated by the automatic location routine with phases at neighbouring stations from other events, resulting in significantly incorrect locations. Thus, it was necessary to carefully re-examine all waveforms to eliminate possible incorrect phase associations due to micro-aftershocks. Finally, back-azimuth information from the closest three-component station was included in the analysis.

Results from these aftershock relocations effectively doubled the size of the CNSN routine earthquake catalogue. The corresponding root-mean-square (RMS) time residual was 0.6 s or less. The distribution of aftershocks formed two linear trends roughly parallel to the strike of the plate margin in the NW–SE direction (Figure 6.10). The band located up-dip from the mainshock within the subducting Pacific plate appears to have three clusters spanning a lateral distance of ~80 km. The other band is distributed along the surface trace of the QCF. The apparent lack of seismicity along the southern part of the QCF in the source region suggests that the accumulated stress along the QCF was only partially released during the 2012 Haida Gwaii earthquake. The projected hypocentre of the mainshock coincides well with the inferred location of the interplate thrust zone at the ~16 km depth near the bottom of the seismogenic (locked) zone (Profile A1–A2, Figure 6.11). The overall area of aftershock distribution is ~120 km by ~40 km, which overlaps the southern part of the estimated rupture zone of the 1949 M 8.1 Queen Charlotte earthquake (Rogers, 1986; Cassidy *et al.*, 2014).

6.2.4 Physical Impacts

Landslides, debris flows and rock falls were noted by many inhabitants in late-October and November 2012. Several were catalogued by Parks Canada officers and Natural Resources Canada field crews in the weeks following the earthquake as they travelled over the largely uninhabited Moresby Island (e.g., Leonard and Bednarski, 2015). As there was only one helicopter available on the islands and the weather in the months following the mainshock was generally too poor for flight safety, the opportunity to conduct aerial field surveys was extremely limited. Dedicated landslide surveys were, however, conducted by the BC Ministry of Forests, Lands and Natural Resource Operations (Millard, 2012; Millard *et al.*, 2012) and by the Gowgaia Institute (Gowgaia Institute, personal communication, 2012). Numerous slides were documented along the slopes of the islands (Figure 6.12): nearly 100 by the provincial government and many more by the Gowgaia Institute, whose efforts focused on a small area between Gowgaia Bay and Upper Victoria Lake within the Gwaii Haanas National Park.

The thermal springs in Gwaii Haanas National Park having become dry in the wake of the earthquake was a great disappointment to the people of Haida Gwaii. The hot springs' pools were a draw to the kayak and boat visitors to Gwaii Haanas, but they are also a sacred site of the Haida Nation. It is not unusual, however, for water levels in geothermal springs and wells to change height as a result of stress perturbations within the crust, such as for earthquakes (Hurwitz *et al.*, 2014; Husen *et al.*, 2004; Hutchinson, 1985; Rinehart, 1972). No such effects on the Gwaii Haanas hot springs were recorded after the more distant 1949, M_W 8.1 event. It should be noted that within a year some thermal spring activity was detected in the area (CBC, 2014) and in 2015 the springs showed signs of returning (Council of the Haida Nation, 2015).

Shaking from the mainshock caused slumping of the roadway between Port Clements and Masset; although not threatening the pavement itself, the supporting berm failed almost completely in one area. Building damage was generally light and locally variable; physical effects of the shaking on construction

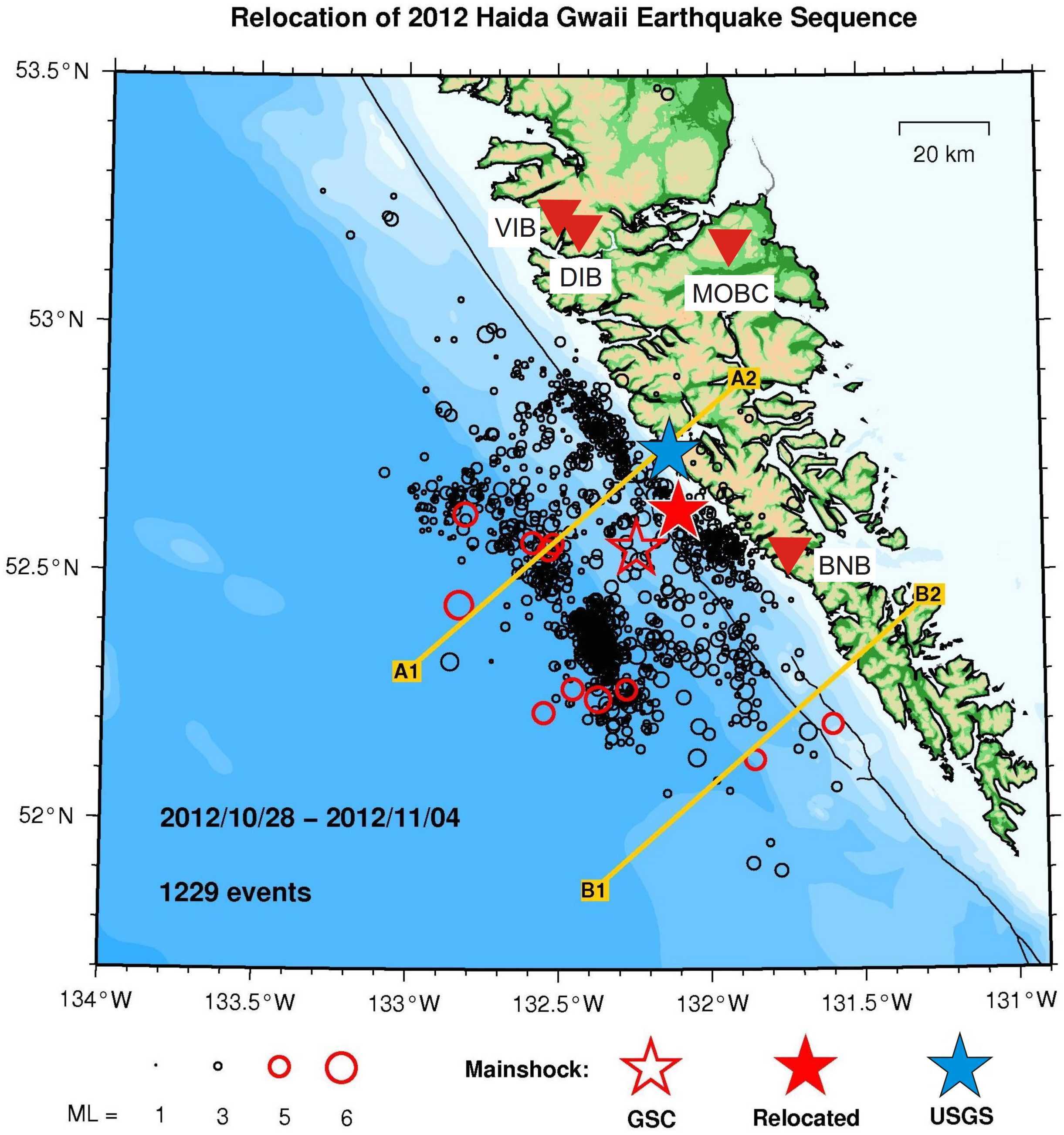

Figure 6.10: Epicentral distribution of the 2012 Haida Gwaii earthquake sequence (adopted from Farahbod & Kao, 2015). Re-analysed aftershocks that occurred during the first week are indicated by black open circles. Mainshock epicentres are shown by stars: the red and blue solid stars correspond to our relocated result and the US Geological Survey (USGS) report, respectively; the red open star corresponds to the location reported by the Geological Survey of Canada (GSC). Triangles indicate the closest seismic stations. Cross-sections along the two profiles (A1-A2 and B1-B2) are shown in Figure 6.11.

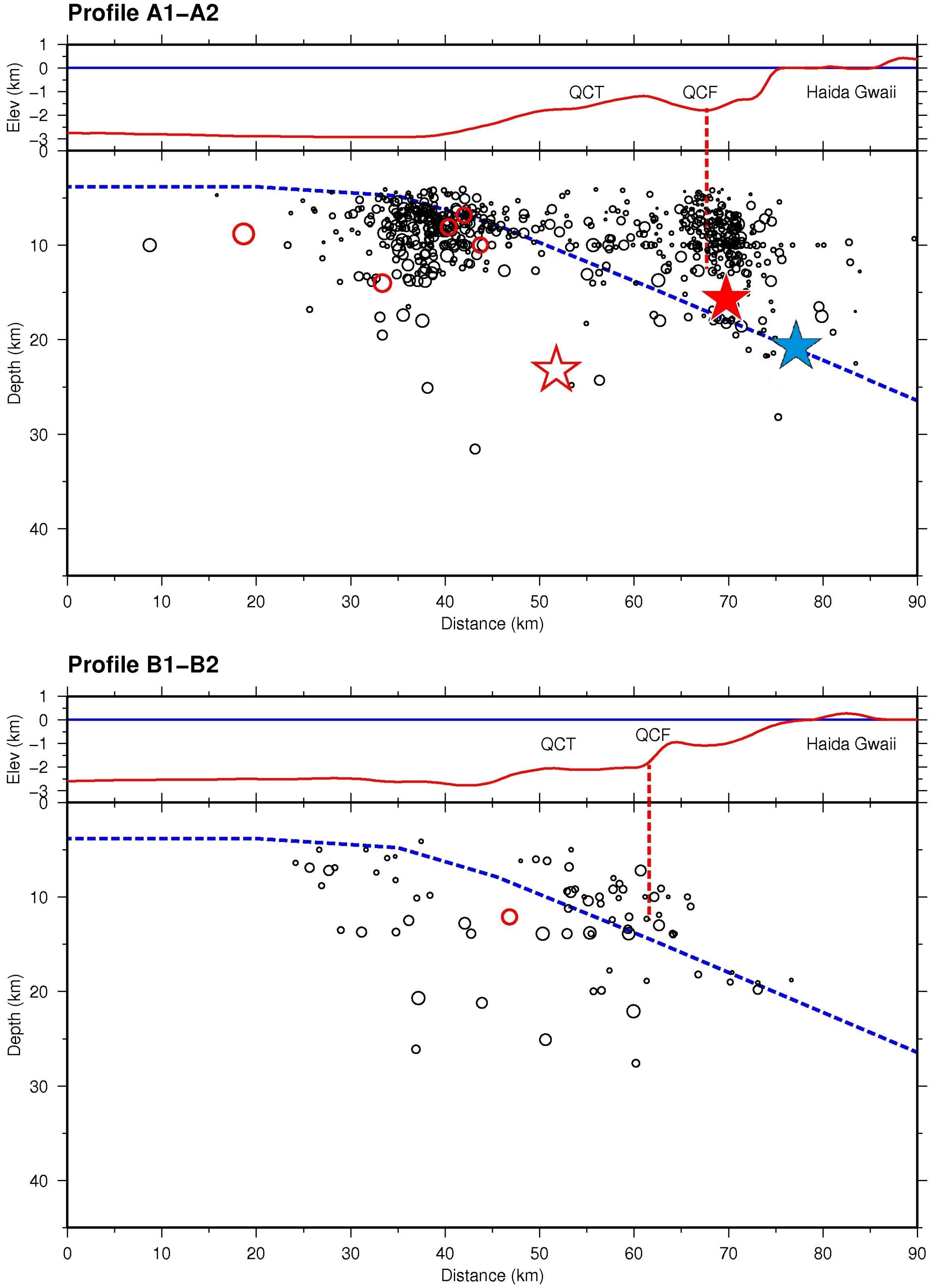

Figure 6.11: *Depth distribution of the 2012 Haida Gwaii earthquake sequence along two cross-sections (adopted from Farahbod and Kao, 2015). Geographic locations of the two profiles are marked in Figure 6.10. Events within 25 km from each side of the profiles are projected onto a vertical plane. Stars represent the projected hypocentres of the mainshock (red and blue solid stars are for relocated results of Farahbod and Kao (2015) and the USGS report, respectively; the red open star is the location reported by the GSC). The vertical dashed line marks the approximate location of the QCF. QCT indicates the location of the Queen Charlotte Terrace.*

Figure 6.12: *Map showing locations of geological observations (from Bird and Lamontagne, 2015a), including a rock-fall, indicated by a green triangle (#1: D. Gould) and other landslides (#2: I. Gould ; #3: M. Schmidt; #4: J. Reggler), indicated by red stars or red curves. Landslide surveys were conducted by the BC Ministry of Forests, Lands and Natural Resource Operations (red boxes) and by the Gowgaia Institute (turquoise box). The dried-up thermal springs at Hotspring Island are indicated by the blue diamond (#5: B. Schofield).*

consisted primarily of chimney damage, with a small number of failed chimneys documented as far away as Tlell (115 km from fault rupture), and minor cracks in foundations and walls (Figure 6.13). In contrast, chimney and other building damage was prevalent throughout the islands in the wake of the larger and generally closer, 1949 (M_W 8.1) earthquake, after which only one chimney on the islands is rumoured to have remained standing (Sergis Debussy, personal communication, 2012). Despite the strong shaking experienced on the islands ($\sim$0.2g), many objects in precarious positions were not damaged or displaced. The Queen Bee Café in the village of Queen Charlotte has numerous tall, thin bottles of syrup on a shelf barely wide enough to hold them but none seemed to have moved, yet the entire contents of refrigerators and china cabinets were emptied onto floors in the neighbouring village of Skidegate. It is likely some of the local variations in shaking effects are due to differences in site conditions; all the communities are located close to the water, with sites varying from bedrock to poorly consolidated sediments. Also, while most buildings are of low, wood-frame construction, other structural elements, such as foundations and reinforcement, vary considerably.

6.2.5 Community Decimal Intensities

A combined total of 3,005 reports were submitted to the "Did you feel it?"(DYFI) section of the Geological Survey of Canada (GSC) and United States Geological Survey (USGS) web sites. For each report, a Community Decimal Intensity (CDI; Wald *et al.*, 2011; Dengler and Dewey, 1998) was calculated – details can be found in Bird and Lamontagne (2015a).

Of the DYFI reports, a total of 88 were submitted by the people of Haida Gwaii, representing only about 2% of the population for that time of year. Additionally, the islands lie roughly 100 km from the mainland coast. This results in the intensity data close to the event's epicentre being relatively sparse. The Haida Gwaii dataset was, however, somewhat augmented by information gathered by Bird in November 2012 and February 2014. Regional CDI measurements from individual reports can be seen on Figure 6.13. Further details can be found in Bird and Lamontagne (2015a,b).

ShakeMap for the October 2012 $\mathbf{M_W}$ 7.8 Haida Gwaii Earthquake

Following the M_W 7.8 Haida Gwaii earthquake in 2012, a ShakeMap of the event was produced by the U.S. Geological Survey (USGS) through the Global ShakeMap system (Wald *et al.*, 1999; 2006), augmented with macroseismic intensity data from the USGS "Did You Feel It?" system (Wald *et al.*, 1999 and 2011; Worden *et al.*, 2010; Figure 6.14). The ground motions in this representation were calculated relative to a point-source rupture using an approach defined by the Electric Power Research Institute (2003), whereby a distance adjustment is determined for cases where the rupture orientation is assumed to be uniformly distributed in azimuth for combinations of strike-slip and dip-slip ruptures (Allen *et al.*, 2008).

Several extended-source fault-models for this event have since been developed (e.g., Lay *et al.*, 2013), allowing for an updated ShakeMap for the 2012 earthquake. The Lay *et al.* (2013) fault model was used as the source for calculating closest distance to rupture for the ground-motion calculations. Additionally, DYFI data from the USGS and NRCan on-line systems, along with field reconnaissance reports (Bird and Lamontagne, 2015a), were employed.

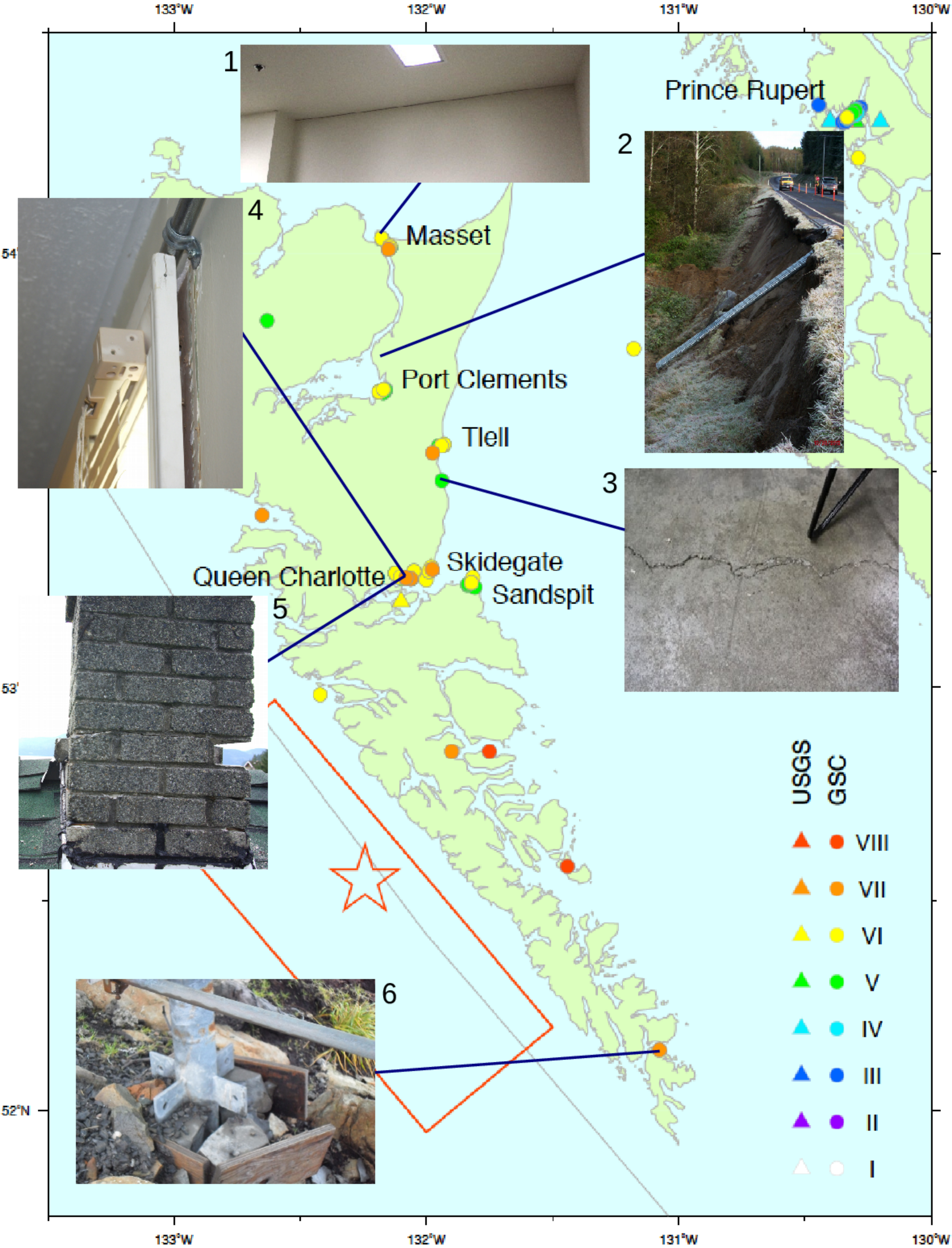

Figure 6.13: *Close-up map of individual intensities (from Bird and Lamontagne, 2015a), together with a selection of images of damage: wall-ceiling separation (#1: A. Bird), road slump (#2: A. Cober), cracked slab (#3: A. Bird), trim separation (#4: J. Goetzinger), chimney damage (#5: J. Goetzinger), and support-strut failure (#6: Canadian Coast Guard).*

Allen and Brillon (in press) found that no one ground-motion model (GMM) adequately captured all characteristics of ground-motion attenuation in the Haida Gwaii region. Zhao *et al.* (2006) was determined to be the most appropriate GMM for this event and was used in the development of the updated ShakeMap. The map (Figure 6.15) includes the effects of site response based on the topographic slope method (Wald and Allen, 2007). The PGV (Peak Ground Velocity) was subsequently converted to macroseismic intensity using the conversion equation of Worden *et al.* (2012) (Figure 6.16). The attenuation of intensity with distance was generally comparable to the assumed model, with the intensity map adjusted by a small inter-event residual of -0.14 macroseismic intensity units (Figure 6.16). The NRCan ShakeMap shows generally higher levels of ground-shaking on Haida Gwaii relative to the USGS ShakeMap. This is primarily due to the inclusion of the extended source model not in the other ShakeMap.

6.2.6 Source Characteristics

Kao *et al.* (2015) systematically determined regional moment-tensor solutions for all significant ($M_L \geq 4$) events in the 2012 Haida Gwaii earthquake sequence. Three-component waveforms from broadband stations of the CNSN at regional distances (≤1500 km) were retrieved for each event. Waveform data from broadband stations in the neighbouring states (Alaska and Washington) were also obtained from the Data Management Center of the Incorporated Research Institutions for Seismology (IRIS DMC) to further improve the azimuthal coverage. The moment-tensor inversion was solved by singular value decomposition of a linear system consisting of observed waveforms and Green's functions of synthetic seismograms, as described in detail by Kao *et al.* (2012).

The focal mechanism of the M_W 7.8 mainshock shows low-angle thrust faulting along a shallowly dipping plane with a strike parallel to the QCF, consistent with the inference of Pacific Plate under-thrusting beneath the overriding North American Plate (Figure 6.17). The results clearly indicate that many seismogenic structures were involved in the 2012 Haida Gwaii earthquake sequence (Figures 6.18 and 6.19). The majority of significant aftershocks show normal-faulting mechanisms that are probably associated with the bending stress within the Pacific plate near the deformation front. Several normal and strike-slip events at greater depths within the subducted Pacific slab show a consistent pattern of T-axis in the down-dip direction, implying that the subducted plate is under a stress regime of down-dip extension. The forearc region is also in extension, but only a few strike-slip events are located along the QCF. The limited size and distribution of the strike-slip events along the QCF suggest that most of the accumulated elastic strain was not released during the 2012 Haida Gwaii sequence. The likelihood of having major strike-slip earthquakes along the southernmost part of the QCF system in the future cannot be ignored.

6.2.7 Coulomb Stress Studies and Overall Rupture Characteristics

Hobbs *et al.* (2015a) studied potential stress triggering resulting from the Haida Gwaii M_W 7.8 mainshock by comparing predicted Coulomb stress changes with the location and mechanism of aftershocks. In addition, they investigated Coulomb stress changes on the nearby Queen Charlotte Transform Fault (Figure 6.20). Using existing rupture models, a high proportion of aftershocks (large and small) were

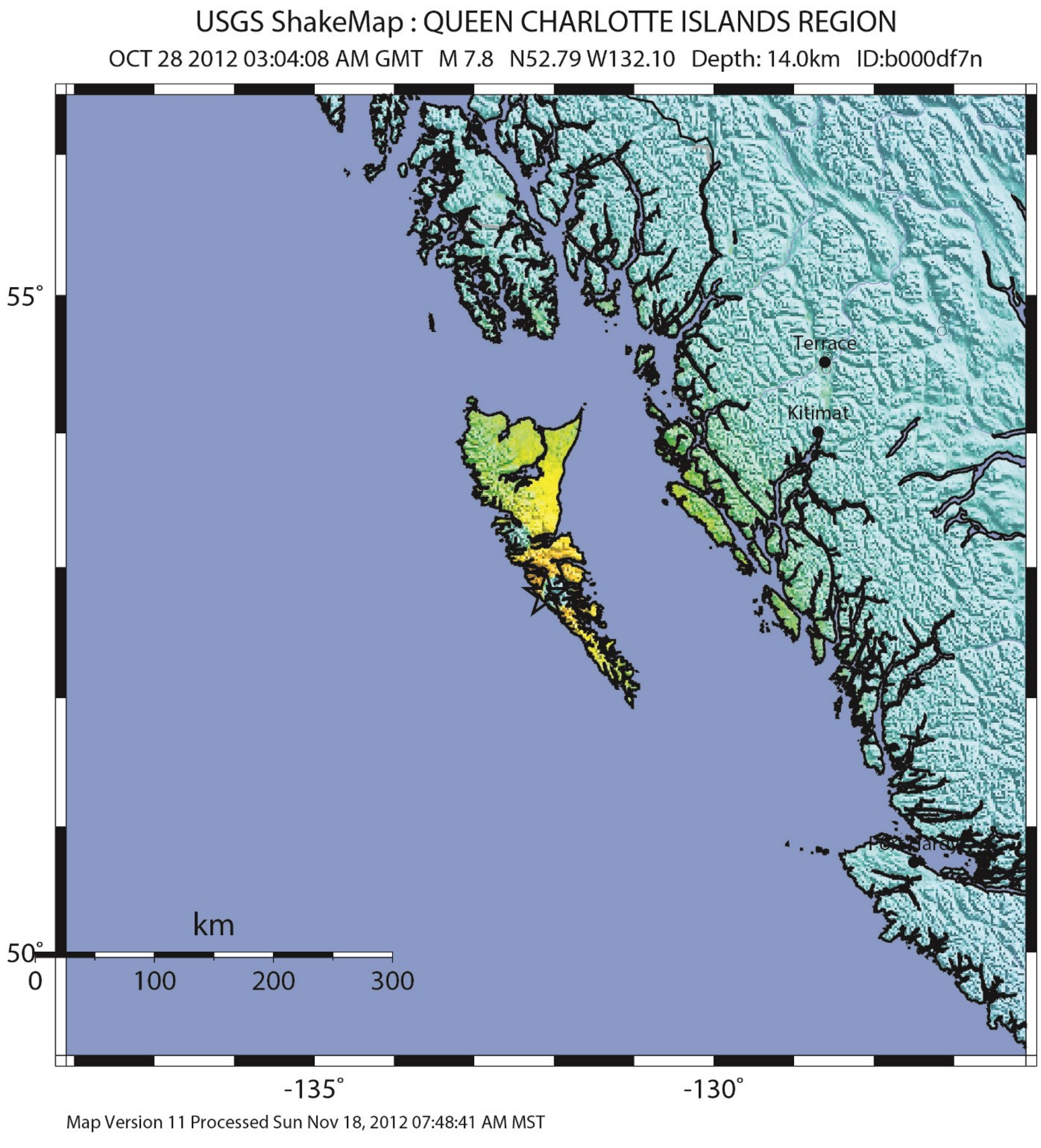

PERCEIVED SHAKING	Not felt	Weak	Light	Moderate	Strong	Very strong	Severe	Violent	Extreme
POTENTIAL DAMAGE	none	none	none	Very light	Light	Moderate	Mod./Heavy	Heavy	Very Heavy
PEAK ACC.(%g)	<0.05	0.3	2.8	6.2	12	22	40	75	>139
PEAK VEL.(cm/s)	<0.02	0.1	1.4	4.7	9.6	20	41	86	>178
INSTRUMENTAL INTENSITY	I	II-III	IV	V	VI	VII	VIII	IX	X+

Scale based upon Worden et al. (2011)

Figure 6.14: *USGS ShakeMap showing the earthquake epicentre (black star). The base shaking was determined through combining the Chiou and Youngs (2008) ground-motion model with the Worden et al. (2012) ground-motion-to-intensity conversion equation (Source: `http://earthquake.usgs.gov/earthquakes/shakemap/global/shake/b000df7n/`).*

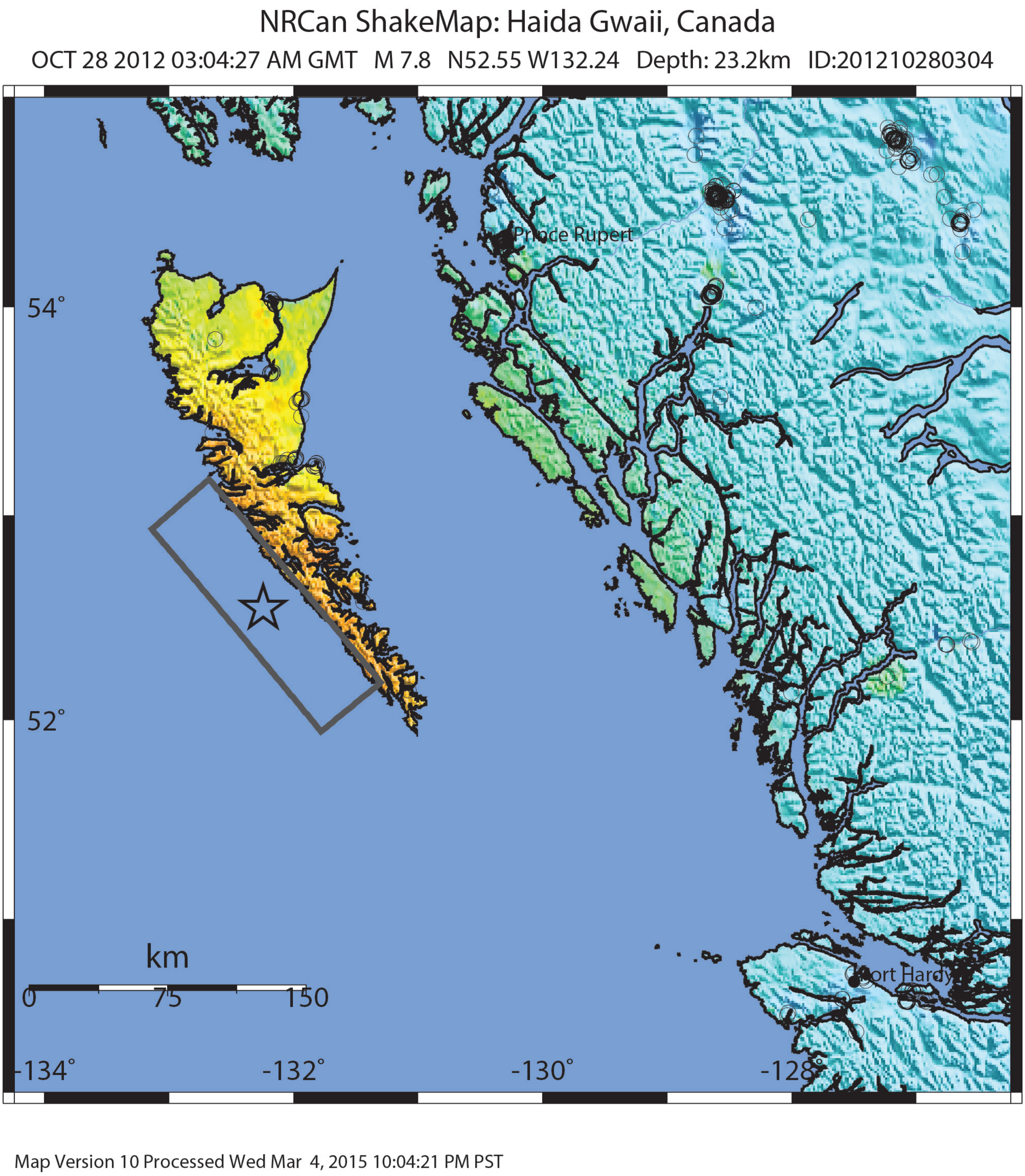

PERCEIVED SHAKING	Not felt	Weak	Light	Moderate	Strong	Very strong	Severe	Violent	Extreme
POTENTIAL DAMAGE	none	none	none	Very light	Light	Moderate	Mod./Heavy	Heavy	Very Heavy
PEAK ACC.(%g)	<0.05	0.3	2.8	6.2	12	22	40	75	>139
PEAK VEL.(cm/s)	<0.02	0.1	1.4	4.7	9.6	20	41	86	>178
INSTRUMENTAL INTENSITY	I	II-III	IV	V	VI	VII	VIII	IX	X+

Scale based upon Worden et al. (2011)

Figure 6.15: *NRCan ShakeMap showing the earthquake epicentre (black star) and the surface projection of the extended fault model of Lay et al. (2013; black polygon). The base shaking was determined through combining the Zhao et al. (2006) ground-motion model with the Worden et al. (2012) ground-motion-to-intensity conversion equation. Open grey circles indicate sites from which a DYFI report was submitted.*

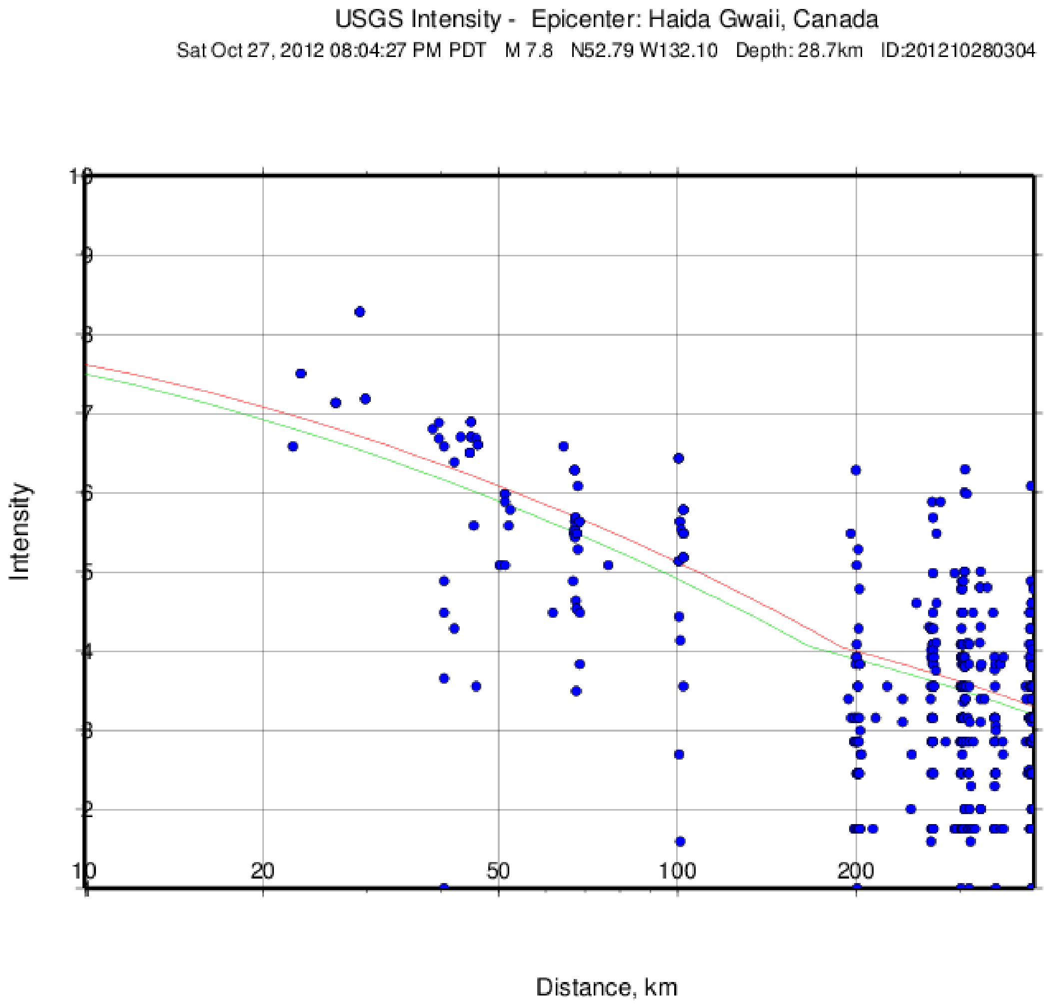

Figure 6.16: *The modelled macroseismic intensity attenuation curve (red line) superimposed by the intensity observations (filled blue circles). The green line indicates the attenuation curve adjusted by the inter-event intensity residual.*

found to be consistent with triggering by the mainshock Coulomb stress changes. For example, up to 86% of all $M_W \geq 4.5$ aftershocks had at least one nodal plane that was positively stressed. Additionally the observed cluster of aftershocks seaward of the main thrust falls within the modelled zone of promoted normal failure, likely related to extension in the footwall. Further, Hobbs *et al.* (2015a) found loading greater than the triggering threshold on nearby portions of the Queen Charlotte Fault, in particular the region to the south of the 2012 mainshock (Figure 6.20b). This segment of the Queen Charlotte Fault was identified (Rogers 1986) as a seismic gap with the potential for an event as large as M 7.5. With increased stress loading from the 2012 earthquake, this suggests increased seismic hazard in the region.

Hobbs *et al.* (2015b) used global Rayleigh and Love wave recordings of the M_W 7.8 mainshock with an Empirical Greens Function (EGF) deconvolution technique (using a nearby well-recorded M_W 6.3 thrust event as the EGF) to determine Relative Source Time Functions (RSTFs) that yield information on the overall rupture characteristics of the mainshock. Resulting RSTFs commonly displayed two peaks, confirming the presence of two dominant sub-events. This was suggested originally by Hayes (2013) and Lay *et al.* (2013).

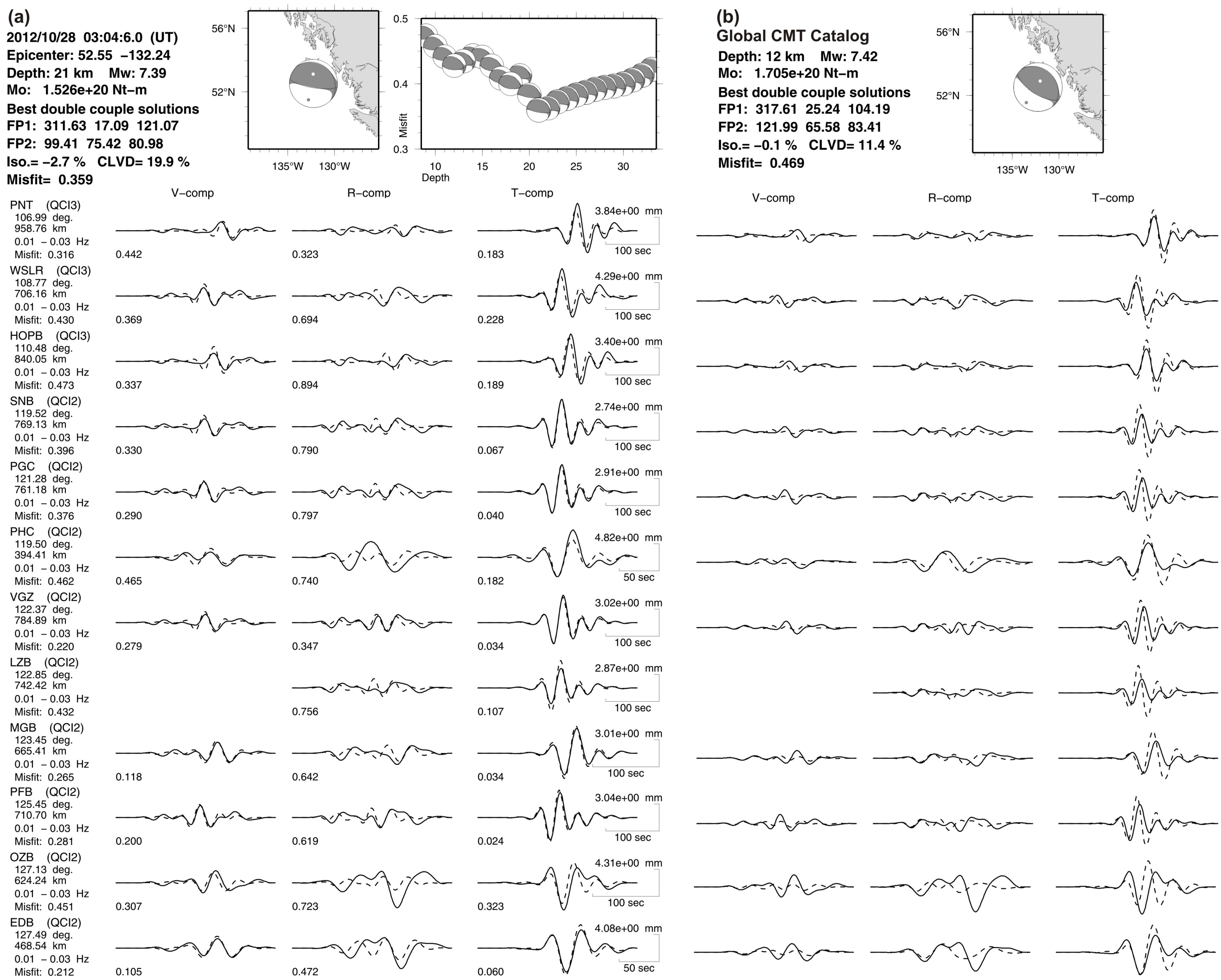

Figure 6.17: Moment-tensor inversion result for the 2012 Haida Gwaii earthquake mainshock (adopted from Kao et al., 2015). (a) Source parameters are summarised on the top with a map showing the epicentral location and the focal mechanism. The best-fitting depth is 21 km, as shown by the misfit vs depth curve. Observed and synthetic waveforms for each station are plotted as solid and dashed lines, respectively. Waveform misfit of each component is listed at the lower-left corner of each trace and the station average is shown on the left. Kao et al.'s solution has a minor strike-slip component that is compatible with the relative plate motion. Overall the waveform fit is excellent. (b) Results of forward modelling based on the solution reported in the Global CMT Project database. The waveform fit is clearly not as satisfactory.

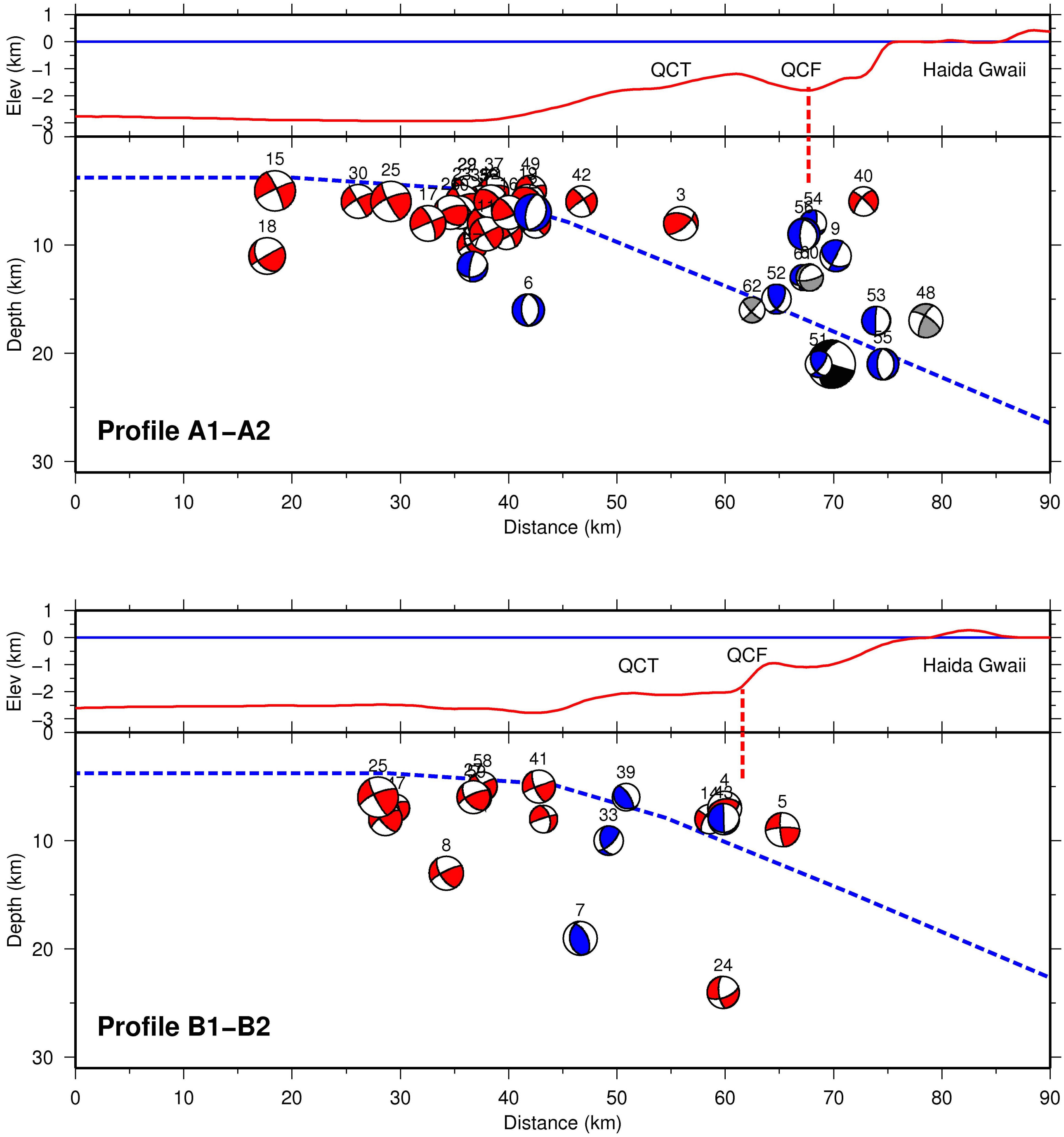

Figure 6.18: *Vertical profiles showing the hypocentral distribution and focal mechanisms (in back-hemisphere projection) of significant aftershocks in the 2012 Haida Gwaii earthquake sequence (adapted from Kao et al., 2015). Different colours/shadings correspond to different types of faulting (red: normal-faulting; blue: strike-slip faulting; grey: thrust-faulting). The mainshock is plotted in black. Local bathymetry and topography are plotted at the top of each profile. Dashed blue and red lines mark the top of the under-thrusting Pacific plate and the Queen Charlotte Fault (QCF), respectively. QCT denotes the Queen Charlotte Terrace. Vertical exaggeration of the bathymetry/topography is 2.5. Geographic locations of the two profiles are available in Figure 6.10.*

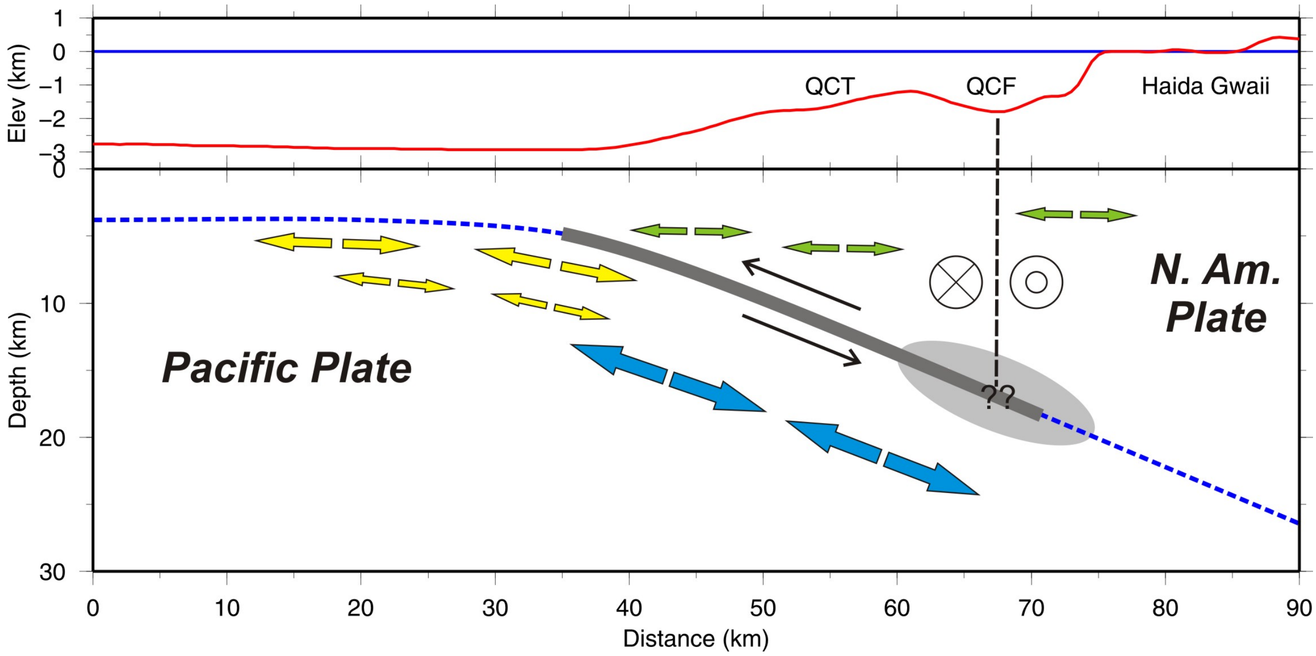

Figure 6.19: *A schematic diagram summarising the seismogenic structures of the 2012 Haida Gwaii earthquake sequence. The layout is similar to that in Figure 6.18 with symbols representing the Queen Charlotte Fault (QCF, vertical dashed line) and the rupture zone of the mainshock (thick dark line). A pair of black arrows represents the relative plate motion along the interface; target signs on the two sides of the QCF symbolise the dextral shear motion across the fault zone. Pairs of arrows near the deformation front correspond to the extensional stress regime due to plate bending. Pairs of arrows beneath the Queen Charlotte Terrace (QCT) and Haida Gwaii indicate the existence of extension within the overriding North America crust. Large arrows symbolise the stress regime of down-dip extension within the down-going Pacific plate. The grey area marks the location where complex interactions between the QCF and the interplate thrust zone might have occurred.*

Overall, Hobbs *et al.* (2015b) found compelling evidence that the 2012 Haida Gwaii earthquake had uneven bilateral overall rupture with a well-resolved component to the northwest (Figure 6.20a). The first, largest sub-event, approximately 14 s after the onset of rupture, was located roughly 12 km to the south of the epicentre. The second sub-event, 17 s after the first sub-event (i.e. ∼31 s after the onset of rupture), was located directly along strike to the northwest at about 28 km from the first sub-event. The overall rupture (from the beginning to end of the RSTFs) migrated a distance of approximately 50 km at 308.5° azimuth and took about 43 s to break. Interestingly, this overall northwest-directed rupture may aid in explaining the observed focusing of surface waves at Alaskan seismic stations (Gomberg, 2013). Future work could examine the potential for delayed-onset dynamic triggering of the Craig, Alaska, earthquake of January 2013 (Gomberg, 2013; Lay *et al.*, 2013) that occurred two months later and ∼300 km to the NW of the 2012 Haida Gwaii mainshock.

6.2.8 GPS Observed Crustal Displacements

A geodetic study of the coseismic and postseismic displacements resulting from this earthquake was carried out by Nykolaishen *et al.* (2015). Global Positioning System (GPS) data collected in the weeks following the event were used along with historical data sets to determine coseismic offsets at sites throughout southern Haida Gwaii. The largest measured offset was 115 cm in a SSW direction, accompanied by 30 cm of subsidence measured at Barry Inlet (Figure 6.21). These offsets are consistent

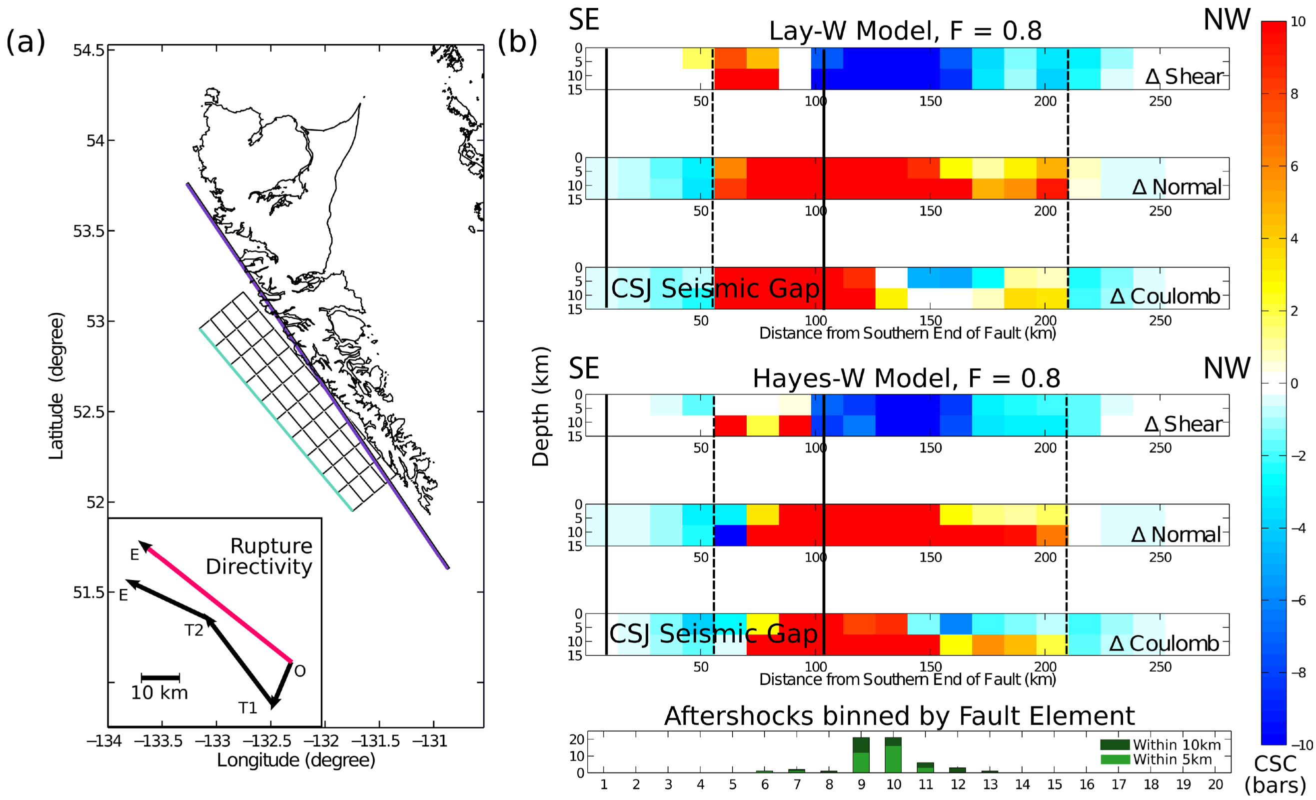

Figure 6.20: *(a) The Haida Gwaii rupture zone (pictured as a fault-element grid with a turquoise surface trace) is considered based on its geometry relative to the Queen Charlotte Fault (purple line). Results of empirical Green's function deconvolution and directivity analysis are inset, with apparent directivity sub-parallel to the Haida Gwaii mainshock's rupture-zone strike and the strike of the Queen Charlotte Fault (from Hobbs et al., 2015b). (b) Shear, normal, and total Coulomb stress changes (CSC), in bars, projected onto the Queen Charlotte Fault, as indicated in (a), using the Lay-W and Hayes-W models and a friction coefficient of 0.8. The extent of the Cape St. James (CSJ) Seismic Gap is indicated at the southern end of the fault. The bottom trace indicates the numbers of aftershocks whose surface projections are within 5 and 10 km, horizontally, of the Queen Charlotte Fault. (from Hobbs et al., 2015a)*

with a shallow dipping thrust beneath the Queen Charlotte Terrace, as identified by static finite-fault rupture models based solely on other observations (seismic/tsunami). These preliminary fault-rupture models, however, do not replicate the magnitudes of GPS-observed horizontal offsets or subsidence throughout the region. Nykolaishen *et al.* (2015) updated selected existing finite-fault models (e.g., Lay *et al.*, 2013) through inversion of the three-component GPS observations and by constraining the rupture to occur offshore Haida Gwaii, in an attempt to replicate the observed subsidence on western Haida Gwaii. Overall, the inversions yielded two important differences compared to the starting models used: (1) the observed subsidence at the Barry Inlet station on the west coast of Haida Gwaii was correctly predicted, and (2) the slip along the fault surface was concentrated at the southern end of the rupture zone (Figure 6.21).

Continued monitoring of displacements resulting from this event has indicated up to 6 cm of cumulative horizontal motion in the first year following the mainshock. These postseismic motions range in direction from south-southwest at stations on northern Moresby Island (similar to the coseismic offsets), to southeast or east-southeast at stations on southern Moresby Island (Figure 6.22). The nature of the postseismic displacements over time are similar to those observed at other subduction zones (e.g., Ozawa *et al.*, 2012; Wang *et al.*, 2012; Sun *et al.*, 2014), with the fastest displacement rate occurring in the

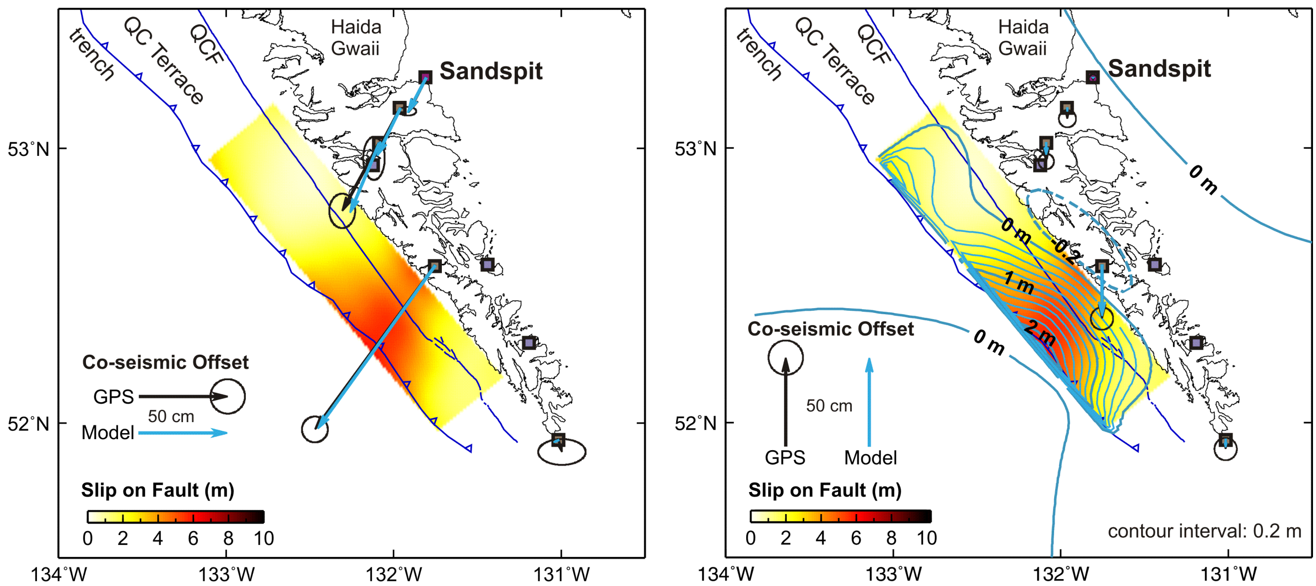

Figure 6.21: *Comparison of observed coseismic offsets (black arrows) at GPS stations on Haida Gwaii to those predicted from non-linear Bayesian inversions of three-component GPS observations (blue arrows) using the finite-fault rupture model of Lay et al. (2013) as the starting model. (Left) Horizontal component of inversion results. Error ellipses represent 95% confidence intervals using standard deviation values five times the values of uncertainties reported in Nykolaishen et al. (2015) for coseismic offsets in the north and east components. (Right) Vertical component of inversion results. The direction of arrows denotes uplift or subsidence and blue contours show the predicted coseismic vertical deformation pattern in southern Haida Gwaii from the inversion. The diameters of the error circles represent 95% confidence intervals using standard deviation values twice the values of uncertainties reported in Nykolaishen et al. (2015) for the vertical coseismic offsets. QCF denotes the Queen Charlotte Fault.*

first few weeks after the earthquake. Preliminary analysis of the time series from the station at Sandspit (Figure 6.21 and 6.22) necessitated fitting a function with multiple decay terms to accommodate this fast displacement rate immediately post-earthquake, along with a slower decay of the postseismic signal over hundreds of days (Nykolaishen *et al.*, 2015).

The spatial variations in the observed postseismic deformation pattern over the GPS network, along with preliminary curve-fitting of postseismic time-series, may indicate that more than one physical process is contributing to the surface deformation. The processes likely include after-slip and viscoelastic stress relaxation, as observed after other subduction zone earthquakes (e.g., Hu and Wang, 2012; Sun *et al.*, 2014). In addition, Nykolaishen *et al.* (2015) suggest that the eastward component of motions observed at the southern stations (Figure 6.22) could indicate a contribution from aseismic slip (creep) along the Queen Charlotte Fault or along sub-parallel faults (Rohr, 2015) offshore southern Moresby Island.

6.2.9 Tsunami

The Haida Gwaii thrust earthquake caused displacement of the seafloor off the west coast of Moresby Island that triggered the largest locally-generated tsunami along the British Columbia coastline documented in written history (the last ∼150 years). The tsunami was recorded by tide gauges and Deep-ocean Assessment and Reporting of Tsunamis (DART) buoys throughout the Pacific Ocean, as well as by NEPTUNE Canada bottom-pressure sensors offshore Vancouver Island (Fine *et al.*, 2015). The largest recorded peak-to-trough wave height of 1.52 m occurred at Kahului, Maui, Hawaii, but only 0.52 m

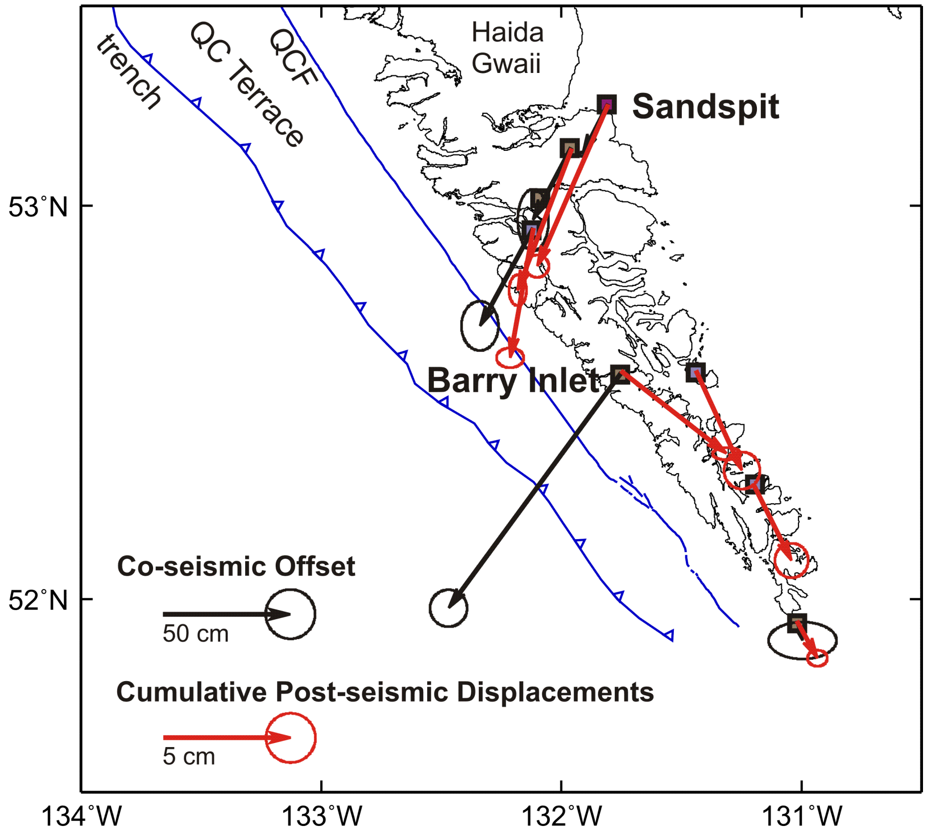

Figure 6.22: *Observed coseismic offsets at GPS stations on Haida Gwaii (black arrows) compared to cumulative postseismic displacements with interseismic deformation signal removed (red arrows). Postseismic displacements were calculated with data available from 28 October 2012 to 31 December 2013. Error ellipses represent 95% confidence interval using standard deviation values five time the values of uncertainties reported in Nykolaishen et al. (2015) for coseismic offsets and cumulative postseismic displacements, respectively, in the north and east components. QCF denotes the Queen Charlotte Fault.*

was recorded at Henslung Cove, Langara Island, off northern Haida Gwaii (Figure 6.23; NGDC/WDS Global Historical Tsunami Database, 2013). Larger waves were, however, expected to have occurred on the unpopulated, non-instrumented west coast of Moresby Island.

Three field surveys in November 2012, February 2013 and June 2013 documented evidence that tsunami run-up exceeded 3 m above the state of tide at the time of the tsunami at sites spanning ∼230 km of the western Haida Gwaii coastline (Figure 6.23; details in Leonard and Bednarski, 2014). Greatest impacts were apparent at the heads of narrow inlets and bays on western Moresby Island, where natural and man-made debris with a clear ocean-ward origin was found on the forest floor and caught in tree branches, inferring flow depths and run-up heights of up to 2.5 m and 13 m, respectively (Figures 6.23 and 6.24). Logs disturbed from their apparent former footprints on the forest floor at the head of Pocket Inlet (Figure 6.24) provided evidence of complex tsunami run-up, backwash and oblique flow patterns. Discontinuous muddy sediments were found at a few sites, but the thickness of deposits was not proportional to run-up. Given the limited sedimentological signature of the Haida Gwaii tsunami and evidence for long-term uplift of this coastline (e.g., Clague *et al.*, 1982), it is likely that evidence of the tsunami has a very low preservation potential (Leonard and Bednarski, 2015).

A numerical tsunami model was initially designed to provide preliminary run-up estimates on the west coast of Moresby Island and was used as an aid to the post-tsunami survey teams in 2012 and 2013. The

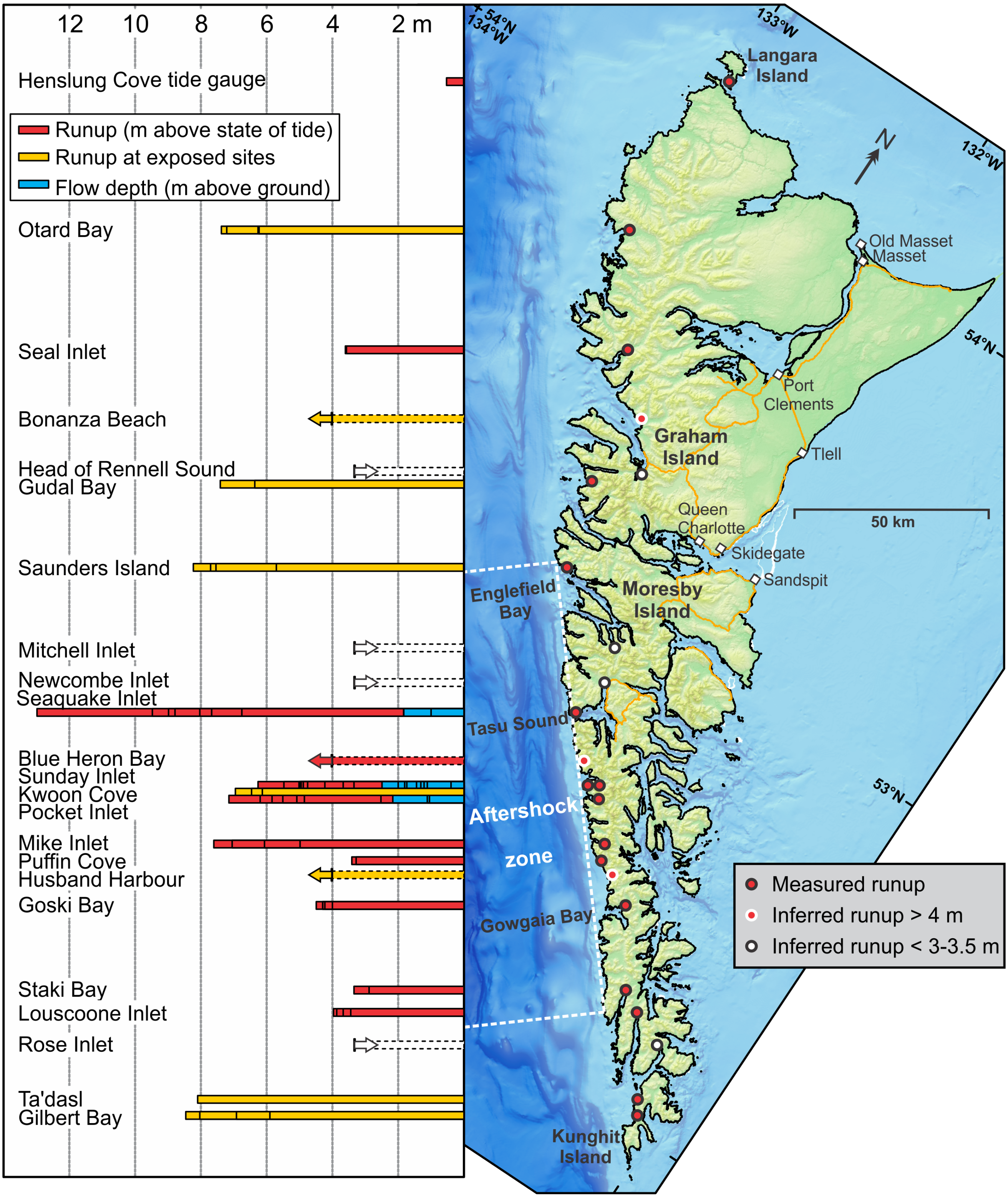

Figure 6.23: *Haida Gwaii survey locations, run-up and flow depth data. Dashed bars indicate inferred minimum/maximum run-up at non-surveyed sites; red/orange indicates that debris was seen to exceed the elevation of the forest edge by at least 1 m; white indicates that debris was not observed to exceed the forest edge elevation. The "run-up" value from Henslung Cove tide gauge is the measured peak-to-trough tsunami amplitude (from Leonard and Bednarski, 2015).*

Figure 6.24: *Tsunami evidence from western Moresby Island (see Figure 6.23 for locations). (a) Variety of debris at Seaquake Inlet. This uncharted inlet has no official name. It was referred to as Davidson Inlet by Leonard and Bednarski (2014) on the basis of its proximity to Davidson Point; the alternative name Seaquake Inlet was proposed by the captain of the CCGS Bartlett following a bathymetric survey of the inlet in August 2013. (b) Fucus seaweed in tree branches at Sunday Inlet. (c) Disturbed logs at Pocket Inlet. (d) Mud deposit at Staki Bay (from Leonard and Bednarski, 2014).*

tsunami source in the more recent version of this model (Fine *et al.*, 2015) was based on the updated finite-fault model of Hayes (2013). To match the tsunami wave arrival-times observed in the DART data, the source region was shifted in the model about 30 km to the southeast. The model-simulated tsunami run-up exceeded 6 m in many places along the coast (Figure 6.25), in good agreement with the post-tsunami surveys (Figure 6.26). This comparison was, however, limited to the bays that are well sheltered from storm-generated waves. Thus the maximum modelled elevation of about 9 m (Figure 6.26) was in a small open bay that has not been surveyed. Furthermore, the largest run-up of 13 m found by the post-tsunami survey team was in a small semi-sheltered inlet just north of Tasu Sound. This large run-up value is not reproduced in the models, a discrepancy that is still under investigation.

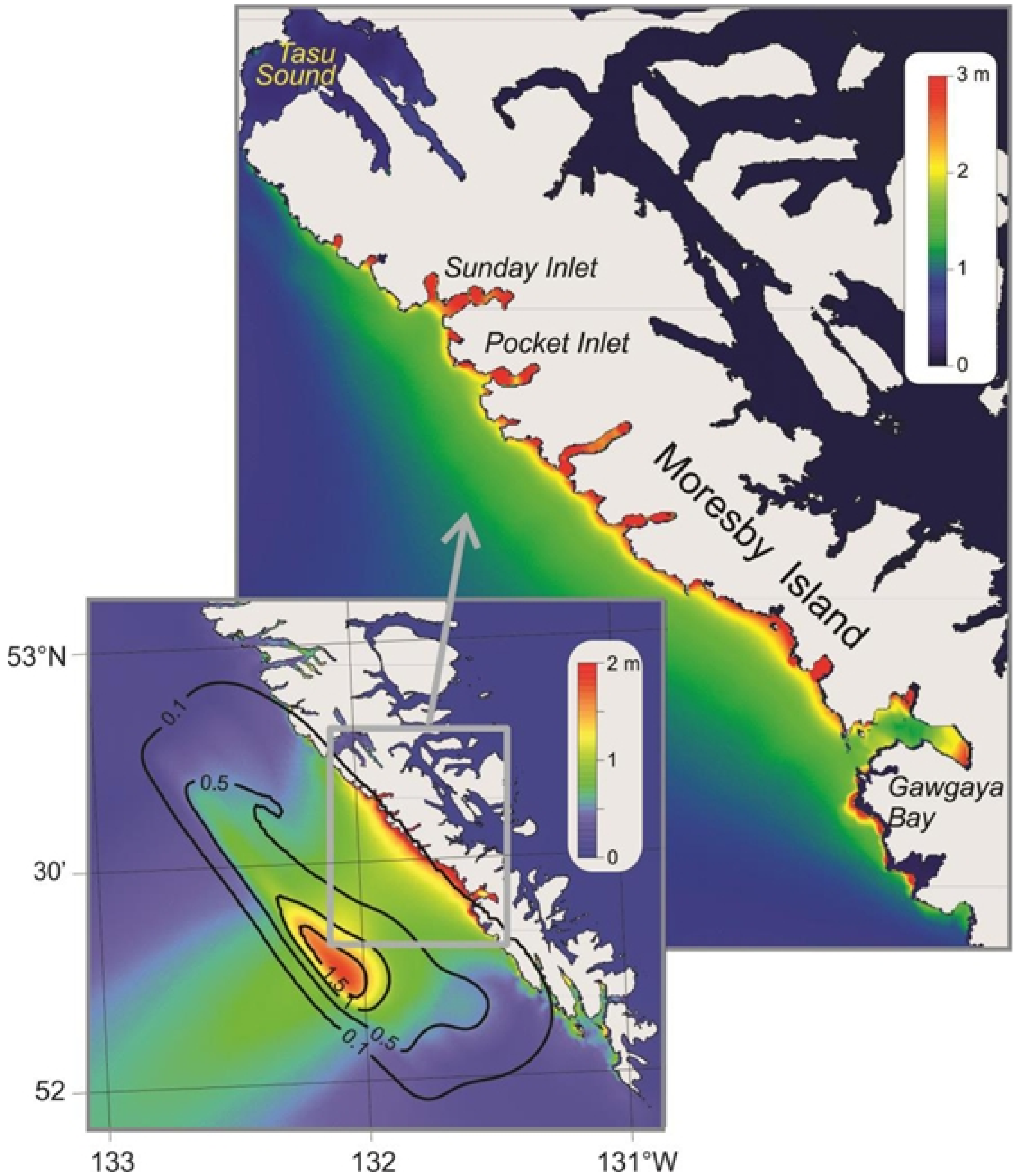

Figure 6.25: *Maximum modelled tsunami elevations off the west coast of Moresby Island. The inset also shows the contours of the initial sea surface uplift (modified from Fine et al., 2015).*

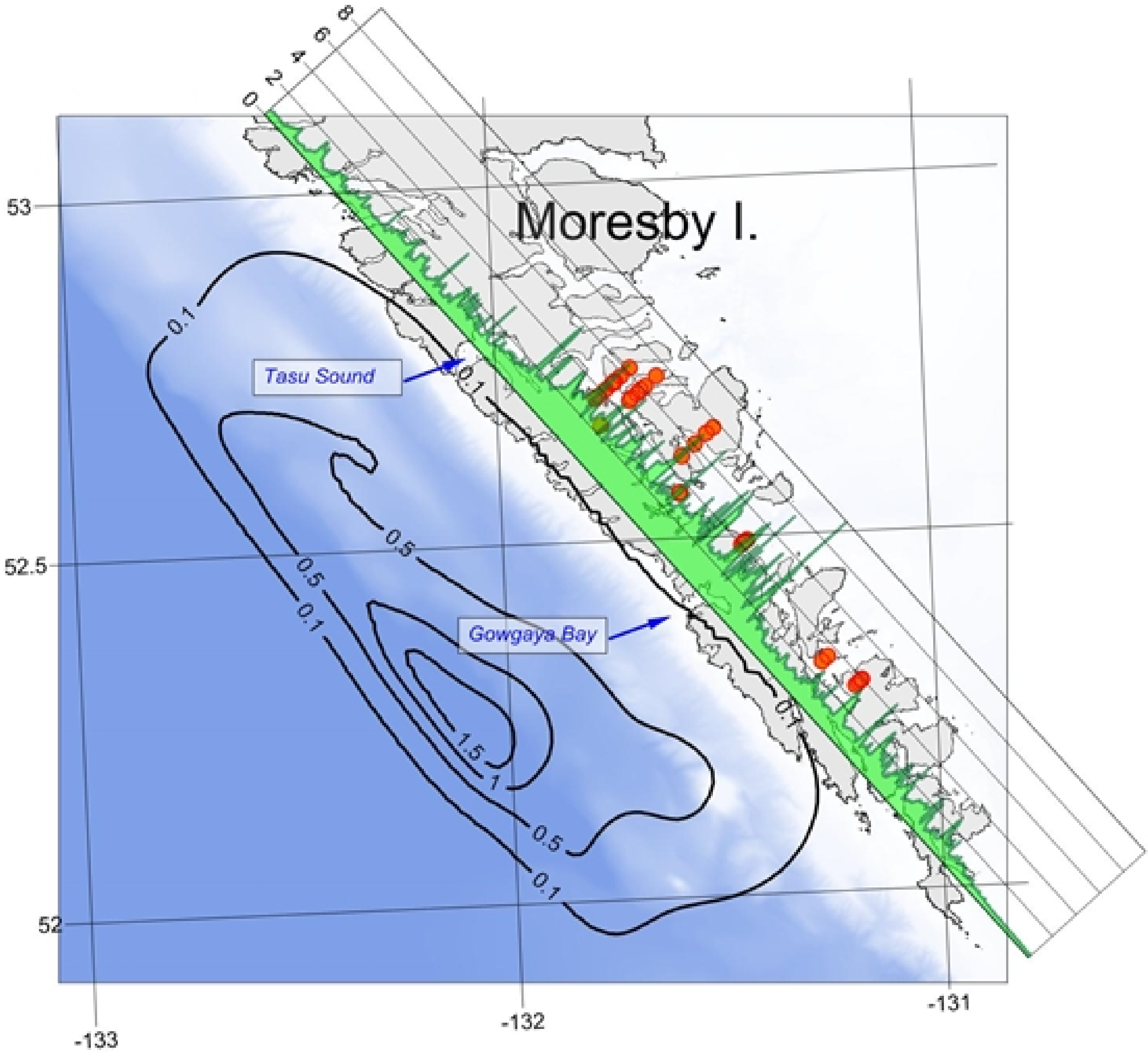

Figure 6.26: *Comparison between the modelled maximum elevations (Fine et al., 2015; green line) and the maximum run-up heights in sheltered bays (Leonard and Bednarski, 2014; red circles) on the west coast of Moresby Island. Black contours show the initial tsunami source used in the model.*

6.2.10 Conclusions

The M_W 7.8 earthquake which struck offshore Haida Gwaii in October of 2012 was the largest thrust event to hit the region in recent Canadian history and cemented the belief that the islands are prone to a complex combination of transform and oblique subduction dynamics. The M_W 7.8 earthquake occurred on a shallow, north-east dipping fault below the QCF, and studies (of aftershock distribution, moment tensor and coulomb stress) suggest the stress along the QCF's seismic gap increased. Part of Moresby Island was measured to have moved over a metre to the south-west and the ground motion lasted roughly 90 s, triggering numerous landslides and the cessation of thermal spring activity, but resulted in only minor damage in the islands' communities. The earthquake also created the largest tsunami of 2012, globally, with run-ups of over 6 m above tidal levels in inlets along the western coast of Moresby Island and possibly as high as 13 m just north of Tasu Sound. Aftershocks lasted months and were distributed in two trends; one up-dip from the mainshock (exhibiting predominantly normal and some strike-slip mechanisms) and another along the trace of the QCF (with strike-slip motion). With help from the USGS, a ShakeMap was created from submissions to the "Did You Feel It?" section of the GSC and USGS web sites. Through scientific observation and interaction with the people of Haida Gwaii, NRCan scientists learned, and continue to learn, a great deal about the complicated tectonics and the resulting earthquakes of the remote, beautiful islands of Haida Gwaii, Canada.

6.2.11 Acknowledgements

It should be noted that several figures were generated with the aid of Generic Mapping Tools software (Wessel and Smith, 1998). The authors are grateful for the assistance they received from colleagues (at NRCan), and associates (at the USGS), including the terrestrial and marine field crews. We are appreciative of Andreas Rosenberger for the data and discussion surrounding the strong-motion recordings. And, we acknowledge the valuable contribution of reviewers Malaika Ulmi, Nicky Hastings and Wayne Richardson. Finally, we respectfully thank the people of Haida Gwaii who took the time to share their experiences, and who helped the first author and NRCan field crews during their time on the islands, particularly Parks Canada and the First Nation Peoples of Haida Gwaii who assisted in GPS and seismic field deployments. This is Earth Sciences Sector (ESS) contribution number 20150358.

6.2.12 References

Akkar, S., M.A. Sandıkkaya, and J.J. Bommer (2014). Empirical ground-motion models for point- and extended-source crustal earthquake scenarios in Europe and the Middle East, *Bulletin of Earthquake Engineering*, **12**: 359–387, doi: 10.1007/s10518-013-9461-4.

Allen, T. I., and C. Brillon (2015). Assessment of Ground-Motion Models for use in the British Columbia North Coast Region, Canada, *Bulletin of the Seismological Society of America*, **105**: 1193-1205, doi: 10.1785/0120140266.

Allen, T. I., D. J. Wald, A. J. Hotovec, K. Lin, P. S. Earle, and K. D. Marano (2008). An Atlas of ShakeMaps for selected global earthquakes, *United States Geological Survey Open-File Report* 2008-1236 Open-File Report 2008-1236, Golden, 47 pp.

Atkinson, G. M. (2005). Ground motions for earthquakes in southwestern British Columbia and northwestern Washington: Crustal, in-slab, and offshore events, *Bulletin of the Seismological Society of America*, **95**: 1027–1044, doi: 10.1785/0120040182.

Atkinson, G. M., and J. Adams (2013). Ground motion prediction equations for application to the 2015 Canadian national seismic hazard maps, *Canadian Journal of Civil Engineering*, **40**: 988–998, dx.doi.org/10.1139/cjce-2012-0544.

Barrie, J.V., K.W. Conway, and P.T. Harris (2013). The Queen Charlotte Fault, British Columbia: seafloor anatomy of a transform fault and its influence on sediment processes. *Geo-Marine Letters*, **33**: 311-318, doi:10.1007/s00367-013-0333-3.

Bird, A. L., and M. Lamontagne (2015a). Impacts of the October 2012 Magnitude 7.8 Earthquake near Haida Gwaii, Canada, *Bulletin of the Seismological Society of America* (in press), doi: 10.1785/0120140167.

Bird, A. L., and M. Lamontagne (2015b). How Scientists' Communications helped mitigate the Psychosocial Effects of the October 2012 Magnitude 7.8 Earthquake near Haida Gwaii, Canada, *Seismological Research Letters*, **86**: 1301-1309,doi: 10.1785/0220140231.

Bird, A.L., G. C. Rogers, and G. D. Spence (1997). Earthquakes in the Queen Charlotte Islands Region: 1984-1996. *Lithoprobe Seismic Processing Facility Newsletter*, **10.1**: 39-44.

Bird, A.L. (1997). Earthquakes in the Queen Charlotte Islands Region: 1982 – 1996; Master of Science Thesis, University of Victoria, Victoria, BC, 134 pp. http://www.collectionscanada.gc.ca/obj/s4/f2/dsk2/tape17/PQDD_0001/MQ34480.pdf.

Bostwick, T. K. (1984). A Re-examination of the August 22, 1949 Queen Charlotte Earthquake: Master of Science Thesis, University of British Columbia, Vancouver, BC, 115 pp.

Cassidy, J. F., G. C. Rogers, and R. D. Hyndman (2014). An overview of the 28 October 2012 M_W 7.7 Earthquake in Haida Gwaii, Canada: A Tsunamigenic Thrust Event Along a Predominantly Strike-Slip Margin, *Pure and Applied Geophysics*, 1-9, doi: 10.1007/s00024-014-0775-1.

CBC (2014). "Haida Gwaii hot springs show more signs of returning", by Marissa Harvey, 06 June 2014: http://www.cbc.ca/news/canada/british-columbia/haida-gwaii-hot-springs-show-more-signs-of-returning-1.2667320 (last accessed June 2014).

Chiou, B. S.-J., and R. R. Youngs (2008). An NGA model for the average horizontal component of peak ground motion and response spectra, *Earthquake Spectra* **24**: 173–215, doi: 10.1193/1.2894832.

Clague, J., J. R. Harper, R. J. Hebda, and D. E. Howes (1982). Late Quaternary sea levels and crustal movements, coastal British Columbia, *Canadian Journal of Earth Science*, **19**: 597-618, doi: 10.1139/e82-048.

Council of the Haida Nation (2015). "Hot pools filling at Gandll K'in Gwaay.yaay (Hotspring Island)!", by haidanation, 13 November 2015: https://haidanation.wordpress.com/2015/11/13/hot-pools-filling-at-g%cc%b2andl-kin-gwaay-yaay-hotspring-island/ (last accessed December 2015).

DeMets, C., R. G. Gordon, D. F. Argus, and S. Stein (1990). Current Plate Motions, *Geophysical Journal International*, **101**: 425-478.

DeMets, C., R. G. Gordon, and D. F. Argus (2010). Geologically current plate motions, *Geophysical Journal International*, **181**: 1-80, doi: 10.1111/j.1365-246X.2009.04491.x.

Dengler, L. A., and J. W. Dewey (1998). An Intensity Survey of Households Affected by the Northridge, California, Earthquake of 17 January, 1994, *Bulletin of the Seismological Society of America*, **88**: 441-462.

Electric Power Research Institute (2003). CEUS Ground Motion Project: Model Development and Results, Palo Alto, CA, 105 pp.

Farahbod, A. M., and H. Kao (2015).Spatiotemporal Distribution of Events during the First Week of the 2012 Haida Gwaii Aftershock Sequence, *Bulletin of the Seismological Society of America*, **105**: 1231-1240, doi:10.1785/0120140173.

Fine, I. V., J. Y. Cherniawsky, R. E. Thomson, A. B. Rabinovich, and M. V. Krassovski (2015). Observations and numerical modeling of the 2012 Haida Gwaii tsunami off the coast of British Columbia, *Pure and Applied Geophysics*, doi: 10.1007/s00024-014-1012-7.

Gomberg, J. (2013). Permanently enhanced dynamic triggering probabilities as evidenced by two M 7.5 earthquakes. *Geophysical Research Letters*, **40**: 4828–4833, doi: 10.1002/grl.50933.

Hayes, G. (2013). Updated Finite Fault Results for the Oct 28, 2012 M_W 7.8 141 km S of Masset, Canada, Earthquake (Version 2): `http://comcat.cr.usgs.gov/earthquakes/eventpage/pde20121028030408820_14#scientific_finite-fault` (last accessed January 2015).

Hobbs, T. E., J. F. Cassidy, S. E. Dosso, and C. Brillon (2015a). Coulomb stress changes following the M_W 7.8 2012 Haida Gwaii, Canada earthquake: Implications for seismic hazard, *Bulletin of the Seismological Society of America*, **105**: 1253-1264, doi: 10.1785/0120140158.

Hobbs, T. E., J .F. Cassidy, and S. E. Dosso (2015b). Rupture properties of the M_W 7.8 2012 Haida Gwaii Earthquake from an Empirical Green's Function Method, *Bulletin of the Seismological Society of America*, **105**: 1219-1230, doi: 10.1785/0120140175.

Hu, Y., and K. Wang (2012). Spherical-Earth finite element model of short-term postseismic deformation following the 2004 Sumatra earthquake, *Journal of Geophysical Research*, **117**: B05404, doi: 10.1029/2012JB009153.

Hurwitz, S., R. A. Sohn, K. Luttrell, and M. Manga (2014). Triggering and modulation of geyser eruptions in Yellowstone National Park by earthquakes, earth tides, and weather, *Journal of Geophysical Research: Solid Earth*, **119**: 1718-1737, doi: 10.1002/2013JB010803.

Husen, S., R. Taylor, R. B. Smith, and H. Healser (2004). Changes in geyser eruption behavior and remotely triggered seismicity in Yellowstone National Park produced by the 2002 M7.9 Denali fault earthquake, Alaska: *Geology*, **32**: 537–540, doi: 10.1130/G20381.1.

Hutchinson, R. A. (1985). Hydrothermal changes in the Upper Geyser Basin, Yellowstone National Park, after the 1983 Borah Peak, Idaho, earthquake, in Proceedings of Workshop 28 on the 1983 Borah Peak, Idaho, Earthquake: *U.S. Geological Survey Open-File Report*, **85-290-A**: 612–624.

Hyndman, R. D. (2015). Tectonics and Structure of the Queen Charlotte Fault Zone, Haida Gwaii, and Large Thrust Earthquakes, *Bulletin of the Seismological Society of America*, **105**: 1058-1075, doi: 10.1785/0120140181

James, T., G. C. Rogers, J. F. Cassidy, H. Dragert, R. Hyndman, L. Leonard, L. Nykolaishen, M. Riedel, M. Schmidt, and K. Wang (2013). Field studies target 2012 Haida Gwaii earthquake, *EOS Transactions of the American Geophysical Union*, **94 (22)**: 197-198, doi: 10.1002/2013EO220002.

Kao, H., S.-J. Shan, A. Bent, C. Woodgold, G. Rogers, J. F. Cassidy, and J. Ristau (2012). Regional centroid-moment-tensor analysis for earthquakes in Canada and adjacent regions: an update, *Seismological Research Letters*, **83**: 505-515, doi: 10.1785/gssrl.83.3.505.

Kao, H., S.-J. Shan, and A. M. Farahbod (2015). Source characteristics of the 2012 Haida Gwaii earthquake sequence, submitted to the 2012 Haida Gwaii Special Volume, *Bulletin of the Seismological Society of America*, **105**: 1206-1218, doi: 10.1785/0120140165

Lamontagne, M., S. Halchuk, J. F. Cassidy, and G. C. Rogers (2008). Significant Canadian Earthquakes of the period 1600-2006. *Seismological Research Letters*, **79**: 211-223, doi: 1.1785/gssrl.79.2.211.

Lay, T., L., Ye, H. Kanamori, Y. Yamazaki, K. F. Cheung, K. Kwong, and K. D. Koper (2013). The October 28, 2012 M_W 7.8 Haida Gwaii underthrusting earthquake and tsunami: Slip partitioning along the Queen Charlotte Fault transpressional plate boundary. *Earth and Planetary Science Letters*, **375**: 57–70, doi: 10.1016/j.epsl.2013.05.005.

Leonard, L. J., and Bednarski, J. M. (2014). Field survey following the 28 October 2012 Haida Gwaii tsunami, *Pure and Applied Geophysics*, **171**: 3467-3482, doi: 10.1007/s00024-014-0792-0.

Leonard, L. J., and J. M. Bednarski (2015). The Preservation Potential of Coastal Coseismic and Tsunami Evidence Observed Following the 2012 M_W 7.8 Haida Gwaii Thrust Earthquake, *Bulletin of the Seismological Society of America*, **105**: 1280-1289, doi:10.1785/0120140193.

Millard, T. (2012). Landslides associated with the October 27, 2012 earthquake in Haida Gwaii, *Memorandum of the BC Ministry of Forests, Lands and Natural Resource Operations*, 9 pp.

Millard, T., M. Geertsema, J. J. Clague, P. Bobrowsky, A. Hasler, and M. Sakals (2012). Landslides on Haida Gwaii during and after the Earthquake, *Risky Ground*, **winter edition**: 12-13.

Milne, W.G. (1956). Seismic activity in Canada west of the 113° meridian, 1841-1951: *Publications of the Dominion Observatory*, Ottawa, **18**: 119-145.

National Geophysical Data Center/World Data System (NGDC/WDS) Global Historical Tsunami Database, Boulder, CO, USA. Available at: `http://www.ngdc.noaa.gov/hazard/tsu_db.shtml` (last accessed October 2013).

Natural Resources Canada / Geological Survey of Canada's "Did you feel it?" reports: `http://www.earthquakescanada.ca` (last accessed 27 January 2015).

Nykolaishen, L., H. Dragert, K. Wang, T. James, and M. Schmidt (2015). GPS Observations of Crustal Deformation Associated with the 2012 M_W 7.8 Haida Gwaii Earthquake, *Bulletin of the Seismological Society of America*, **105**: 1241-1252, doi:10.1785/0120140177.

Ottemöller, L., P. Voss, and J. Havskov (2012). SEISAN Earthquake Analysis Software, University of Bergen.

Ozawa, S., T. Nishimura, H. Munekane, H. Suito, T. Kobayashi, M. Tobia, and T. Imakiire (2012). Preceding, coseismic, and postseismic slips of the 2011 Tohoku earthquake, Japan. *Journal of Geophysical Research*, **117**: B07404, doi: 10.1029/2011JB009120.

Rinehart, J.S. (1972). Fluctuations in geyser activity caused by variations in earth tidal forces, barometric pressure, and tectonic stress, *Journal of Geophysical Research*, **77**: 342–350.

Ristau, J., G. C. Rogers, and J. F. Cassidy (2007). Stress in western Canada from regional moment tensor analysis, *Canadian Journal of Earth Sciences*, **44**: 127-148, doi: 10.1139/e06-057.

Roberts, R. G., A. Christoffersson, and F. Cassidy (1989). Real-time event detection, phase identification and source location estimation using single station three-component seismic data, *Geophysics Journal International*, **97**: 471-480.

Rohr, K. (2015). Plate boundary adjustment of the southernmost Queen Charlotte fault. *Bulletin of the Seismological Society of America*, **105**: 1076-1089, doi: 10.1785/0120140162.

Rogers, G. C. (1986). Seismic gaps along the Queen Charlotte Fault. *Earthquake Prediction Research*, **4**: 1–11.

Rosenberger, A., A. Bird, M. E. Turek, S. Huffman, G. Rogers, J. Cassidy, and T. Mulder (2013). Strong motion data from the magnitude 7.7 "Haida Gwaii" earthquake on October 27, 2012 (local time). *Geological Survey of Canada Open File 7324*, 35 pp, doi: 10.4095/292275.

Sun, T., K. Wang, T. Iinuma, R. Hino, J. He, H. Fujimoto, M. Kido, Y. Osada, S. Miura, Y. Ohta, and Y. Hu (2014). Prevalence of viscoelastic relaxation after the 2011 Tohoku-oki earthquake. *Nature*, **514**: 84-87, doi:10.1038/nature13778.

United States Geological Survey's "Did you feel it?" reports: `http://earthquake.usgs.gov/research/dyfi` (last accessed 27 January 2015).

Wald, D. J., V. Quitoriano, B. Worden, M. Hopper, and J. W. Dewey (2011). USGS "Did You Feel It?" Internet-based macroseismic intensity maps; *Annals of Geophysics*, **54**: 688-707, doi: 10.4401/ag-5354 plus appendix.

Wald, D. J., and T. I. Allen (2007). Topographic slope as a proxy for seismic site conditions and amplification, *Bulletin of the Seismological Society of America*, **97**: 1379-1395, doi: 10.1785/0120060267.

Wald, D. J., P. S. Earle, K. Lin, V. Quitoriano, and B. Worden (2006). Challenges in rapid ground motion estimation for the prompt assessment of global urban earthquakes, *Bulletin of the Earthquake Research Institute*, **81**: 272-281.

Wald, D. J., V. Quitoriano, T. H. Heaton, H. Kanamori, C. W. Scrivner, and B. C. Worden (1999). TriNet "ShakeMaps": Rapid generation of peak ground-motion and intensity maps for earthquakes in southern California, *Earthquake Spectra*, **15**: 537-556, doi: 10.1193/1.1586057.

Wang, K., Y. Hu, and J. He (2012). Deformation cycles of subduction earthquakes in a viscoelastic Earth. *Nature*, **484**: 327-332, doi: 10.1038/nature11032.

Wessel, P., and W. H. F. Smith (1998). New, improved version of the Generic Mapping Tools Released, *EOS Transactions, AGU*, **79**: 579, doi: 10.1029/98EO00426.

Worden, C. B., M. C. Gerstenberger, D. A. Rhoades, and D. J. Wald (2012). Probabilistic relationships between ground-motion parameters and Modified Mercalli Intensity in California, *Bulletin of the Seismological Society of America*, **102**: 204-221, doi: 10.1785/0120110156.

Worden, C. B., D. J. Wald, T. I. Allen, K. Lin, D. Garcia, and G. Cua (2010). A revised ground-motion and intensity interpolation scheme for ShakeMap, *Bulletin of the Seismological Society of America*, **100**: 3083–3096, doi: 10.1785/0120100101.

Zhao, J. X., J. Zhang, A. Asano, Y. Ohno, T. Oouchi, T. Takahashi, H. Ogawa, K. Irikura, H. K. Thio, P. G. Somerville, Y. Fukushima, and Y. Fukushima (2006). Attenuation relations of strong ground motion in Japan using site classification based on predominant period, *Bulletin of the Seismological Society of America*, **96**: 898–913, doi: 10.1785/0120050122.

7

Statistics of Collected Data

7.1 Introduction

The ISC Bulletin is based on the parametric data reports received from seismological agencies around the world. With rare exceptions, these reports include the results of waveform review done by analysts at network data centres and observatories. These reports include combinations of various bulletin elements such as event hypocentre estimates, moment tensors, magnitudes, event type and felt and damaging data as well as observations of the various seismic waves recorded at seismic stations.

Data reports are received in different formats that are often agency specific. Once an authorship is recognised, the data are automatically parsed into the ISC database and the original reports filed away to be accessed when necessary. Any reports not recognised or processed automatically are manually checked, corrected and re-processed. This chapter describes the data that are received at the ISC before the production of the reviewed Bulletin.

Notably, the ISC integrates all newly received data reports into the automatic ISC Bulletin (available on-line) soon after these reports are made available to ISC, provided it is done before the submission deadline that currently stands at 12 months following an event occurrence.

With data constantly being reported to the ISC, even after the ISC has published its review, the total data shown as collected, in this chapter, is limited to two years after the time of the associated reading or event, i.e. any hypocentre data collected two years after the event are not reflected in the figures below.

7.2 Summary of Agency Reports to the ISC

A total of 142 agencies have reported data for July 2012 to December 2012. The parsing of these reports into the ISC database is summarised in Table 7.1.

Table 7.1: *Summary of the parsing of reports received by the ISC from a total of 142 agencies, containing data for this summary period.*

	Number of reports
Total collected	3948
Automatically parsed	3218
Manually parsed	730

Data collected by the ISC consists of multiple data types. These are typically one of:

- Bulletin, hypocentres with associated phase arrival observations.

- Catalogue, hypocentres only.
- Unassociated phase arrival observations.

In Table 7.2, the number of different data types reported to the ISC by each agency is listed. The number of each data type reported by each agency is also listed. Agencies reporting indirectly have their data type additionally listed for the agency that reported it. The agencies reporting indirectly may also have 'hypocentres with associated phases' but with no associated phases listed - this is because the association is being made by the agency reporting directly to the ISC. Summary maps of the agencies and the types of data reported are shown in Figure 7.1 and Figure 7.2.

Table 7.2: *Agencies reporting to the ISC for this summary period. Entries in bold are for new or renewed reporting by agencies since the previous six-month period.*

Agency	Country	Directly or indirectly reporting (D/I)	Hypocentres with associated phases	Hypocentres without associated phases	Associated phases	Unassociated phases	Amplitudes
TIR	Albania	D	363	60	2904	271	0
CRAAG	Algeria	D	436	23	2213	439	0
LPA	Argentina	D	0	0	0	398	10
SJA	Argentina	D	3628	14	59000	0	9191
NSSP	Armenia	D	60	10	293	0	0
AUST	Australia	D	908	5	19266	0	0
IDC	Austria	D	17077	0	376391	0	347771
VIE	Austria	D	3641	232	31536	206	30856
AZER	Azerbaijan	D	410	25	13735	0	0
BELR	Belarus	D	0	0	0	2892	605
UCC	Belgium	D	0	1	0	3743	947
SCB	Bolivia	D	23	0	617	0	92
SAR	Bosnia and Herzegovina	D	663	137	12588	6430	0
MASS	**Brazil**	**I IASPEI**	**0**	**0**	**0**	**30**	**0**
VAO	Brazil	D	0	0	0	1113	0
SOF	Bulgaria	D	37	10	233	2111	0
OTT	Canada	D	1093	1728	28428	0	2641
PGC	Canada	I OTT	782	1635	18981	0	0
GUC	Chile	D	2640	59	55109	963	15310
BJI	China	D	2304	33	122800	20931	69927
ASIES	Chinese Taipei	D	0	42	0	0	0
TAP	Chinese Taipei	D	13985	8	431622	0	0
RSNC	Colombia	D	6466	1	110602	13279	32975
ICE	**Costa Rica**	**I UCR**	**24**	**1**	**0**	**0**	**0**
UCR	Costa Rica	D	840	7	25257	0	2719
ZAG	Croatia	D	0	0	0	9996	0
NIC	Cyprus	D	184	22	1278	445	0
IPEC	Czech Republic	D	382	58	2479	21388	1137
PRU	Czech Republic	D	4238	413	31621	289	9118
WBNET	Czech Republic	D	112	0	2284	0	2238
DNK	Denmark	D	1	18	0	6221	2009
ARO	Djibouti	D	91	0	858	0	0
IGQ	Ecuador	D	95	2	3185	39	104
HLW	Egypt	D	174	23	1466	0	0
SNET	El Salvador	I NEIC	6	28	0	0	0
EST	Estonia	I HEL	304	13	0	0	0
AAE	Ethiopia	D	25	2	163	773	4
SKO	FYR Macedonia	D	1169	1	9930	3676	3612
FIA0	Finland	I HEL	172	22	0	0	0
HEL	Finland	D	5964	3318	104782	0	16941
CSEM	France	D	8519	11130	151753	0	30682
LDG	France	D	1854	280	36859	44	15260
STR	France	D	444	51	6721	16	0
PPT	French Polynesia	D	1449	0	11886	378	12234
TIF	Georgia	D	0	592	0	17341	0

Table 7.2: *(continued)*

Agency	Country	Directly or indirectly reporting (D/I)	Hypocentres with associated phases	Hypocentres without associated phases	Associated phases	Unassociated phases	Amplitudes
AWI	Germany	D	1813	3	6599	1619	0
BGR	Germany	D	99	141	3495	0	106
BNS	Germany	I BGR	1	23	0	0	0
BRG	Germany	D	0	0	0	5291	4167
BUG	Germany	I BGR	10	1	0	0	0
CLL	Germany	D	0	0	0	8122	2916
GDNRW	Germany	I BGR	0	12	0	0	0
GFZ	Germany	I NEIC	8	2	0	0	0
LEDBW	Germany	I BGR	10	5	0	0	0
ATH	Greece	D	10638	1816	305149	0	105233
THE	Greece	D	3228	535	71202	8781	22819
UPSL	Greece	I CSEM	0	13	0	0	0
HKC	Hong Kong	D	0	0	0	39	0
BUD	Hungary	D	0	3	0	3153	0
REY	Iceland	D	83	9	2863	0	0
HYB	India	D	754	0	1717	11	326
NDI	India	D	623	363	17911	6186	5910
DJA	Indonesia	D	3849	44	74686	0	47063
TEH	Iran	D	939	67	43815	0	25371
THR	Iran	D	254	100	2074	2	631
ISN	Iraq	D	308	38	1979	0	94
DIAS	Ireland	D	0	0	0	212	0
GII	Israel	D	419	19	6976	0	0
GEN	Italy	D	606	87	6721	837	0
MED_RCMT	Italy	D	0	116	0	0	0
OSUB	Italy	D	0	0	0	2682	0
ROM	Italy	D	9605	64	389410	0	245308
TRI	Italy	D	0	0	0	5569	0
LIC	Ivory Coast	D	802	0	2406	0	1603
JSN	Jamaica	D	128	0	736	4	0
JMA	Japan	D	78313	0	605789	447	0
MAT	Japan	D	0	0	0	11874	0
NIED	Japan	D	0	1290	0	0	0
SYO	Japan	D	0	0	0	4392	0
JSO	Jordan	D	11	0	99	0	10
NNC	Kazakhstan	D	8545	14	61611	0	57082
SOME	Kazakhstan	D	3958	164	59991	0	57250
KNET	Kyrgyzstan	D	1386	0	11482	0	2647
KRNET	Kyrgyzstan	D	3423	0	57838	0	0
LVSN	Latvia	D	402	40	5020	483	2671
GRAL	Lebanon	D	268	61	1919	477	0
LIT	Lithuania	D	93	118	769	2431	1507
MCO	Macao, China	D	0	0	0	135	0
GSDM	Malawi	D	0	0	0	226	0
KLM	Malaysia	D	303	1	1148	0	0
ECX	Mexico	D	924	7	14841	0	2164
MEX	Mexico	D	2697	196	19994	0	0
MOLD	Moldova	D	0	3	0	2089	762
PDG	Montenegro	D	498	60	11800	0	6167
CNRM	Morocco	D	1141	401	5658	0	0
DMN	Nepal	D	1712	0	17339	0	13359
DBN	Netherlands	D	0	0	0	1475	383
WEL	New Zealand	D	1326	7	62903	220	14702
BER	Norway	D	2427	1092	31876	3611	7903
NAO	Norway	D	2735	780	5260	0	2239
OMAN	Oman	D	725	35	8717	0	0
MSSP	Pakistan	D	0	0	0	952	0
UPA	**Panama**	**I NEIC**	**0**	**1**	**0**	**0**	**0**
ARE	Peru	I NEIC	1	31	0	0	0
LIM	Peru	I IRIS	2	0	0	0	0
MAN	Philippines	D	0	1712	0	33623	7486
QCP	Philippines	D	0	0	0	92	0
WAR	Poland	D	0	216	0	14571	489
IGIL	Portugal	D	736	1	3852	0	1307

Table 7.2: *(continued)*

Agency	Country	Directly or indirectly reporting (D/I)	Hypocentres with associated phases	Hypocentres without associated phases	Associated phases	Unassociated phases	Amplitudes
INMG	Portugal	D	1327	134	39821	3131	14275
PDA	Portugal	I CSEM	419	94	0	0	0
SVSA	Portugal	D	536	0	8683	3970	4444
KMA	Republic of Korea	D	23	0	244	0	0
BUC	Romania	D	789	10	12076	47121	0
ASRS	Russia	D	26	18	343	0	0
BYKL	Russia	D	128	0	9175	0	3213
CMWS	Russia	I MOS	4	0	0	0	0
DRS	Russia	I MOS	85	218	0	0	0
IDG	**Russia**	**I MOS**	**0**	**285**	**0**	**0**	**0**
IEPN	Russia	D	96	9	409	2054	788
KOLA	Russia	D	165	217	647	0	0
KRAR	**Russia**	**I MOS**	**0**	**177**	**0**	**0**	**0**
KRSC	Russia	D	625	0	21378	0	0
MIRAS	Russia	D	44	42	474	20	293
MOS	Russia	D	3234	1557	434575	0	164523
NERS	Russia	D	16	15	392	0	168
NORS	Russia	I MOS	105	216	0	0	0
SKHL	Russia	D	609	724	21773	0	11890
VKMS	**Russia**	**I MOS**	**0**	**49**	**0**	**0**	**0**
YARS	Russia	D	491	499	10225	0	4107
SGS	Saudi Arabia	D	126	2	719	0	0
BEO	Serbia	D	1471	209	24711	0	10
BRA	Slovakia	D	0	0	0	15175	0
LJU	Slovenia	D	1421	511	20530	5440	6766
HNR	Solomon Islands	D	0	0	0	1829	0
PRE	South Africa	D	792	0	12391	12	4147
MDD	Spain	D	3003	1785	87686	0	72003
MRB	Spain	D	360	3	9181	0	2946
SFS	Spain	D	400	34	2467	231	0
UPP	Sweden	D	1234	1828	13920	0	0
ZUR	Switzerland	D	288	51	5008	0	2606
NSSC	Syria	D	27	0	275	0	112
BKK	Thailand	D	2731	601	18537	0	21711
TRN	Trinidad and Tobago	D	0	1067	0	31859	0
TUN	Tunisia	D	7	2	54	0	0
ATA	Turkey	D	10	0	176	0	34
DDA	Turkey	D	12216	1587	136429	6787	0
ISK	Turkey	D	10671	1644	136183	11067	66662
AEIC	U.S.A.	I NEIC	59	47	0	0	0
ANF	U.S.A.	I IRIS	1379	915	0	0	0
BRK	U.S.A.	I NEIC	0	0	0	0	0
BUT	U.S.A.	I NEIC	2	11	0	0	0
CERI	U.S.A.	I IRIS	60	23	0	0	0
GCMT	U.S.A.	D	0	3323	0	0	0
HVO	U.S.A.	I NEIC	0	1	0	0	0
IASPEI	U.S.A.	D	0	0	0	30	0
IRIS	U.S.A.	D	3477	3705	322244	0	0
LDO	U.S.A.	I NEIC	0	7	0	0	0
NCEDC	U.S.A.	I NEIC	161	93	0	0	0
NEIC	U.S.A.	D	15174	4950	816609	0	321001
OGSO	**U.S.A.**	**I NEIC**	**0**	**1**	**0**	**0**	**0**
PAS	U.S.A.	I NEIC	211	75	0	0	0
PNSN	U.S.A.	D	0	98	0	0	0
REN	U.S.A.	I IRIS	30	22	0	0	0
RSPR	U.S.A.	D	2123	3	24231	0	0
SCEDC	U.S.A.	I IRIS	262	218	0	0	0
SEA	U.S.A.	I IRIS	22	10	57	0	0
SLC	U.S.A.	I IRIS	8	1	0	0	0
SLM	U.S.A.	I NEIC	0	1	0	0	0
TUL	U.S.A.	I IRIS	18	0	0	0	0
UUSS	U.S.A.	I IRIS	0	8	0	0	0
WES	U.S.A.	I IRIS	1	2	0	0	0

Table 7.2: *(continued)*

Agency	Country	Directly or indirectly reporting (D/I)	Hypocentres with associated phases	Hypocentres without associated phases	Associated phases	Unassociated phases	Amplitudes
SIGU	Ukraine	D	63	61	1681	0	543
DSN	United Arab Emirates	D	562	30	7246	0	0
BGS	United Kingdom	D	233	59	7868	67	3014
EAF	Unknown	D	373	3	1978	18464	602
MOSS	**Unknown**	**I MOS**	**0**	**0**	**13656**	**0**	**0**
SIK	Unknown	D	54	16	539	0	0
CAR	Venezuela	I NEIC	0	3	0	0	0
FUNV	Venezuela	I IRIS	1	0	0	0	0
PLV	Vietnam	D	11	0	378	0	210
DHMR	Yemen	D	110	8	1097	1110	479
LSZ	Zambia	D	7	0	24	98	4
BUL	Zimbabwe	D	171	1	796	586	0

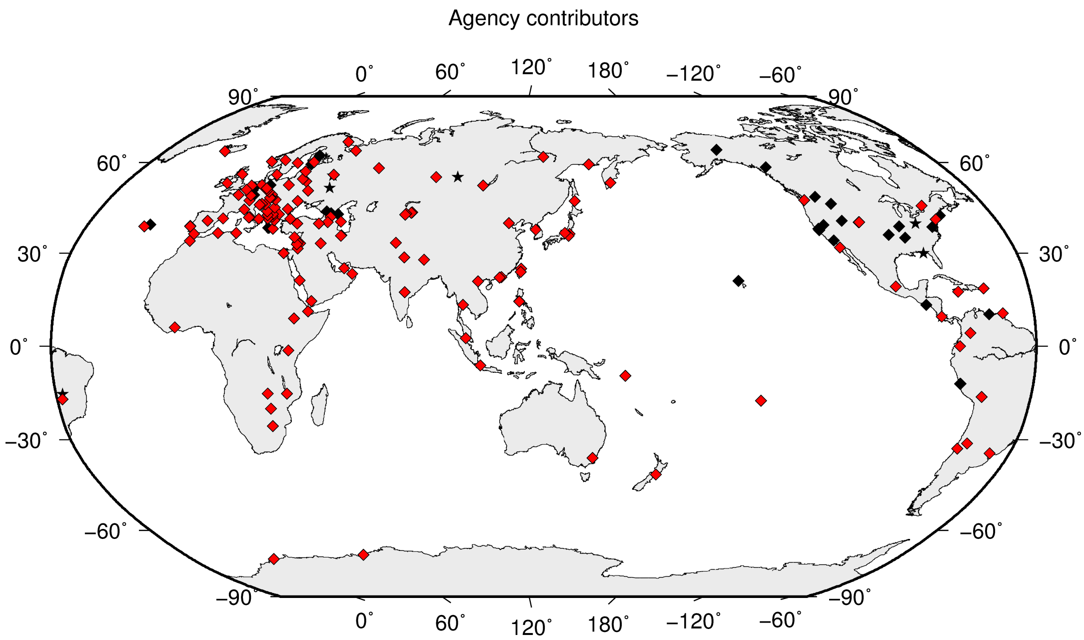

Figure 7.1: *Map of agencies that have contributed data to the ISC for this summary period. Agencies that have reported directly to the ISC are shown in red. Those that have reported indirectly (via another agency) are shown in black. Any new or renewed agencies, since the last six-month period, are shown by a star. Each agency is listed in Table 7.2.*

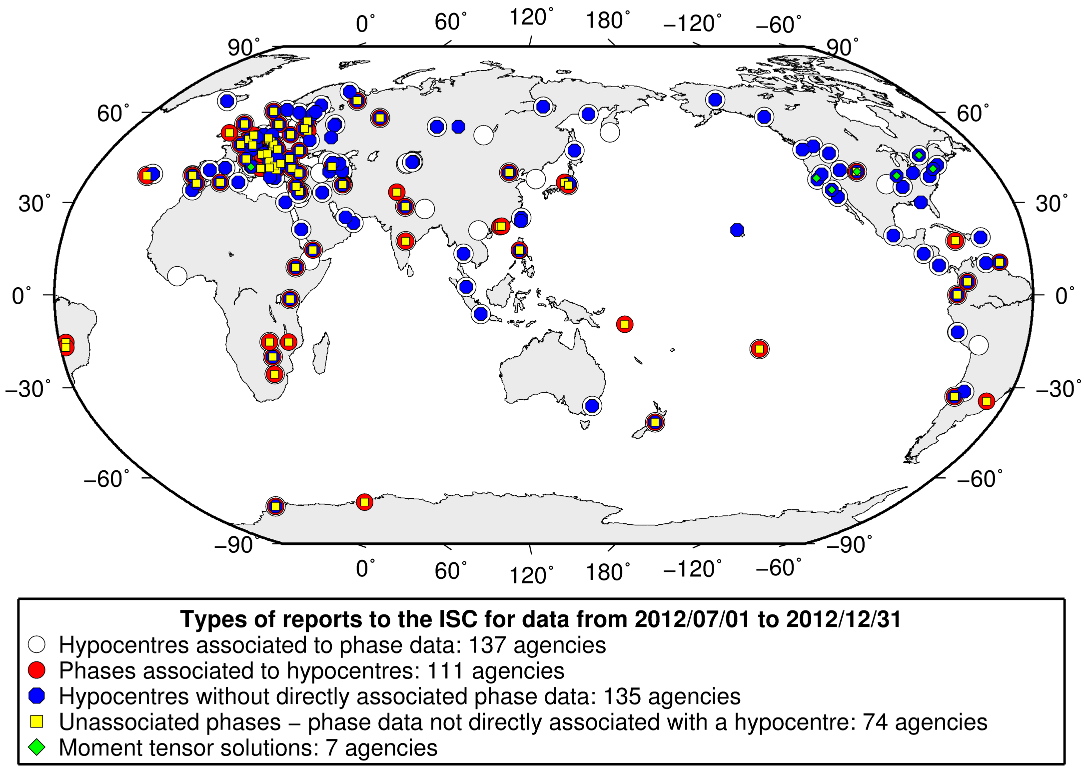

Figure 7.2: *Map of the different data types reported by agencies to the ISC. A full list of the data types reported by each agency is shown in Table 7.2.*

7.3 Arrival Observations

The collection of phase arrival observations at the ISC has increased dramatically with time. The increase in reported phase arrival observations is shown in Figure 7.3.

The reports with phase data are summarised in Table 7.3. This table is split into three sections, providing information on the reports themselves, the phase data, and the stations reporting the phase data. A map of the stations contributing these phase data is shown in Figure 7.4.

The ISC encourages the reporting of phase arrival times together with amplitude and period measurements whenever feasible. Figure 7.5 shows the percentage of events reported by each station was accompanied with amplitude and period measurements.

Figure 7.6 indicates the number of amplitude and period measurement for each station.

Together with the increase in the number of phases (Figure 7.3), there has been an increase in the number of stations reported to the ISC. The increase in the number of stations is shown in Figure 7.7. This increase can also be seen on the maps for stations reported each decade in Figure 7.8.

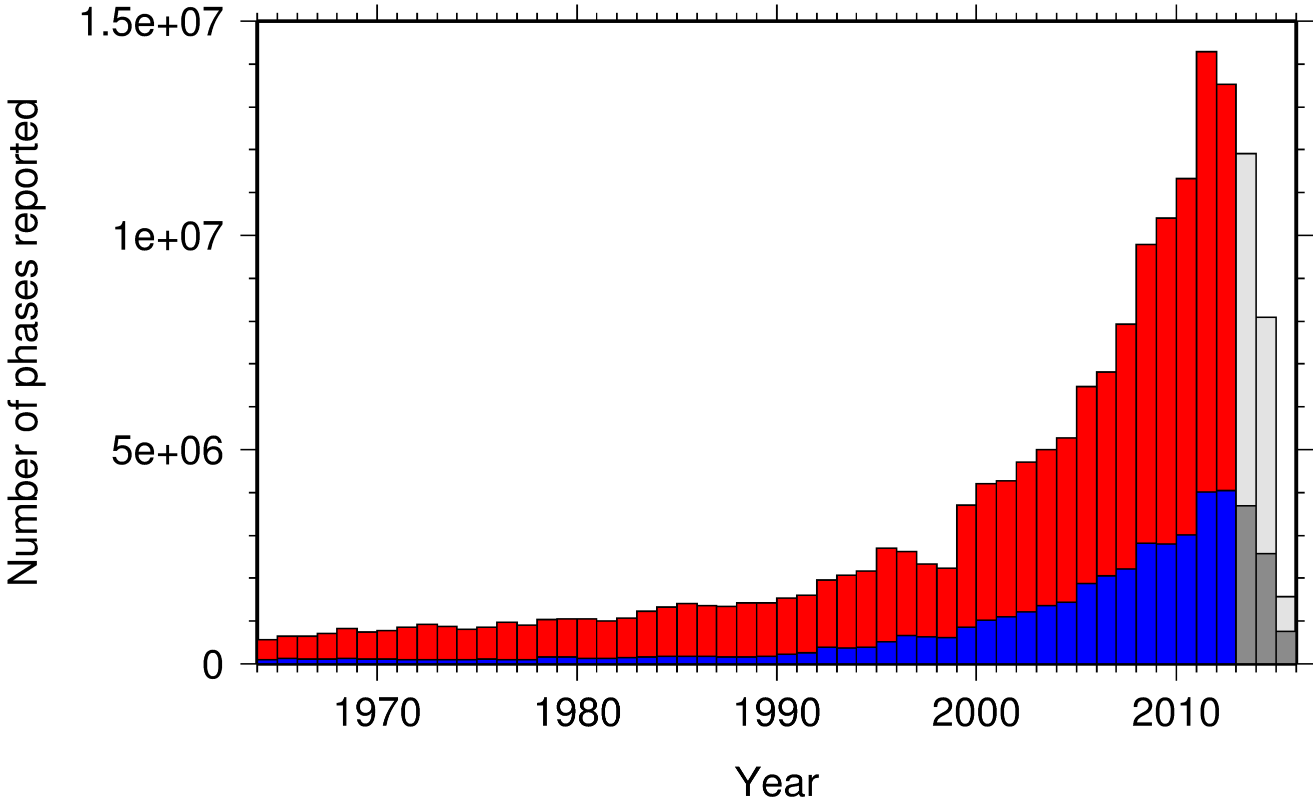

Figure 7.3: *Histogram showing the number of phases (red) and number of amplitudes (blue) collected by the ISC for events each year since 1964. The data in grey covers the current period where data are still being collected before the ISC review takes place and is accurate at the time of publication.*

Table 7.3: *Summary of reports containing phase arrival observations.*

Reports with phase arrivals	3394
Reports with phase arrivals including amplitudes	660
Reports with only phase arrivals (no hypocentres reported)	287
Total phase arrivals received	6177316
Total phase arrival-times received	5639438
Number of duplicate phase arrival-times	575703 (10.2%)
Number of amplitudes received	1952326
Stations reporting phase arrivals	6969
Stations reporting phase arrivals with amplitude data	3500
Max number of stations per report	2161

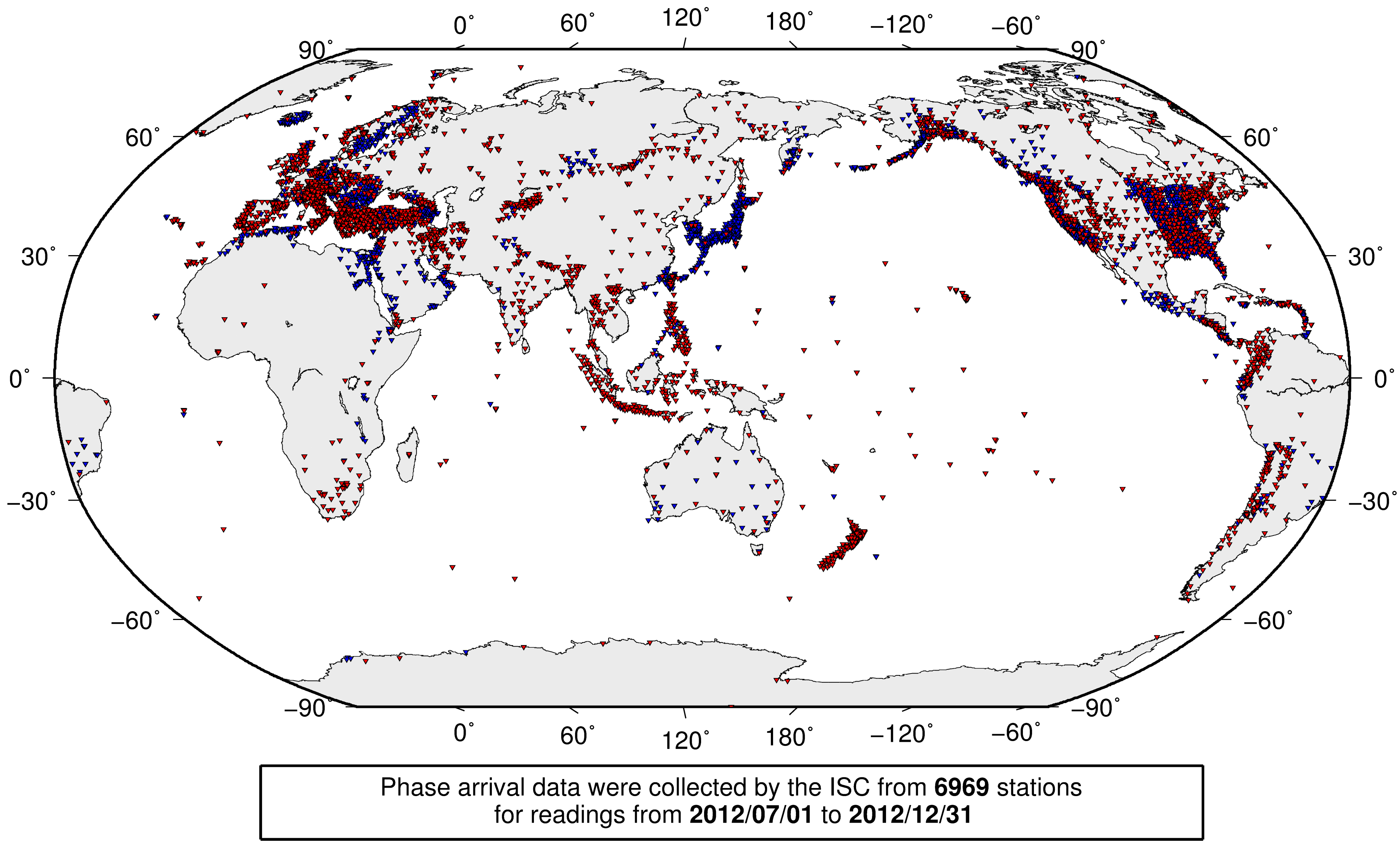

Figure 7.4: *Stations contributing phase data to the ISC for readings from July 2012 to the end of December 2012. Stations in blue provided phase arrival times only; stations in red provided both phase arrival times and amplitude data.*

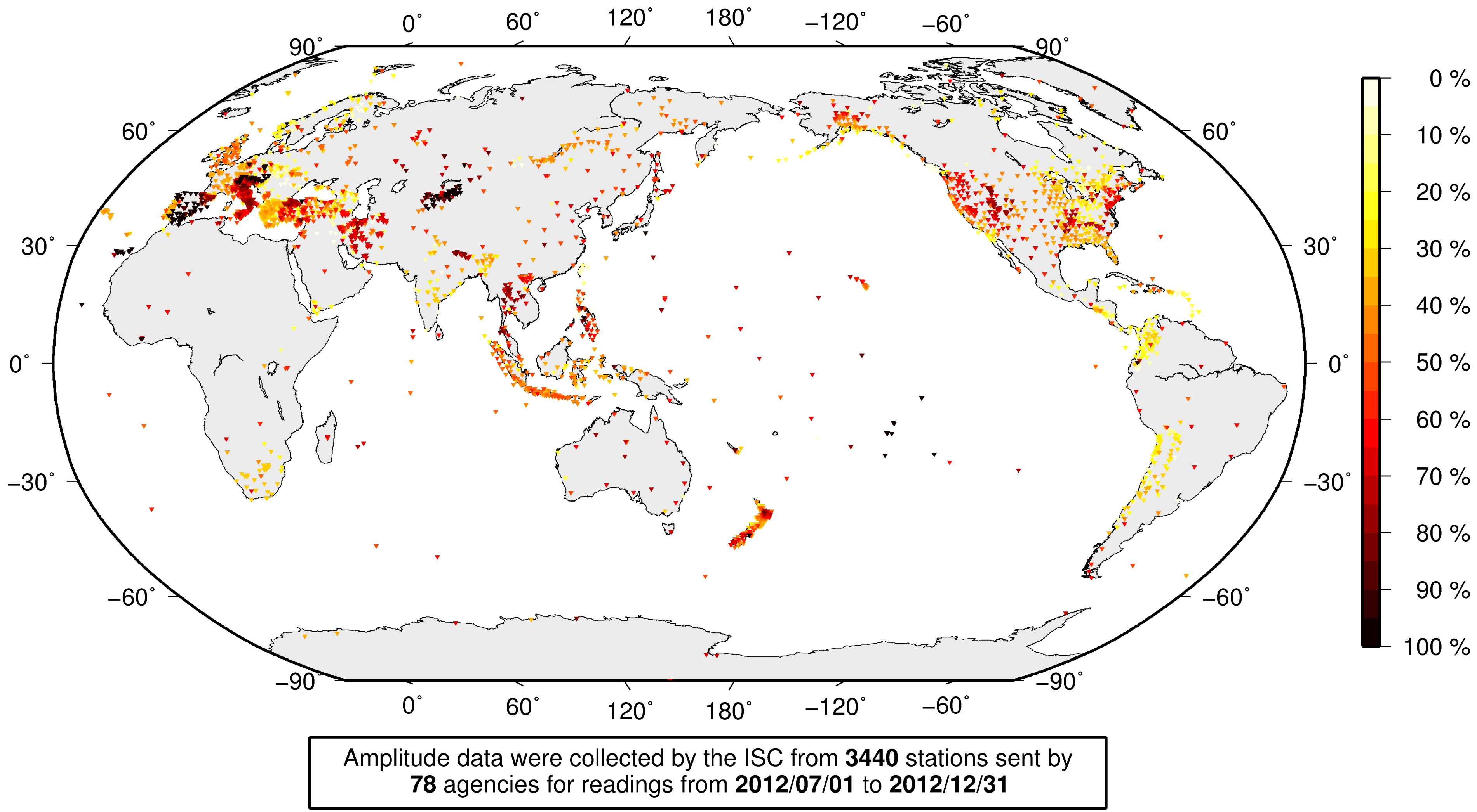

Figure 7.5: *Percentage of events for which phase arrival times from each station are accompanied with amplitude and period measurements.*

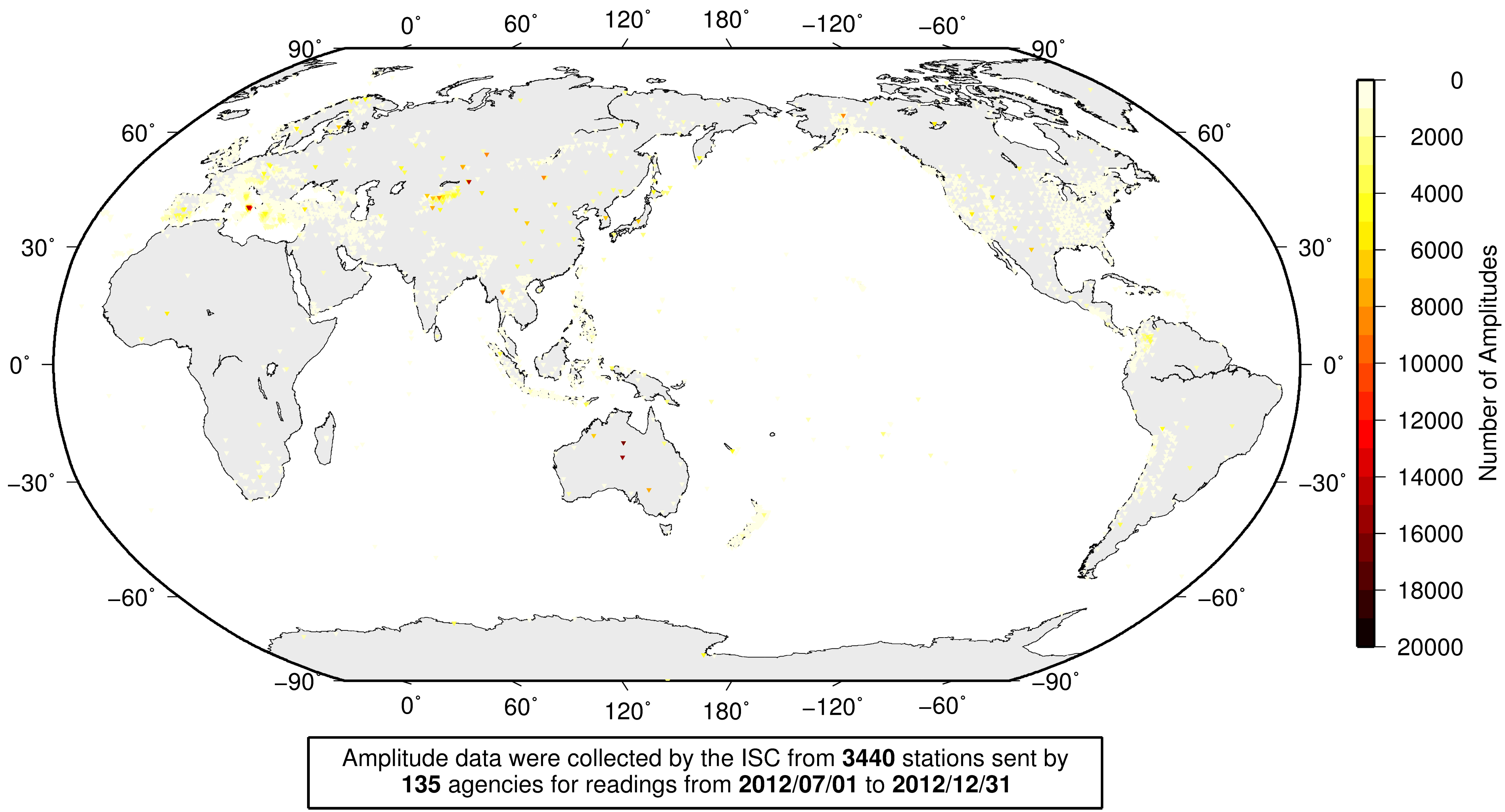

Figure 7.6: *Number of amplitude and period measurements for each station.*

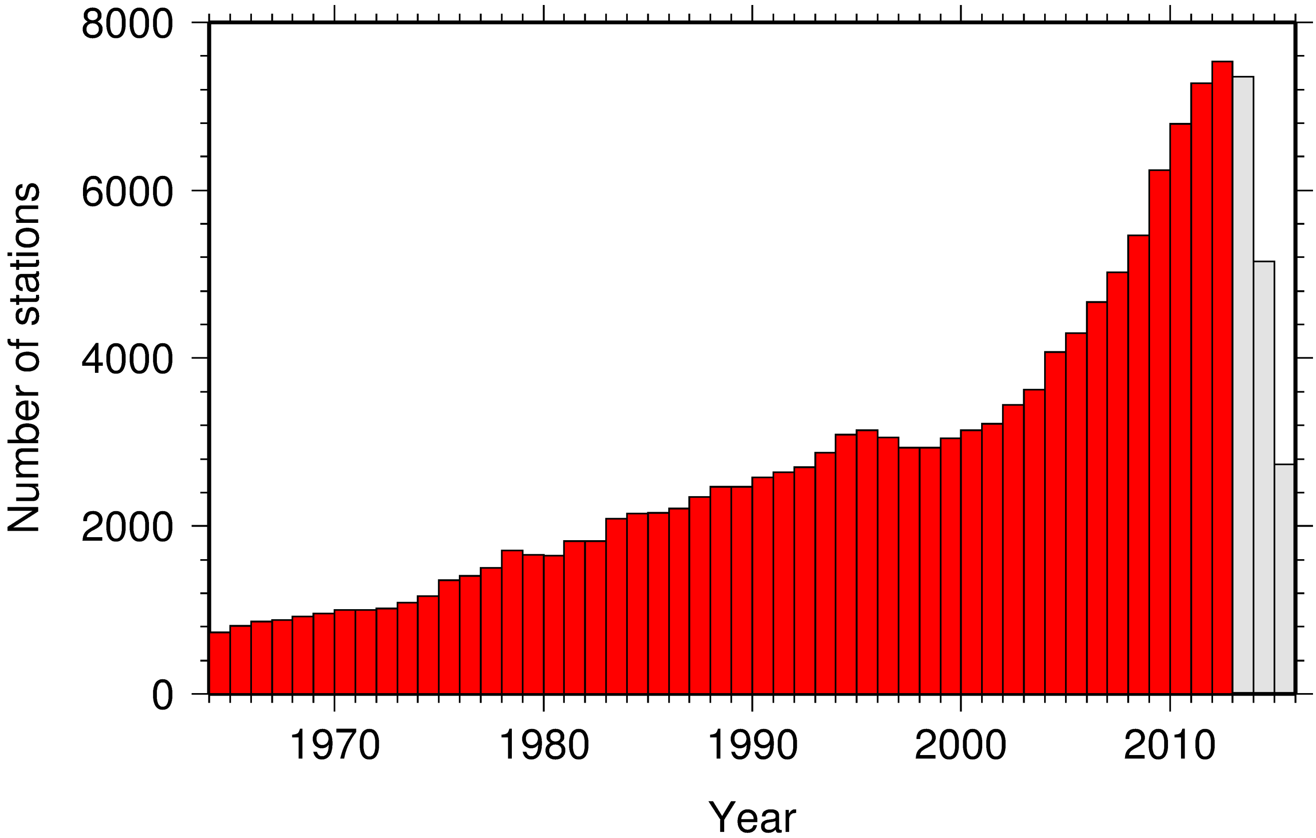

Figure 7.7: *Histogram showing the number of stations reporting to the ISC each year since 1964. The data in grey covers the current period where station information is still being collected before the ISC review of events takes place and is accurate at the time of publication.*

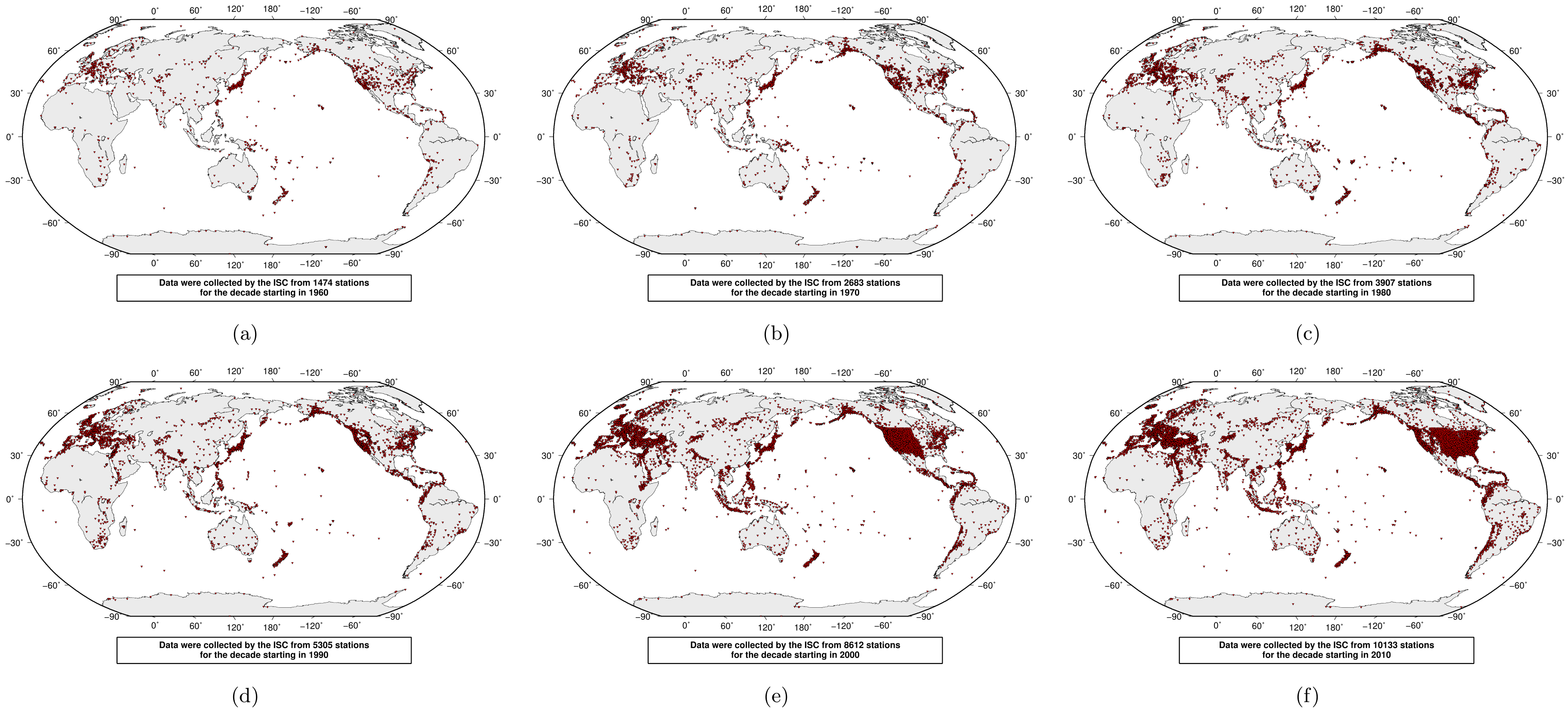

Figure 7.8: *Maps showing the stations reported to the ISC for each decade since 1960. Note that the last map covers a shorter time period.*

7.4 Hypocentres Collected

The ISC Bulletin groups multiple estimates of hypocentres into individual events, with an appropriate prime hypocentre solution selected. The collection of these hypocentre estimates are described in this section.

The reports containing hypocentres are summarised in Table 7.4. The number of hypocentres collected by the ISC has also increased significantly since 1964, as shown in Figure 7.9. A map of all hypocentres reported to the ISC for this summary period is shown in Figure 7.10. Where a network magnitude was reported with the hypocentre, this is also shown on the map, with preference given to reported values, first of M_W followed by M_S, m_b and M_L respectively (where more than one network magnitude was reported).

Table 7.4: *Summary of the reports containing hypocentres.*

Reports with hypocentres	3661
Reports of hypocentres only (no phase readings)	554
Total hypocentres received	317853
Number of duplicate hypocentres	22234 (7.0%)
Agencies determining hypocentres	161

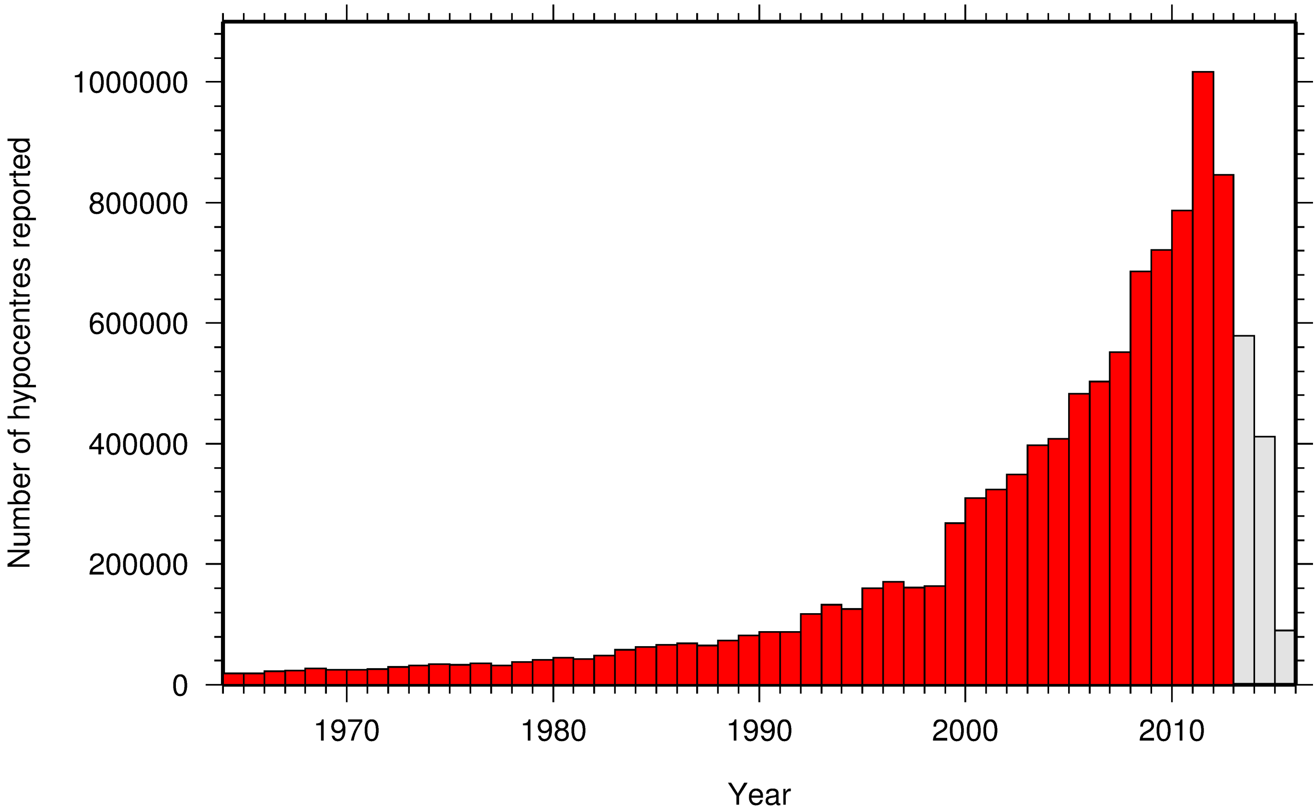

Figure 7.9: *Histogram showing the number of hypocentres collected by the ISC for events each year since 1964. For each event, multiple hypocentres may be reported.*

All the hypocentres that are reported to the ISC are automatically grouped into events, which form the basis of the ISC Bulletin. For this summary period 350966 hypocentres (including ISC) were grouped

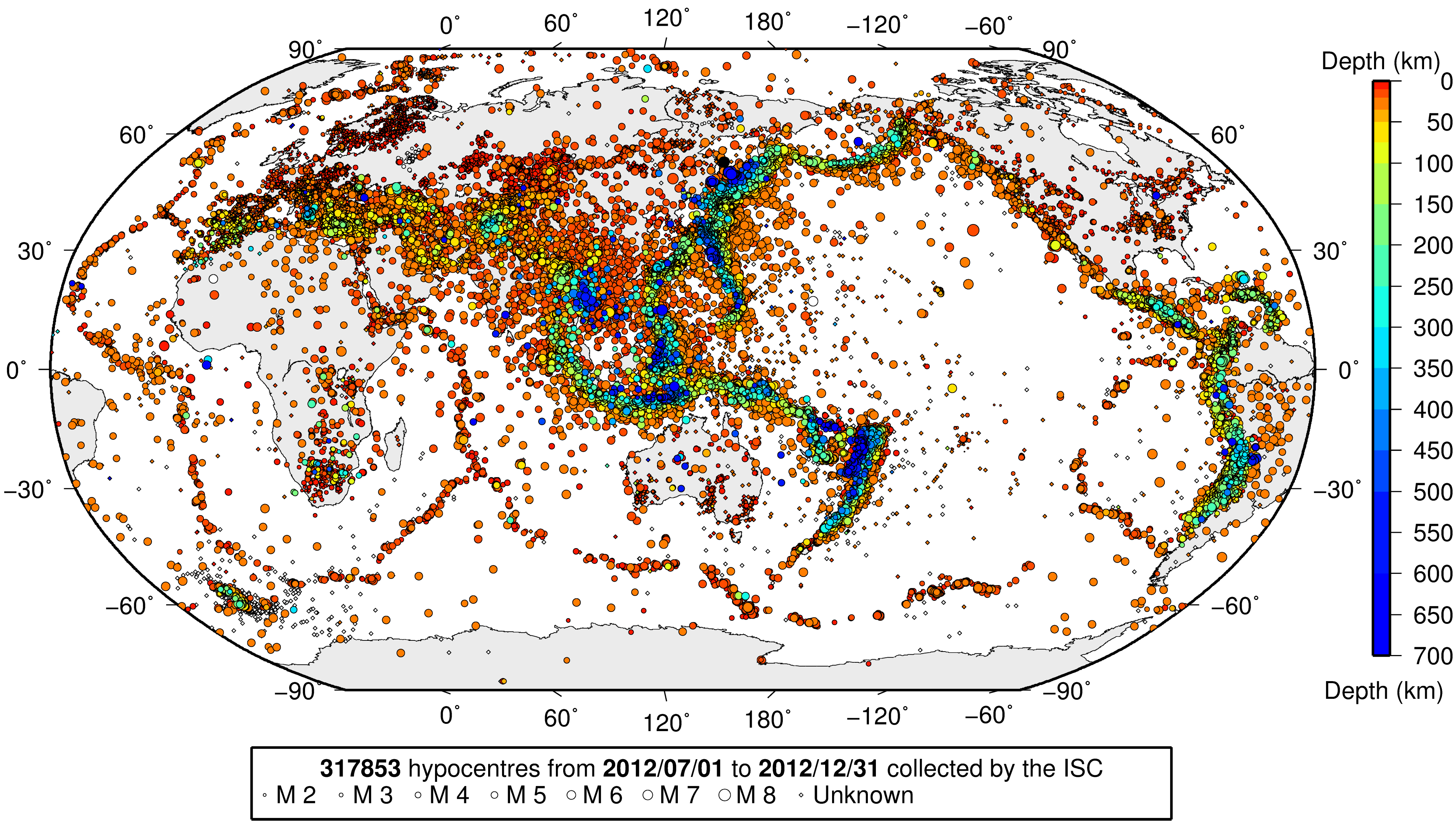

Figure 7.10: *Map of all hypocentres collected by the ISC. The scatter shows the large variation of the multiple hypocentres that are reported for each event. The magnitude corresponds with the reported network magnitude. If more than one network magnitude type was reported, preference was given to values of* M_W*,* M_S*,* m_b *and* M_L *respectively. Compare with Figure 8.2*

into 216109 events, the largest of these having 68 hypocentres in one event. The total number of events shown here is the result of an automatic grouping algorithm, and will differ from the total events in the published ISC Bulletin, where both the number of events and the number of hypocentre estimates will have changed due to further analysis. The process of grouping is detailed in Section 3.3.1 of January to June 2012 Bulletin Summary. Figure 8.2 on page 99 shows a map of all prime hypocentres.

7.5 Collection of Network Magnitude Data

Data contributing agencies normally report earthquake hypocentre solutions along with magnitude estimates. For each seismic event, each agency may report one or more magnitudes of the same or different types. This stems from variability in observational practices at regional, national and global level in computing magnitudes based on a multitude of wave types. Differences in the amplitude measurement algorithm, seismogram component(s) used, frequency range, station distance range as well as the instrument type contribute to the diversity of magnitude types. Table 7.5 provides an overview of the complexity of reported network magnitudes reported for seismic events during this summary period.

Table 7.5: *Statistics of magnitude reports to the ISC; M – average magnitude of estimates reported for each event.*

	M<3.0	3.0≤M<5.0	M≥5.0
Number of seismic events	163183	32838	398
Average number of magnitude estimates per event	1.3	5.0	30.2
Average number of magnitudes (by the same agency) per event	1.1	2.7	4.3
Average number of magnitude types per event	1.1	4.1	11.2
Number of magnitude types	19	28	29

Table 7.6 gives the basic description, main features and scientific paper references for the most commonly reported magnitude types.

Table 7.6: *Description of the most common magnitude types reported to the ISC.*

Magnitude type	Description	References	Comments
M	Unspecified		Often used in real or near-real time magnitude estimations
mB	Medium-period and Broad-band body-wave magnitude	*Gutenberg* (1945a); *Gutenberg* (1945b); *IASPEI* (2005); *IASPEI* (2013); *Bormann et al.* (2009); *Bormann and Dewey* (2012)	
mb	Short-period body-wave magnitude	*IASPEI* (2005); *IASPEI* (2013); *Bormann et al.* (2009); *Bormann and Dewey* (2012)	Classical mb based on stations between 21°-100° distance

Table 7.6: *continued*

Magnitude type	Description	References	Comments
mb1	Short-period body-wave magnitude	*IDC* (1999) and references therein	Reported only by the IDC; also includes stations at distances less than 21°
mb1mx	Maximum likelihood short-period body-wave magnitude	*Ringdal* (1976); *IDC* (1999) and references therein	Reported only by the IDC
mbtmp	short-period body-wave magnitude with depth fixed at the surface	*IDC* (1999) and references therein	Reported only by the IDC
mbLg	Lg-wave magnitude	*Nuttli* (1973); *IASPEI* (2005); *IASPEI* (2013); *Bormann and Dewey* (2012)	Also reported as MN
Mc	Coda magnitude		
MD (Md)	Duration magnitude	*Bisztricsany* (1958); *Lee et al.* (1972)	
ME (Me)	Energy magnitude	*Choy and Boatwright* (1995)	Reported only by NEIC
MJMA	JMA magnitude	*Tsuboi* (1954)	Reported only by JMA
ML (Ml)	Local (Richter) magnitude	*Richter* (1935); *Hutton and Boore* (1987); *IASPEI* (2005); *IASPEI* (2013)	
MLSn	Local magnitude calculated for Sn phases	*Balfour et al.* (2008)	Reported by PGC only for earthquakes west of the Cascadia subduction zone
MLv	Local (Richter) magnitude computed from the vertical component		Reported only by DJA and BKK
MN (Mn)	Lg-wave magnitude	*Nuttli* (1973); *IASPEI* (2005)	Also reported as mbLg
MS (Ms)	Surface-wave magnitude	*Gutenberg* (1945c); *Vaněk et al.* (1962); *IASPEI* (2005)	Classical surface-wave magnitude computed from station between 20°-160° distance
Ms1	Surface-wave magnitude	*IDC* (1999) and references therein	Reported only by the IDC; also includes stations at distances less than 20°
ms1mx	Maximum likelihood surface-wave magnitude	*Ringdal* (1976); *IDC* (1999) and references therein	Reported only by the IDC

Table 7.6: *continued*

Magnitude type	Description	References	Comments
Ms7	Surface-wave magnitude	*Bormann et al.* (2007)	Reported only by BJI and computed from records of a Chinese-made long-period seismograph in the distance range 3°-177°
MW (Mw)	Moment magnitude	*Kanamori* (1977); *Dziewonski et al.* (1981)	Computed according to the *IASPEI* (2005) and *IASPEI* (2013) standard formula
Mw(mB)	Proxy Mw based on mB	*Bormann and Saul* (2008)	Reported only by DJA and BKK
Mwp	Moment magnitude from P-waves	*Tsuboi et al.* (1995)	Reported only by DJA and BKK and used in rapid response
mbh	Unknown		
mbv	Unknown		
MG	Unspecified type		Contact contributor
Mm	Unknown		
msh	Unknown		
MSV	Unknown		

Table 7.7 lists all magnitude types reported, the corresponding number of events in the ISC Bulletin and the agency codes along with the number of earthquakes.

Table 7.7: *Summary of magnitude types in the ISC Bulletin for this summary period. The number of events with values for each magnitude type is listed. The agencies reporting these magnitude types are listed, together with the total number of values reported.*

Magnitude type	Events	Agencies reporting magnitude type (number of values)
M	2181	SKO (900), STR (299), IDG (285), KRAR (170), MOS (144), SKHL (111), KOLA (85), VKMS (49), FDF (35), PRU (20), IGQ (19), ASRS (17), MIRAS (16), NERS (15), JSO (10), YARS (8), BKK (1)
mB	2189	BJI (1890), DJA (735), IGQ (15), STR (3), BKK (1), BER (1)
MB	13	NEIC (13)
mb	25738	IDC (16382), NEIC (6134), NNC (4709), KRNET (3418), MOS (2199), BJI (1853), MAN (1664), VIE (1263), DJA (1138), MDD (275), CSEM (92), NIC (55), PGC (51), DSN (43), SIGU (38), IASPEI (33), KLM (31), GII (24), IGQ (14), NDI (14), STR (7), UCR (3), PDA (3), CRAAG (2), DMN (2), PDG (2), IGIL (1), JSO (1), BER (1), DHMR (1), BKK (1), AZER (1), BGS (1)
mb1	16884	IDC (16884)
mb1mx	16884	IDC (16884)
mbLg	2721	MDD (2718), NEIC (2), TUL (1)

Table 7.7: *Continued.*

Magnitude type	Events	Agencies reporting magnitude type (number of values)
mbtmp	16884	IDC (16884)
MD	12079	RSPR (3114), MEX (3047), LDG (1495), ECX (889), ROM (887), TRN (854), BUC (789), DDA (527), TIR (364), UCR (363), PDA (297), GRAL (268), GII (223), NCEDC (161), HLW (126), PDG (107), PNSN (80), SNET (75), JSN (63), SJA (52), CSEM (50), EAF (50), INMG (48), SVSA (43), CERI (36), HVO (29), ISK (27), SOF (21), SEA (18), BUL (17), BUT (14), TUN (7), HDC (5), LSZ (5), SIGU (4), IGQ (4), PGC (2), THR (2), WES (1), JSO (1), FDF (1), UPA (1), CAR (1), NEIC (1)
ME	76	NEIC (76)
Mjma	5	JSO (5)
MJMA	76057	JMA (76057)
ML	96198	TAP (14004), DDA (11678), ISK (10676), ATH (10634), IDC (9371), ROM (8837), CSEM (7196), RSNC (6461), HEL (5487), SJA (3429), THE (3266), GUC (2818), UPP (2507), VIE (2032), BER (1820), AEIC (1775), LDG (1775), MAN (1665), BEO (1447), LJU (923), ECX (921), SKO (913), TEH (906), INMG (876), PRE (790), WEL (753), CNRM (744), PGC (706), GEN (689), ANF (677), UCR (670), SAR (662), KRSC (622), NAO (471), IGIL (465), AZER (412), PDG (410), BJI (386), PAS (370), IPEC (366), MRB (360), PDA (343), SFS (313), CRAAG (310), ISN (307), LVSN (292), THR (288), NDI (241), FIA0 (193), NIC (185), KNET (184), HLW (141), DSN (141), NEIC (134), ZUR (125), WB-NET (112), PPT (110), OTT (109), DHMR (104), BGR (98), ARO (82), ARE (62), BGS (58), HVO (57), SVSA (49), SIK (45), SEA (44), MIRAS (43), REN (41), TUL (37), NCEDC (31), SLC (30), DMN (25), BNS (24), SCB (22), BUT (15), PLV (11), BUG (11), NSSC (10), ATA (10), GDNRW (9), LDO (7), LEDBW (6), TIF (6), TIR (5), JSO (4), BUC (4), AUST (3), HYB (3), DNK (3), IGQ (3), REY (2), NORS (2), LSZ (1), UCC (1), SOF (1), DBN (1), GFZ (1), ZAG (1), IASPEI (1), RSPR (1)
MLh	161	ZUR (161)
MLSn	162	PGC (162)
MLv	3615	DJA (3100), STR (435), IGQ (73), JSO (10), BKK (1)
MN	396	OTT (271), TEH (95), NEIC (46), WES (4), CERI (2), TUL (2), OGSO (1)
mpv	4785	NNC (4785)
MPVA	882	MOS (772), NORS (214), CMWS (3)
MS	9494	IDC (8129), MAN (1665), BJI (1515), MOS (480), NEIC (197), NSSP (61), SOME (27), ASRS (23), VIE (14), IASPEI (10), DSN (8), AZER (8), CSEM (4), LVSN (3), LDG (3), IGIL (1), BER (1), THR (1), ECX (1)
Ms1	8128	IDC (8128)
ms1mx	8129	IDC (8129)
Ms7	1472	BJI (1472)

Table 7.7: *Continued.*

Magnitude type	Events	Agencies reporting magnitude type (number of values)
MW	6782	SJA (3424), NIED (1288), GCMT (1170), NEIC (511), RSNC (476), PGC (259), WAR (212), OTT (73), BRK (49), GUC (23), ASIES (18), PAS (14), CAR (11), CSEM (10), ATA (10), UCR (7), UPA (6), SIGU (4), SLM (3), IGQ (2), BER (2), CRAAG (1), NCEDC (1), IEC (1), PDA (1)
Mw(mB)	19	IGQ (15), STR (3), BKK (1)
MwMwp	1	IGQ (1)
Mwp	47	DJA (45), IGQ (2)

The most commonly reported magnitude types are short-period body-wave, surface-wave, local (or Richter), moment, duration and JMA magnitude type. For a given earthquake, the number and type of reported magnitudes greatly vary depending on its size and location. The large earthquake of October 25, 2010 gives an example of the multitude of reported magnitude types for large earthquakes (Listing 7.1). Different magnitude estimates come from global monitoring agencies such as the IDC, NEIC and GCMT, a local agency (GUC) and other agencies, such as MOS and BJI, providing estimates based on the analysis of their networks. The same agency may report different magnitude types as well as several estimates of the same magnitude type, such as NEIC estimates of M_W obtained from W-phase, centroid and body-wave inversions.

Listing 7.1: *Example of reported magnitudes for a large event*

```
Event   15264887 Southern  Sumatera
   Date        Time         Err   RMS Latitude Longitude  Smaj  Smin   Az Depth   Err Ndef Nsta Gap  mdist  Mdist Qual   Author      OrigID
2010/10/25 14:42:22.18    0.27 1.813  -3.5248  100.1042 4.045 3.327  54  20.0  1.37 2102 2149  23   0.76 176.43 m i de ISC       01346132
 (#PRIME)

Magnitude  Err Nsta Author      OrigID
mb      6.1       61 BJI       15548963
mB      6.9       68 BJI       15548963
Ms      7.7       85 BJI       15548963
Ms7     7.5       86 BJI       15548963
mb      5.3 0.1   48 IDC       16686694
mb1     5.3 0.1   51 IDC       16686694
mb1mx   5.3 0.0   52 IDC       16686694
mbtmp   5.3 0.1   51 IDC       16686694
ML      5.1 0.2    2 IDC       16686694
MS      7.1 0.0   31 IDC       16686694
Ms1     7.1 0.0   31 IDC       16686694
ms1mx   6.9 0.1   44 IDC       16686694
mb      6.1      243 ISCJB     01677901
MS      7.3      228 ISCJB     01677901
M       7.1      117 DJA       01268475
mb      6.1 0.2  115 DJA       01268475
mB      7.1 0.1  117 DJA       01268475
MLv     7.0 0.2   26 DJA       01268475
        7.1 0.4  117 DJA       01268475
Mwp     6.9 0.2  102 DJA       01268475
mb      6.4       49 MOS       16742129
MS      7.2       70 MOS       16742129
mb      6.5      110 NEIC      01288303
ME      7.3          NEIC      01288303
MS      7.3      143 NEIC      01288303
MW      7.7          NEIC      01288303
MW      7.8      130 GCMT      00125427
mb      5.9          KLM       00255772
ML      6.7          KLM       00255772
MS      7.6          KLM       00255772
mb      6.4       20 BGR       16815854
Ms      7.2        2 BGR       16815854
mb      6.3 0.3  250 ISC       01346132
MS      7.3 0.1  237 ISC       01346132
```

An example of a relatively small earthquake that occurred in northern Italy for which we received magnitude reports of mostly local and duration type from six agencies in Italy, France and Austria is given in Listing 7.2.

Listing 7.2: *Example of reported magnitudes for a small event*

```
Event 15089710 Northern Italy
   Date        Time         Err   RMS Latitude Longitude  Smaj  Smin   Az Depth   Err Ndef Nsta Gap  mdist  Mdist Qual   Author      OrigID
2010/08/08 15:20:46.22    0.94 0.778  45.4846    8.3212 2.900 2.539 110  28.6  9.22  172  110  82   0.41   5.35 m i ke ISC       01249414
 (#PRIME)

Magnitude  Err Nsta Author      OrigID
ML      2.4       10 ZUR       15925566
```

```
Md        2.6 0.2   19 ROM         16861451
Ml        2.2 0.2    9 ROM         16861451
ML        2.5          GEN         00554757
ML        2.6 0.3   28 CSEM        00554756
Md        2.3 0.0    3 LDG         14797570
Ml        2.6 0.3   32 LDG         14797570
```

Figure 7.11 shows a distribution of the number of agencies reporting magnitude estimates to the ISC according to the magnitude value. The peak of the distribution corresponds to small earthquakes where many local agencies report local and/or duration magnitudes. The number of contributing agencies rapidly decreases for earthquakes of approximately magnitude 5.5 and above, where magnitudes are mostly given by global monitoring agencies.

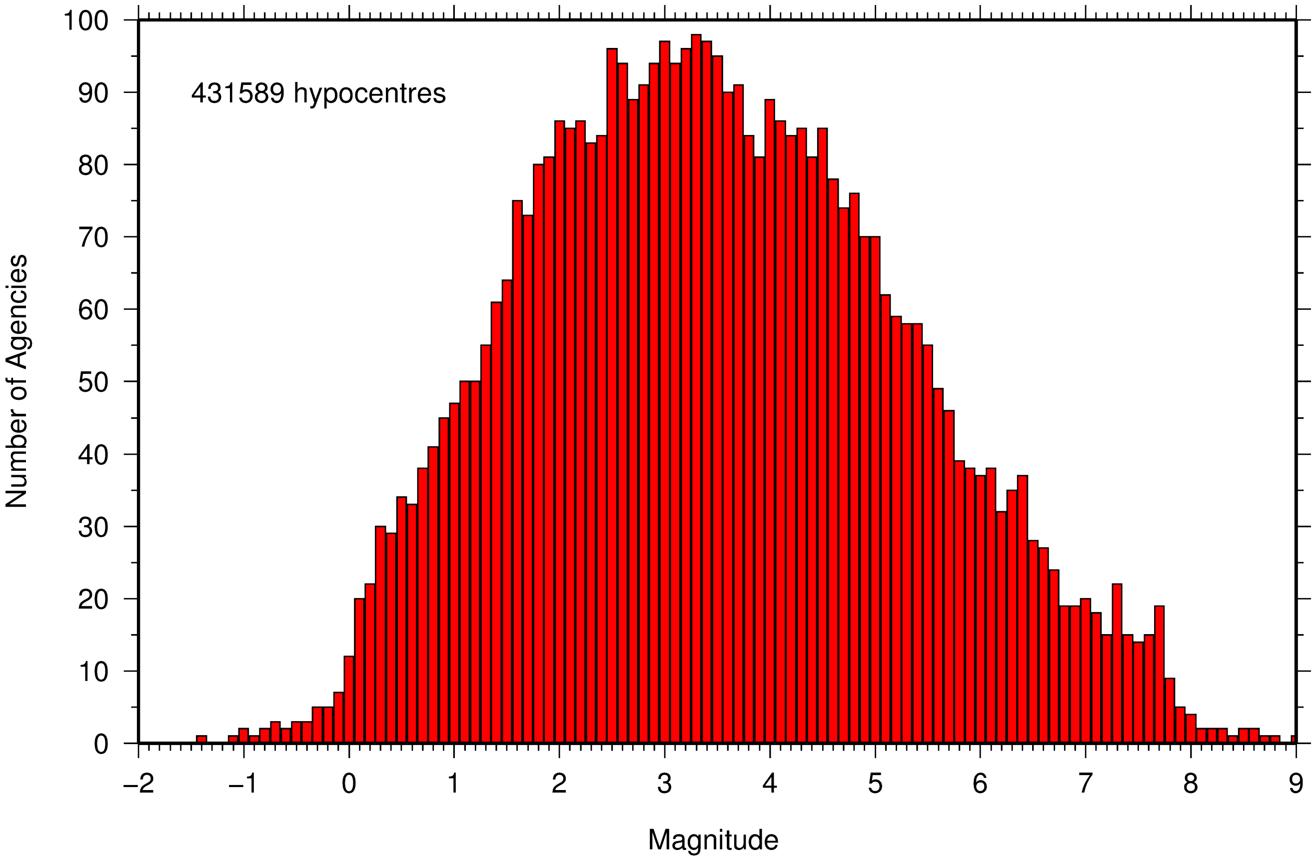

Figure 7.11: *Histogram showing the number of agencies that reported network magnitude values. All magnitude types are included.*

7.6 Moment Tensor Solutions

The ISC Bulletin publishes moment tensor solutions, which are reported to the ISC by other agencies. The collection of moment tensor solutions is summarised in Table 7.8. A histogram showing all moment tensor solutions collected throughout the ISC history is shown in Figure 7.12. Several moment tensor solutions from different authors and different moment tensor solutions calculated by different methods from the same agency may be present for the same event.

The number of moment tensors for this summary period, reported by each agency, is shown in Table 7.9. The moment tensor solutions are plotted in Figure 7.13.

Table 7.8: Summary of reports containing moment tensor solutions.

Reports with Moment Tensors	14
Total moment tensors received	4460
Agencies reporting moment tensors	7

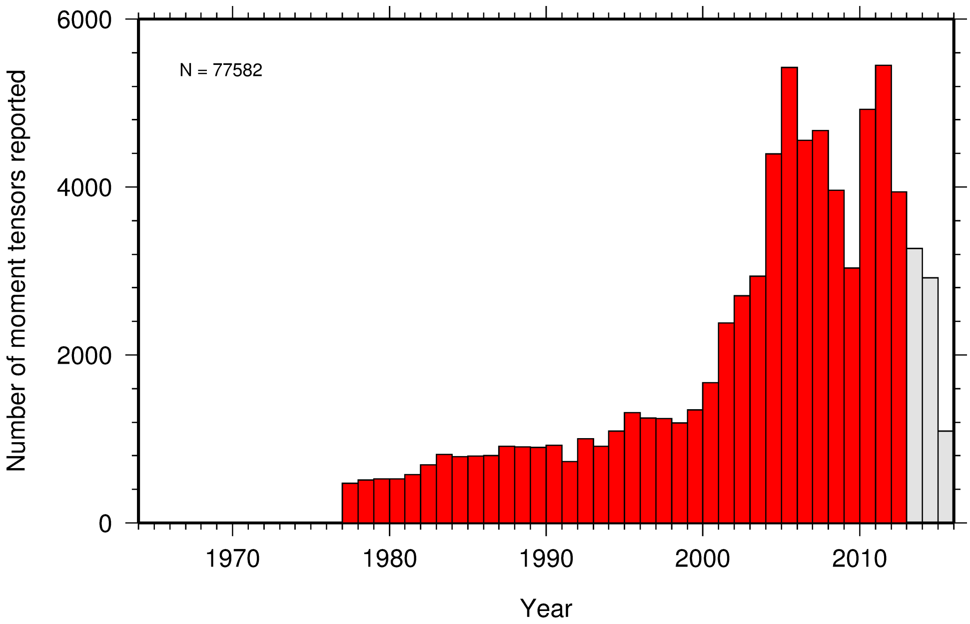

Figure 7.12: *Histogram showing the number of moment tensors reported to the ISC since 1964. The regions in grey represent data that are still being actively collected.*

Table 7.9: *Summary of moment tensor solutions in the ISC Bulletin reported by each agency.*

Agency	Number of moment tensor solutions
GCMT	1169
NEIC	469
MED_RCMT	58
OTT	55
BRK	39
SLM	3
PAS	2

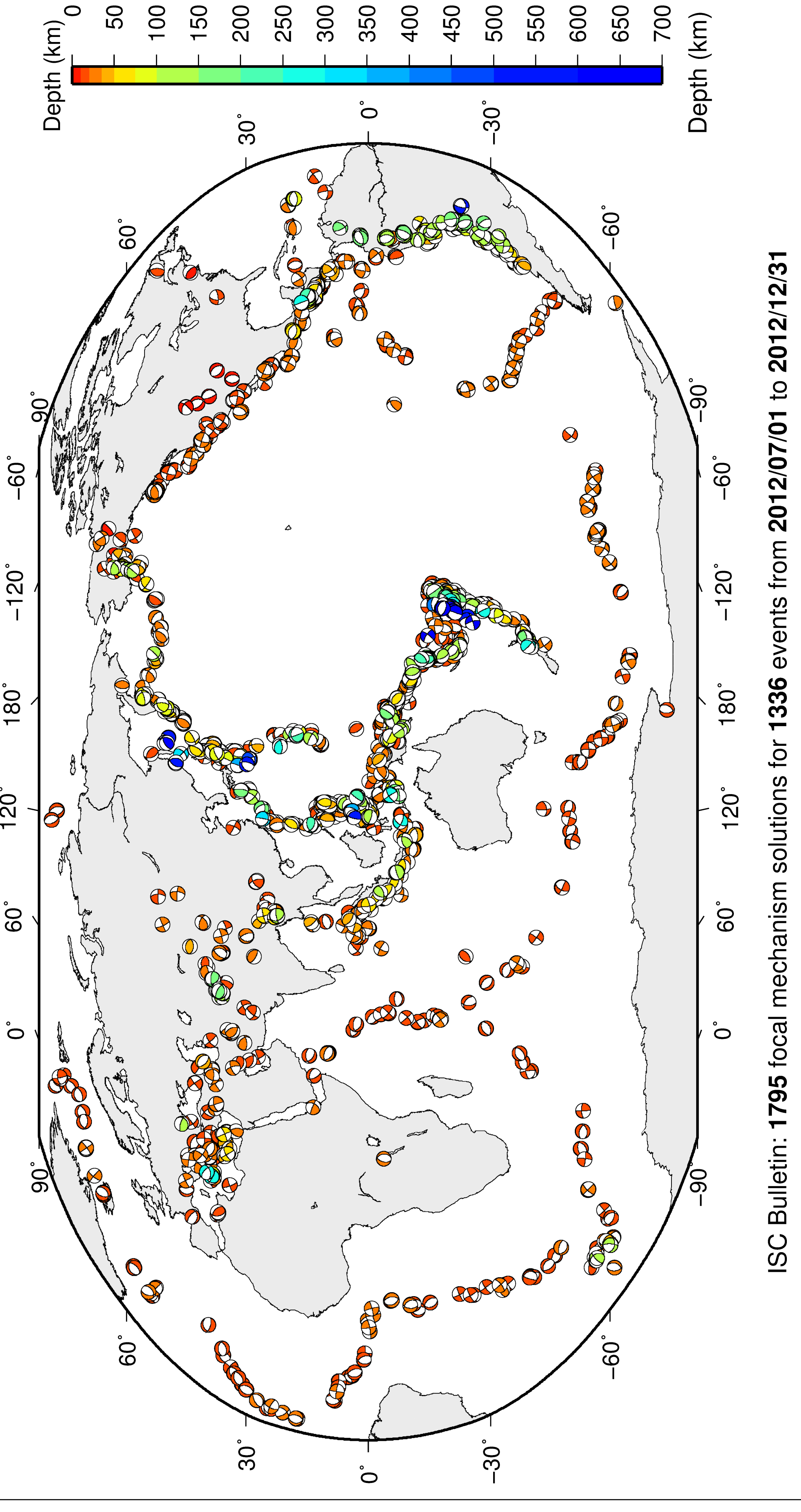

Figure 7.13: *Map of all moment tensor solutions in the ISC Bulletin for this summary period.*

7.7 Timing of Data Collection

Here we present the timing of reports to the ISC. Please note, this does not include provisional alerts, which are replaced at a later stage. Instead, it reflects the final data sent to the ISC. The absolute timing of all hypocentre reports, regardless of magnitude, is shown in Figure 7.14. In Figure 7.15 the reports are grouped into one of six categories - from within three days of an event origin time, to over one year. The histogram shows the distribution with magnitude (for hypocentres where a network magnitude was reported) for each category, whilst the map shows the geographic distribution of the reported hypocentres.

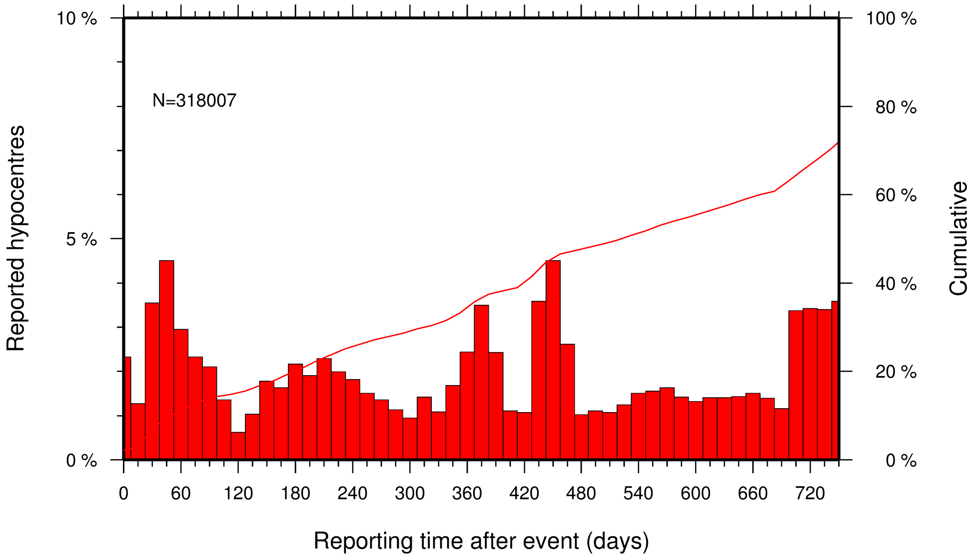

Figure 7.14: *Histogram showing the timing of final reports of the hypocentres (total of N) to the ISC. The cumulative frequency is shown by the solid line.*

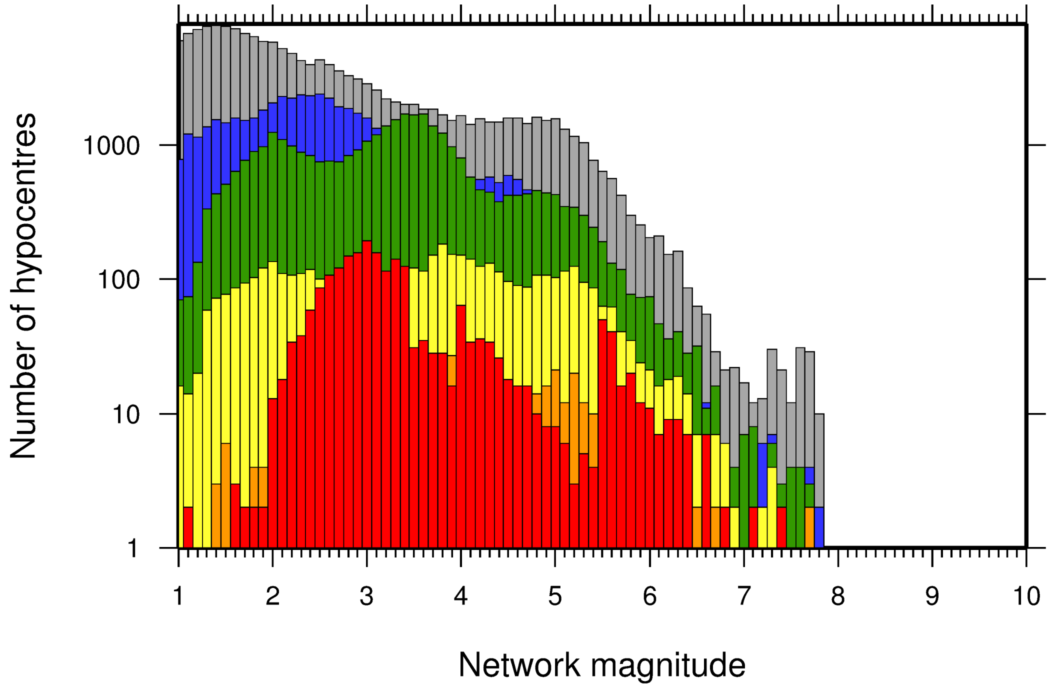

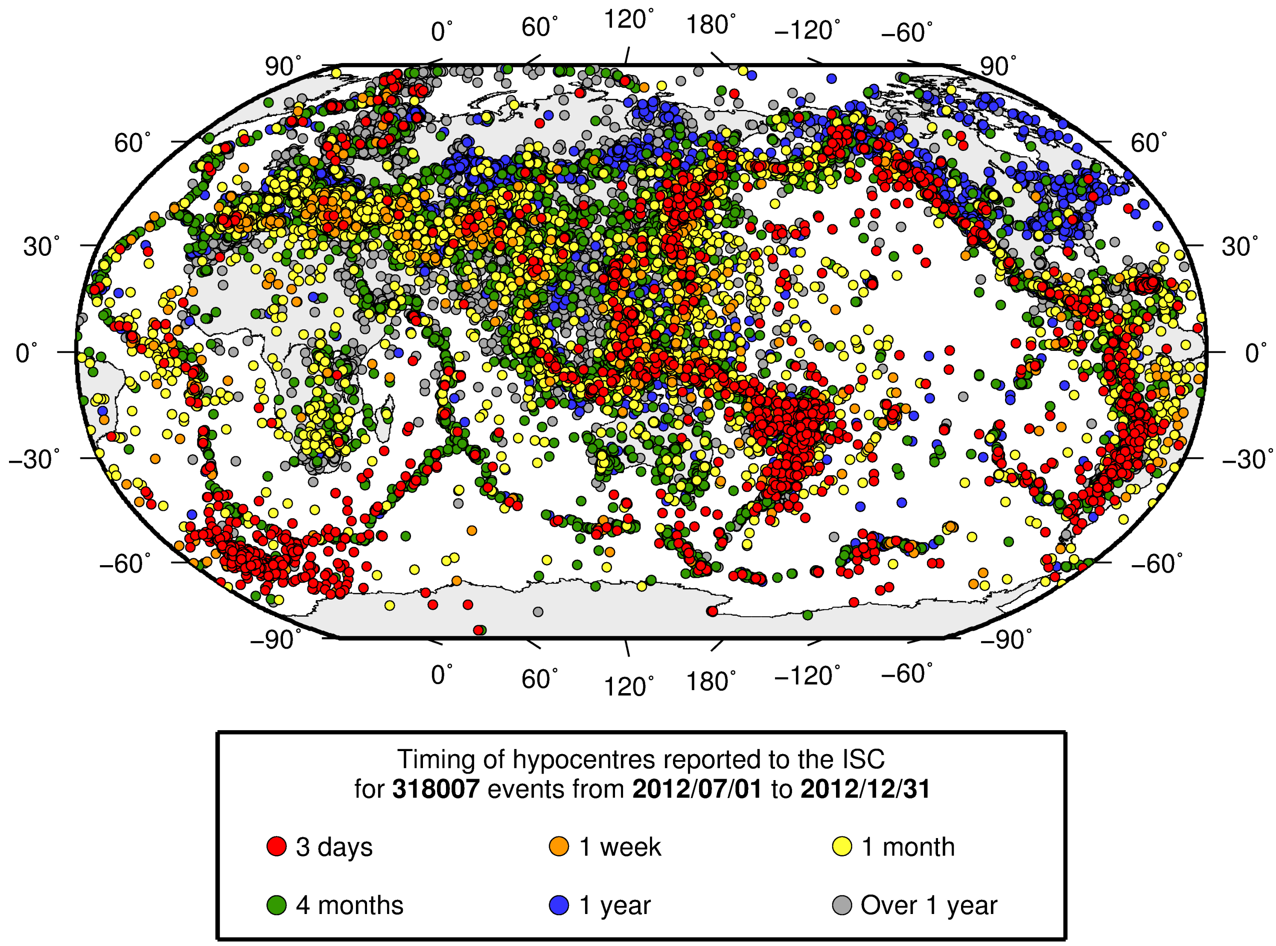

Figure 7.15: *Timing of hypocentres reported to the ISC. The colours show the time after the origin time that the corresponding hypocentre was reported. The histogram shows the distribution with magnitude. If more than one network magnitude was reported, preference was given to a value of M_W followed by M_S, m_b and M_L respectively; all reported hypocentres are included on the map. Note: early reported hypocentres are plotted over later reported hypocentres, on both the map and histogram.*

8

Overview of the ISC Bulletin

This chapter provides an overview of the seismic event data in the ISC Bulletin. We indicate the differences between all ISC events and those ISC events that are reviewed or located. We describe the wealth of phase arrivals and phase amplitudes and periods observed at seismic stations worldwide, reported in the ISC Bulletin and often used in the ISC location and magnitude determination. Finally, we make some comparisons of the ISC magnitudes with those reported by other agencies, and discuss magnitude completeness of the ISC Bulletin.

8.1 Events

The ISC Bulletin had 206379 reported events in the summary period between July and December 2012. Some 92% (190518) of the events were identified as earthquakes, the rest (15861) were of anthropogenic origin (including mining and other chemical explosions, rockbursts and induced events) or of unknown origin. As discussed in Section 3.3.3 of January to June 2012 Bulletin Summary, typically about 20% of the events are selected for ISC review, and about half of the events selected for review are located by the ISC. In this summary period 14% of the events were reviewed and 8% of the events were located by the ISC. For events that are not located by the ISC, the prime hypocentre is identified according to the rules described in Section 3.3.1 of January to June 2012 Bulletin Summary.

Of the 6178635 reported phase observations, 45% are associated to ISC-reviewed events, and 42% are associated to events selected for ISC location. Note that all large events are reviewed and located by the ISC. Since large events are globally recorded and thus reported by stations worldwide, they will provide the bulk of observations. This explains why only about one-fifth of the events in any given month is reviewed although the number of phases associated to reviewed events has increased nearly exponentially in the past decades.

Figure 8.1 shows the daily number of events throughout the summary period. Figure 8.2 shows the locations of the events in the ISC Bulletin; the locations of ISC-reviewed and ISC-located events are shown in Figures 8.3 and 8.4, respectively.

Figure 8.5 shows the hypocentral depth distributions of events in the ISC Bulletin for the summary period. The vast majority of events occur in the Earth's crust. Note that the peaks at 0, 10, 35 km, and at every 50 km intervals deeper than 100 km are artifacts of analyst practices of fixing the depth to a nominal value when the depth cannot be reliably resolved.

Figure 8.6 shows the depth distribution of free-depth solutions in the ISC Bulletin. The depth of a hypocentre reported to the ISC is assumed to be determined as a free parameter, unless it is explicitly labelled as a fixed-depth solution. On the other hand, as described in Section 3.4.3 of January to June

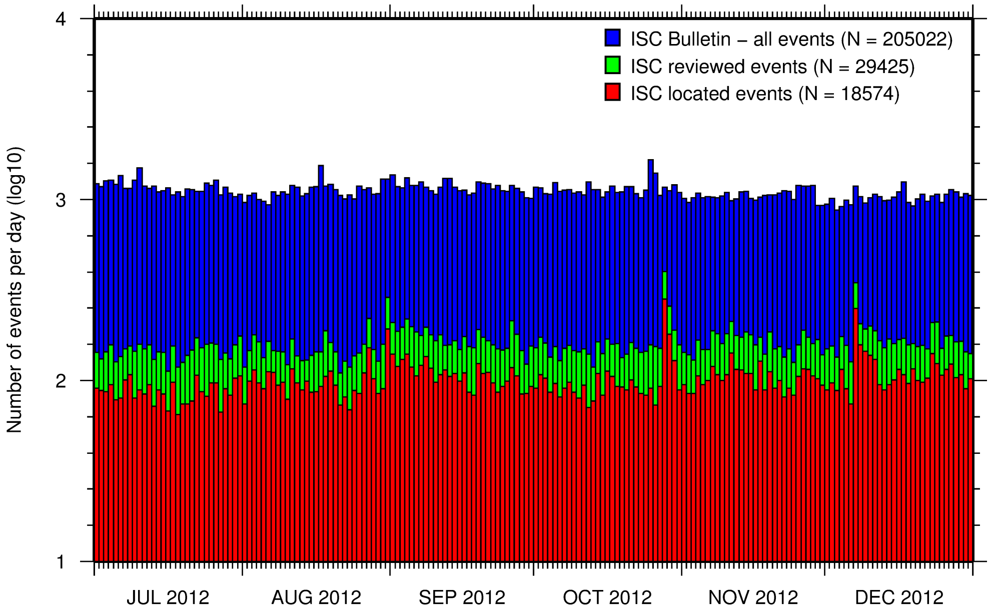

Figure 8.1: *Histogram showing the number of events in the ISC Bulletin for the current summary period. The vertical scale is logarithmic.*

2012 Bulletin Summary, the ISC locator attempts to get a free-depth solution if, and only if, there is resolution for the depth in the data, i.e. if there is a local network and/or sufficient depth-sensitive phases are reported.

Figure 8.7 shows the depth distribution of fixed-depth solutions in the ISC Bulletin. Except for a fraction of events whose depth is fixed to a shallow depth, this set comprises mostly ISC-located events. If there is no resolution for depth in the data, the ISC locator fixes the depth to a value obtained from the ISC default depth grid file, or if no default depth exists for that location, to a nominal default depth assigned to each Flinn-Engdahl region (see details in Section 3.4.3 of January to June 2012 Bulletin Summary). During the ISC review editors are inclined to accept the depth obtained from the default depth grid, but they typically change the depth of those solutions that have a nominal (10 or 35 km) depth. When doing so, they usually fix the depth to a round number, preferably divisible by 50.

For events selected for ISC location, the number of stations typically increases as arrival data reported by several agencies are grouped together and associated to the prime hypocentre. Consequently, the network geometry, characterised by the secondary azimuthal gap (the largest azimuthal gap a single station closes), is typically improved. Figure 8.8 illustrates that the secondary azimuthal gap is indeed generally smaller for ISC-located events than that for all events in the ISC Bulletin. Figure 8.9 shows the distribution of the number of associated stations. For large events the number of associated stations is usually larger for ISC-located events than for any of the reported event bulletins. On the other hand, events with just a few reporting stations are rarely selected for ISC location. The same is true for the number of defining stations (stations with at least one defining phase that were used in the location). Figure 8.10 indicates that because the reported observations from multiple agencies are associated to the prime, large ISC-located events typically have a larger number of defining stations than any of the reported event bulletins.

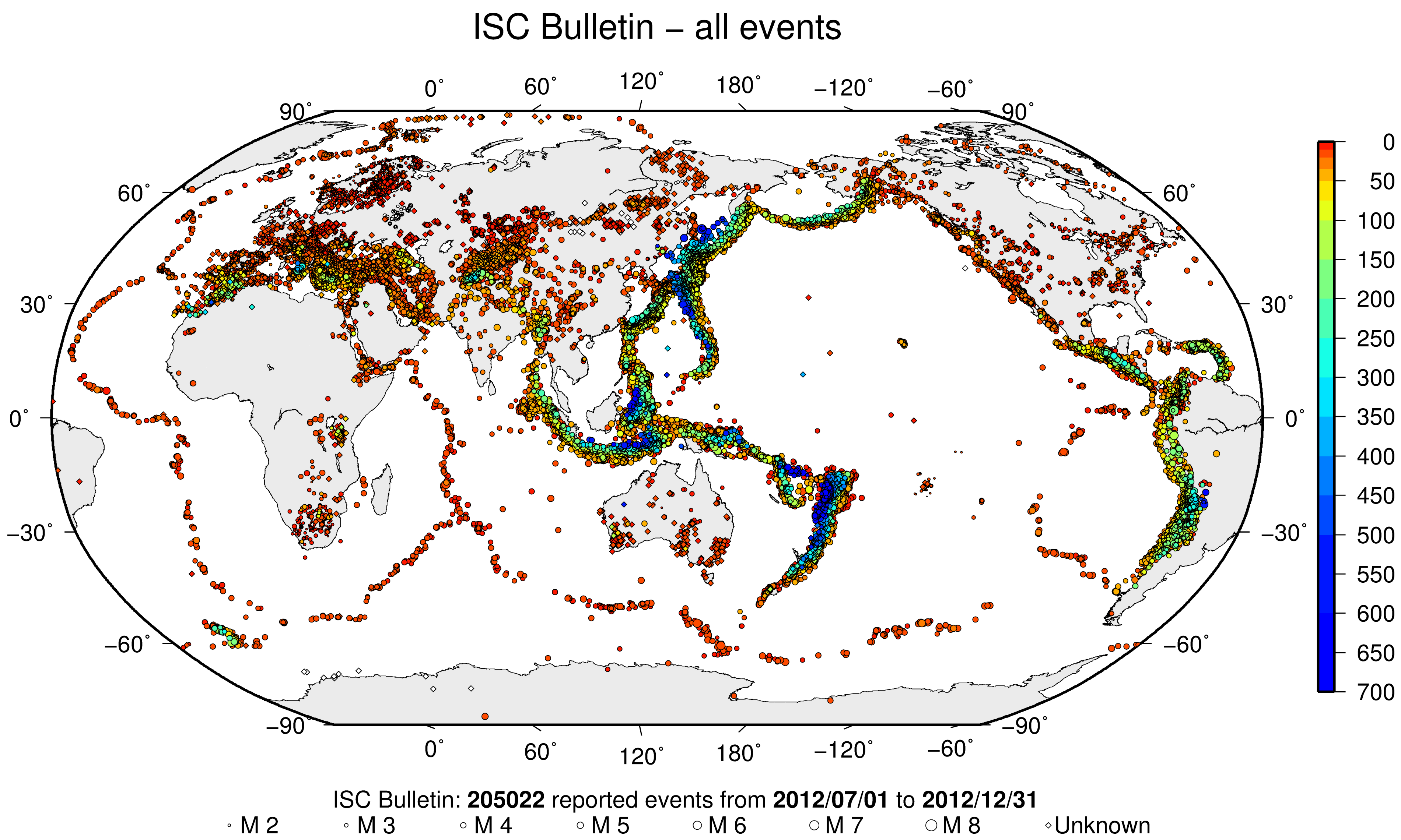

Figure 8.2: *Map of all events in the ISC Bulletin. Prime hypocentre locations are shown. Compare with Figure 7.10.*

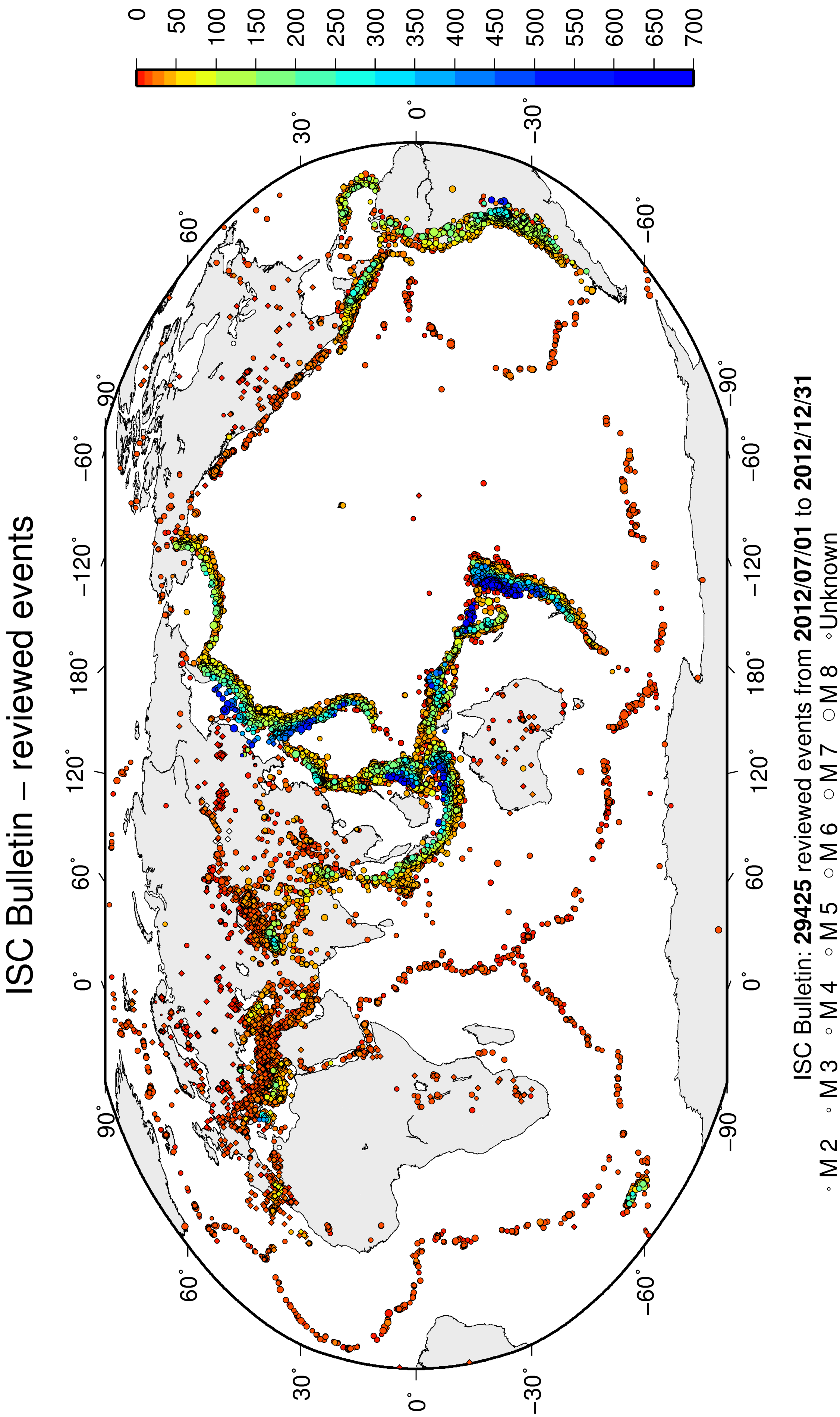

Figure 8.3: *Map of all events reviewed by the ISC for this time period. Prime hypocentre locations are shown.*

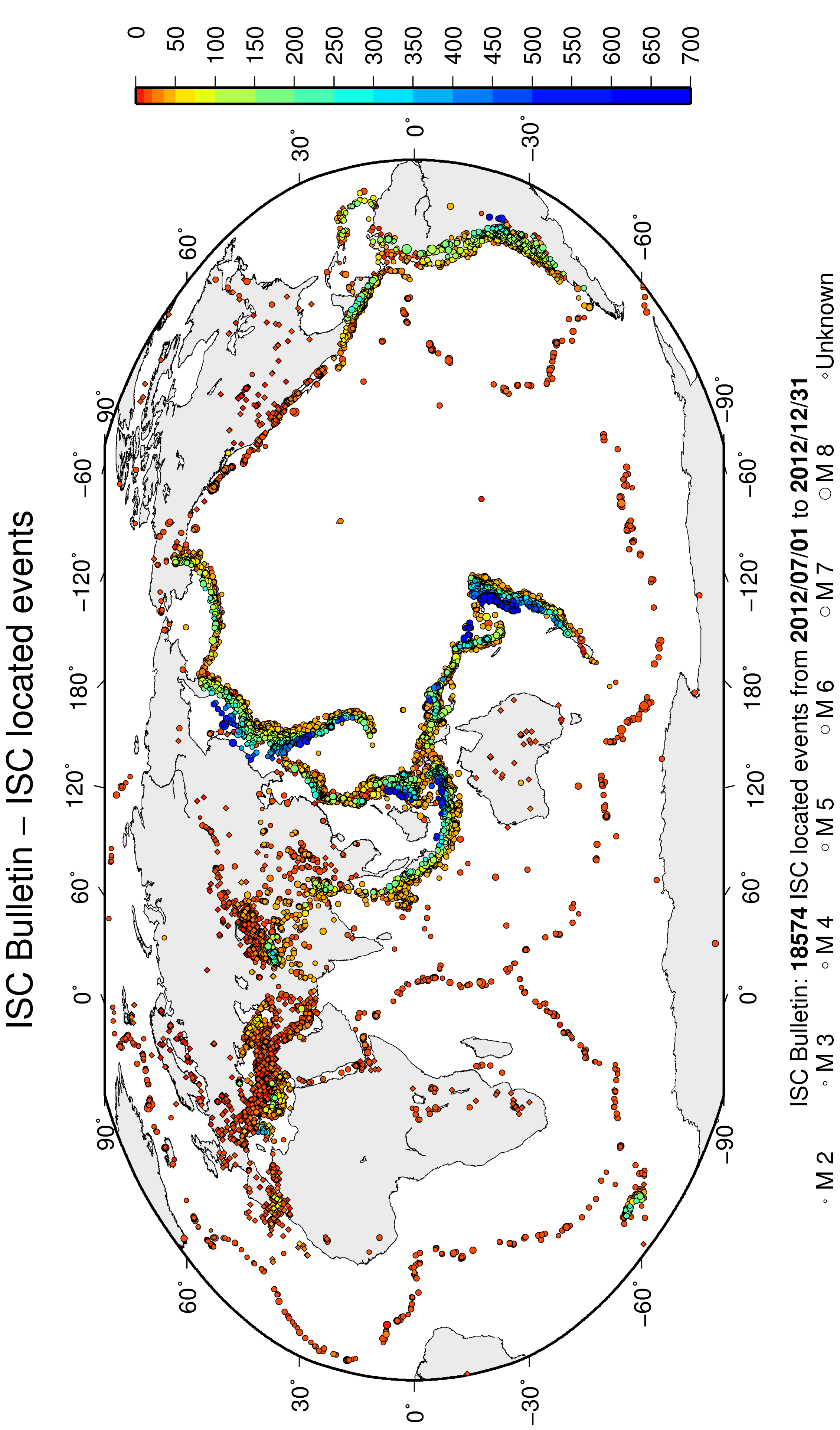

Figure 8.4: *Map of all events located by the ISC for this time period. ISC determined hypocentre locations are shown.*

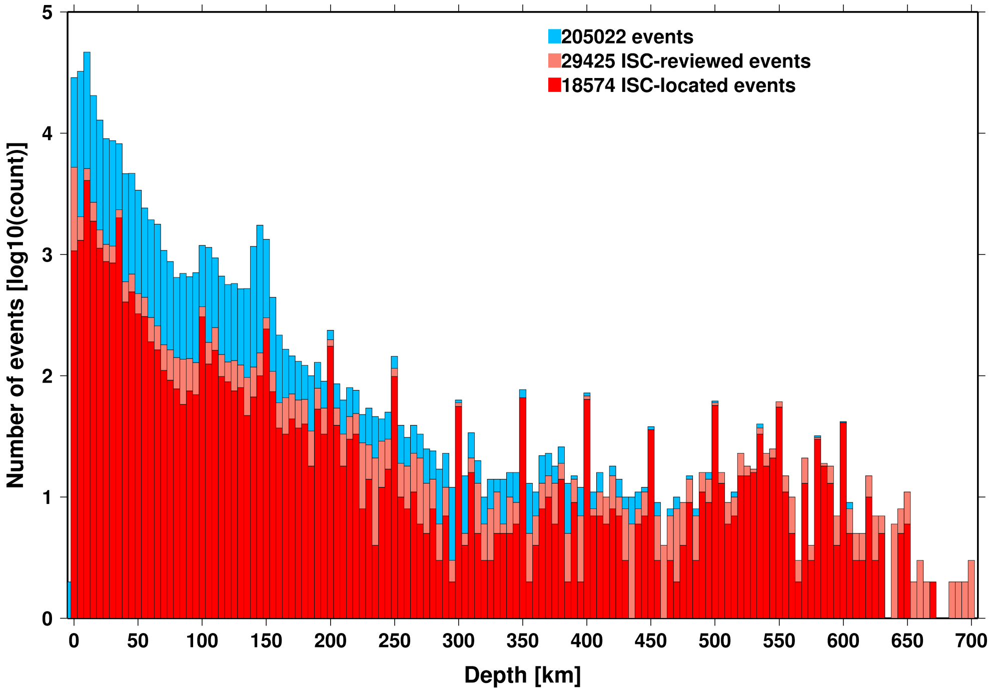

Figure 8.5: *Distribution of event depths in the ISC Bulletin (blue) and for the ISC-reviewed (pink) and the ISC-located (red) events during the summary period. All ISC-located events are reviewed, but not all reviewed events are located by the ISC. The vertical scale is logarithmic.*

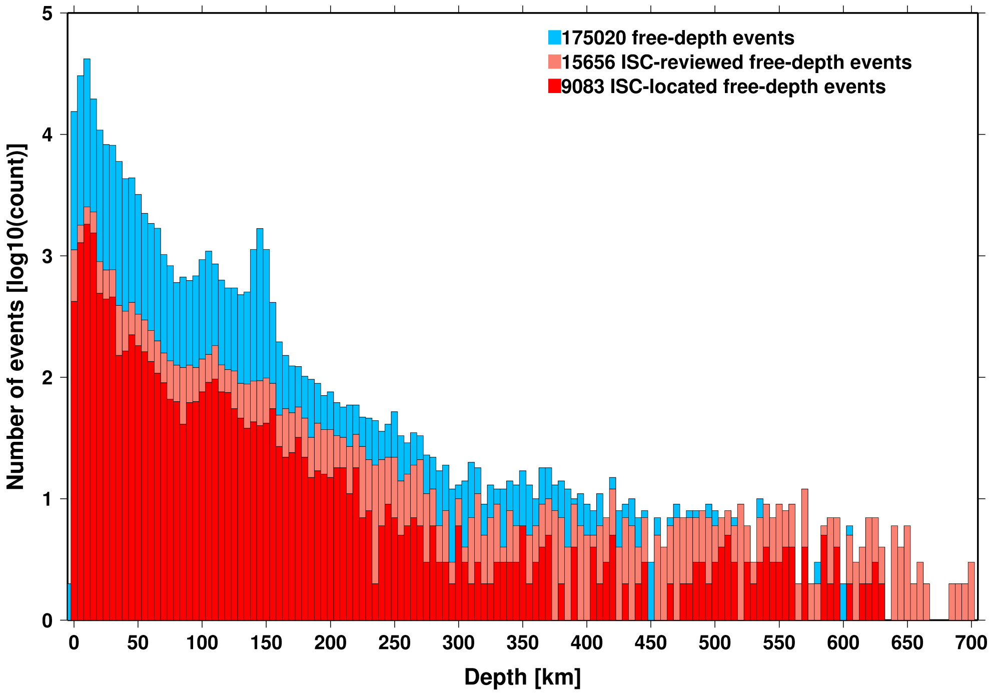

Figure 8.6: *Hypocentral depth distribution of events where the prime hypocentres are reported/located with a free-depth solution in the ISC Bulletin. The vertical scale is logarithmic.*

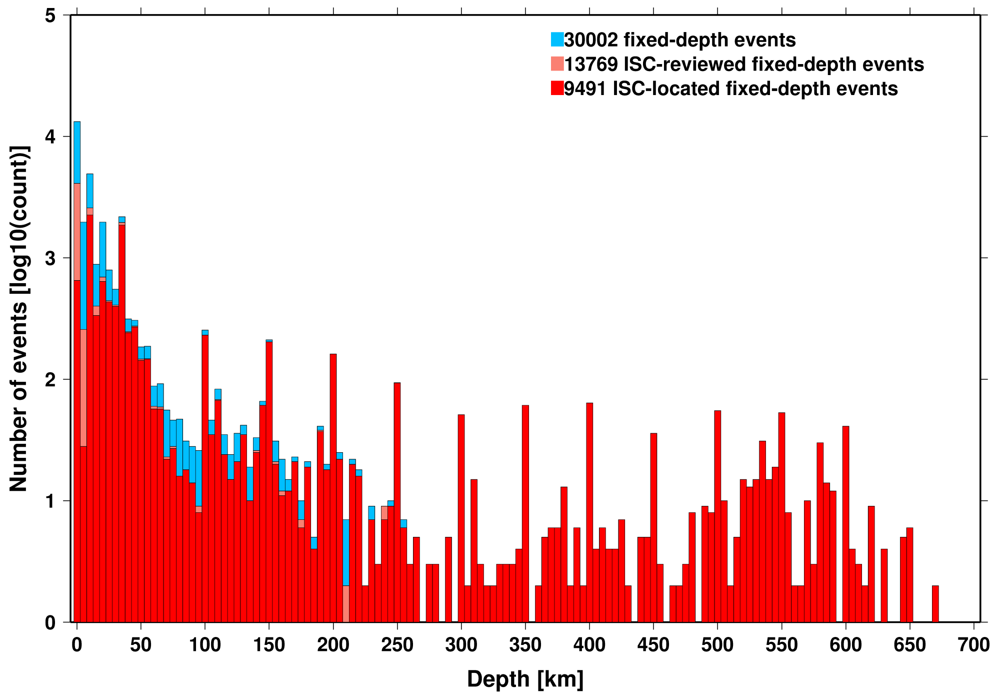

Figure 8.7: *Hypocentral depth distribution of events where the prime hypocentres are reported/located with a fixed-depth solution in the ISC Bulletin. The vertical scale is logarithmic.*

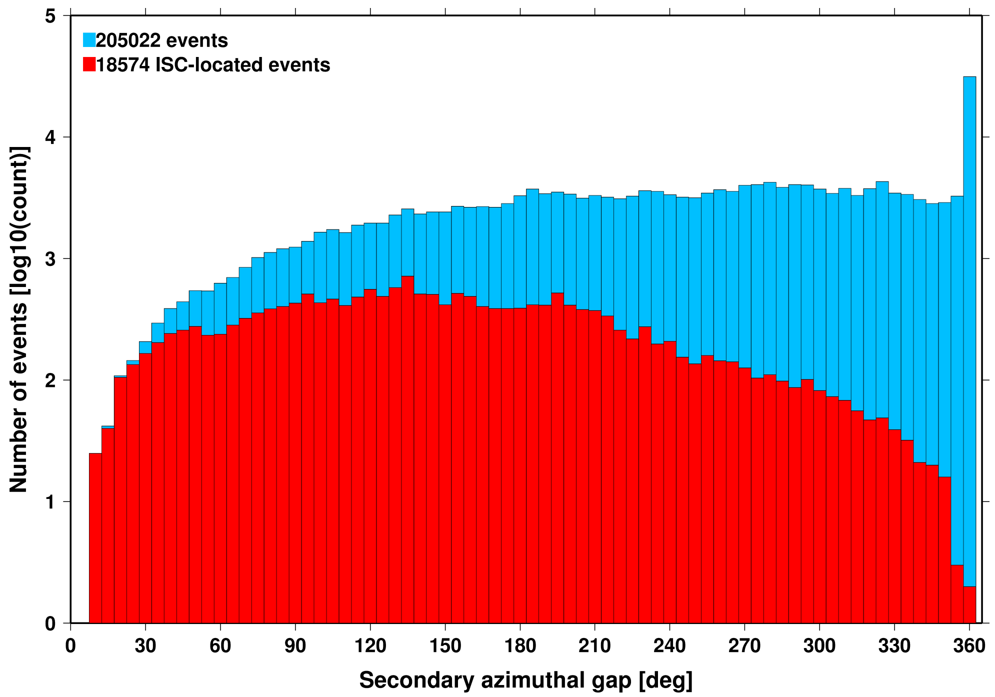

Figure 8.8: *Distribution of secondary azimuthal gap for events in the ISC Bulletin (blue) and those selected for ISC location (red). The vertical scale is logarithmic.*

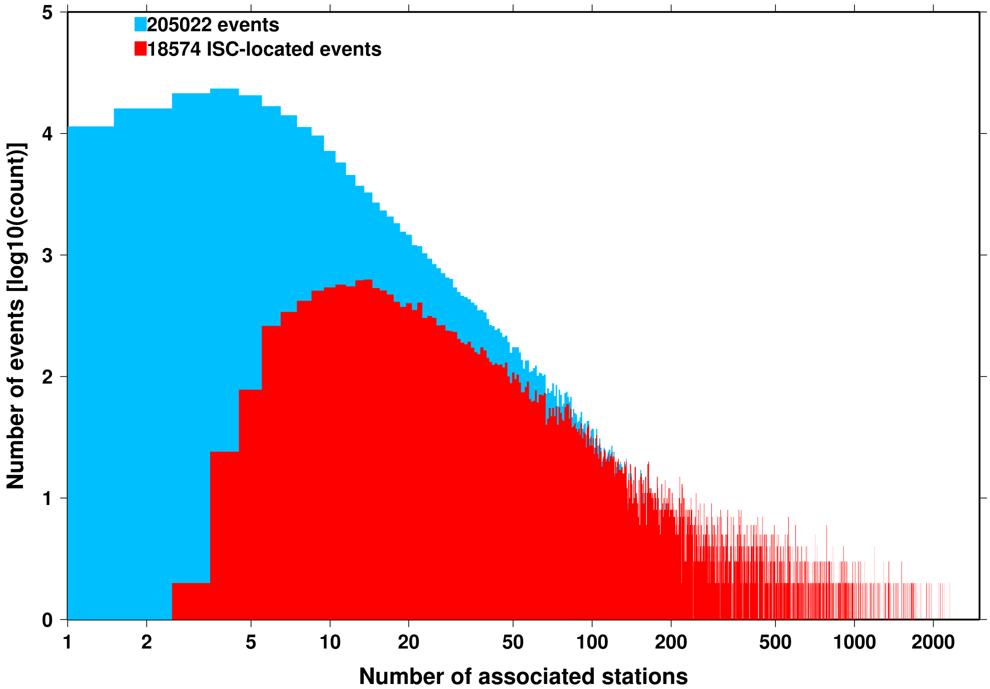

Figure 8.9: *Distribution of the number of associated stations for events in the ISC Bulletin (blue) and those selected for ISC location (red). The vertical scale is logarithmic.*

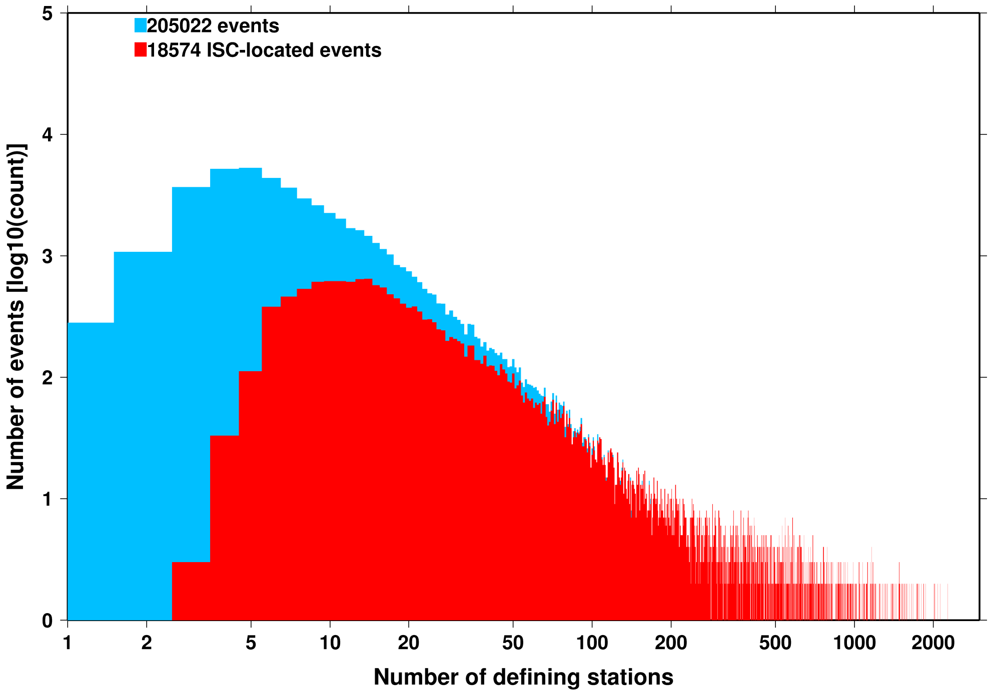

Figure 8.10: *Distribution of the number of defining stations for events in the ISC Bulletin (blue) and those selected for ISC location (red). The vertical scale is logarithmic.*

The formal uncertainty estimates are also typically smaller for ISC-located events. Figure 8.11 shows the distribution of the area of the 90% confidence error ellipse for ISC-located events during the summary period. The distribution suffers from a long tail indicating a few poorly constrained event locations. Nevertheless, half of the events are characterised by an error ellipse with an area less than 194 km^2, 90% of the events have an error ellipse area less than 1050 km^2, and 95% of the events have an error ellipse area less than 1699 km^2.

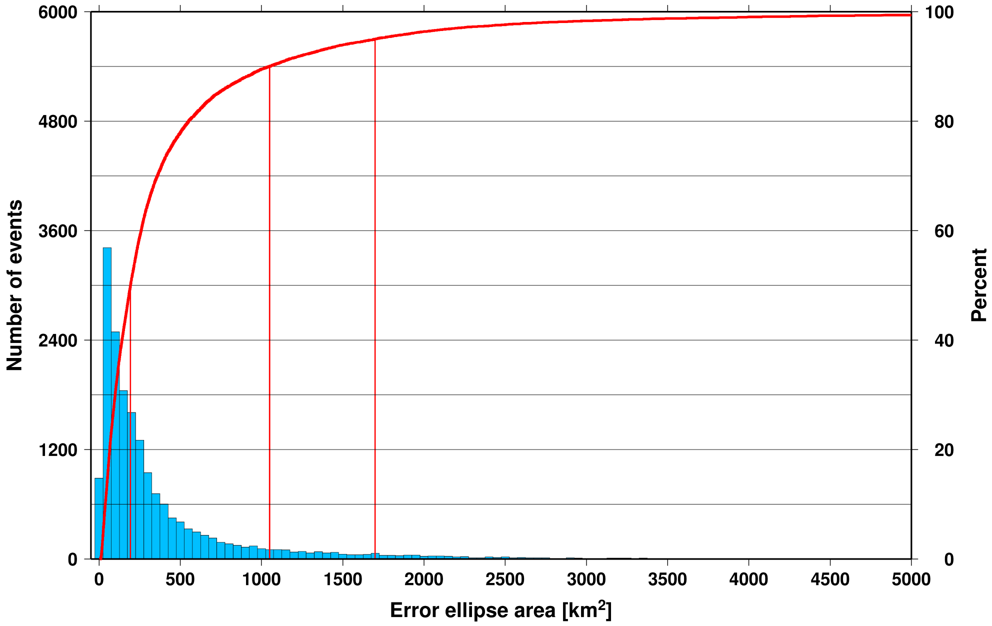

Figure 8.11: *Distribution of the area of the 90% confidence error ellipse of the ISC-located events. Vertical red lines indicate the 50th, 90th and 95th percentile values.*

Figure 8.12 shows one of the major characteristic features of the ISC location algorithm (Bondár and Storchak, 2011). Because the ISC locator accounts for correlated travel-time prediction errors due to unmodelled velocity heterogeneities along similar ray paths, the area of the 90% confidence error ellipse does not decrease indefinitely with increasing number of stations, but levels off once the information carried by the network geometry is exhausted, thus providing more realistic uncertainty estimates.

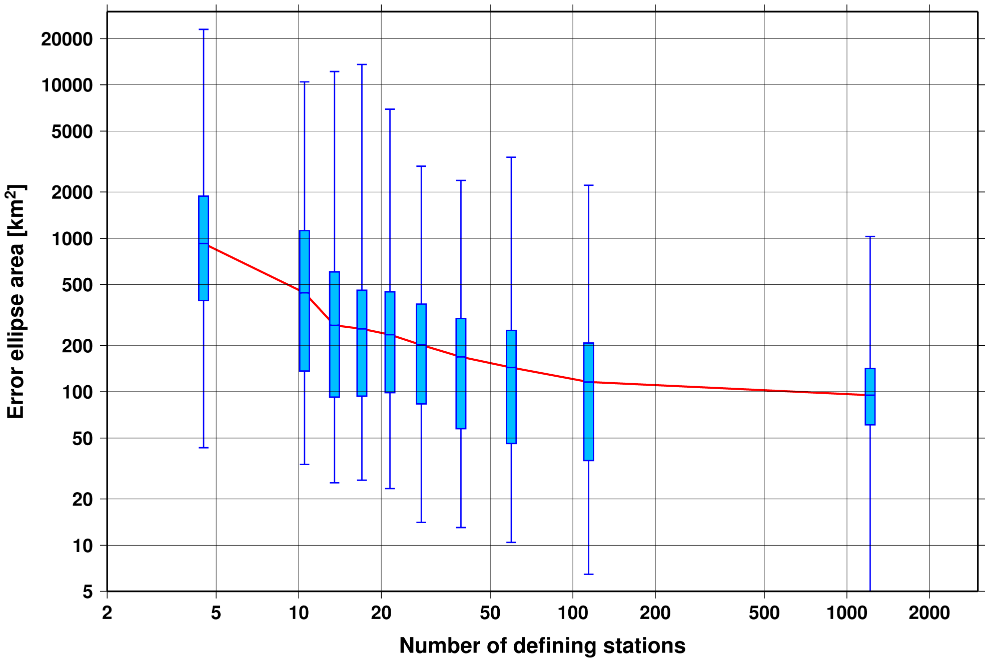

Figure 8.12: *Box-and-whisker plot of the area of the 90% confidence error ellipse of the ISC-located events as a function of the number of defining stations. Each box represents one-tenth-worth of the total number of data. The red line indicates the median 90% confidence error ellipse area.*

8.2 Seismic Phases and Travel-Time Residuals

The number of phases that are associated to events over the summary period in the ISC Bulletin is shown in Figure 8.13. Phase types and their total number in the ISC Bulletin is shown in the Appendix, Table 10.2. A summary of phase types is indicated in Figure 8.14.

In computing ISC locations, the current (for events since 2009) ISC location algorithm (*Bondár and Storchak*, 2011) uses all *ak135* phases where possible. Within the Bulletin, the phases that contribute to an ISC location are labelled as *time defining*. In this section, we summarise these time defining phases.

In Figure 8.15, the number of defining phases is shown in a histogram over the summary period. Each defining phase is listed in Table 8.1, which also provides a summary of the number of defining phases per event. A pie chart showing the proportion of defining phases is shown in Figure 8.16. Figure 8.17 shows travel times of seismic waves. The distribution of residuals for these defining phases is shown for the top five phases in Figures 8.18 through 8.22.

Table 8.1: *Numbers of 'time defining' phases (N) within the ISC Bulletin for 18574 ISC located events.*

Phase	Number of 'defining' phases	Number of events	Max per event	Median per event
P	975545	12890	2800	11
Pn	434287	17201	1032	12
Sn	143574	15045	194	5
PKPdf	85088	4679	864	3
Pb	74285	8347	86	5
Pg	61464	6709	155	6
Sg	49152	6467	117	4
Sb	47999	7935	80	4
PKPbc	38977	4013	373	2
S	35527	3556	344	3
PKPab	17807	2952	332	2
PcP	17430	3641	115	2

Table 8.1: *(continued)*

Phase	Number of 'defining' phases	Number of events	Max per event	Median per event
pP	14395	1436	350	3
Pdif	10755	1005	766	2
PP	8390	1655	105	2
PKiKP	7187	1039	222	2
ScP	4633	1055	205	2
SS	3762	1110	62	2
sP	3573	979	159	2
PKKPbc	2257	391	115	3
SKSac	2076	513	88	1
PnPn	1595	782	13	1
SnSn	1417	662	9	2
ScS	1153	504	31	1
pPKPdf	1148	414	33	1
SKPbc	1008	269	180	2
P'P'df	581	138	54	2
PKKPdf	535	213	22	1
PKKPab	523	216	30	2
pPKPbc	506	255	14	1
SKiKP	492	257	15	1
sS	492	267	16	1
PS	464	129	28	1
PcS	417	316	6	1
pPKPab	349	150	35	1
PKSdf	314	208	17	1
PnS	304	152	9	1
sPKPdf	288	185	9	1
SKKSac	287	161	10	1
SKSdf	265	152	12	1
SKPab	218	108	15	1
SP	194	67	18	1
SKPdf	187	45	63	1
Sdif	167	73	11	1
sPKPbc	147	92	13	1
pS	63	57	2	1
pPdif	55	25	7	1
SKKPbc	51	26	7	1
sPKPab	40	29	7	1
pPKiKP	39	20	9	1
SPn	38	26	5	1
P'P'ab	19	12	5	1
sPdif	17	5	8	1
PKSbc	12	10	3	1
SKKSdf	10	6	2	2
SbSb	9	8	2	1
SKKPdf	7	6	2	1
P'P'bc	7	5	3	1
sPKiKP	6	3	3	2
SKKPab	5	5	1	1
PbPb	5	5	1	1
sPn	4	4	1	1
pSKSac	4	1	4	4
PKKSbc	2	2	1	1
PKKSdf	1	1	1	1
SgSg	1	1	1	1
pwP	1	1	1	1
sSKSac	1	1	1	1
PKSab	1	1	1	1
PgPg	1	1	1	1
S'S'ac	1	1	1	1

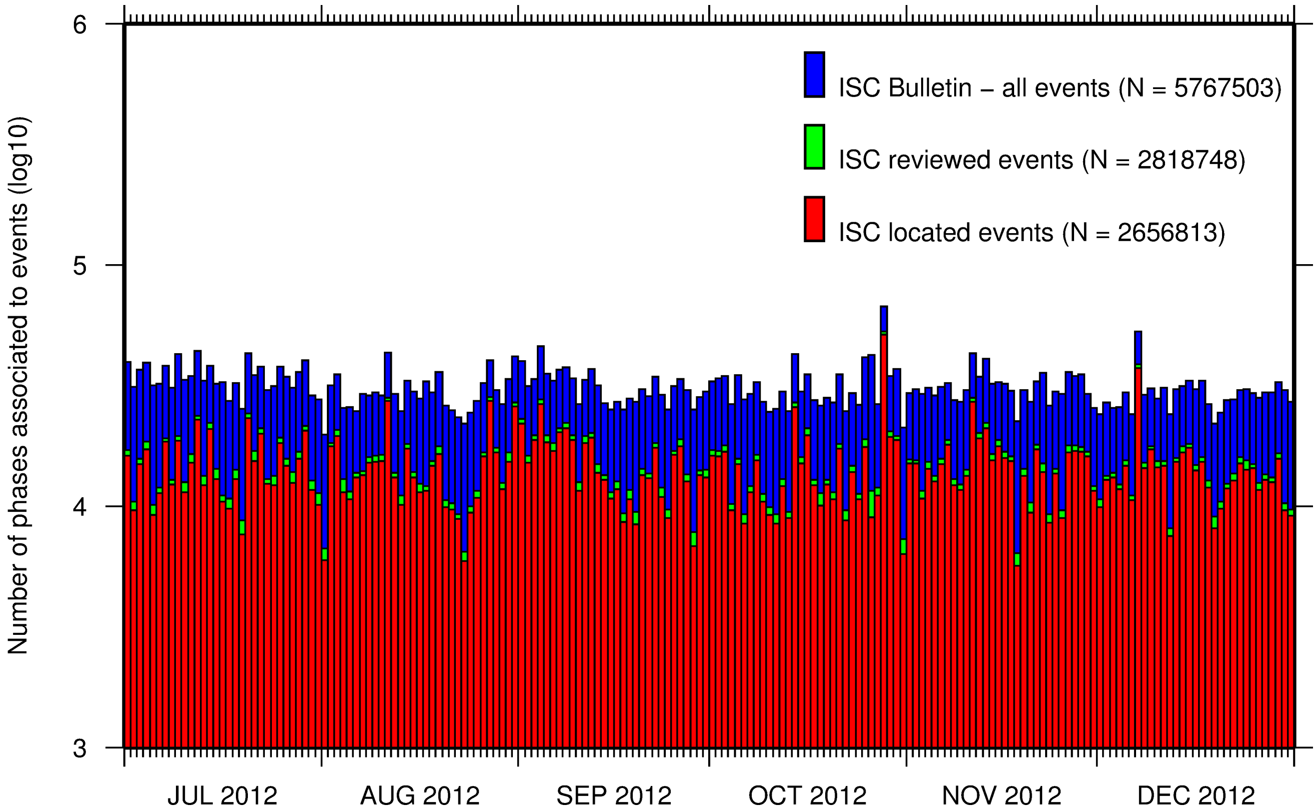

Figure 8.13: *Histogram showing the number of phases (N) that the ISC has associated to events within the ISC Bulletin for the current summary period.*

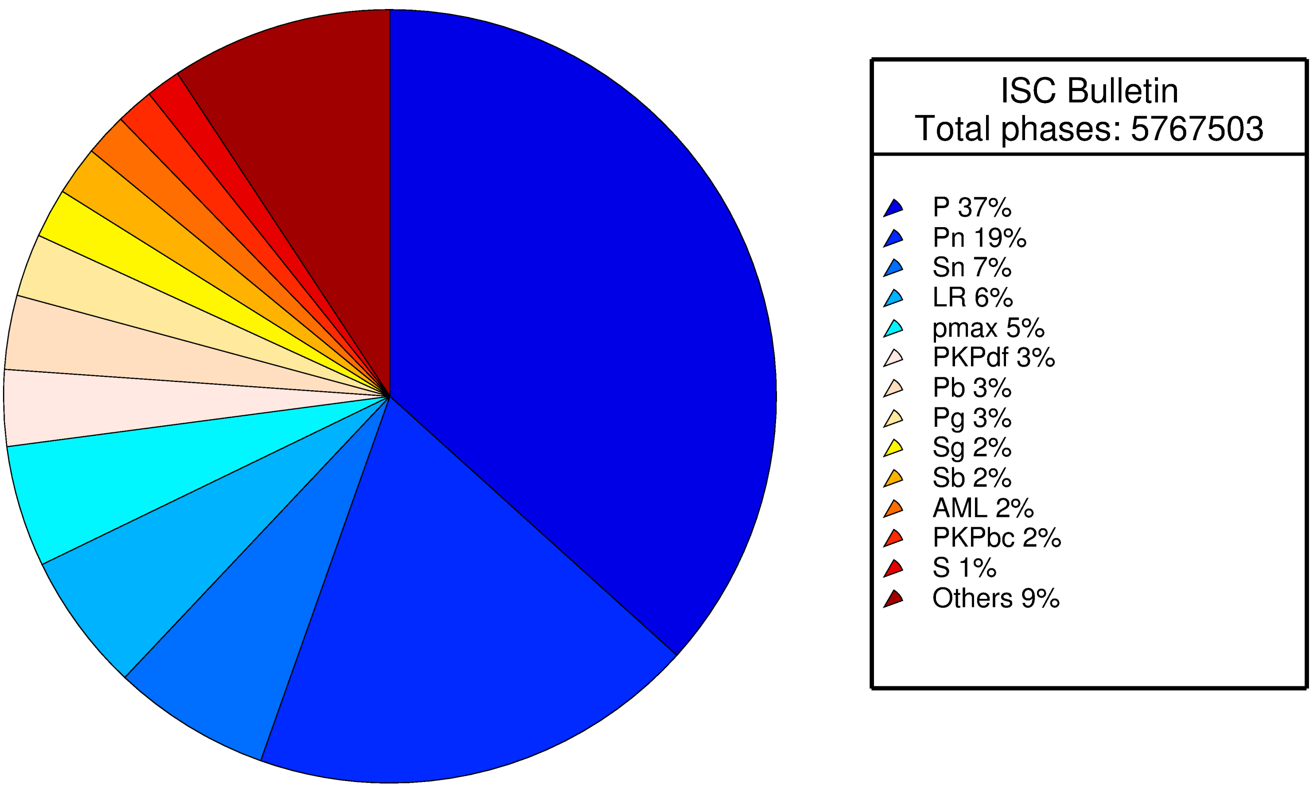

Figure 8.14: *Pie chart showing the fraction of various phase types in the ISC Bulletin for this summary period.*

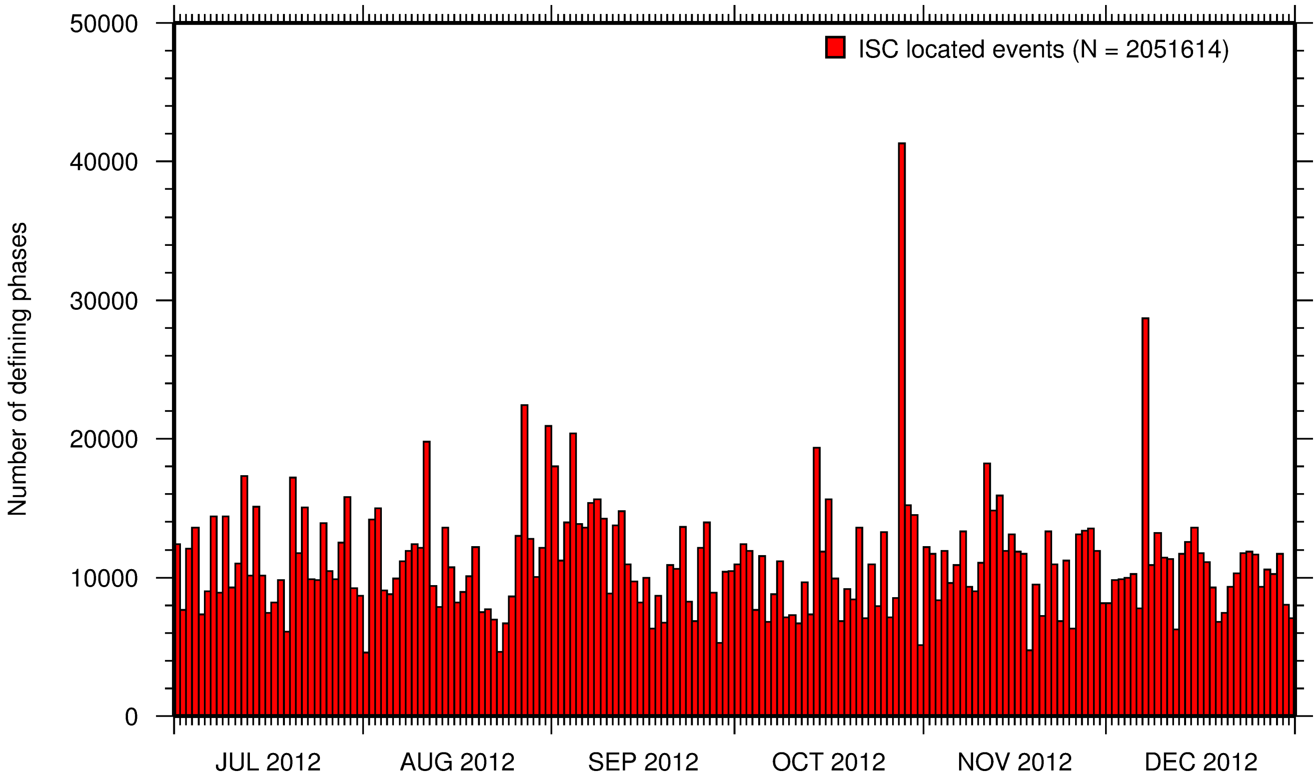

Figure 8.15: *Histogram showing the number of defining phases in the ISC Bulletin, for events located by the ISC.*

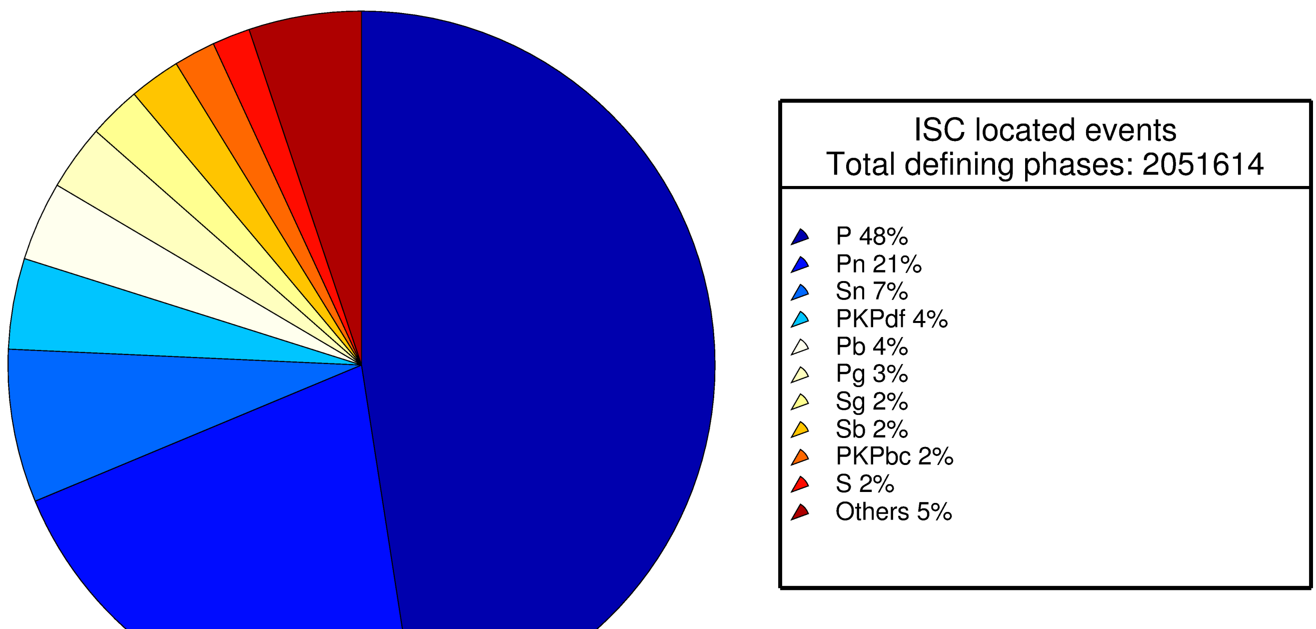

Figure 8.16: *Pie chart showing the defining phases in the ISC Bulletin, for events located by the ISC. A complete list of defining phases is shown in Table 8.1.*

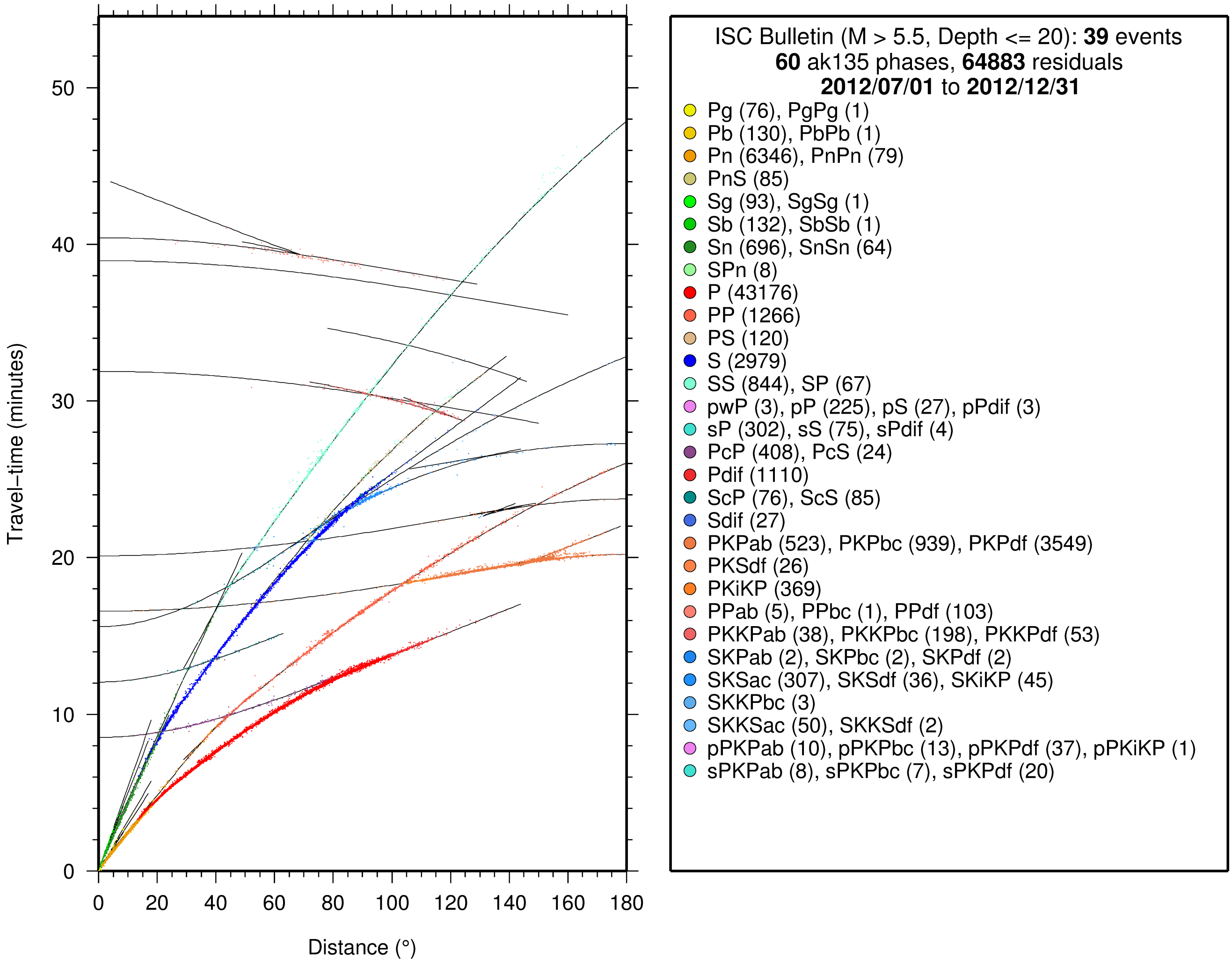

Figure 8.17: *Distribution of travel-time observations in the ISC Bulletin for events with M > 5.5 and depth less than 20 km. The travel-time observations are shown relative to a 0 km source and compared with the theoretical ak135 travel-time curves (solid lines). The legend lists the number of each phase plotted.*

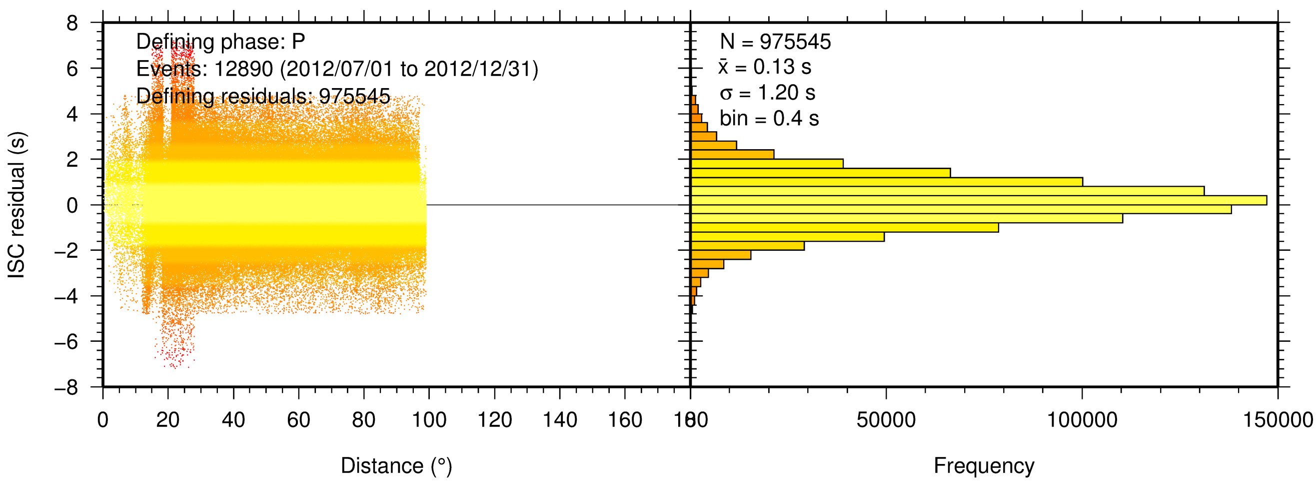

Figure 8.18: *Distribution of travel-time residuals for the defining P phases used in the computation of ISC located events in the Bulletin.*

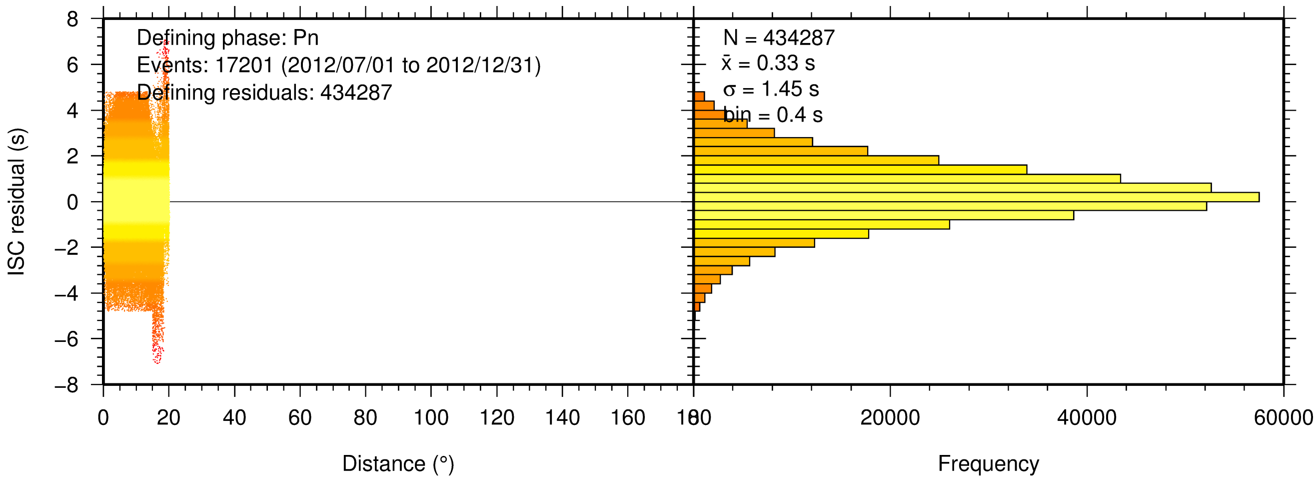

Figure 8.19: *Distribution of travel-time residuals for the defining Pn phases used in the computation of ISC located events in the Bulletin.*

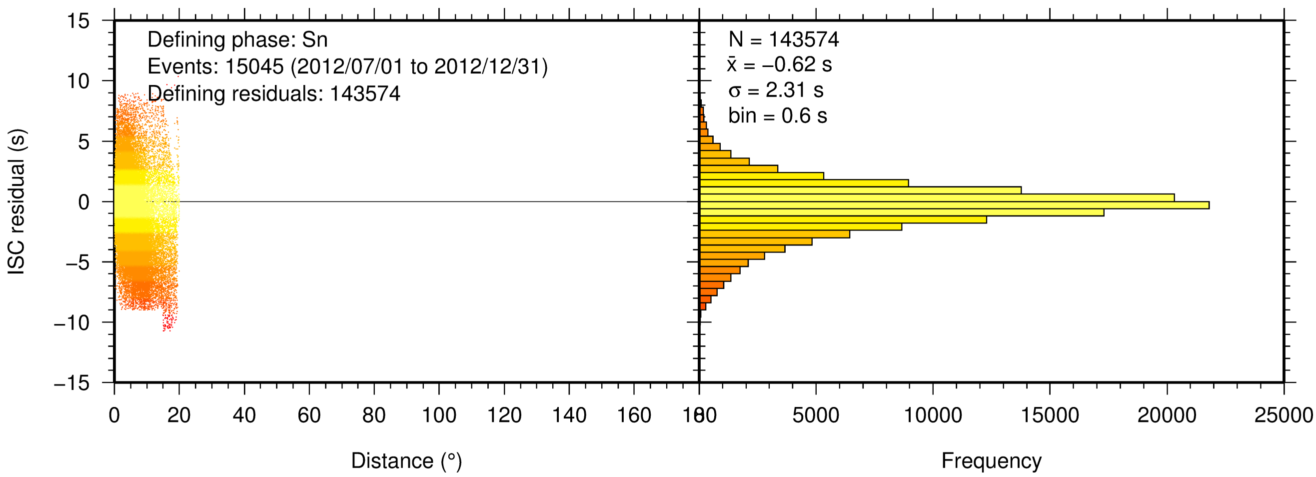

Figure 8.20: *Distribution of travel-time residuals for the defining Sn phases used in the computation of ISC located events in the Bulletin.*

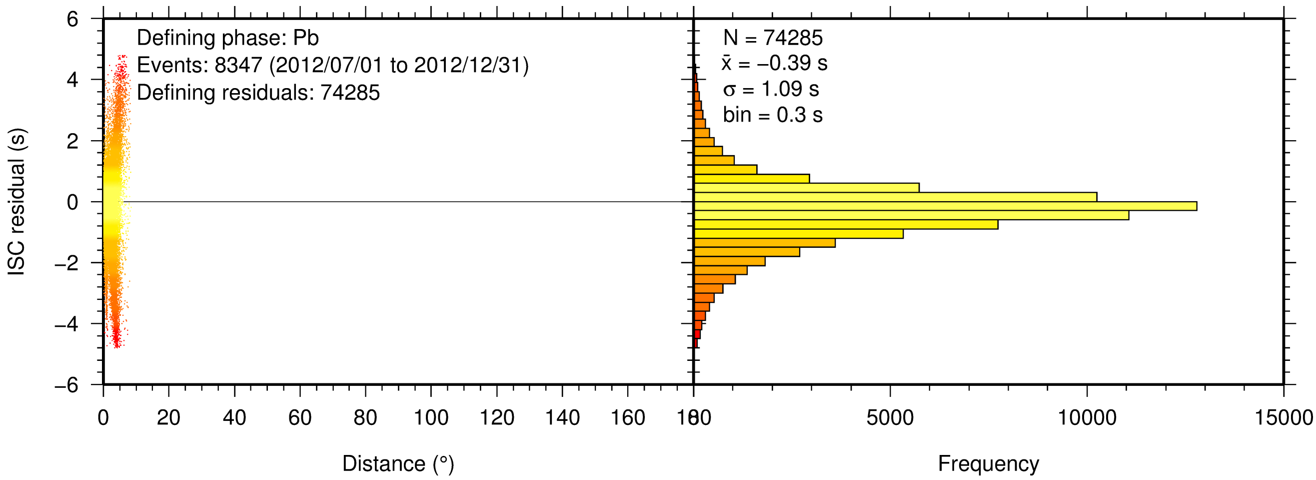

Figure 8.21: *Distribution of travel-time residuals for the defining Pb phases used in the computation of ISC located events in the Bulletin.*

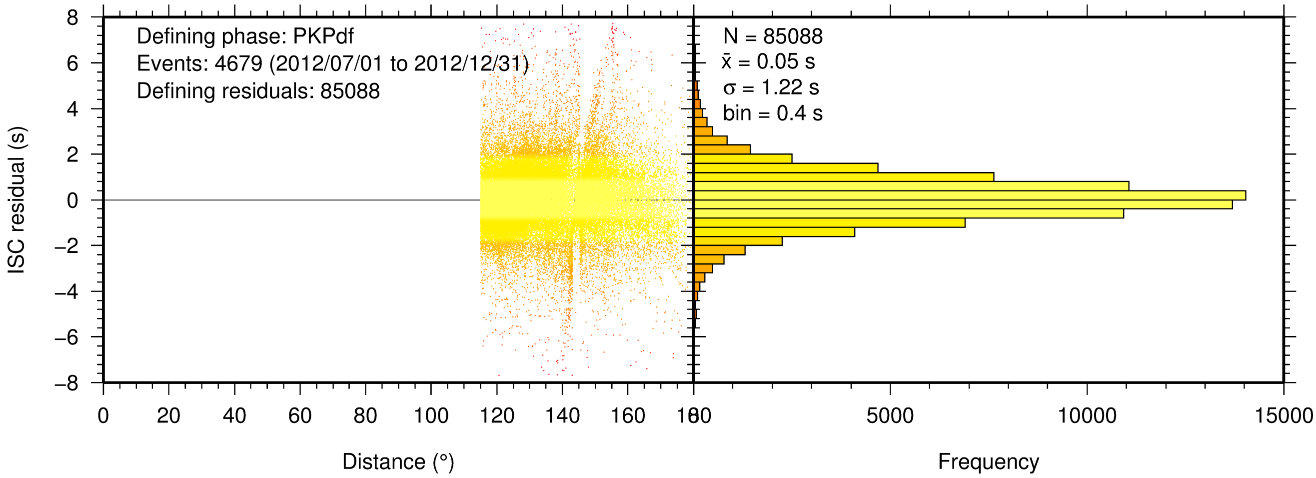

Figure 8.22: *Distribution of travel-time residuals for the defining PKPdf phases used in the computation of ISC located events in the Bulletin.*

8.3 Seismic Wave Amplitudes and Periods

The ISC Bulletin contains a variety of seismic wave amplitudes and periods measured by reporting agencies. For this Bulletin Summary, the total of collected amplitudes and periods is 642655 (see Section 7.3). For the determination of the ISC magnitudes MS and mb, only a fraction of such data can be used. Indeed, the ISC network magnitudes are computed only for ISC located events. Here we recall the main features of the ISC procedure for MS and mb computation (see detailed description in Section 3.4 of January to June 2012 Bulletin Summary). For each amplitude-period pair in a reading the ISC algorithm computes the magnitude (a reading can include several amplitude-period measurements) and the reading magnitude is assigned to the maximum A/T in the reading. If more than one reading magnitude is available for a station, the station magnitude is the median of the reading magnitudes. The network magnitude is computed then as the 20% alpha-trimmed median of the station magnitudes (at least three required). MS is computed for shallow earthquakes (depth $\leq$ 60 km) only and using amplitudes and periods on all three components (when available) if the period is within 10-60 s and the epicentral distance is between 20° and 160°. mb is computed also for deep earthquakes (depth down to 700 km) but only with amplitudes on the vertical component measured at periods $\leq$ 3 s in the distance range 21°-100°.

Table 8.2 is a summary of the amplitude and period data that contributed to the computation of station and ISC MS and mb network magnitudes for this Bulletin Summary.

Table 8.2: *Summary of the amplitude-period data used by the ISC Locator to compute MS and mb.*

	MS	mb
Number of amplitude-period data	131505	511150
Number of readings	115969	506329
Percentage of readings in the ISC located events with qualifying data for magnitude computation	13.5	51.0
Number of station magnitudes	108636	442705
Number of network magnitudes	2982	11325

A small percentage of the readings with qualifying data for MS and mb calculation have more than one amplitude-period pair. Notably, only 13% of the readings for the ISC located (shallow) events included qualifying data for MS computation, whereas for mb the percentage is much higher at 51%. This is due to the seismological practice of reporting agencies. Agencies contributing systematic reports of amplitude and period data are listed in Appendix Table 10.3. Obviously the ISC Bulletin would benefit if more agencies included surface wave amplitude-period data in their reports.

Figure 8.23 shows the distribution of the number of station magnitudes versus distance. For mb there is a significant increase in the distance range 70°-90°, whereas for MS most of the contributing stations are below 100°. The increase in number of station magnitude between 70°-90° for mb is partly due to the very dense distribution of seismic stations in North America and Europe with respect to earthquake occurring in various subduction zones around the Pacific Ocean.

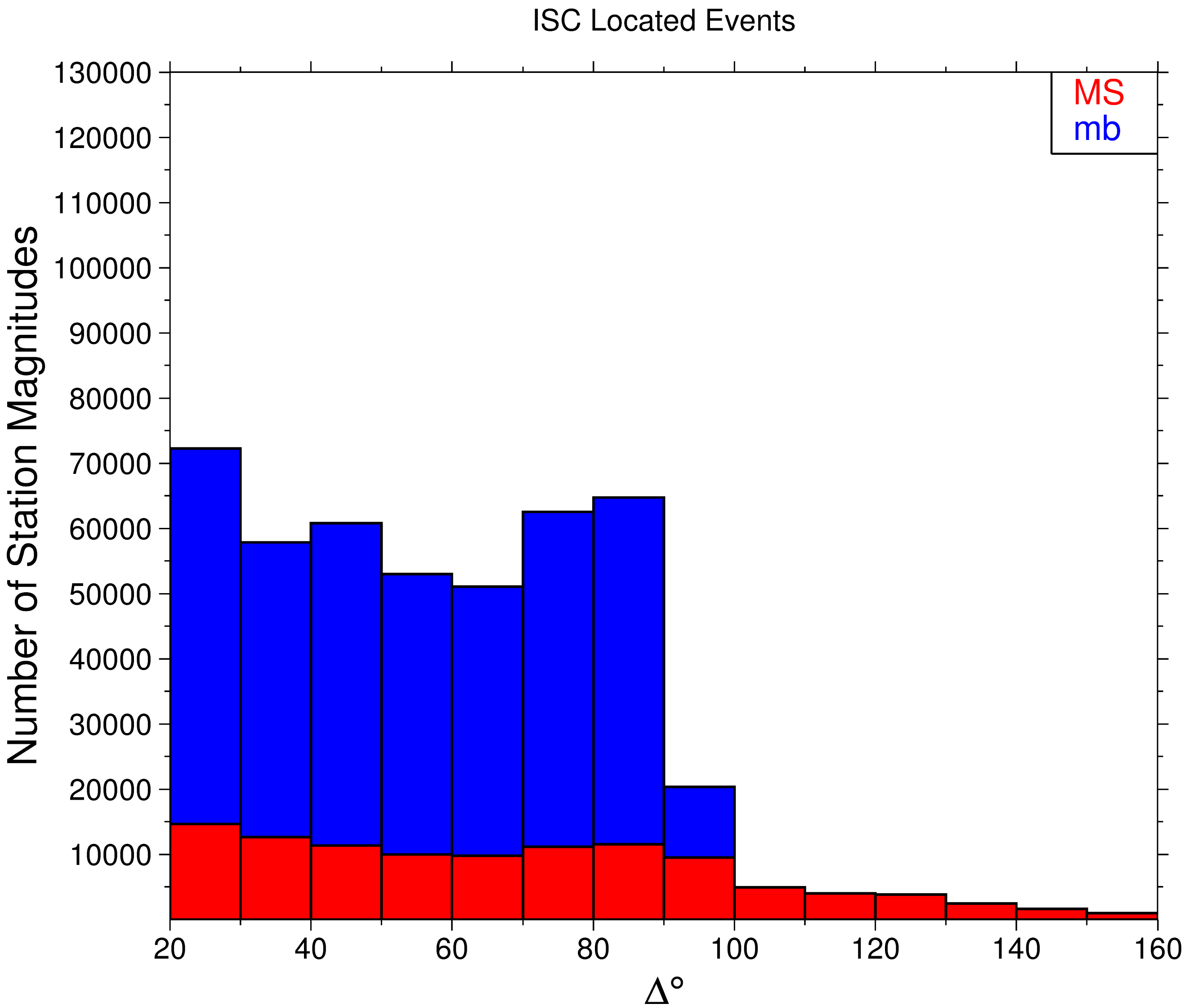

Figure 8.23: *Distribution of the number of station magnitudes computed by the ISC Locator for mb (blue) and MS (red) versus distance.*

Finally, Figure 8.24 shows the distribution of network MS and mb as well as the median number of stations for magnitude bins of 0.2. Clearly with increasing magnitude the number of events is smaller but with a general tendency of having more stations contributing to the network magnitude.

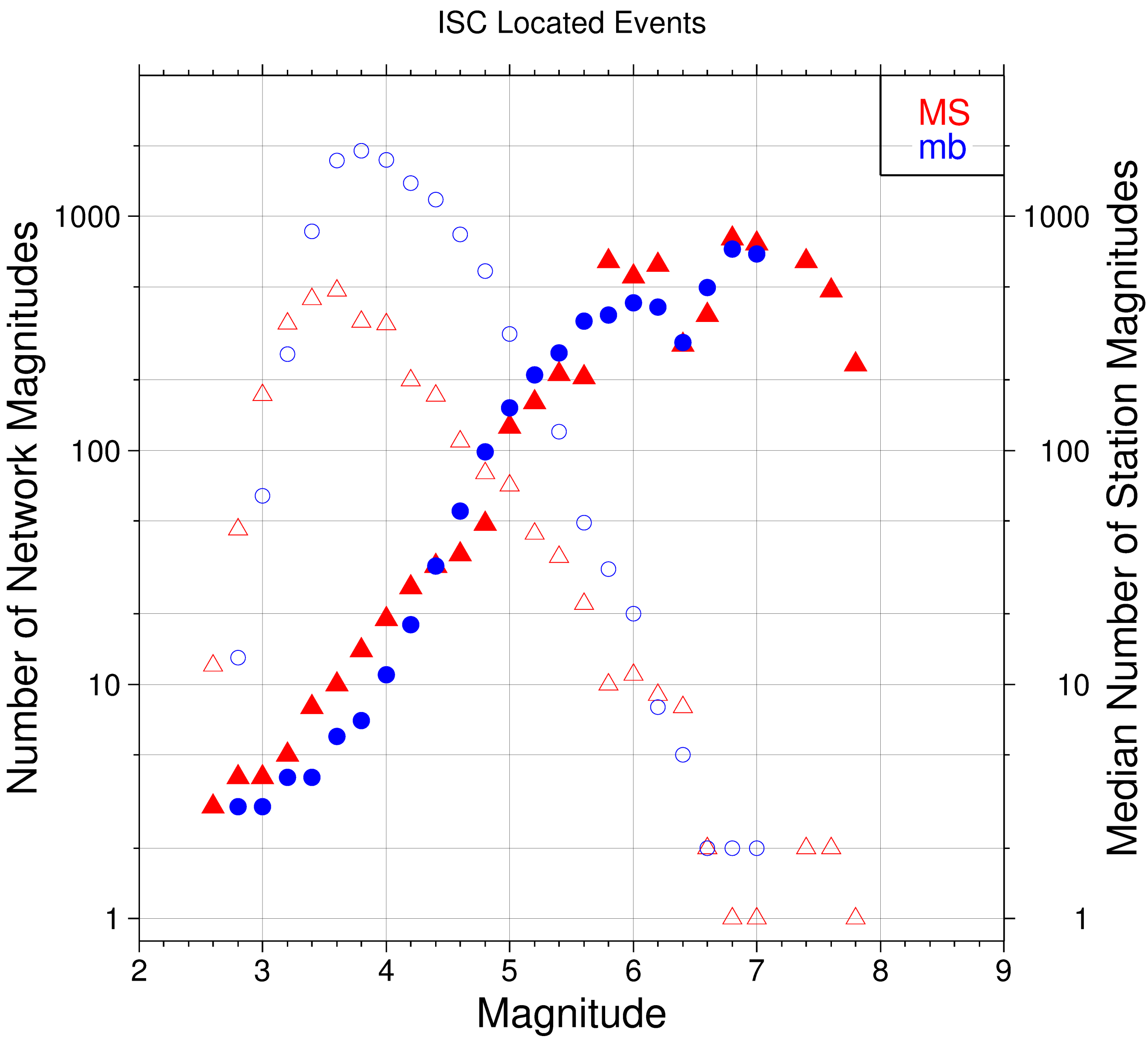

Figure 8.24: *Number of network magnitudes (open symbols) and median number of stations magnitudes (filled symbols). Blue circles refer to mb and red triangles to MS. The width of the magnitude interval δM is 0.2, and each symbol includes data with magnitude in $M \pm \delta M/2$.*

8.4 Completeness of the ISC Bulletin

The completeness of the ISC Bulletin can be expressed as a magnitude value, above which we expect the Bulletin to contain 100% of events. This magnitude of completeness, M_C can be measured as the point where the seismicity no longer follows the Gutenberg-Richter relationship. We compute an estimate of M_C using the maximum curvature technique of *Woessner and Wiemer* (2005).

The completeness of the ISC Bulletin for this summary period is shown in Figure 8.25. A history of completeness for the ISC Bulletin is shown in Figure 8.26. The step change in 1996 corresponds with the inclusion of the Prototype IDC (EIDC) Bulletin, followed by the Reviewed Event Bulletin (REB) of the IDC.

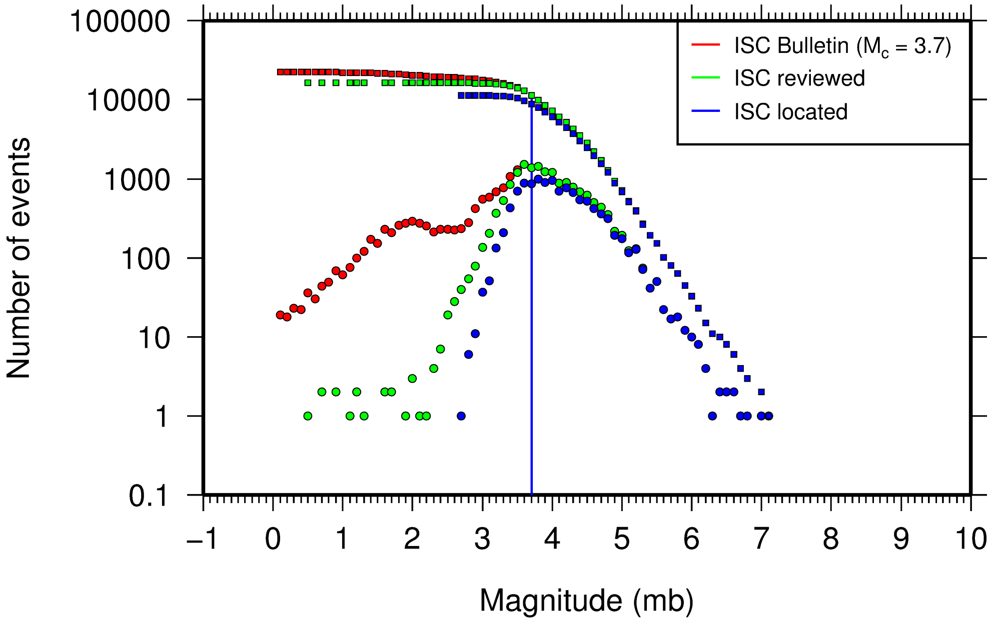

Figure 8.25: *Frequency and cumulative frequency magnitude distribution for all events in the ISC Bulletin, ISC reviewed events and events located by the ISC. The magnitude of completeness (M_C) is shown for the ISC Bulletin. Note: only events with values of mb are represented in the figure.*

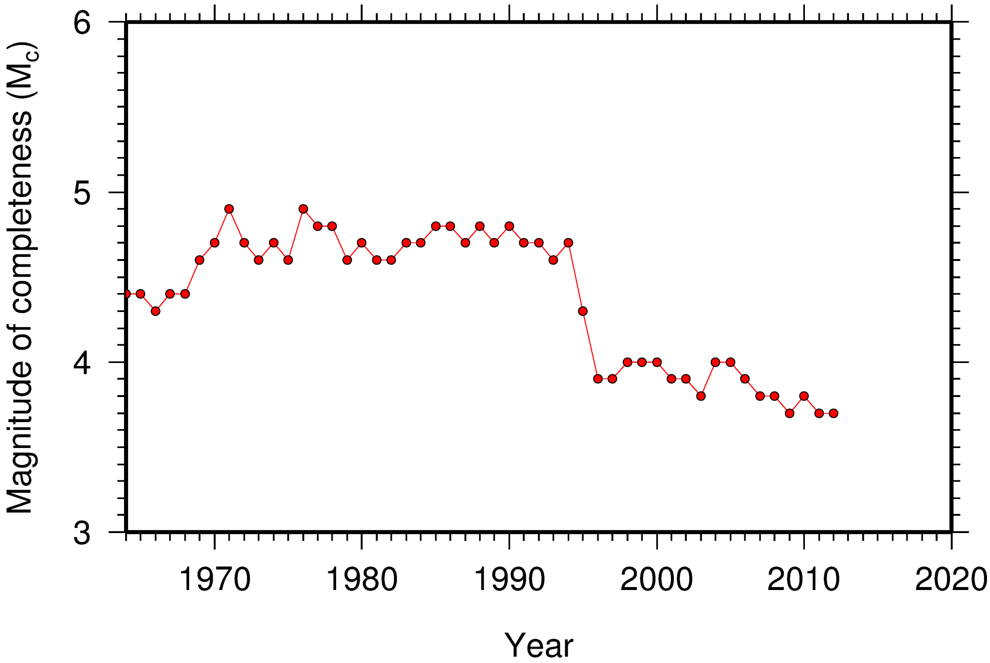

Figure 8.26: *Variation of magnitude of completeness (M_C) for each year in the ISC Bulletin. Note: M_C is calculated only using those events with values of mb.*

8.5 Magnitude Comparisons

The ISC Bulletin publishes network magnitudes reported by multiple agencies to the ISC. For events that have been located by the ISC, where enough amplitude data has been collected, the MS and mb magnitudes are calculated by the ISC (MS is computed only for depths $\leq$ 60 km). In this section, ISC magnitudes and some other reported magnitudes in the ISC Bulletin are compared.

The comparison between MS and mb computed by the ISC locator for events in this summary period is shown in Figure 8.27, where the large number of data pairs allows a colour coding of the data density. The scatter in the data reflects the fundamental differences between these magnitude scales.

Similar plots are shown in Figure 8.28 and 8.29, respectively, for comparisons of ISC mb and ISC MS with M_W from the GCMT catalogue. Since M_W is not often available below magnitude 5, these distributions are mostly for larger, global events. Not surprisingly, the scatter between mb and M_W is larger than the scatter between MS and M_W. Also, the saturation effect of mb is clearly visible for earthquakes with $M_W > 6.5$. In contrast, MS scales well with $M_W > 6$, whereas for smaller magnitudes MS appears to be systematically smaller than M_W.

In Figure 8.30 ISC values of mb are compared with all reported values of mb, values of mb reported by NEIC and values of mb reported by IDC. Similarly in Figure 8.31, ISC values of MS are compared with all reported values of MS, values of MS reported by NEIC and values of MS reported by IDC. There is a large scatter between the ISC magnitudes and the mb and MS reported by all other agencies.

The scatter decreases both for mb and MS when ISC magnitudes are compared just with NEIC and IDC magnitudes. This is not surprising as the latter two agencies provide most of the amplitudes and periods used by the ISC locator to compute MS and mb. However, ISC mb appears to be smaller than NEIC mb for $mb < 4$ and larger than IDC mb for $mb > 4$. Since NEIC does not include IDC amplitudes, it seems these features originate from observations at the high-gain, low-noise sites reported by the IDC. For the MS comparisons between ISC and NEIC a similar but smaller effect is observed for $MS < 4.5$, whereas a good scaling is generally observed for the MS comparisons between ISC and IDC.

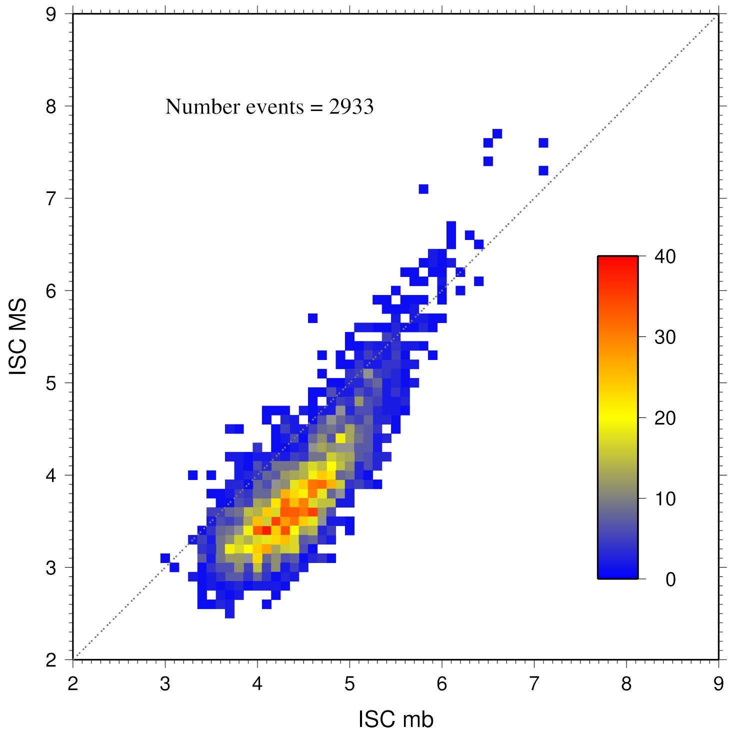

Figure 8.27: *Comparison of ISC values of MS with mb for common event pairs.*

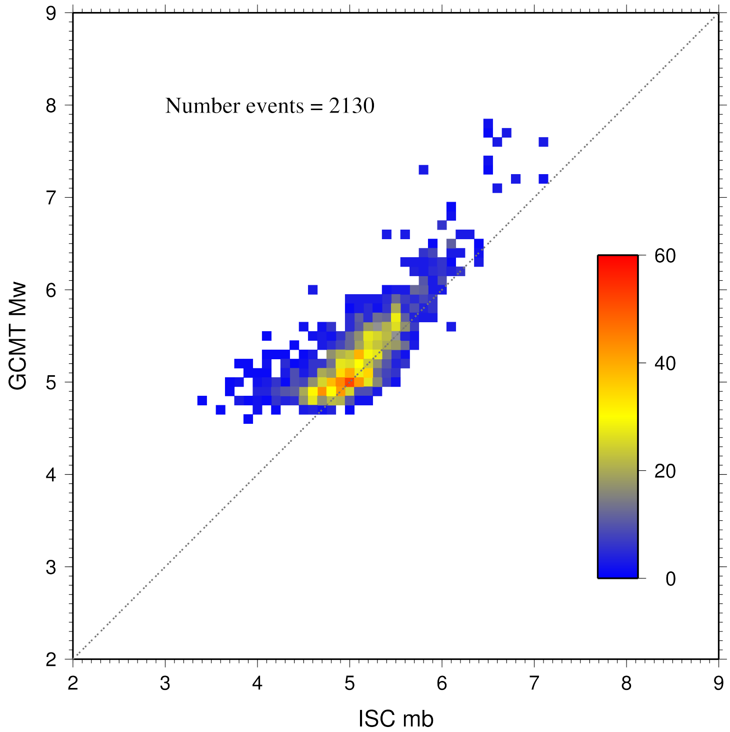

Figure 8.28: *Comparison of ISC values of mb with GCMT M_W for common event pairs.*

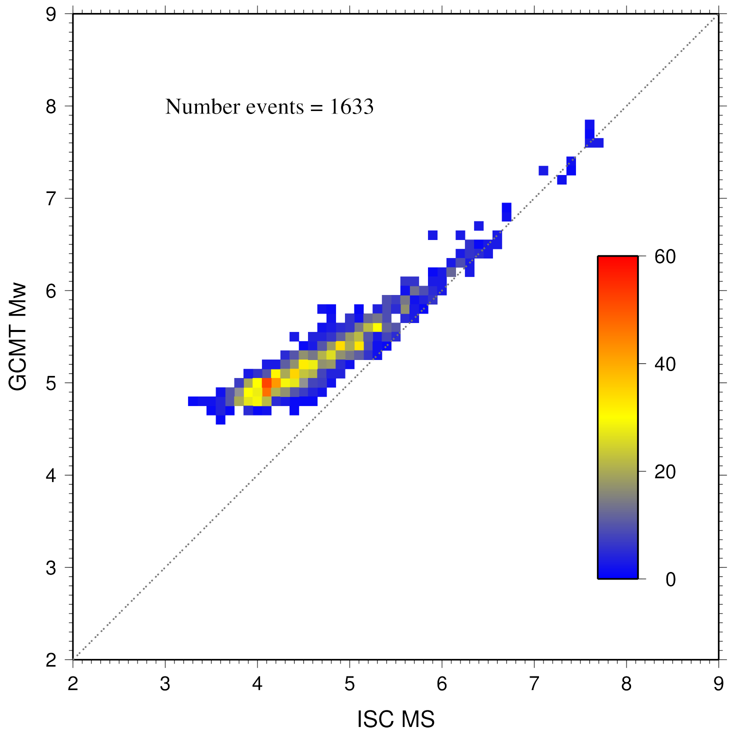

Figure 8.29: *Comparison of ISC values of MS with GCMT M_W for common event pairs.*

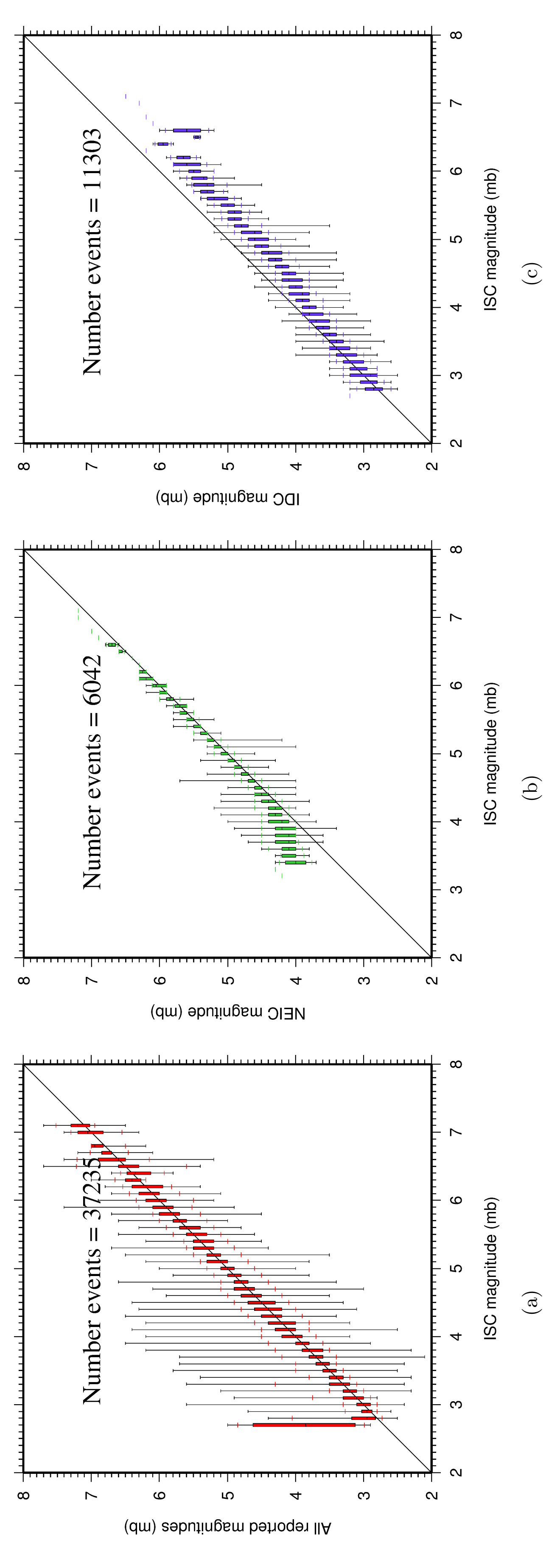

Figure 8.30: *Comparison of ISC magnitude data (mb) with additional agency magnitudes (mb). The statistical summary is shown in box-and-whisker plots where the 10th and 90th percentiles are shown in addition to the max and min values. (a): All magnitudes reported; (b): NEIC magnitudes; (c): IDC magnitudes.*

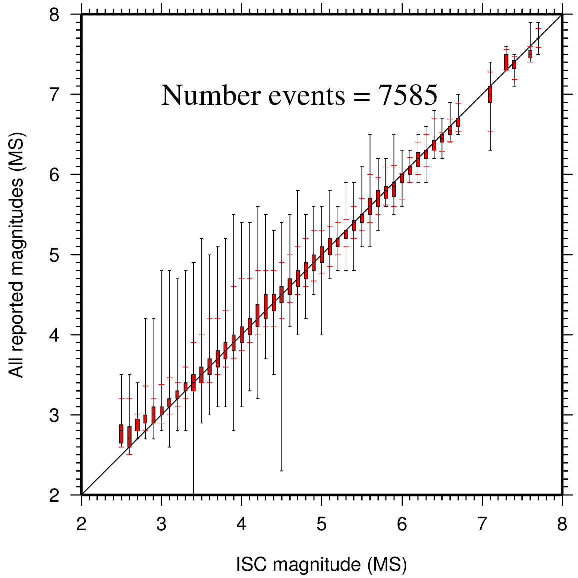

(a)

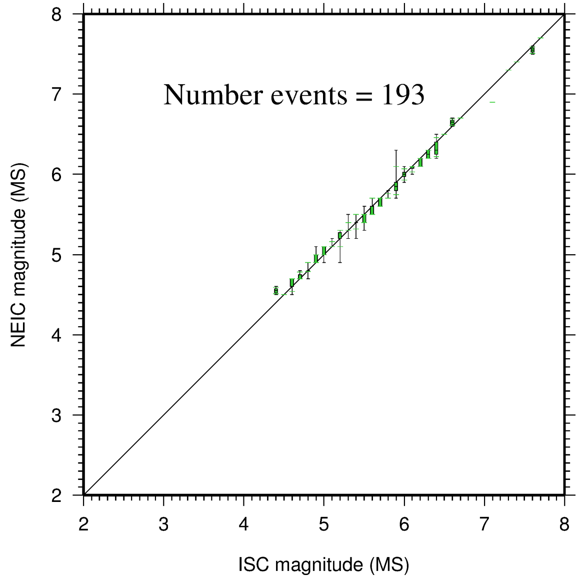

(b)

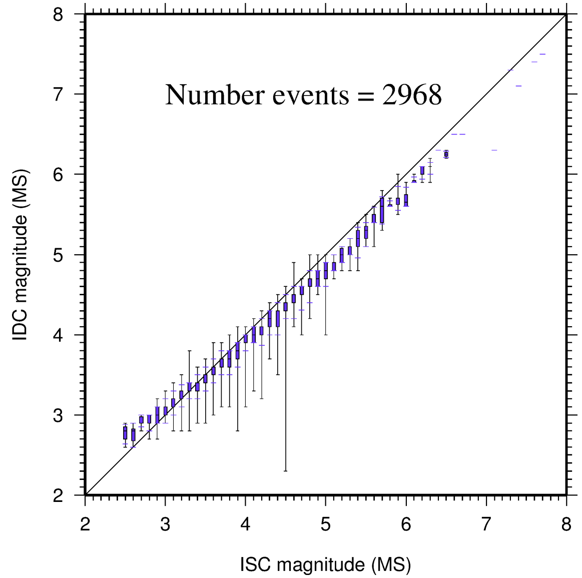

(c)

Figure 8.31: *Comparison of ISC magnitude data (MS) with additional agency magnitudes (MS). The statistical summary is shown in the box-and-whisker plots where the 10th and 90th percentiles are shown in addition to the max and min values. (a): All magnitudes reported; (b): NEIC magnitudes; (c): IDC magnitudes.*

9

The Leading Data Contributors

For the current six-month period, 142 agencies reported related bulletin data. Although we are grateful for every report, we nevertheless would like to acknowledge those agencies that made the most useful or distinct contributions to the contents of the ISC Bulletin. Here we note those agencies that:

- provided a comparatively large volume of parametric data (see Section 9.1),
- reported data that helped quite considerably to improve the quality of the ISC locations or magnitude determinations (see Section 9.2),
- helped the ISC by consistently reporting data in one of the standard recognised formats and in-line with the ISC data collection schedule (see Section 9.3).

We do not aim to discourage those numerous small networks who provide comparatively smaller yet still most essential volumes of regional data regularly, consistently and accurately. Without these reports the ISC Bulletin would not be as comprehensive and complete as it is today.

9.1 The Largest Data Contributors

We acknowledge the contribution of MOS, BJI, USArray, GCMT, NEIC, IDC, PRU, CLL and a few others (Figure 9.1) that reported the majority of moderate to large events recorded at teleseismic distances. The contributions of NEIC, IDC, BJI and several others are also acknowledged with respect to smaller seismic events. The contributions of IDC, JMA, NEIC, TAP, DDA, MEX, ATH, ISK and a number of others are also acknowledged with respect to small seismic events. Note that the NEIC bulletin accumulates a contribution of all regional networks in the USA. Similarly, the CSEM communicates contributions of many tens of European and Mediterranean networks a few of which the ISC does not always receive directly. Several agencies monitoring highly seismic regions routinely report large volumes of small to moderate magnitude events, such as those in Japan, Chinese Taipei, Turkey, Chile, Italy, Greece, New Zealand, Norway, Mexico and Columbia. Contributions of small magnitude events by agencies in regions of low seismicity, such as Finland and Saudia Arabia are also gratefully received.

We also would like to acknowledge contributions of those agencies that report a large portion of arrival time and amplitude data (Figure 9.2). For small magnitude events, these are local agencies in charge of monitoring local and regional seismicity. For moderate to large events, contributions of NEIC, USArray, MOS and IDC are especially acknowledged. Notably, three agencies (IDC, NEIC and MOS) together reported approximately 80% of all amplitude measurements made for teleseismically recorded events. We hope that other agencies would also be able to update their monitoring routines in the future to include the amplitude reports for teleseismic events compliant with the IASPEI standards.

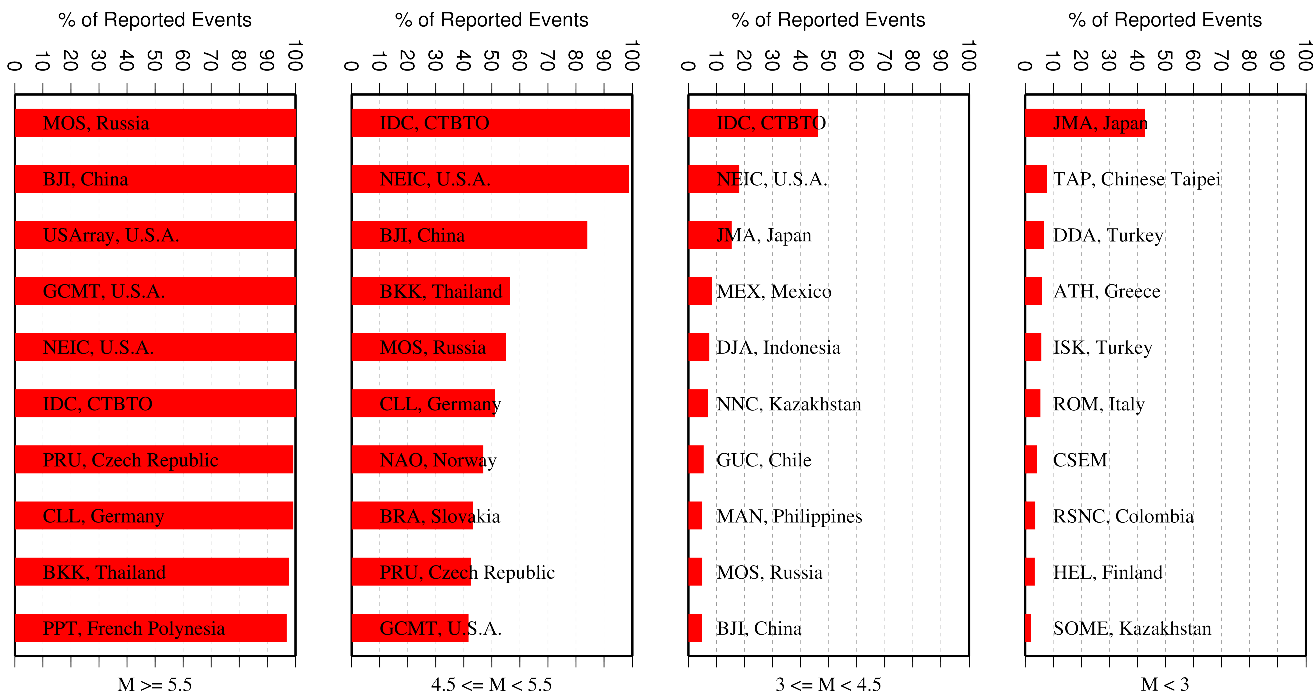

Figure 9.1: *Frequency of events in the ISC Bulletin for which an agency reported at least one item of data: a moment tensor, a hypocentre, a station arrival time or an amplitude. The top ten agencies are shown for four magnitude intervals.*

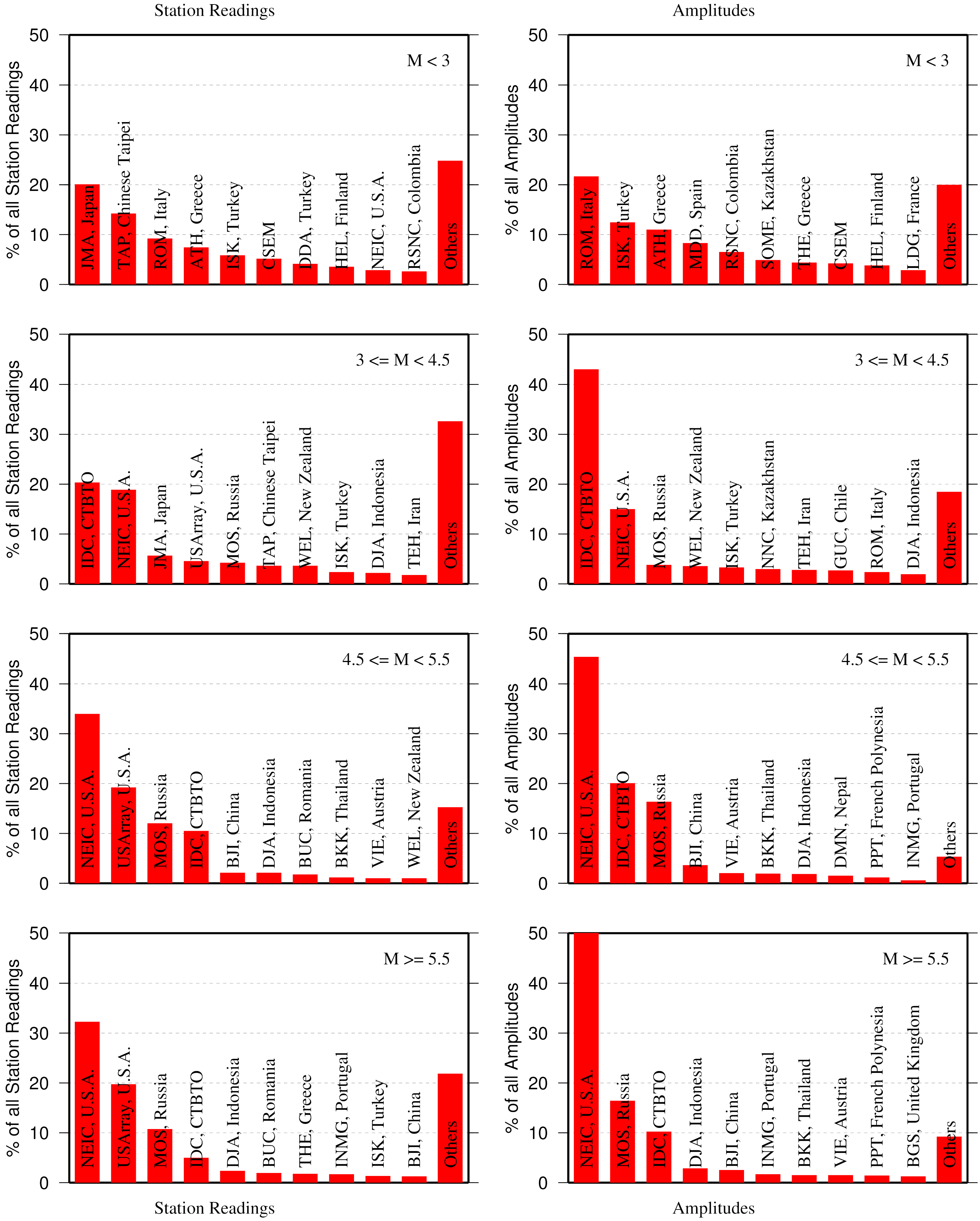

Figure 9.2: *Contributions of station arrival time readings (left) and amplitudes (right) of agencies to the ISC Bulletin. Top ten agencies are shown for four magnitude intervals.*

9.2 Contributors Reporting the Most Valuable Parameters

One of the main ISC duties is to re-calculate hypocentre estimates for those seismic events where a collective wealth of all station reports received from all agencies is likely to improve either the event location or depth compared to the hypocentre solution from each single agency. For areas with a sparse local seismic network or an unfavourable station configuration, readings made by other networks at teleseismic distances are very important. All events near mid-oceanic ridges as well as those in the majority of subduction zones around the world fall into this category. Hence we greatly appreciate the effort made by many agencies that report data for remote earthquakes (Figure 9.3). For some agencies, such as the IDC and the NEIC, it is part of their mission. For instance, the IDC reports almost every seismic event that is large enough to be recorded at teleseismic distance (20 degrees and beyond). This is largely because the International Monitoring System of primary arrays and broadband instruments is distributed at quiet sites around the world in order to be able to detect possible violations of the Comprehensive Nuclear-Test-Ban Treaty. The NEIC reported approximately 35% of those events as their mission requires them to report events above magnitude 4.5 outside the United States of America. For other agencies reporting distant events it is an extra effort that they undertake to notify their governments and relief agencies as well as to help the ISC and academic research in general. Hence these agencies usually report on the larger magnitude events. BJI, NAO, MOS, CLL, BKK, BRA, PRU and PPT each reported individual station arrivals for several percent of all relevant events. We encourage other agencies to report distant events to us.

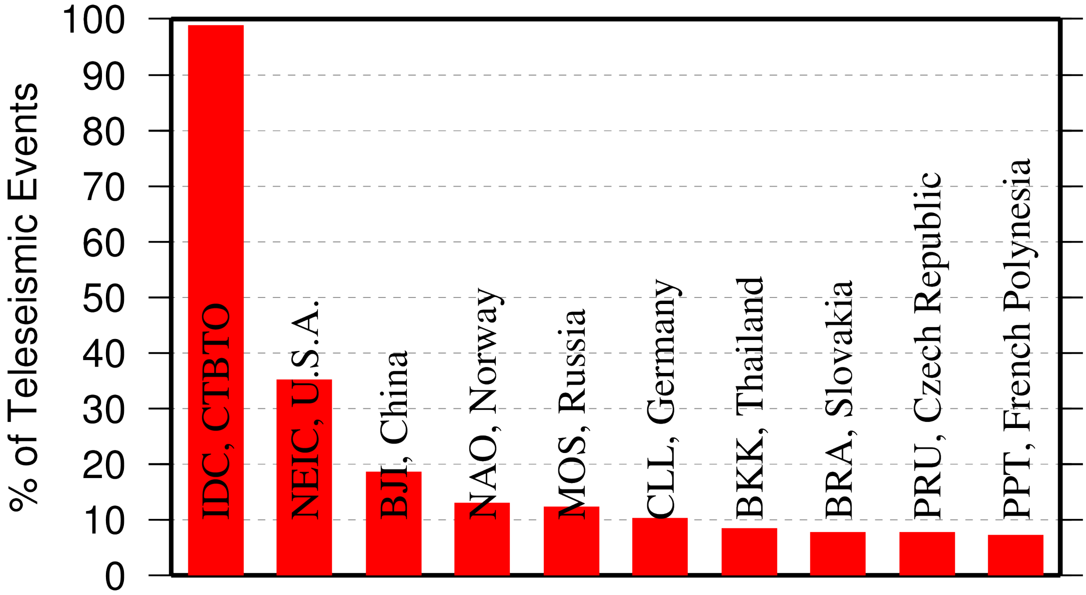

Figure 9.3: *Top ten agencies that reported teleseismic phase arrivals for a large portion of ISC events.*

In addition to the first arriving phase we encourage reporters to contribute observations of secondary seismic phases that help constrain the event location and depth: S, Sn, Sg and pP, sP, PcP (Figure 9.4). We expect though that these observations are actually made from waveforms, rather than just predicted by standard velocity models and modern software programs. It is especially important that these arrivals are manually reviewed by an operator (as we know takes place at the IDC and NEIC), as opposed to some lesser attempts to provide automatic phase readings that are later rejected by the ISC due to a generally poor quality of unreviewed picking.

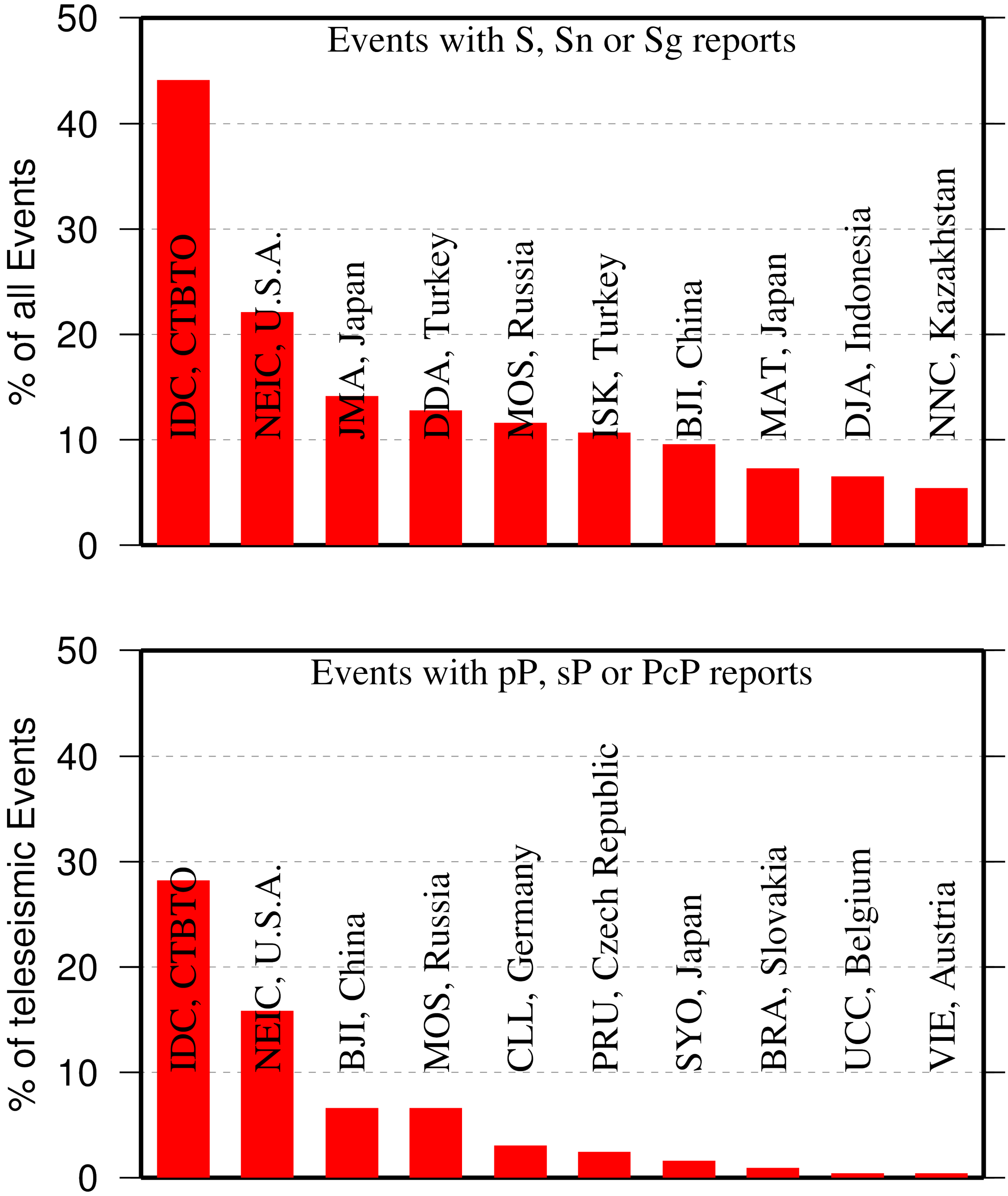

Figure 9.4: *Top ten agencies that reported secondary phases important for an accurate epicentre location (top) and focal depth determination (bottom).*

Another important long-term task that the ISC performs is to compute the most definitive values of MS and mb network magnitudes that are considered reliable due to removal of outliers and consequent averaging (using alpha-trimmed median) across the largest network of stations, generally not feasible for a single agency. Despite concern over the bias at the lower end of mb introduced by the body wave amplitude data from the IDC, other agencies are also known to bias the results. This topic is further discussed in Section 8.5.

Notably, the IDC reports almost 100% of all events for which MS and mb are estimated. This is due to the standard routine that requires determination of body and surface wave magnitudes useful for discrimination purposes. NEIC, MOS, BJI, NAO, PRU and a few other agencies (Figure 9.5) are also responsible for the majority of the amplitude and period reports that contribute towards the ISC magnitudes.

Since the ISC does not routinely process waveforms, we rely on other agencies to report moment magnitudes as well as moment tensor determinations (Figure 9.6).

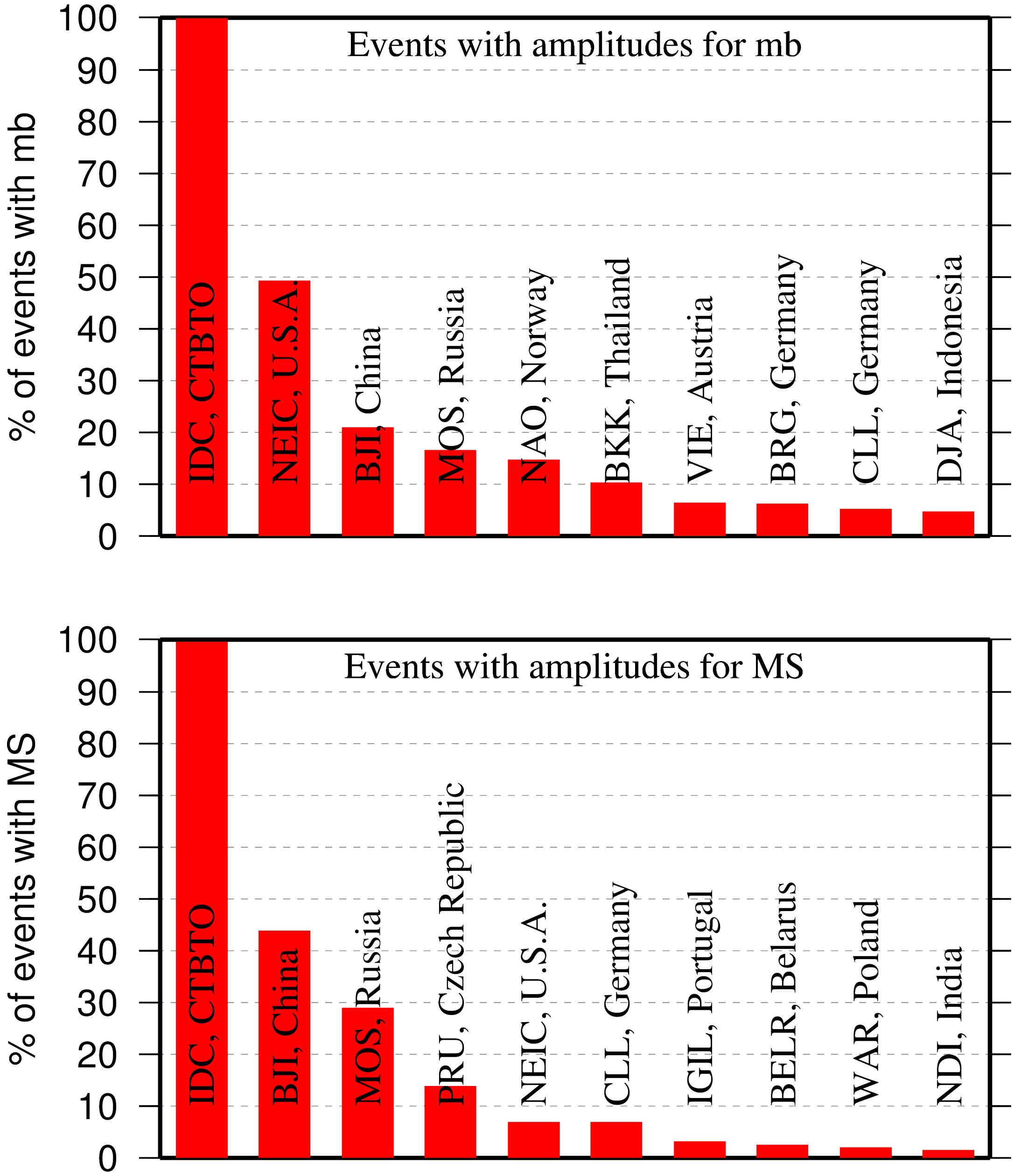

Figure 9.5: *Agencies that report defining body (top) and surface (bottom) wave amplitudes and periods for the largest fraction of those ISC Bulletin events with MS/mb determinations.*

Among other event parameters the ISC Bulletin also contains information on event type. We cannot independently verify the type of each event in the Bulletin and thus rely on other agencies to report the event type to us. Practices of reporting non-tectonic events vary greatly from country to country. Many agencies do not include anthropogenic events in their reports. Suppression of such events from reports to the ISC may lead to a situation where a neighbouring agency reports the anthropogenic event as an earthquake for which expected data are missing. This in turn is detrimental to ISC Bulletin users studying natural seismic hazard. Hence we encourage all agencies to join the agencies listed on Figure 9.7 and several others in reporting both natural and anthropogenic events to the ISC.

The ISC Bulletin also contains felt and damaging information when local agencies have reported it to us. Agencies listed on Figure 9.8 provide such information for the majority of all felt or damaging events in the ISC Bulletin.

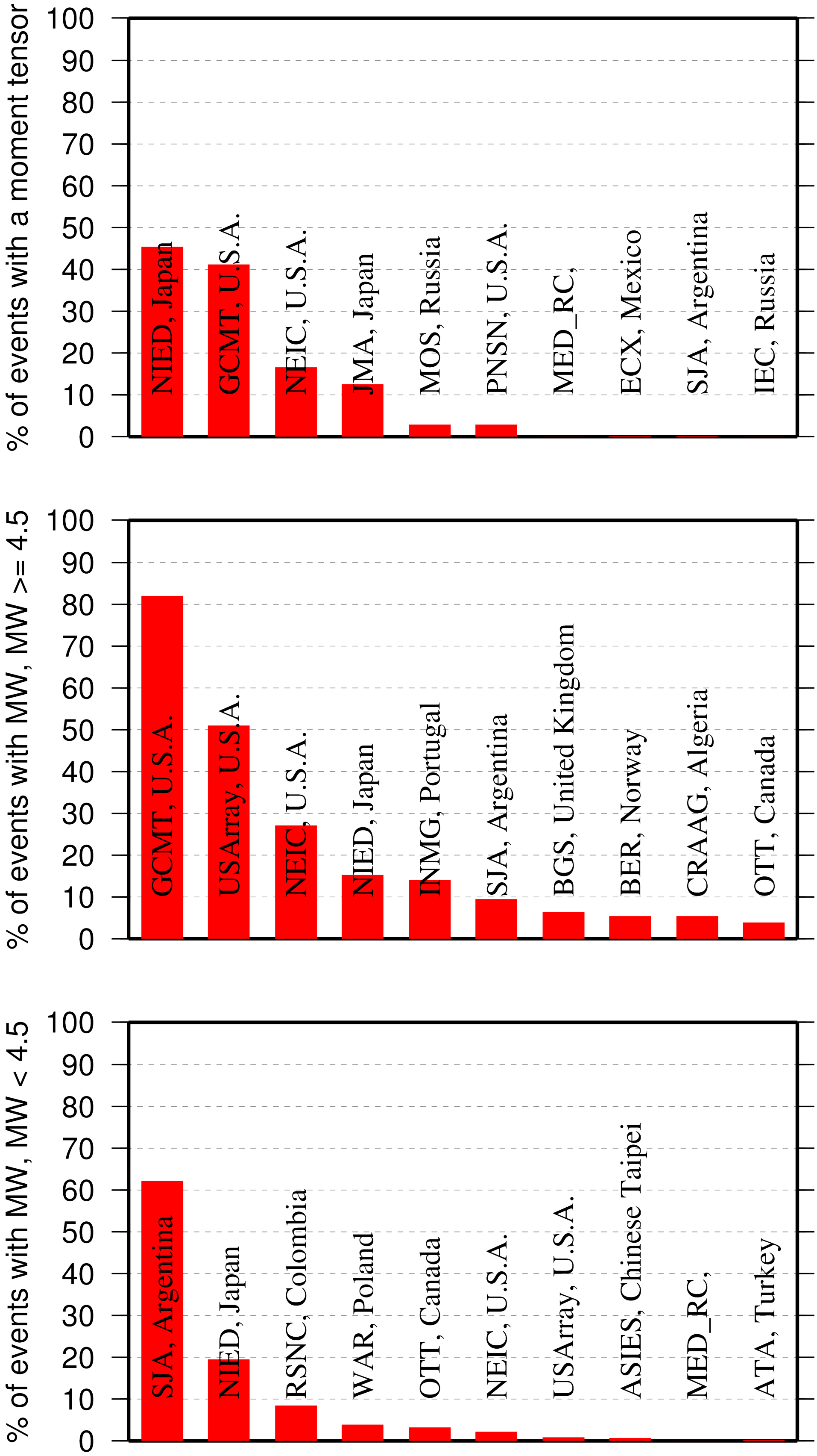

Figure 9.6: *Top ten agencies that most frequently report determinations of seismic moment tensor (top) and moment magnitude (middle/bottom for M greater/smaller than 4.5).*

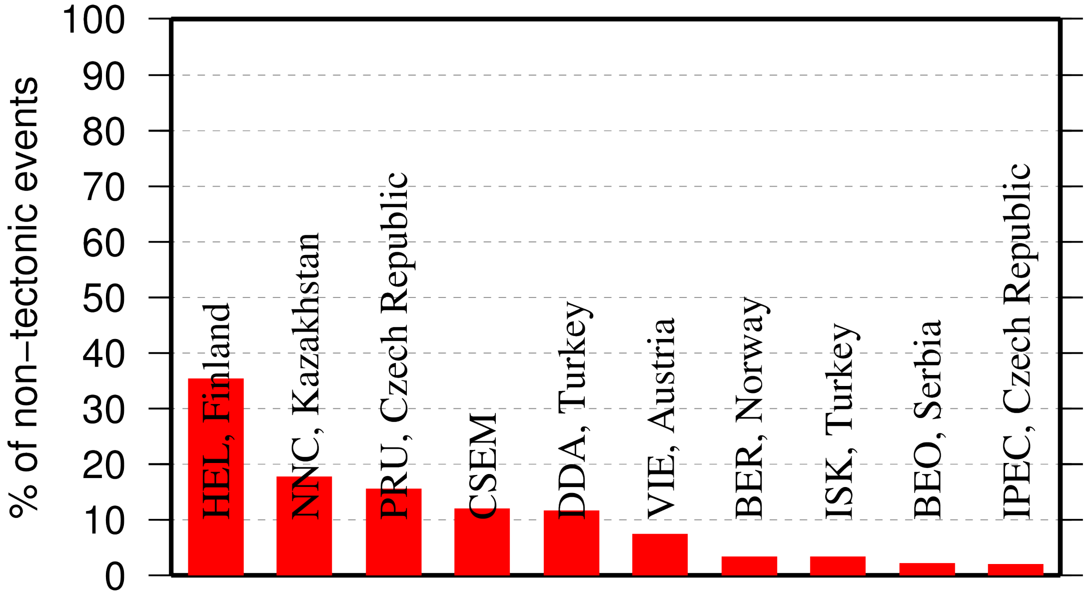

Figure 9.7: *Top ten agencies that most frequently report non-tectonic seismic events to the ISC.*

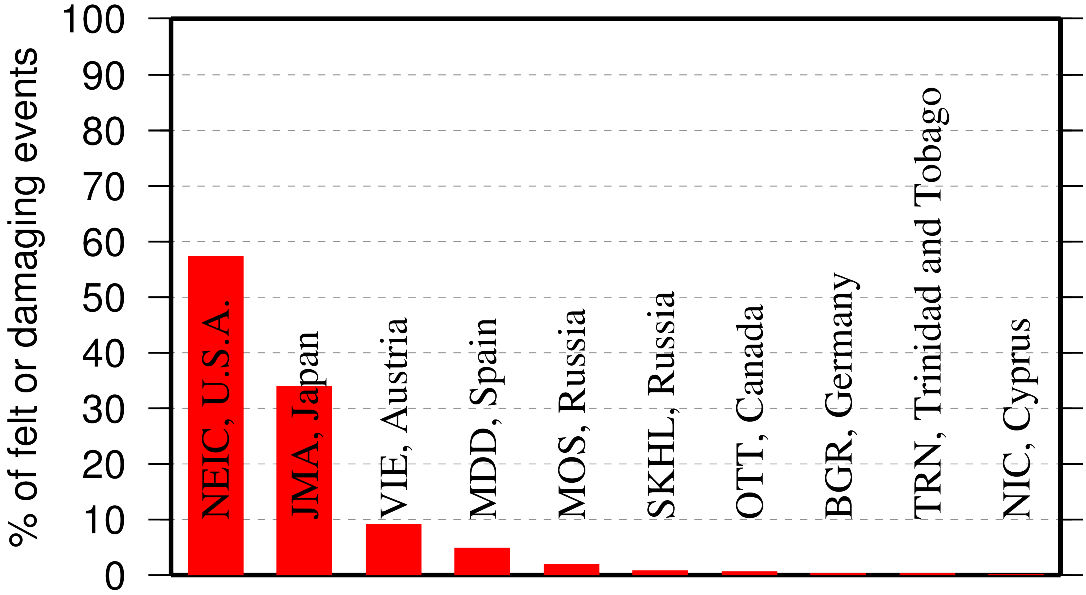

Figure 9.8: *Top ten agencies that most frequently report macroseismic information to the ISC.*

9.3 The Most Consistent and Punctual Contributors

During this six-month period, 30 agencies reported their bulletin data in one of the standard seismic formats (ISF, IMS, GSE, Nordic or QuakeML) and within the current 12-month deadline. Here we must reiterate that the ISC accepts reviewed bulletin data after a final analysis as soon as they are ready. These data, even if they arrive before the deadline, are immediately parsed into the ISC database, grouped with other data and become available to the ISC users on-line as part of the preliminary ISC Bulletin. There is no reason to wait until the deadline to send the data to the ISC. Table 9.1 lists all agencies that have been helpful to the ISC in this respect during the six-month period.

Table 9.1: *Agencies that contributed reviewed bulletin data to the ISC in one of the standard international formats before the submission deadline.*

Agency Code	Country	Average Delay from real time (days)
PPT	French Polynesia	20
NAO	Norway	27
LIC	Ivory Coast	28
LDG	France	29
IGIL	Portugal	32
PDG	Montenegro	42
KRSC	Russia	47
BUL	Zimbabwe	48
UCC	Belgium	50
DMN	Nepal	57
IDC	Austria	58
SVSA	Portugal	64
BGR	Germany	70
ISK	Turkey	72
BEO	Serbia	76
ISN	Iraq	79
NSSC	Syria	79
AUST	Australia	84
BJI	China	88
ATA	Turkey	129
ASRS	Russia	137
NERS	Russia	145
BGS	United Kingdom	151
THE	Greece	156
INMG	Portugal	169
LIT	Lithuania	186
ECX	Mexico	204
BYKL	Russia	226
DDA	Turkey	254
ATH	Greece	255
IRIS	U.S.A.	265
QCP	Philippines	274
GSDM	Malawi	297
DBN	Netherlands	298
KNET	Kyrgyzstan	313
MOS	Russia	329

10

Appendix

Table 10.1: *Listing of all 324 agencies that have directly reported to the ISC. The 142 agencies highlighted in bold have reported data to the ISC Bulletin for the period of this Bulletin Summary.*

Agency Code	Agency Name
AAA	Alma-ata, Kazakhstan
AAE	**University of Addis Ababa, Ethiopia**
AAM	University of Michigan, USA
ADE	Primary Industries and Resources SA, Australia
ADH	Observatorio Afonso Chaves, Portugal
AEIC	Alaska Earthquake Information Center, USA
AFAR	The Afar Depression: Interpretation of the 1960-2000 Earthquakes, Israel
ALG	Algiers University, Algeria
ANF	USArray Array Network Facility, USA
ANT	Antofagasta, Chile
ARE	Instituto Geofisico del Peru, Peru
ARO	**Observatoire Géophysique d'Arta, Djibouti**
ASIES	**Institute of Earth Sciences, Academia Sinica, Chinese Taipei**
ASL	Albuquerque Seismological Laboratory, USA
ASM	University of Asmara, Eritrea
ASRS	**Altai-Sayan Seismological Centre, GS SB RAS, Russia**
ATA	**The Earthquake Research Center Ataturk University, Turkey**
ATH	**National Observatory of Athens, Greece**
AUST	**Geoscience Australia, Australia**
AWI	**Alfred Wegener Institute for Polar and Marine Research, Germany**
AZER	**Republic Center of Seismic Survey, Azerbaijan**
BCIS	Bureau Central International de Sismologie, France
BDF	Observatório Sismológico da Universidade de Brasília, Brazil
BELR	**Centre of Geophysical Monitoring, Belarus**
BEO	**Seismological Survey of Serbia, Serbia**
BER	**University of Bergen, Norway**
BERK	Berkheimer H, Germany
BGR	**Bundesanstalt für Geowissenschaften und Rohstoffe, Germany**
BGS	**British Geological Survey, United Kingdom**
BHUJ2	Study of Aftershocks of the Bhuj Earthquake by Japanese Research Team, Japan
BIAK	Biak earthquake aftershocks (17-Feb-1996), USA
BJI	**China Earthquake Networks Center, China**
BKK	**Thai Meteorological Department, Thailand**
BNS	Erdbebenstation, Geologisches Institut der Universität, Köl, Germany
BOG	Universidad Javeriana, Colombia
BRA	**Geophysical Institute, Slovak Academy of Sciences, Slovakia**

Table 10.1: Continued.

Agency Code	Agency Name
BRG	**Seismological Observatory Berggießhübel, TU Bergakademie Freiberg**, **Germany**
BRK	Berkeley Seismological Laboratory, USA
BRS	Brisbane Seismograph Station, Australia
BUC	**National Institute for Earth Physics**, **Romania**
BUD	**Geodetic and Geophysical Research Institute**, **Hungary**
BUG	Institute of Geology, Mineralogy & Geophysics, Germany
BUL	**Goetz Observatory**, **Zimbabwe**
BUT	Montana Bureau of Mines and Geology, USA
BYKL	**Baykal Regional Seismological Centre, GS SB RAS**, **Russia**
CADCG	Central America Data Centre, Costa Rica
CAN	Australian National University, Australia
CANSK	Canadian and Scandinavian Networks, Sweden
CAR	Instituto Sismologico de Caracas, Venezuela
CASC	Central American Seismic Center, Costa Rica
CERI	Center for Earthquake Research and Information, USA
CLL	**Geophysikalisches Observatorium Collm**, **Germany**
CMWS	Laboratory of Seismic Monitoring of Caucasus Mineral Water Region, GSRAS, Russia
CNG	Seismographic Station Changalane, Mozambique
CNRM	**Centre National de Recherche**, **Morocco**
COSMOS	Consortium of Organizations for Strong Motion Observations, USA
CRAAG	**Centre de Recherche en Astronomie, Astrophysique et Géophysique**, **Algeria**
CSC	University of South Carolina, USA
CSEM	**Centre Sismologique Euro-Méditerranéen (CSEM/EMSC)**, **France**
DASA	Defense Atomic Support Agency, USA
DBN	**Koninklijk Nederlands Meteorologisch Instituut**, **Netherlands**
DDA	**Disaster and Emergency Management Presidency**, **Turkey**
DHMR	**Yemen National Seismological Center**, **Yemen**
DIAS	**Dublin Institute for Advanced Studies**, **Ireland**
DJA	**Badan Meteorologi, Klimatologi dan Geofisika**, **Indonesia**
DMN	**Department of Mines and Geology, Ministry of Industry of Nepal**, **Nepal**
DNK	**Geological Survey of Denmark and Greenland**, **Denmark**
DRS	Dagestan Branch, Geophysical Survey, Russian Academy of Sciences, Russia
DSN	**Dubai Seismic Network**, **United Arab Emirates**
DUSS	Damascus University, Syria, Syria
EAF	**East African Network**, **Unknown**
EAGLE	Ethiopia-Afar Geoscientific Lithospheric Experiment, Unknown
EBR	Observatori de l'Ebre, Spain
EBSE	Ethiopian Broadband Seismic Experiment, Unknown
ECX	**Red Sismica del Noroeste de Mexico (RESOM)**, **Mexico**
EFATE	OBS Experiment near Efate, Vanuatu, USA
EHB	Engdahl, van der Hilst and Buland, USA

Table 10.1: Continued.

Agency Code	Agency Name
EIDC	Experimental (GSETT3) International Data Center, USA
EKA	Eskdalemuir Array Station, United Kingdom
ENT	Geological Survey and Mines Department, Uganda
EPSI	Reference events computed by the ISC for EPSI project, United Kingdom
ERDA	Energy Research and Development Administration, USA
EST	Geological Survey of Estonia, Estonia
FBR	Fabra Observatory, Spain
FDF	Fort de France, Martinique
FIA0	Finessa Array, Finland
FOR	Unknown Historical Agency, Unknown - historical agency
FUNV	Fundación Venezolana de Investigaciones Sismológicas, Venezuela
FUR	Geophysikalisches Observatorium der Universität München, Germany
GBZT	Marmara Research Center, Turkey
GCG	INSIVUMEH, Guatemala
GCMT	**The Global CMT Project, USA**
GDNRW	Geologischer Dienst Nordrhein-Westfalen, Germany
GEN	**Dipartimento per lo Studio del Territorio e delle sue Risorse (RSNI), Italy**
GFZ	Helmholtz Centre Potsdam GFZ German Research Centre For Geo-sciences, Germany
GII	**The Geophysical Institute of Israel, Israel**
GOM	Observatoire Volcanologique de Goma, Democratic Republic of the Congo
GRAL	**National Council for Scientific Research, Lebanon**
GSDM	**Geological Survey Department Malawi, Malawi**
GTFE	German Task Force for Earthquakes, Germany
GUC	**Departamento de Geofísica, Universidad de Chile, Chile**
HAN	Hannover, Germany
HDC	Observatorio Vulcanológico y Sismológico de Costa Rica, Costa Rica
HEL	**Institute of Seismology, University of Helsinki, Finland**
HFS	Hagfors Observatory, Sweden
HFS1	Hagfors Observatory, Sweden
HFS2	Hagfors Observatory, Sweden
HKC	**Hong Kong Observatory, Hong Kong**
HLUG	Hessisches Landesamt für Umwelt und Geologie, Germany
HLW	**National Research Institute of Astronomy and Geophysics, Egypt**
HNR	**Ministry of Mines, Energy and Rural Electrification, Solomon Islands**
HON	Pacific Tsunami Warning Center - NOAA, USA
HRVD	Harvard University, USA
HRVD_LR	Department of Geological Sciences, Harvard University, USA
HVO	Hawaiian Volcano Observatory, USA
HYB	**National Geophysical Research Institute, India**
HYD	National Geophysical Research Institute, India
IAG	Instituto Andaluz de Geofisica, Spain
IASPEI	**IASPEI Working Group on Reference Events, USA**

Table 10.1: Continued.

Agency Code	Agency Name
ICE	Instituto Costarricense de Electricidad, Costa Rica
IDC	**International Data Centre, CTBTO**, **Austria**
IDG	Institute of Dynamics of Geosphere, Russian Academy of Sciences, Russia
IEPN	**Institute of Environmental Problems of the North, Russian Academy of Sciences**, **Russia**
IGIL	**Instituto Geofisico do Infante Dom Luiz**, **Portugal**
IGQ	**Servicio Nacional de Sismología y Vulcanología**, **Ecuador**
IGS	Institute of Geological Sciences, United Kingdom
INDEPTH3	International Deep Profiling of Tibet and the Himalayas, USA
INET	Instituto Nicaragüense de Estudios Territoriales, Nicaragua
INMG	**Instituto Português do Mar e da Atmosfera, I.P.**, **Portugal**
IPEC	**The Institute of Physics of the Earth (IPEC)**, **Czech Republic**
IPER	Institute of Physics of the Earth, Academy of Sciences, Moscow, Russia
IPGP	Institut de Physique du Globe de Paris, France
IPRG	Institute for Petroleum Research and Geophysics, Israel
IRIS	**IRIS Data Management Center**, **USA**
IRSM	Institute of Rock Structure and Mechanics, Czech Republic
ISK	**Kandilli Observatory and Research Institute**, **Turkey**
ISN	**Iraqi Meteorological and Seismology Organisation**, **Iraq**
ISS	International Seismological Summary, United Kingdom
IST	Institute of Physics of the Earth, Technical University of Istanbul, Turkey
JEN	Geodynamisches Observatorium Moxa, Germany
JMA	**Japan Meteorological Agency**, **Japan**
JOH	Bernard Price Institute of Geophysics, South Africa
JSN	**Jamaica Seismic Network**, **Jamaica**
JSO	**Jordan Seismological Observatory**, **Jordan**
KBC	Institut de Recherches Géologiques et Minières, Cameroon
KEW	Kew Observatory, United Kingdom
KHC	Geofysikalni Ustav, Ceske Akademie Ved, Czech Republic
KISR	Kuwait Institute for Scientific Research, Kuwait
KLM	**Malaysian Meteorological Service**, **Malaysia**
KMA	**Korea Meteorological Administration**, **Republic of Korea**
KNET	**Kyrgyz Seismic Network**, **Kyrgyzstan**
KOLA	**Kola Regional Seismic Centre, GS RAS**, **Russia**
KRAR	Krasnoyarsk Scientific Research Inst. of Geology and Mineral Resources, Russia, Russia
KRL	Geodätisches Institut der Universität Karlsruhe, Germany
KRNET	**Institute of Seismology, Academy of Sciences of Kyrgyz Republic**, **Kyrgyzstan**
KRSC	**Kamchatkan Experimental and Methodical Seismological Department, GS RAS**, **Russia**
KSA	Observatoire de Ksara, Lebanon
KUK	Geological Survey Department of Ghana, Ghana
LAO	Large Aperture Seismic Array, USA
LDG	**Laboratoire de Détection et de Géophysique/CEA**, **France**
LDN	University of Western Ontario, Canada

Table 10.1: Continued.

Agency Code	Agency Name
LDO	Lamont-Doherty Earth Observatory, USA
LED	Landeserdbebendienst Baden-Württemberg, Germany
LEDBW	Landeserdbebendienst Baden-Württemberg, Germany
LER	Besucherbergwerk Binweide Station, Germany
LIB	Tripoli, Libya
LIC	**Station Géophysique de Lamto**, **Ivory Coast**
LIM	Lima, Peru
LIS	Instituto de Meteorologia, Portugal
LIT	**Geological Survey of Lithuania**, **Lithuania**
LJU	**Environmental Agency of the Republic of Slovenia**, **Slovenia**
LPA	**Universidad Nacional de La Plata**, **Argentina**
LSZ	**Geological Survey Department of Zambia**, **Zambia**
LVSN	**Latvian Seismic Network**, **Latvia**
MAN	**Philippine Institute of Volcanology and Seismology**, **Philippines**
MAT	**The Matsushiro Seismological Observatory**, **Japan**
MCO	**Macao Meteorological and Geophysical Bureau**, **Macao, China**
MDD	**Instituto Geográfico Nacional**, **Spain**
MED_RCMT	**MedNet Regional Centroid - Moment Tensors**, **Italy**
MES	Messina Seismological Observatory, Italy
MEX	**Instituto de Geofísica de la UNAM**, **Mexico**
MIRAS	**Mining Institute of the Ural Branch of the Russian Academy of Sciences**, **Russia**
MOLD	**Institute of Geophysics and Geology**, **Moldova**
MOS	**Geophysical Survey of Russian Academy of Sciences**, **Russia**
MOZ	Direccao Nacional de Geologia, Mozambique
MRB	**Institut Cartogràfic de Catalunya**, **Spain**
MSI	Messina Seismological Observatory, Italy
MSSP	**Micro Seismic Studies Programme, PINSTECH**, **Pakistan**
MUN	Mundaring Observatory, Australia
NAI	University of Nairobi, Kenya
NAM	The Geological Survey of Namibia, Namibia
NAO	**Stiftelsen NORSAR**, **Norway**
NCEDC	Northern California Earthquake Data Center, USA
NDI	**India Meteorological Department**, **India**
NEIC	**National Earthquake Information Center**, **USA**
NEIS	National Earthquake Information Service, USA
NERS	**North Eastern Regional Seismological Centre, GS RAS**, **Russia**
NIC	**Cyprus Geological Survey Department**, **Cyprus**
NIED	**National Research Institute for Earth Science and Disaster Prevention**, **Japan**
NNC	**National Nuclear Center**, **Kazakhstan**
NORS	North Ossetia (Alania) Branch, Geophysical Survey, Russian Academy of Sciences, Russia
NOU	IRD Centre de Nouméa, New Caledonia
NSSC	**National Syrian Seismological Center**, **Syria**
NSSP	**National Survey of Seismic Protection**, **Armenia**
OBM	Research Centre of Astronomy and Geophysics, Mongolia

Table 10.1: *Continued.*

Agency Code	Agency Name
OGSO	Ohio Geological Survey, USA
OMAN	**Sultan Qaboos University**, **Oman**
ORF	Orfeus Data Center, Netherlands
OSUB	**Osservatorio Sismologico Universita di Bari**, **Italy**
OTT	**Canadian Hazards Information Service, Natural Resources Canada**, **Canada**
PAL	Palisades, USA
PAS	California Institute of Technology, USA
PDA	Universidade dos Açores, Portugal
PDG	**Seismological Institute of Montenegro**, **Montenegro**
PEK	Peking, China
PGC	Pacific Geoscience Centre, Canada
PLV	**National Center for Scientific Research**, **Vietnam**
PMEL	Pacific seismicity from hydrophones, USA
PMR	Alaska Tsunami Warning Center,, USA
PNSN	**Pacific Northwest Seismic Network**, **USA**
PPT	**Laboratoire de Géophysique/CEA**, **French Polynesia**
PRE	**Council for Geoscience**, **South Africa**
PRU	**Geophysical Institute, Academy of Sciences of the Czech Republic**, **Czech Republic**
PTO	Instituto Geofísico da Universidade do Porto, Portugal
PTWC	Pacific Tsunami Warning Center, USA
QCP	**Manila Observatory**, **Philippines**
QUE	Pakistan Meteorological Department, Pakistan
QUI	Escuela Politécnica Nacional, Ecuador
RAB	Rabaul Volcanological Observatory, Papua New Guinea
RBA	Université Mohammed V, Morocco
REN	MacKay School of Mines, USA
REY	**Icelandic Meteorological Office**, **Iceland**
RISSC	Laboratory of Research on Experimental and Computational Seimology, Italy
RMIT	Royal Melbourne Institute of Technology, Australia
ROC	Odenbach Seismic Observatory, USA
ROM	**Istituto Nazionale di Geofisica e Vulcanologia**, **Italy**
RRLJ	Regional Research Laboratory Jorhat, India
RSMAC	Red Sísmica Mexicana de Apertura Continental, Mexico
RSNC	**Red Sismológica Nacional de Colombia**, **Colombia**
RSPR	**Red Sísmica de Puerto Rico**, **USA**
RYD	King Saud University, Saudi Arabia
SAPSE	Southern Alps Passive Seismic Experiment, New Zealand
SAR	**Sarajevo Seismological Station**, **Bosnia and Herzegovina**
SCB	**Observatorio San Calixto**, **Bolivia**
SCEDC	Southern California Earthquake Data Center, USA
SDD	Universidad Autonoma de Santo Domingo, Dominican Republic
SEA	Geophysics Program AK-50, USA
SEPA	Seismic Experiment in Patagonia and Antarctica, USA
SET	Setif Observatory, Algeria

Table 10.1: Continued.

Agency Code	Agency Name
SFS	**Real Instituto y Observatorio de la Armada**, **Spain**
SGS	**Saudi Geological Survey**, **Saudi Arabia**
SHL	Central Seismological Observatory, India
SIGU	**Subbotin Institute of Geophysics, National Academy of Sciences**, **Ukraine**
SIK	**Seismic Institute of Kosovo**, **Unknown**
SIO	Scripps Institution of Oceanography, USA
SJA	**Instituto Nacional de Prevención Sísmica**, **Argentina**
SJS	Instituto Costarricense de Electricidad, Costa Rica
SKHL	**Sakhalin Experimental and Methodological Seismological Expedition, GS RAS**, **Russia**
SKL	Sakhalin Complex Scientific Research Institute, Russia
SKO	**Seismological Observatory Skopje**, **FYR Macedonia**
SLC	Salt Lake City, USA
SLM	Saint Louis University, USA
SNET	Servicio Nacional de Estudios Territoriales, El Salvador
SNM	New Mexico Institute of Mining and Technology, USA
SNSN	Saudi National Seismic Network, Saudi Arabia
SOF	**Geophysical Institute, Bulgarian Academy of Sciences**, **Bulgaria**
SOME	**Seismological Experimental Methodological Expedition**, **Kazakhstan**
SPA	USGS - South Pole, Antarctica
SPGM	Service de Physique du Globe, Morocco
SRI	Stanford Research Institute, USA
SSN	Sudan Seismic Network, Sudan
SSNC	Servicio Sismológico Nacional Cubano, Cuba
SSS	Centro de Estudios y Investigaciones Geotecnicas del San Salvador, El Salvador
STK	Stockholm Seismological Station, Sweden
STR	**Institut de Physique du Globe**, **France**
STU	Stuttgart Seismological Station, Germany
SVSA	**Sistema de Vigilância Sismológica dos Açores**, **Portugal**
SYO	**National Institute of Polar Research**, **Japan**
SZGRF	Seismologisches Zentralobservatorium Gräfenberg, Germany
TAC	Estación Central de Tacubaya, Mexico
TAN	Antananarivo, Madagascar
TANZANIA	Tanzania Broadband Seismic Experiment, USA
TAP	**CWB**, **Chinese Taipei**
TAU	University of Tasmania, Australia
TEH	**Tehran University**, **Iran**
TEIC	Center for Earthquake Research and Information, USA
THE	**Department of Geophysics, Aristotle University of Thessaloniki**, **Greece**
THR	**International Institute of Earthquake Engineering and Seismology (IIEES)**, **Iran**
TIF	**Seismic Monitoring Centre of Georgia**, **Georgia**

Table 10.1: *Continued.*

Agency Code	Agency Name
TIR	**The Institute of Seismology, Academy of Sciences of Albania, Albania**
TRI	**Istituto Nazionale di Oceanografia e di Geofisica Sperimentale (OGS), Italy**
TRN	**University of the West Indies, Trinidad and Tobago**
TTG	Titograd Seismological Station, Montenegro
TUL	Oklahoma Geological Survey, USA
TUN	**Institut National de la Météorologie, Tunisia**
TVA	Tennessee Valley Authority, USA
TZN	University of Dar Es Salaam, Tanzania
UAV	Red Sismológica de Los Andes Venezolanos, Venezuela
UCC	**Royal Observatory of Belgium, Belgium**
UCR	**Sección de Sismología, Vulcanología y Exploración Geofísica, Costa Rica**
UGN	Institute of Geonics AS CR, Czech Republic
ULE	University of Leeds, United Kingdom
UNAH	Universidad Nacional Autonoma de Honduras, Honduras
UPA	Universidad de Panama, Panama
UPP	**University of Uppsala, Sweden**
UPSL	University of Patras, Department of Geology, Greece
USAEC	United States Atomic Energy Commission, USA
USCGS	United States Coast and Geodetic Survey, USA
USGS	**United States Geological Survey, USA**
UUSS	The University of Utah Seismograph Stations, USA
UVC	Universidad del Valle, Colombia
VAO	**Instituto Astronomico e Geofísico, Brazil**
VIE	**Österreichischer Geophysikalischer Dienst, Austria**
VKMS	Lab. of Seismic Monitoring, Voronezh region, GSRAS & Voronezh State University, Russia
VLA	Vladivostok Seismological Station, Russia
VSI	University of Athens, Greece
WAR	**Institute of Geophysics, Polish Academy of Sciences, Poland**
WBNET	**West Bohemia Seismic Network, Czech Republic**
WEL	**Institute of Geological and Nuclear Sciences, New Zealand**
WES	Weston Observatory, USA
YARS	**Yakutiya Regional Seismological Center, GS SB RAS, Russia**
ZAG	**Seismological Survey of the Republic of Croatia, Croatia**
ZUR	**Swiss Seismological Sevice (SED), Switzerland**
ZUR_RMT	Zurich Moment Tensors, Switzerland

Table 10.2: *Phases reported to the ISC. These include phases that could not be matched to an appropriate* ak135 *phases. Those agencies that reported at least 10% of a particular phase are also shown.*

Reported Phase	Total	Agencies reporting
P	2791086	NEIC (17%), JMA (11%)
S	1199129	JMA (24%), TAP (16%)
AML	348853	ROM (67%), ATH (30%)
Pn	234771	NEIC (46%)
pmax	161447	MOS (81%), BJI (19%)
LR	159544	IDC (43%), NEIC (30%), BJI (23%)
Pg	151463	MDD (15%), CSEM (14%)
Sg	103209	CSEM (14%)
PG	97087	ISK (62%), HEL (16%)
NULL	87649	RSNC (38%), MOS (28%), TEH (11%)
Sn	87226	NEIC (25%), IDC (12%)
PN	77127	ISK (66%), MOS (19%)
SG	70230	ISK (39%), HEL (26%), PRU (15%), IPEC (11%)
Lg	60372	MDD (49%), NNC (23%)
IAML	46378	GUC (33%), SJA (20%), BER (15%)
PKP	36413	IDC (41%), NEIC (26%)
PKPdf	30727	NEIC (87%)
PKPbc	27946	NEIC (53%), IDC (37%)
pP	26437	NEIC (39%), BJI (33%), IDC (13%)
PFAKE	24907	NEIC (100%)
MLR	24612	MOS (100%)
T	23658	IDC (90%)
PcP	23144	NEIC (49%), IDC (37%)
A	19294	INMG (51%), SKHL (28%), SVSA (21%)
PKIKP	16753	MOS (97%)
MSG	16471	HEL (100%)
Sb	15576	IRIS (95%)
SN	15139	HEL (53%), ISK (16%), OTT (13%), BRA (11%)
PP	13958	BJI (37%), NEIC (20%), IDC (17%)
smax	11350	MOS (85%), BJI (15%)
IAMB	11102	TEH (100%)
PKPab	9885	NEIC (49%), IDC (30%)
END	9867	ROM (100%)
sP	9157	BJI (84%)
Pb	7910	IRIS (89%)
SS	7442	BJI (43%), MOS (32%)
SB	6902	HEL (100%)
x	6792	NDI (70%), PRU (22%)
AMB	6786	SKHL (86%), BJI (14%)
PB	6701	HEL (100%)
ScP	5922	IDC (49%), NEIC (40%)
IAmb	5827	NDI (33%), LIT (26%), BGS (23%), BER (14%)
PKiKP	5313	NEIC (30%), IDC (27%), VIE (23%)
AMS	4491	PRU (73%), SKHL (14%)
Smax	3997	YARS (62%), BYKL (38%)
*PP	3783	MOS (100%)
PKP2	3736	MOS (95%)
PKKPbc	3598	IDC (53%), NEIC (44%)
sS	2909	BJI (97%)
Pmax	2851	YARS (56%), BYKL (42%)
PKPpre	2828	NEIC (98%)
Pdiff	2698	IRIS (59%), IDC (21%), VIE (12%)
Trac	2639	OTT (100%)
Pdif	2574	NEIC (80%)
LG	2515	BRA (62%), OTT (31%)
pPKP	1763	IDC (34%), BJI (31%), NEIC (20%)
SKPbc	1666	IDC (55%), NEIC (44%)
PKhKP	1609	IDC (100%)
PKHKP	1602	MOS (100%)
LQ	1500	PPT (60%), BELR (13%), INMG (11%), IEPN (11%)
PPP	1442	MOS (77%)
X	1375	JMA (83%), SYO (16%)
SKS	1336	BJI (58%), PRU (15%)
IAMs_20	1284	BGS (72%), NDI (21%)
PS	1147	MOS (48%), CLL (12%)

Table 10.2: *(continued)*

Reported Phase	Total	Agencies reporting
ScS	1110	BJI (74%), IDC (12%)
AMP	1033	IEPN (67%), HLW (15%)
SSS	926	MOS (54%), CLL (26%), BELR (13%)
sPKP	885	BJI (97%)
pPKPbc	756	IDC (54%), NEIC (29%)
LRM	726	MOLD (60%), BELR (38%)
PKKP	699	IDC (54%), NEIC (35%)
PKPPKP	671	IDC (94%)
SKP	632	IDC (33%), IRIS (28%), NEIC (20%)
*SP	597	MOS (100%)
pPKPdf	586	NEIC (64%), VIE (23%)
PKKPab	564	IDC (54%), NEIC (40%)
SP	507	MOS (36%), PRU (25%), PPT (12%)
max	453	BYKL (100%)
LMZ	453	WAR (100%)
PKP1	448	LIC (82%), SFS (15%)
PcS	442	BJI (94%)
P'P'	430	NEIC (100%)
SKKS	426	BJI (69%)
PKPAB	391	PRU (100%)
L	374	BRA (35%), MOLD (26%), DBN (23%), CLL (16%)
PKS	371	BJI (79%)
P*	369	NEIC (61%), BGR (35%)
Lm	354	CLL (100%)
*SS	341	MOS (100%)
PDIFF	331	BRA (35%), PRU (33%), IPEC (22%)
pPKPab	328	NEIC (44%), IDC (27%), CLL (15%), VIE (11%)
SKSac	324	CLL (23%), WAR (17%), LJU (17%), PPT (11%)
LmV	303	CLL (100%)
PKP2bc	256	IDC (100%)
PM	245	BELR (100%)
AMb	243	IGIL (83%)
(P)	229	BRG (66%), CLL (24%)
SKKPbc	227	IDC (56%), NEIC (38%)
PCP	211	PRU (51%), BRA (18%)
PPS	207	CLL (59%), MOS (22%), MOLD (11%)
P3KPbc	190	IDC (100%)
Sm	184	SIGU (100%)
Pm	181	SIGU (99%)
IVMs_BB	175	BER (53%), HYB (43%)
Rg	163	NNC (33%), DBN (20%), NAO (17%), IDC (13%), BER (13%)
LmH	160	CLL (100%)
SKPdf	148	NEIC (49%), WAR (14%), CLL (12%)
PA	145	THR (82%), JSN (18%)
pPcP	132	IDC (66%), NEIC (30%)
PKPDF	122	PRU (100%)
Snm	121	SIGU (100%)
PC	120	SFS (100%)
Sgmax	112	NERS (100%)
PKP2ab	112	IDC (100%)
AP	112	UCC (85%), MOS (15%)
S*	111	BGR (87%), NEIC (13%)
PKKPdf	110	NEIC (50%), BUD (35%)
SKPab	109	IDC (54%), NEIC (44%)
P4KPbc	105	IDC (100%)
IVmB_BB	103	BER (93%)
E	101	ZAG (75%), UCC (22%)
SSSS	98	CLL (99%)
Sdif	92	CLL (43%), NEIC (29%), INMG (13%), PPT (11%)
Sgm	90	SIGU (100%)
AMSG	77	SJA (100%)
Lmax	76	CLL (100%)
P'P'ab	76	NEIC (100%)
pPKiKP	72	VIE (50%), CLL (18%), SYO (12%), BUD (11%)
PmP	72	BGR (94%)
Pu	72	NEIC (100%)
SH	71	SYO (100%)

Table 10.2: *(continued)*

Reported Phase	Total	Agencies reporting
PD	60	SFS (100%)
SmS	58	BGR (100%)
RG	53	HEL (98%)
del	52	AUST (98%)
Pgmax	52	NERS (100%)
PKPdif	50	NEIC (96%)
P3KP	50	IDC (100%)
SDIF	48	PRU (92%)
pPP	47	CLL (45%), LPA (40%)
(sP)	47	CLL (100%)
PKPPKPdf	47	BUD (64%), CLL (36%)
Pnm	46	SIGU (100%)
SKKPdf	45	BUD (91%)
m	45	SIGU (100%)
P'P'df	44	NEIC (84%), PPT (16%)
pPn	41	BUD (54%), OMAN (44%)
Pgm	41	SIGU (100%)
LQM	40	BELR (92%)
AMPG	40	SJA (90%)
PKKKP	39	NEIC (100%)
SKKSac	38	CLL (66%), WAR (16%), LJU (11%)
PsP	37	MOLD (78%), BELR (22%)
SKKP	35	IDC (37%), NEIC (31%), SVSA (17%)
pPdiff	34	SYO (68%), BUD (15%), IDC (12%)
XS	32	PRU (100%)
sPP	32	CLL (100%)
XP	31	UCC (94%)
PSKS	30	CLL (97%)
PDIF	30	BRA (83%), BRG (13%)
PgPg	30	BYKL (97%)
MSN	29	HEL (100%)
PPPP	28	CLL (100%)
Sdiff	28	IDC (57%), LJU (21%), WAR (18%)
APKP	27	UCC (100%)
rx	26	SKHL (100%)
(SS)	26	CLL (100%)
SM	26	BELR (100%)
Plp	25	CLL (100%)
(pP)	25	CLL (100%)
sSS	24	CLL (100%)
(PP)	24	CLL (100%)
SCP	22	BRG (50%), PRU (27%), IPEC (18%)
SDIFF	21	BRG (81%), LPA (19%)
SKIKP	21	LPA (81%), IPEC (19%)
pwP	21	NEIC (100%)
SKSP	19	MOLD (37%), BELR (21%), CLL (21%), DBN (16%)
SCS	19	LPA (63%), IPEC (21%), DIAS (11%)
P4KP	19	IDC (68%), NEIC (32%)
PKKSdf	19	NEIC (89%), CLL (11%)
SgSg	19	BYKL (100%)
SKIKS	18	LPA (100%)
PKIKS	18	LPA (100%)
PPM	18	BELR (100%)
SPP	17	CLL (47%), BELR (24%), WAR (24%)
M	14	MOLD (100%)
PSPS	14	CLL (100%)
SKSdf	14	BUD (71%), CLL (14%), WAR (14%)
PKPc	13	WAR (100%)
Sglp	13	CLL (100%)
Li	13	MOLD (100%)
SKiKP	12	IDC (100%)
(SSS)	12	CLL (100%)
PPPrev	12	CLL (100%)
sPKPdf	12	CLL (58%)
pPdif	12	CLL (83%), SOME (17%)
SMZ	12	BJI (100%)
Lm(360	11	CLL (100%)

Table 10.2: *(continued)*

Reported Phase	Total	Agencies reporting
(PcP)	11	CLL (100%)
sPKPbc	11	CLL (73%), IDC (18%)
s	11	MAN (64%), SFS (36%)
IVmBB	11	BER (100%)
PN5	11	ISN (100%)
PKPdiff	11	CLL (100%)
P5KP	10	IDC (60%), NEIC (40%)
R	10	LDG (100%)
P(2)	10	CLL (100%)
IVmBBB	10	BER (100%)
XM	10	MOLD (100%)
(S)	10	CLL (70%), VAO (30%)
pScP	9	IDC (56%), NEIC (44%)
P*P	9	ZUR (100%)
PPlp	9	CLL (100%)
sSSS	9	CLL (100%)
IVMsB	9	BER (100%)
PKPlp	9	CLL (100%)
SN4	9	ISN (100%)
PKSbc	9	CLL (78%), LJU (22%)
PKSdf	9	CLL (100%)
(Pg)	8	CLL (88%), OSUB (12%)
TT	8	NEIC (100%)
sPdif	8	CLL (100%)
PSP	7	LPA (100%)
sPKPab	7	CLL (100%)
LV	7	CLL (100%)
(sPP)	7	CLL (100%)
LMN	7	WAR (100%)
sPKiKP	7	CLL (43%), BUD (29%), IDC (14%), SYO (14%)
PbPb	7	VIE (100%)
SKKKS	6	BELR (100%)
pPg	6	SKHL (100%)
pPN	6	IPEC (67%), BRA (33%)
(SSSS)	6	CLL (100%)
SN5	6	ISN (100%)
pSKS	6	SVSA (100%)
sPPP	6	CLL (100%)
SKKSacre	6	CLL (100%)
SKSp	6	BRA (100%)
sPS	6	CLL (100%)
(pPKPab)	6	CLL (100%)
(pPKPdf)	6	CLL (100%)
(Sn)	6	OSUB (67%), CLL (33%)
(PKiKP)	6	CLL (100%)
(PPP)	5	CLL (100%)
(Sg)	5	OSUB (100%)
(ES)	5	VAO (100%)
PKPPKPbc	5	CLL (80%), BUD (20%)
LRM2	5	MOLD (100%)
PKPM	5	BELR (80%), MOLD (20%)
P'P'bc	5	PPT (100%)
p	5	OMAN (60%), MAN (40%)
sPdiff	5	SYO (60%), BUD (40%)
(PKPdf)	5	CLL (100%)
sPn	5	BUD (80%), BJI (20%)
PGN	5	HEL (100%)
IVMsBB	5	HYB (40%), BER (40%), BGS (20%)
(Pn)	5	OSUB (60%), CLL (40%)
(PS)	4	CLL (100%)
Lg1	4	MOLD (100%)
LH	4	CLL (100%)
LRM1	4	MOLD (100%)
Lg2	4	MOLD (100%)
I	4	NDI (50%), BER (50%)
pPS	4	CLL (100%)
PSS	4	CLL (100%)

Table 10.2: *(continued)*

Reported Phase	Total	Agencies reporting
SSSrev	4	CLL (100%)
pPKP1	4	BELR (100%)
SSmax	4	CLL (100%)
EeS	3	SFS (100%)
APKPbc	3	UCC (100%)
PKKPB	3	BRA (100%)
(Pdif)	3	CLL (100%)
sPcP	3	CLL (100%)
mb	3	OTT (100%)
(PPS)	3	CLL (100%)
sPKP1	3	BELR (100%)
pPPS	3	CLL (100%)
sPg	3	SKHL (67%), BUD (33%)
PKP1M	3	BELR (100%)
PSSrev	3	CLL (100%)
PPmax	3	CLL (100%)
PPk	3	CLL (100%)
pPKS	3	LPA (100%)
pPKPPKPd	2	CLL (100%)
PN4	2	ISN (100%)
pPDIFF	2	BRG (100%)
PKPPKPma	2	CLL (100%)
(Sdif)	2	CLL (100%)
PnPn	2	OMAN (50%), SYO (50%)
SSP	2	CLL (100%)
SSSmax	2	CLL (100%)
(PPPP)	2	CLL (100%)
sSKKSac	2	CLL (100%)
SKKPab	2	NEIC (50%), IDC (50%)
PKPabd	2	WAR (100%)
SKPa	2	NAO (100%)
PKKS	2	PRU (100%)
(pPKiKP)	2	CLL (100%)
PCS	2	LPA (100%)
PnPN	2	SYO (100%)
(PKP)	2	CLL (100%)
SKPPKPbc	2	CLL (100%)
(SKSac)	2	CLL (100%)
(PSKS)	2	CLL (100%)
sSKSac	2	CLL (100%)
P–	2	BUD (100%)
sSSSS	2	CLL (100%)
PKKPDF	2	BRA (100%)
PDS	2	NDI (100%)
sPDIF	2	BRA (100%)
sPPS	2	CLL (100%)
SKSSKSac	2	CLL (100%)
(SKKSdf)	2	CLL (100%)
SSrev	2	CLL (100%)
IP	2	BELR (100%)
LME	2	WAR (100%)
(PKPab)	2	CLL (100%)
SSS(2)	2	LPA (100%)
(pPP)	2	CLL (100%)
sPDIFF	2	BRG (100%)
(SKKSac)	2	CLL (100%)
pPKSdf	2	CLL (100%)
PGCS	2	NDI (100%)
pZP	1	SYO (100%)
ScSmax	1	CLL (100%)
pSKPdf	1	CLL (100%)
(SKPbc)	1	CLL (100%)
RQ	1	MOLD (100%)
(pPKPbc)	1	CLL (100%)
pn	1	ISN (100%)
sPKKPdf	1	CLL (100%)
Cod	1	SFS (100%)

Table 10.2: *(continued)*

Reported Phase	Total	Agencies reporting
sPSPS	1	CLL (100%)
sPKKPbc	1	CLL (100%)
PCN	1	NDI (100%)
PPPPrev	1	CLL (100%)
(sSdiff)	1	CLL (100%)
Gg	1	BER (100%)
sSKSB	1	BRA (100%)
SSPrev	1	CLL (100%)
(sPKPdf)	1	CLL (100%)
AMSN	1	SJA (100%)
pPKPdiff	1	CLL (100%)
3PKPmax	1	CLL (100%)
pP(2)	1	CLL (100%)
sPKP2	1	BJI (100%)
(PSPS)	1	CLL (100%)
sg	1	BUD (100%)
(sSSS)	1	CLL (100%)
(PSS)	1	CLL (100%)
PKSDF	1	BRA (100%)
PGCN	1	NDI (100%)
pC	1	SFS (100%)
pS	1	BRA (100%)
SKPPKPdf	1	CLL (100%)
AnL	1	INMG (100%)
SKKSdf	1	NEIC (100%)
pPKKPbc	1	CLL (100%)
sZP	1	SYO (100%)
(sSS)	1	CLL (100%)
(pPcP)	1	CLL (100%)
PKPab(2)	1	CLL (100%)
KSK	1	IPEC (100%)
pPmax	1	CLL (100%)
Lgg	1	MDD (100%)
sPSKS	1	CLL (100%)
pPlp	1	CLL (100%)
(pPdif)	1	CLL (100%)
3PKPdf	1	CLL (100%)
LPM	1	MOLD (100%)
(sS)	1	CLL (100%)
sPmax	1	CLL (100%)
PMP	1	BER (100%)
pPKKPab	1	CLL (100%)
(sPPP)	1	CLL (100%)
(PG)	1	BRG (100%)
SKKPDF	1	BRA (100%)
pSKKSac	1	CLL (100%)
(PKKPdf)	1	CLL (100%)
N	1	DSN (100%)
pPPP	1	CLL (100%)
Coda	1	SFS (100%)
sPPPP	1	CLL (100%)
PN8	1	DHMR (100%)
(PPPrev)	1	CLL (100%)
sSKKSdf	1	CLL (100%)
SKPDF	1	BRA (100%)
PGG	1	AAE (100%)
3PKPbc	1	CLL (100%)
SKPB	1	BRA (100%)
(PKKSdf)	1	CLL (100%)
PKPbc(2)	1	CLL (100%)
SKPpB	1	BRA (100%)
pPKPPKPb	1	CLL (100%)
(PKPbc)	1	CLL (100%)
PKRPbc	1	CLL (100%)
ScSScS	1	CLL (100%)
sSdiff	1	CLL (100%)
sPN	1	BRA (100%)

Table 10.2: *(continued)*

Reported Phase	Total	Agencies reporting
sPPmax	1	CLL (100%)
PcP(2)	1	CLL (100%)
PPdiff	1	SYO (100%)
sPb	1	BUD (100%)
SKKSacr	1	CLL (100%)
PKSB	1	BRA (100%)
P5KPbc	1	IDC (100%)
LRM3	1	MOLD (100%)
PKKPmax	1	CLL (100%)
-ML	1	INMG (100%)
Pn(2)	1	CLL (100%)
(SP)	1	CLL (100%)
SPS	1	CLL (100%)
(Sb)	1	CLL (100%)

Table 10.3: Reporters of amplitude data

Agency	Number of reported amplitudes	Number of amplitudes in ISC located events	Number used for ISC mb	Number used for ISC MS
IDC	347771	323587	136790	42809
NEIC	321001	320505	240341	45959
ROM	245308	21639	0	0
MOS	164523	135835	67829	13053
ATH	105233	10354	0	0
MDD	72003	15064	0	0
BJI	69927	67411	16079	20752
ISK	66662	17496	0	0
SOME	57250	17949	1748	0
NNC	57082	15441	173	0
DJA	47063	28069	5435	0
RSNC	32975	1328	9	0
VIE	30856	17362	7704	0
CSEM	30682	3584	313	0
TEH	25324	16215	0	0
THE	22819	3995	0	0
BKK	21711	18481	8654	0
HEL	16941	361	0	0
GUC	15310	4952	0	0
LDG	15260	3231	1	0
WEL	14702	3686	0	0
INMG	14275	7866	3268	0
DMN	13359	12786	0	0
PPT	12234	10473	1316	0
SKHL	11890	9428	0	0
SJA	9191	2478	0	0
PRU	9118	4293	0	2530
BER	7903	1724	724	75
MAN	7486	3870	0	0
LJU	6766	295	0	0
PDG	6167	3912	0	0
NDI	5910	4647	1261	166
SVSA	4444	442	257	0
BRG	4167	2942	740	0
PRE	4147	216	0	0
YARS	4107	59	0	0
SKO	3612	407	0	0
BYKL	3213	845	0	0
BGS	3014	2434	1287	803
MRB	2946	111	0	0
CLL	2916	2715	656	340
UCR	2719	1690	8	0
LVSN	2671	509	2	194
KNET	2647	876	3	0

Table 10.3: Continued.

Agency	Number of reported amplitudes	Number of amplitudes in ISC located events	Number used for ISC mb	Number used for ISC MS
OTT	2641	480	0	0
ZUR	2606	355	40	0
NAO	2239	2200	1677	0
WBNET	2238	0	0	0
ECX	2164	482	0	0
DNK	2009	1884	1304	0
LIC	1603	1351	762	0
LIT	1507	1408	1063	0
IGIL	1307	824	189	279
IPEC	1137	197	0	0
UCC	947	850	570	0
IEPN	788	699	0	0
MOLD	762	462	82	0
THR	631	629	0	0
BELR	605	582	0	222
EAF	602	27	0	0
SIGU	543	394	0	0
WAR	489	488	3	357
DHMR	479	138	5	0
DBN	383	275	171	0
HYB	326	321	164	0
MIRAS	293	8	0	0
PLV	210	116	0	0
NERS	168	25	0	0
NSSC	112	76	0	0
BGR	106	64	0	0
IGQ	104	104	0	0
ISN	94	2	0	0
SCB	92	79	0	0
ATA	34	20	0	0
JSO	10	10	0	0
LPA	10	10	1	0
BEO	10	0	0	0
LSZ	4	0	0	0
AAE	4	0	0	0

11

Glossary of ISC Terminology

- Agency/ISC data contributor

  An academic or government institute, seismological organisation or company, geological/meteorological survey, station operator or author that reports or contributed data in the past to the ISC or one of its predecessors. Agencies may contribute data to the ISC directly, or indirectly through other ISC data contributors.

- Agency code

  A unique, maximum eight-character code for a data reporting agency (e.g. NEIC, GFZ, BUD) or author (e.g. ISC, EHB, IASPEI). Often the agency code is the commonly used acronym of the reporting institute.

- Arrival

  A phase pick at a station is characterised by a phase name and an arrival time.

- Associated phase

  Associated phase arrival or amplitude measurements represent a collection of observations belonging to (i.e. generated by) an event. The complete set of observations are associated to the prime hypocentre.

- Azimuthal gap/Secondary azimuthal gap

  The azimuthal gap for an event is defined as the largest angle between two stations with defining phases when the stations are ordered by their event-to-station azimuths. The secondary azimuthal gap is the largest azimuthal gap a single station closes.

- BAAS

  Seismological bulletins published by the British Association for the Advancement of Science (1913-1917) under the leadership of H.H. Turner. These bulletins are the predecessors of the ISS Bulletins and include reports from stations distributed worldwide.

- Bulletin

  An ordered list of event hypocentres, uncertainties, focal mechanisms, network magnitudes, as well as phase arrival and amplitude observations associated to each event. An event bulletin may list all the reported hypocentres for an event. The convention in the ISC Bulletin is that the preferred (prime) hypocentre appears last in the list of reported hypocentres for an event.

- Catalogue

  An ordered list of event hypocentres, uncertainties and magnitudes. An event catalogue typically lists only the preferred (prime) hypocentres and network magnitudes.

- CoSOI/IASPEI

  Commission on Seismological Observation and Interpretation, a commission of IASPEI that prepares and discusses international standards and procedures in seismological observation and interpretation.

- Defining/Non-defining phase

  A defining phase is used in the location of the event (time-defining) or in the calculation of the network magnitude (magnitude-defining). Non-defining phases are not used in the calculations because they suffer from large residuals or could not be identified.

- Direct/Indirect report

  A data report sent (e-mailed) directly to the ISC, or indirectly through another ISC data contributor.

- Duplicates

  Nearly identical phase arrival time data reported by one or more agencies for the same station. Duplicates may be created by agencies reporting observations from other agencies, or several agencies independently analysing the waveforms from the same station.

- Event

  A natural (e.g. earthquake, landslide, asteroid impact) or anthropogenic (e.g. explosion) phenomenon that generates seismic waves and its source can be identified by an event location algorithm.

- Grouping

  The ISC algorithm that organises reported hypocentres into groups of events. Phases associated to any of the reported hypocentres will also be associated to the preferred (prime) hypocentre. The grouping algorithm also attempts to associate phases that were reported without an accompanying hypocentre to events.

- Ground Truth

  An event with a hypocentre known to certain accuracy at a high confidence level. For instance, GT0 stands for events with exactly known location, depth and origin time (typically explosions); GT5 stands for events with their epicentre known to 5 km accuracy at the 95% confidence level, while their depth and origin time may be known with less accuracy.

- Ground Truth database

  On behalf of IASPEI, the ISC hosts and maintains the IASPEI Reference Event List, a bulletin of ground truth events.

- IASPEI

  International Association of Seismology and Physics of the Earth Interior, www.iaspei.org.

- International Registry of Seismograph Stations (IR)

  Registry of seismographic stations, jointly run by the ISC and the World Data Center for Seismology, Denver (NEIC). The registry provides and maintains unique five-letter codes for stations participating in the international parametric and waveform data exchange.

- ISC Bulletin

  The comprehensive bulletin of the seismicity of the Earth stored in the ISC database and accessible through the ISC website. The bulletin contains both natural and anthropogenic events. Currently the ISC Bulletin spans more than 50 years (1960-to date) and it is constantly extended by adding both recent and past data. Eventually the ISC Bulletin will contain all instrumentally recorded events since 1900.

- ISC Governing Council

  According to the ISC Working Statutes the Governing Council is the governing body of the ISC, comprising one representative for each ISC Member.

- ISC-located events

  A subset of the events selected for ISC review are located by the ISC. The rules for selecting an event for location are described in Section 3.3.4 of January to June 2012 Bulletin Summary; ISC-located events are denoted by the author ISC.

- ISC Member

  An academic or government institute, seismological organisation or company, geological/meteorological survey, station operator, national/international scientific organisation that contribute to the ISC budget by paying membership fees. ISC members have voting rights in the ISC Governing Council.

- ISC-reviewed events

  A subset of the events reported to the ISC are selected for ISC analyst review. These events may or may not be located by the ISC. The rules for selecting an event for review are described in Section 3.3.3 of January to June 2012 Bulletin Summary. Non-reviewed events are explicitly marked in the ISC Bulletin by the comment following the prime hypocentre "Event not reviewed by the ISC".

- ISF

  International Seismic Format (www.isc.ac.uk/standards/isf). A standard bulletin format approved by IASPEI. The ISC Bulletin is presented in this format at the ISC website.

- ISS

  International Seismological Summary (1918-1963). These bulletins are the predecessors of the ISC Bulletin and represent the major source of instrumental seismological data before the digital era. The ISS contains regionally and teleseismically recorded events from several hundreds of globally distributed stations.

- Network magnitude

The event magnitude reported by an agency or computed by the ISC locator. An agency can report several network magnitudes for the same event and also several values for the same magnitude type. The network magnitude obtained with the ISC locator is defined as the median of station magnitudes of the same magnitude type.

- Phase

  A maximum eight-character code for a seismic, infrasonic, or hydroacoustic phase. During the ISC processing, reported phases are mapped to standard IASPEI phase names. Amplitude measurements are identified by specific phase names to facilitate the computation of body-wave and surface-wave magnitudes.

- Prime hypocentre

  The preferred hypocentre solution for an event from a list of hypocentres reported by various agencies or calculated by the ISC.

- Reading

  Parametric data that are associated to a single event and reported by a single agency from a single station. A reading typically includes one or more phase names, arrival time and/or amplitude/period measurements.

- Report/Data report

  All data that are reported to the ISC are parsed and stored in the ISC database. These may include event bulletins, focal mechanisms, moment tensor solutions, macroseismic descriptions and other event comments, as well as phase arrival data that are not associated to events. Every single report sent to the ISC can be traced back in the ISC database via its unique report identifier.

- Shide Circulars

  Collections of station reports for large earthquakes occurring in the period 1899-1912. These reports were compiled through the efforts of J. Milne. The reports are mainly for stations of the British Empire equipped with Milne seismographs. After Milne's death, the Shide Circulars were replaced by the Seismological Bulletins of the BAAS.

- Station code

  A unique, maximum six-character code for a station. The ISC Bulletin contains data exclusively from stations registered in the International Registry of Seismograph Stations.

12

Acknowledgements

We thank Mathilde Sørensen of the University of Bergen in Norway and Alison Bird and her colleagues at the Pacific Geoscience Centre in Canada for kindly accepting our invitation and submitting the articles on notable earthquakes for this issue of the Summary.

We are also grateful to the developers of the Generic Mapping Tools (GMT) suite of software (Wessel and Smith, 1998) that was extensively used for producing the graphical figures.

Finally, we thank the ISC Member Institutions, Data Contributors, Funding Agencies (including NSF Award EAR-1417970 and USGS Award G14AC00149) and Sponsors for supporting the long-term operation of the ISC.

References

Balfour, N., R. Baldwin, and A. Bird (2008), Magnitude calculations in Antelope 4.10, *Analysis Group Note of Geological Survey of Canada*, pp. 1–13.

Bisztricsany, E. A. (1958), A new method for the determination of the magnitude of earthquakes, *Geofiz. Kozl*, pp. 69–76.

Bondár, I., and D. Storchak (2011), Improved location procedures at the International Seismological Centre, *Geophysical Journal International*, *186*, 1220–1244.

Bormann, P., and J. W. Dewey (2012), The new iaspei standards for determining magnitudes from digital data and their relation to classical magnitudes, is 3.3, *New Manual of Seismological Observatory Practice 2 (NMSOP-2), P. Bormann (Ed.)*, pp. 1–44, doi:10.2312/GFZ.NMSOP-2_IS_3.3,10.2312/GFZ.NMSOP-2, `http://nmsop.gfz-postsdam.de`.

Bormann, P., and J. Saul (2008), The new IASPEI standard broadband magnitude mB, *Seism. Res. Lett*, *79*(5), 698–705.

Bormann, P., R. Liu, X. Ren, R. Gutdeutsch, D. Kaiser, and S. Castellaro (2007), Chinese national network magnitudes, their relation to NEIC magnitudes and recommendations for new IASPEI magnitude standards, *Bulletin of the Seismological Society of America*, *97*(1B), 114–127, doi:10.1785/012006007835.

Bormann, P., R. Liu, Z. Xu, R. Ren, and S. Wendt (2009), First application of the new IASPEI teleseismic magnitude standards to data of the China National Seismographic Network, *Bulletin of the Seismological Society of America*, *99*, 1868–1891, doi:10.1785/0120080010.

Choy, G. L., and J. L. Boatwright (1995), Global patterns of readiated seismic energy and apparent stress, *J. Geophys. Res.*, *100*(B9), 18,205–18,228.

Dziewonski, A. M., T.-A. Chou, and J. H. Woodhouse (1981), Determination of earthquake source parameters from waveform data for studies of global and regional seismicity, *J. Geophys. Res.*, *86*, 2825–2852.

Engdahl, E. R., and A. Villaseñor (2002), Global seismicity: 1900-1999, *International Handbook of Earthquake Engineering and Seismology, International Geophysics series*, *81A*, 665–690.

Engdahl, E. R., R. van der Hilst, and R. Buland (1998), Global teleseismic earthquake relocation with improved travel times and procedures for depth determination, *Bulletin of the Seismological Society of America*, *88*, 722–743.

Gutenberg, B. (1945a), Amplitudes of P, PP and S and magnitude of shallow earthquakes, *Bulletin of the Seismological Society of America*, *35*, 57–69.

Gutenberg, B. (1945b), Magnitude determination of deep-focus earthquakes, *Bulletin of the Seismological Society of America*, *35*, 117–130.

Gutenberg, B. (1945c), Amplitudes of surface waves and magnitudes of shallow earthquakes, *Bulletin of the Seismological Society of America*, *35*, 3–12.

Hutton, L. K., and D. M. Boore (1987), The ML scale in southern California, *Bulletin of the Seismological Society of America*, *77*, 2074–2094.

IASPEI (2005), Summary of magnitude working group recommendations on standard procedures for determining earthquake magnitudes from digital data, `http://www.iaspei.org/commissions/CSOI.html#wgmm,http://www.iaspei.org/commissions/CSOI/summary_of_WG_recommendations_2005.pdf`.

IASPEI (2013), Summary of magnitude working group recommendations on standard procedures for determining earthquake magnitudes from digital data, `http://www.iaspei.org/commissions/CSOI/Summary_of_WG_recommendations_20130327.pdf`.

IDC (1999), IDC processing of seismic, hydroacoustic and infrasonic data, *IDC Documentation*.

Kanamori, H. (1977), The energy release in great earthquakes, *J. Geophys. Res.*, *82*, 2981–2987.

Lee, W. H. K., R. Bennet, and K. Meagher (1972), A method of estimating magnitude of local earthquakes from signal duration, *U.S. Geol. Surv.*, Open-File Rep.

Nuttli, O. W. (1973), Seismic wave attenuation and magnitude relations for eastern North America, *J. Geophys. Res.*, *78*, 876–885.

Richter, C. F. (1935), An instrumental earthquake magnitude scale, *Bulletin of the Seismological Society of America*, *25*, 1–32.

Ringdal, F. (1976), Maximum-likelihood estimation of seismic magnitude, *Bulletin of the Seismological Society of America*, *66*(3), 789–802.

Tsuboi, C. (1954), Determination of the Gutenberg-Richter's magnitude of earthquakes occurring in and near Japan, *Zisin (J. Seism. Soc. Japan)*, *Ser. II*(7), 185–193.

Tsuboi, S., K. Abe, K. Takano, and Y. Yamanaka (1995), Rapid determination of Mw from broadband P waveforms, *Bulletin of the Seismological Society of America*, *85*(2), 606–613.

Vaněk, J., A. Zapotek, V. Karnik, N. V. Kondorskaya, Y. V. Riznichenko, E. F. Savarensky, S. L. Solov'yov, and N. V. Shebalin (1962), Standardization of magnitude scales, *Izvestiya Akad. SSSR.*, *Ser. Geofiz.*(2), 153–158, pages 108–111 in the English translation.

Woessner, J., and S. Wiemer (2005), Assessing the quality of earthquake catalogues: estimating the magnitude of completeness and its uncertainty, *Bulletin of the Seismological Society of America*, *95*(2), doi:10/1785/012040,007.

WHITE PAPER

COMPLETE INTEGRATED AFTERSHOCK SYSTEM PROVIDES QUICK AND EASY SOLUTION FOR RAPID AFTERSHOCK DEPLOYMENT

LEONID ZIMAKOV

TRIMBLE INFRASTRUCTURE, PLANO, TEXAS, USA

INTRODUCTION

Rapid aftershock mobilization plays an essential role in the understanding of both focal mechanism and rupture propagation caused by strong earthquakes. A quick assessment of the data provides a unique opportunity to study the dynamics of the entire earthquake process in-situ. Aftershock study also provides practical information for local authorities regarding post-earthquake activity, which is very important in order to conduct the necessary actions for public safety in the area affected by a strong earthquake.

Due to a relatively short aftershock activity period (several weeks to several months), it is critical to rapidly deploy emergency personnel to the affected area in order to minimize the time required to estimate the extent and amplitude of strong shaking from aftershock events.

A dense array of seismic stations consisting of high resolution seismic recorders with short period seismometers and accelerometers is required in order to reduce the time needed to detect an event and provide high resolution maps of ground accelerations across the affected earthquake region. Therefore, the rapid aftershock mobilization of seismic equipment should comply with the following critical requirements:

- Lightweight and small in size
- Integrated design with minimal or no external peripheral equipment
- Very low power consumption
- Minimal or no field programming
- Easy and quick data download in the field
- Low maintenance

WHAT DOES THE 160-03 OFFER?

The REF TEK High Resolution Aftershock System, Model 160-03, is a self-contained, fully integrated Aftershock System providing the customer with simple and quick deployment during aftershock emergency mobilization. The 160-03, six channel recorder, contains three major components integrated in one case:

- 24-bit resolution low power ADC with CPU and lid interconnect boards;
- power source; and
- three component 2 Hz sensors (two horizontals and one vertical and a triaxial +/-4g MEMS accelerometer.

Figure 1: REF TEK 160-03 High Resolution Aftershock System

Figure 2: Inside the case of the REF TEK 160-03 High Resolution Aftershock System

The self-contained rechargeable battery pack provides power autonomy for up to 7 days during continuous data acquisition at 200 sps on three weak motion and three triggered strong motion recording channels. For longer power autonomy, the 160-03 Aftershock System battery pack can be charged from an external source (solar power system). To download recorded data the customer has two options:

- Connect a laptop to the 160-03 and the data is then automatically uploaded; or
- Connect the REF TEK Wi-Fi Serial Adaptor to upload data to the REF TEK iFSC Controller.

The 160-03 configuration is fixed based on a configuration file stored in the system, so no external command/control interface is required for parameter setup in the field. For visual control of the system performance in the field, the 160-03 has a built-in LED display which indicates the system's recording status, as well as a hot swappable USB drive and battery status. As an added customer convenience, four 160-03 systems can be housed in a small, lightweight, watertight rolling case that will keep the recorders safe during transport. The ease of having an all-in-one aftershock system also provides the customer flexibility in sending the equipment to the affected region via a more cost effective way as the equipment/carrying case can easily be checked on both domestic and international commercial flights.

160-03 SPECIFICATIONS

Model	160-03 (Part No. 97124-00)
Mechanical	
Size: Weight: Watertight Integrity:	6” (15.2cm) high x 8.63” (21.9cm) diameter 11.7 lbs. (5.3 kg) IP67
Environmental	
Operating Temp.:	-30°C to +60°C
Storage Temp.:	-40°C to +70°C
Power	
Average Power:	<400 mW
A/D Convertor	
Type:	Delta-Sigma Modulation, 24-bit output resolution
Dynamic Range:	>138 dB@100 sps
Channels:	6
Input Impedance:	Matched to sensors
Sample Rates:	200 sps default; 100, 250, 500 sps optional
Seismometer	
Type:	Moving coil / mass
Natural Frequency:	2 Hz
Accelerometer	
Type:	± 4g
Frequency Response:	DC – 45 Hz
Damping:	0.7 to critical
Data Storage	
Type:	USB Flash
User Interface	
Type:	LED array consisting of 16 LED display recording status, USB drive status, battery voltage, etc.
Power Control:	Magnetic switch to turn on both power and acquisition

Table 1: 160-03 Specifications

CONTACT US

Phone: +1 (214) 440 1265

Email: sales@reftek.com

Earthquake Early Warning
Rapid Response

Where to be utilized?

- ✓ High seismic risk areas
- ✓ Regions with known active faults or fault zones
- ✓ Densely populated and urban areas
- ✓ Industrial facilities and lifelines

What are the Features and Benefits?

- ✓ Detecting primary non-destructive waves as soon as an earthquake occurs
- ✓ Estimating the magnitude and location of earthquake
- ✓ Indicating approaching destructive waves
- ✓ Real-time operation within scientific reliability
- ✓ Rapid calculation of estimated damages after shake
- ✓ Thematic mapping for damage assessment and action plan (disaster management)
- ✓ Notification of user groups or involved parties
- ✓ Mitigation of risk due to earthquake exposure
- ✓ Automated decision making and emergency actions such as shutdown of facilities
- ✓ Continued monitoring for aftershock events
- ✓ Disaster awareness, prevention and management

Professional Advice and Support from concept to deployment

Our professional and experienced consultants are ready to provide you with the best impartial advice and support from the outset.

Our knowledge of earthquake early warning, seismic monitoring and rapid response systems coupled with an in-depth understanding of our instruments will provide you with an unparalleled advantage to achieve the best results for your requirements on time and on budget.

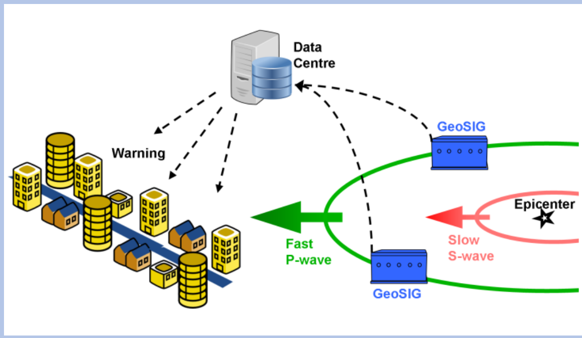

Overview

Earthquakes are perilous and inevitable natural events, causing severe damage and loss of life.

There is no proven method to forecast the precise occurrence time of an earthquake nor its location or size.

Yet, utilising state of the art scientific methodologies as done in GeoSIG Earthquake Early Warning (EEW) solution, it is now possible to quite accurately assess the location and size as soon as an earthquake emerges using its non-destructive primary waves.

Thus, warnings about a potential strong shaking can be generated almost instantaneously, until destructive secondary seismic waves arrive.

Based on fast and reliable communication channels, this provides the crucial seconds to take measures which may help reduce catastrophic impacts of seismic events.

After an earthquake, GeoSIG Rapid Response (RR) solution provides analytic and thematic information on the aftermath of the earthquake in terms of shake maps consisting of observed ground motion parameters as well as estimated damage distribution.

Our Services

Advice

Consulting

Technical Proposal

Financial Offer

Planning

Installation

Training

Maintenance

GeoSIG
swiss made to measure

Earthquake Early Warning
Rapid Response

Where to be utilized?

- ✓ High seismic risk areas
- ✓ Regions with known active faults or fault zones
- ✓ Densely populated and urban areas
- ✓ Industrial facilities and lifelines

What are the Features and Benefits?

- ✓ Detecting primary non-destructive waves as soon as an earthquake occurs
- ✓ Estimating the magnitude and location of earthquake
- ✓ Indicating approaching destructive waves
- ✓ Real-time operation within scientific reliability
- ✓ Rapid calculation of estimated damages after shake
- ✓ Thematic mapping for damage assessment and action plan (disaster management)
- ✓ Notification of user groups or involved parties
- ✓ Mitigation of risk due to earthquake exposure
- ✓ Automated decision making and emergency actions such as shutdown of facilities
- ✓ Continued monitoring for aftershock events
- ✓ Disaster awareness, prevention and management

Professional Advice and Support from concept to deployment

Our professional and experienced consultants are ready to provide you with the best impartial advice and support from the outset.

Our knowledge of earthquake early warning, seismic monitoring and rapid response systems coupled with an in-depth understanding of our instruments will provide you with an unparalleled advantage to achieve the best results for your requirements on time and on budget.

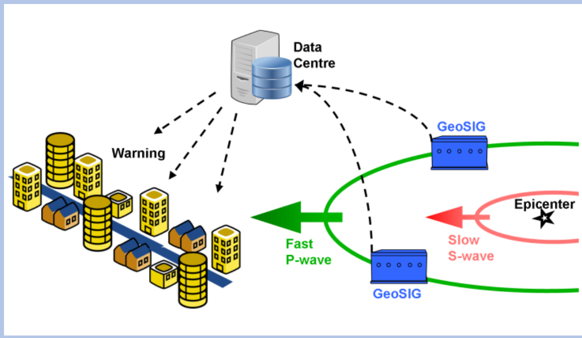

Overview

Earthquakes are perilous and inevitable natural events, causing severe damage and loss of life.

There is no proven method to forecast the precise occurrence time of an earthquake nor its location or size.

Yet, utilising state of the art scientific methodologies as done in GeoSIG Earthquake Early Warning (EEW) solution, it is now possible to quite accurately assess the location and size as soon as an earthquake emerges using its non-destructive primary waves.

Thus, warnings about a potential strong shaking can be generated almost instantaneously, until destructive secondary seismic waves arrive.

Based on fast and reliable communication channels, this provides the crucial seconds to take measures which may help reduce catastrophic impacts of seismic events.

After an earthquake, GeoSIG Rapid Response (RR) solution provides analytic and thematic information on the aftermath of the earthquake in terms of shake maps consisting of observed ground motion parameters as well as estimated damage distribution.

Our Services

- Advice
- Consulting
- Technical Proposal
- Financial Offer
- Planning
- Installation
- Training
- Maintenance